THE ELECTROCHEMISTRY OF LEAD

IN SULPHURIC ACID

Thesis submitted to the University of Newcastle upon Tyne for the degree of Doctor of Philosophy

G. Archdale

July 1973

CONTENTS

INTRODUCTION

This project was initiated in order to investigate the basic electrochemistry of $Pb/PbSO_4$ in sulphuric acid. Very little has appeared in the literature on this subject, workers have been concerned with the $PbSO_4/PbO_2$ region, as can be seen from the literature survey in Chapter 5. However, in the last few years interest has increased in the lead acid battery and I hope this thesis will help further technical advance.

The first four chapters review basic background material against which the measurements were made. The following chapters then describe the experimental work and finally some attempt is made to link the basic electrochemistry to the working of a battery.

CHAPTER 1.

ELECTROCHEMICAL METHODS AND ELECTRON-OPTICAL TECHNIQUES

1.1. Introduction

In this chapter I will discuss interfaces composed of a metal in contact with aqueous solutions. The first section deals with fundamental electrochemical kinetics and the effect of mass transfer. The second section concerns electrochemical techniques used in the elucidation of mechanisms. The third section describes the techniques used to investigate the surface. Particular reference is made to the potentiostatic method and the rotating disc, since these were the techniques most employed in the experimental work.

If a potential is applied to a single metal electrode M in an electrolyte, say HCl, the following reactions can occur:-

Anodic

$$M \rightleftharpoons M^{n+} + ne$$
$$nCl^- + M \rightleftharpoons MCl_n + ne$$
$$M + Cl^- \rightleftharpoons (MCl)_s + e$$
$$Cl^- \rightleftharpoons \tfrac{1}{2} Cl_2 + e$$
$$2H_2O \rightleftharpoons O_2 + 4H^+ + 4e$$

Cathodic

$$M + H^+ + e \rightleftharpoons MH$$
$$H^+ + e \rightleftharpoons \tfrac{1}{2} H_2$$

This is shown diagrammatically in Figure 1.1.

To determine the possible reactions, thermodynamic data can be used, but which particular reaction will be preferred is controlled by

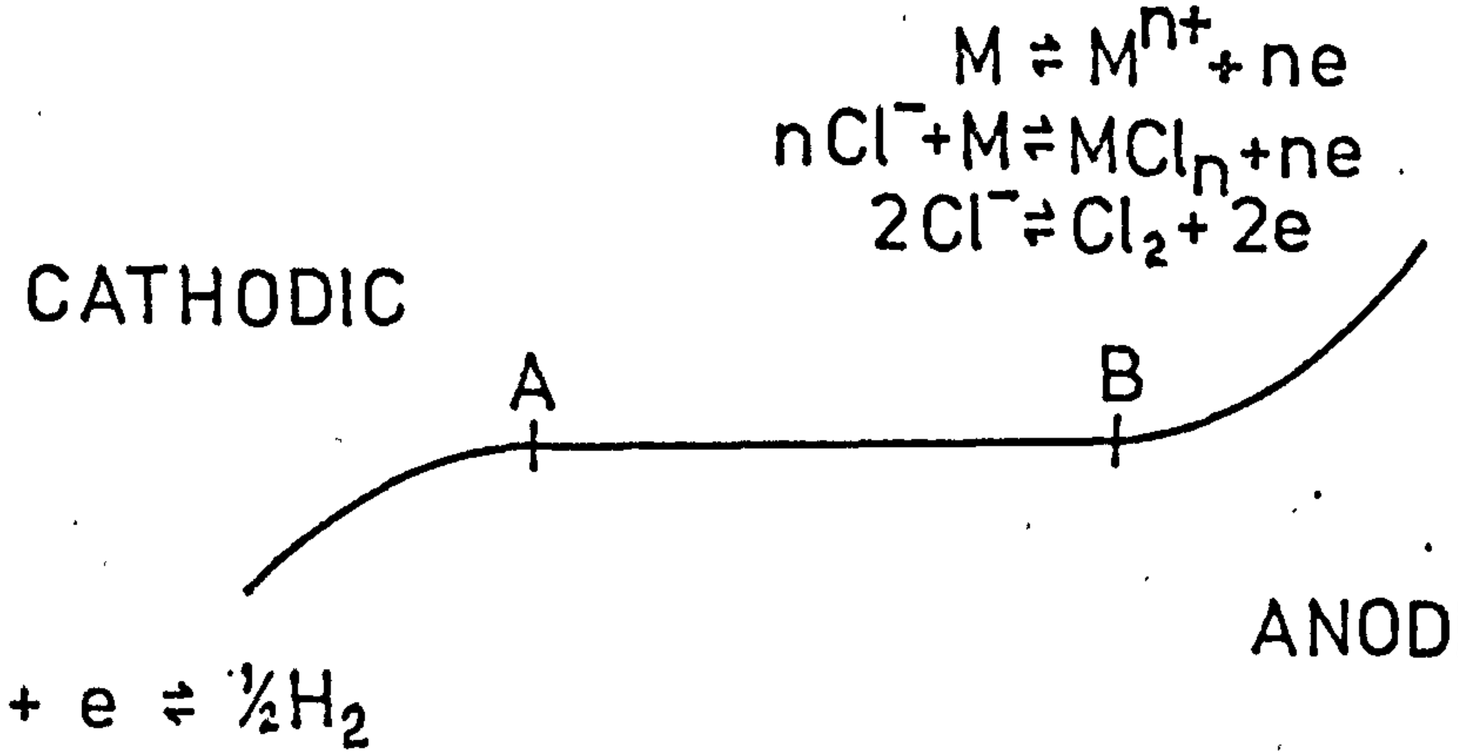

FIG. 1.1. FORM OF THE CURRENT VOLTAGE CURVE FOR A SINGLE METAL ELECTRODE M IN AN ELECTROLYTE HCl.

the kinetics. No permanent current flows in the region AB and the electrode is said to be perfectly polarisable.

The Double Layer

Change in potential in the region AB changes the charge on both sides of the interface, as in a parallel plate condenser. A great deal is now known about the structure of the double layer and an authoritative account has been given by Delahay[1].

The double layer consists of an accumulation of charges of opposite sign and oriented dipoles at the surface; the separation of charge causing an electric field at the interface. The charge on the metal surface, an excess or depletion of electrons, resides with the metal atoms of the first layer of the metal surface. On the solution side however, the double layer penetrates further towards the bulk of the solution. This is shown schematically in Figure (1.2), and consists of an outer or diffuse layer made up of positively and negatively charged ions held in the layer by coulombic forces and a more compact layer held by both coulombic and specific interaction forces. Some anions penetrate to the inner Helmholtz plane (I.H.P.) and are specifically adsorbed. Cations and unadsorbed anions only approach as far as the outer Helmholtz plane (O.H.P.). A layer of water exists between the I.H.P. and the metal surface. The quantities which are measured to deduce double layer structure are differential capacity, interfacial tension, and surface potential. Specialist reviews are available for further details of the interpretation of the effect of inorganic ions[2,3,4,5,6] and organic[7] compounds at the mercury electrolyte interface. Although the interface can be investigated in the double layer region (at mercury) it is

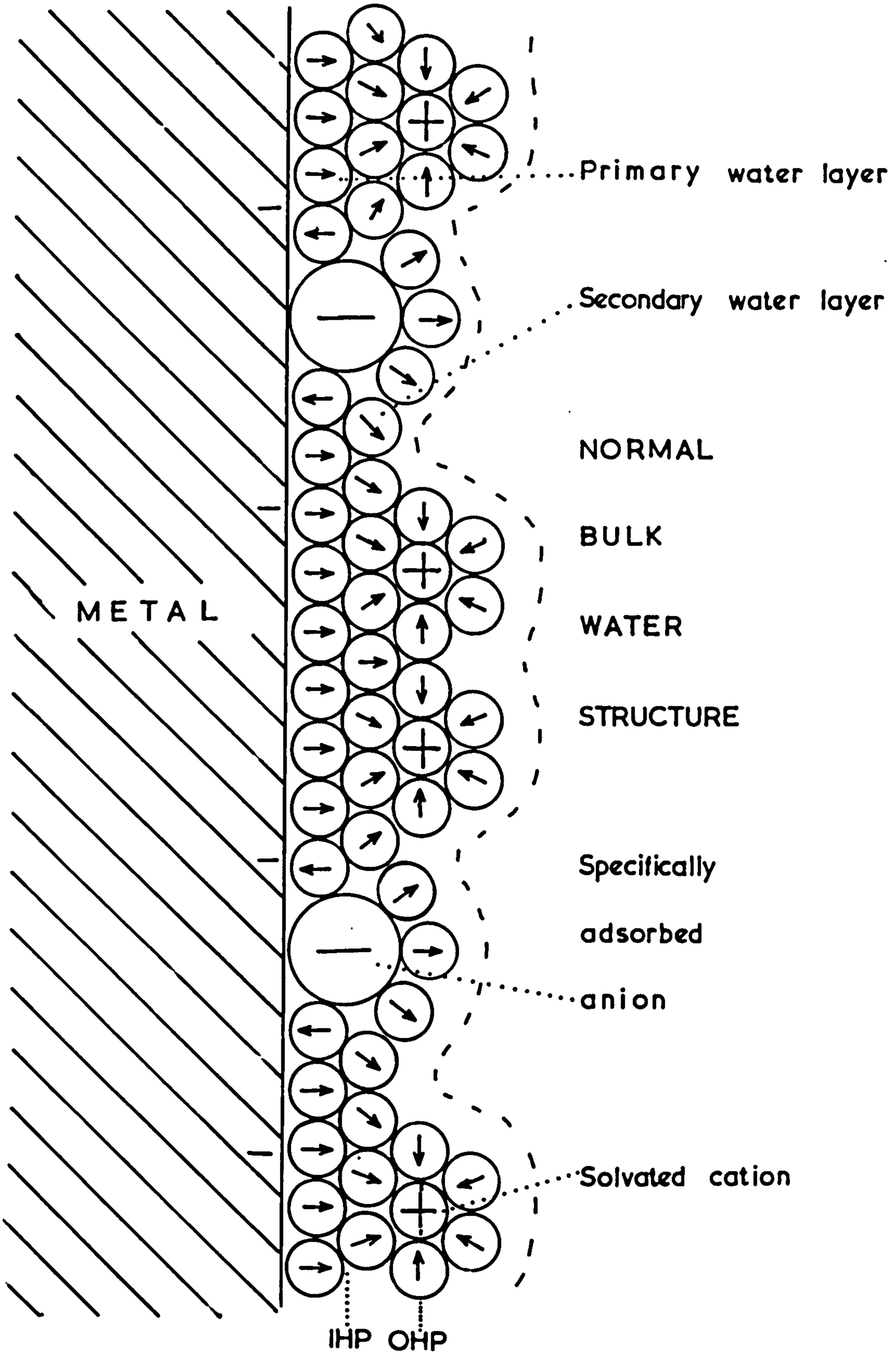

Fig.1.2 Schematic microstructure of a metal-aqueous electrolyte interface

undoubtedly also present when a reaction proceeds. Attempts have been made to match double layer properties measured in the absence of reactant, with the reaction kinetics[1,8,9]. Sluyters A.C. method[10] has been an advance in this direction, since by this method the double layer capacity can be measured in the presence of a reaction.

Differential capacity measurements have almost exclusively been measured on mercury. An extensive review of porous and rough electrodes has been given by De Levie[11]. With a deeper understanding of roughness and surface structure progress could be made in the study of the double layer on other metals. An attempt along these lines has been made by Giles and Harrison[12] with silver.

Generally, in electrode kinetics, double layer effects are not of overriding importance. The presence of excess inert electrolyte, to minimise migration, ensures that the potential at the reaction site remains constant as the overall potential of the electrode is changed. The fact that many reactions under these conditions have a straight Tafel plot of the correct slope and also have the correct dependence of current on reactant concentration at fixed potential supports this argument. If experimentally there is deviation from this rule then the structure of the double layer must be taken into account.

1.2. Electrode Kinetics

Substances O and R present in solution

The basic electrochemical process which occurs when an inert metal is in contact with a redox process is

$$R \underset{K_b}{\overset{K_f}{\rightleftharpoons}} O + ne \qquad (1.1)$$

At a particular potential the current that flows as in equation (1.1), can be expressed as the difference between the forward and reverse rates.

$$i = nFA\left(k_f C_R^s - k_b C_O^s\right) \tag{1.2}$$

k_f and k_b are constants at fixed potential which include the activity coefficients. C_R^s , C_O^s are the concentrations of R and O at the surface. n is the number of electrons involved, A is the area of the electrode and F is the Faraday. Equivalent to equation (1.2) is the statement that the overall current is given by the partial currents

$$i = i_f - i_b \tag{1.3}$$

It is necessary here to define a sign convention. Since this thesis is primarily concerned with anodic processes, anodic currents will be assigned a positive sign, cathodic currents a negative sign. The anodic potentials are defined as positive going, cathodic potentials negative going. k_f and k_b are expected to be exponential functions of potential. This assumption can be justified by the transition state theory of which there are many accounts available.

Transport to the electrode

However, the interfacial rate is not the only component of the overall reaction rate. Reactants and products have to be transported to and away from the electrode; this is achieved by diffusion.

Transport in solution can also occur by convection and migration. Migration is invariably prevented by the addition of excess indifferent

electrolyte. Natural convection can be avoided if the time of measurement is short. Both these effects will not be considered further.

When a diffusion gradient exists between the surface and the bulk of solution, the movement of ions in a concentration gradient is controlled by Fick's first and second laws,

$$\text{flux} = \mathcal{D}\left(\frac{\partial c}{\partial x}\right) \qquad \text{Fick's first law}$$

$$\left(\frac{\partial c}{\partial t}\right) = \mathcal{D}\left(\frac{\partial^2 c}{\partial x^2}\right) \qquad \text{Fick's second law}$$

where $\mathcal{D}$ is the diffusion coefficient of the species.

Solving the second law by integration for a stationary situation, with a fixed diffusion layer, then the flux per unit area is a constant given by

$$i = \frac{nFAD_o\left(C_o^s - C_o^b\right)}{\delta} \qquad (1.4)$$

where δ is the diffusion layer at which the concentration is maintained at C_o^b.

Calculation of C_o^s

The concentrations at the interface C_o^s, C_R^s are not immediately accessible, however equation (1.2) can be used by eliminating C_o^s and C_R^s by means of equation (1.4) in the form

$$C_o^s = \frac{\left(i - i_d^o\right)\delta}{nFAD_o} \qquad (1.5)$$

and a corresponding equation for C_R^s

$$C_R^s = \frac{\left(i_d^R - i\right)\delta}{nFAD_R} \qquad (1.6)$$

where $i_d^{\cdot o}$ and $i_d^{\cdot R}$ represent the diffusion limiting currents of the oxidised and reduced species respectively.

$$i_d^{\cdot o} = - \frac{C_o^b nFAD_o}{\delta} \qquad (1.7)$$

and

$$i_d^{\cdot R} = \frac{C_R^b nFAD_R}{\delta} \qquad (1.8)$$

This method holds in principal for any technique. Techniques that specifically achieve a fixed diffusion layer thickness include polarography and the rotating disc (see later).

1.3. Derivation of the basic equation

The potential E of the working electrode with respect to a reference electrode is the main property which determines the current. K_f, K_b are defined as follows,

$$K_f = K_1 \exp \frac{\alpha nFE}{RT} \qquad (1.9)$$

$$K_b = K_{-1} \exp \frac{(\alpha-1) nFE}{RT} \qquad (1.10)$$

K_1, K_{-1} are potential independent constants, and α is an empirical constant with a value approximately 0.5. Attempts have been made to give α theoretical significance but, as yet, no completely satisfactory theory has emerged[13,6]. The numerical values of K_1, K_{-1} depend on the reference electrode system, that is $K_f = K_1$, $K_b = K_{-1}$ at $E = 0$. In order to define constants equivalent to K_1, K_{-1} which reflect the nature of the electro-

chemical process itself, it is usual to use two alternatives. The first is to define k_f and k_b with respect to E°, the standard potential.

$$k_f = k_a \exp \frac{\alpha n F (E - E^\circ)}{RT} \tag{1.11}$$

$$k_b = k_a \exp \frac{(\alpha - 1) n F (E - E^\circ)}{RT} \tag{1.12}$$

where k_a is the forward rate on the surface. The second method is to define k_f, k_b with respect to the potential E_e, at which experimentally $i = 0$. Using the definition for overpotential

$$\eta = E - E_e \tag{1.13}$$

then

$$k_f = \frac{i_o}{nFC_R^b} \exp \frac{\alpha n F \eta}{RT} \tag{1.14}$$

$$k_b = \frac{i_o}{nFC_o^b} \exp \frac{(\alpha - 1) n F \eta}{RT} \tag{1.15}$$

i_o is the exchange current.

Substituting equations (1.14), (1.15) in equation (1.2) gives the well known equation

$$\frac{i}{A} = i_o \left[\frac{C_R^s}{C_R^b} \exp \frac{\alpha n F \eta}{RT} - \frac{C_o^s}{C_o^b} \exp \frac{(\alpha - 1) n F \eta}{RT} \right] \tag{1.16}$$

Similar expressions are obtained using the other definitions of k_f and k_b.

Equation (1.16) describes generally the relation between overall current and potential when the concentration of the reacting species is different from the bulk concentration, and O and R exist in the bulk of solution.

This equation can be dealt with by the use of two methods namely wave analysis and extrapolation techniques.

1.4. Wave Analysis

General case when O and R present in bulk

Here it is appropriate to use the form of equation (1.16) containing η since E_e is measurable (both components present in the bulk).

The concentrations at the surface are given by equations (1.5) and (1.6).

Hence

$$\frac{C_o^s}{C_o^b} = \frac{i_d^o - i}{i_d^o} \qquad (1.17)$$

$$\frac{C_R^s}{C_R^b} = \frac{i_d^R - i}{i_d^R} \qquad (1.18)$$

Substituting equations (1.17) and (1.18) into equation (1.16) gives,

$$i = Ai_o\left[\left(\frac{i_d^R - i}{i_d^R}\right)\exp\frac{\alpha nF\eta}{RT} - \left(\frac{i_d^o - i}{i_d^o}\right)\exp\frac{(\alpha-1)nF\eta}{RT}\right] \qquad (1.19)$$

and a simple rearrangement[14] gives,

$$\ln\left[\left(\frac{1}{i} - \frac{1}{i_d^R}\right) - \left(\frac{1}{i} - \frac{1}{i_d^o}\right)\exp\frac{-nF\eta}{RT}\right] = \ln\frac{1}{Ai_o} - \frac{\alpha nF\eta}{RT} \qquad (1.20)$$

When only one component is present in the bulk, O, it is more convenient to use E° as the reference point, as E_e is not easily experimentally determined. Using definitions equations (1.11) and (1.12) we have,

$$i = nFAK_a\left[C_R^s \exp\frac{\alpha nF(E-E^\circ)}{RT} - C_O^s \exp\frac{(\alpha-1)nF(E-E^\circ)}{RT}\right] \qquad (1.21)$$

Substituting for C_O^s and C_R^s when the fluxes are equal,

$$i = nFAK_a\left[-C_O^b \frac{i}{i_d^\circ}\frac{D_O}{D_R}\exp\frac{\alpha nF(E-E^\circ)}{RT} - C_O^b\left(\frac{i+i_d^\circ}{i_d^\circ}\right)\exp\frac{(\alpha-1)nF(E-E^\circ)}{RT}\right] \qquad (1.22)$$

which is rearranged to

$$\ln\left[\frac{C_O^b D_O}{i_d^\circ D_R} + C_O^b\left(\frac{1}{i_d^\circ}+\frac{1}{i}\right)\exp\frac{-nF(E-E^\circ)}{RT}\right] = \ln\frac{1}{nFAK_a} - \frac{\alpha nF(E-E^\circ)}{RT} \qquad (1.23)$$

Equation (1.23) has been used for studying polarographic waves. Metal dissolution is, however, a much simpler case.

Metal Dissolution

General case.

Take the situation

$$R \underset{K_b}{\overset{K_f}{\rightleftharpoons}} O + ne$$

R is a metal that dissolves at unit activity. The total anodic current is represented by

$$i = nFA\left(K_f - K_b C_O^s\right) \qquad (1.24)$$

which can be alternatively written as

$$i = nFAK_a\left(\exp\frac{\alpha nF(E-E^\circ)}{RT} - C_o^s \exp\frac{(\alpha-1)nF(E-E^\circ)}{RT}\right) \qquad (1.25)$$

using equations (1.11) and (1.12).

Since $$i = \frac{D_o C_o^s nFA}{\delta} \qquad (1.26)$$

then

$$i = nFAK_a \exp\frac{\alpha nF(E-E^\circ)}{RT} - K_a\frac{i\delta}{D}\exp\frac{(\alpha-1)nF(E-E^\circ)}{RT} \qquad (1.27)$$

Two limiting cases of equation (1.27) exist:-

Reversible case

This case is obtained by equating the two R.H.S. terms of equation (1.25).

$$i = \frac{nFAD_o}{\delta}\exp -\frac{nF(E-E^\circ)}{RT} \qquad (1.28)$$

Irreversible case

Here $$i = nFAK_f \qquad (1.29)$$

hence $$i = nFAK_a \exp\frac{\alpha nF(E-E^\circ)}{RT} \qquad (1.30)$$

Equation (1.27) can be used to describe the whole of an i-E wave for a metal dissolving, this however is a cumbersome equation and has probably never been used. Usually one of the limiting cases equation (1.28) or

equation (1.30) is used at the rotating disc. Since only equation (1.28) contains δ, reversible reactions will be dependent on rotation speed, whereas irreversible reactions will be independent of rotation speed. Also when $\log i$ vs E is plotted the reversible case for a one electron reaction will have a slope of 60 mV/decade and the corresponding irreversible reaction a slope of 120 mV/decade. Since $\frac{2.303\ RT}{F}$ = 60 mV at 25°C.

1.5. Extrapolation Techniques

In a current-voltage curve most of the information about the interfacial reaction is contained at the foot of the wave where measurement is inexact. In addition the maximum interfacial rate which can be measured in a stationary current-voltage curve depends on the diffusion layer thickness. Faster rates can be investigated by non-stationary methods (perturbation methods) in which the interfacial rate, which moves in sympathy with the signal, wins over processes occurring in solution. This amounts to setting up a thinner effective diffusion layer.

There are many techniques available for studying electrode processes including polarography, potentiostatic methods, galvanostatic methods, A.C. method. Since potentiostatic methods were employed in the experimental, only this method will be discussed here.

1.5.1. The Potentiostatic Method

The basis of the potentiostatic method for studying the kinetics of electrode processes was outlined in 1955 by Gerischer and Vielstich[15]. In this method the potential of the electrode under investigation (working electrode (W.E.) against some reference electrode (R.E.), at a constant value E, is controlled by the potentiometer of the potentiostat. Any

current flowing through the cell, from the working electrode to a subsidiary electrode (S.E.), is recorded.

The heterogeneous rate constant for the electrochemical step is potential dependent and the rate of the reaction is determined by the potential difference between the chemical species at the reaction site, usually assumed to be the Helmholtz plane, and the electrode surface. Consequently, the most detailed analysis of the electrode kinetics can be obtained under constant potential conditions. The potential of an electrode is the variable which defines the height of the energy barrier to be surmounted for the occurrence of electron transfer. The resulting current for the electrode process is considered as the net rate of transfer of electrons in one direction over this energy barrier - hence potential control is a very definitive condition.

Potentiostatic control with superimposition of a regular potential perturbation offers powerful techniques with wide application in electrode kinetics e.g. potentiostatic single pulse, linear potential sweep, potentiostatic double pulse, potentiostatic pulse and sweep combined, and the potentiostatic a.c. impedance method. Only the first two methods will be discussed.

The design of potentiostats and pulse generators is now well understood[16,17]. Many types of instrument are commercially available. A versatile system can be built from operational amplifiers[18,19,20].

1.5.2. Potential Step Method

The potentiostatic step or pulse method has found wide application in the study of electrode kinetics for processes in which electron transfer and diffusion are important, and for more complex

reactions, for example, the H_2 reaction[21]. Many reaction schemes have been studied. These have been summarised recently by Thirsk and Harrison[22].

Electron transfer

Consider the straight electron exchange reaction[15] in which both species are diffusing to or away from the electrode

$$O + ne \rightleftharpoons R \tag{1.31}$$

The equations to be solved are

$$\frac{\partial C_O}{\partial t} = D_O\left(\frac{\partial^2 C_O}{\partial x^2}\right), \tag{1.32}$$

$$\frac{\partial C_R}{\partial t} = D_R\left(\frac{\partial^2 C_R}{\partial x^2}\right) \tag{1.33}$$

with the boundary conditions at $x = 0$

$$i = nFAD_R\left(\frac{\partial C_R}{\partial x}\right)_{x=0} = nFA\left(k_b C_R^s - k_f C_O^s\right) \tag{1.34}$$

$$D_R\left(\frac{\partial C_R}{\partial x}\right)_{x=0} = -D_O\left(\frac{\partial C_O}{\partial x}\right)_{x=0} \tag{1.35}$$

with the conditions at $x \longrightarrow \infty$

$$C_O = C_O^b, \quad C_R = C_R^b \tag{1.36}$$

and the initial condition at $t = 0$

$$C_O = C_O^b, \quad C_R = C_R^b \tag{1.37}$$

The well known solution which is achieved using Laplace transforms is given by

$$\frac{i}{A} = i_o\left[\exp\frac{\alpha nF\eta}{RT} - \exp\frac{(\alpha-1)nF\eta}{RT}\right]\exp(\lambda^2 t)\,erfc\,(\lambda t^{1/2}) \qquad (1.38)$$

$$\frac{i}{A} = I\,\exp(\lambda^2 t)\,erfc\,(\lambda t^{1/2}) \qquad (1.39)$$

where I is the current free of diffusion λ is given by

$$\lambda = \frac{i_o}{nF}\left[\frac{\exp\frac{\alpha nF\eta}{RT}}{C_R^b D_R^{1/2}} + \frac{\exp\frac{(\alpha-1)nF\eta}{RT}}{C_o^b D_o^{1/2}}\right] \qquad (1.40)$$

Equation (1.38), which appears to be rather complex is rarely used in this form. Two limiting cases can be calculated, by expanding the exp and erfc terms in equation (1.38).

When $\lambda t^{1/2} > 5$, the kinetic parameters become negligible and the mass transfer polarisation term becomes important. The current-time relationship simplifies to

$$i = nFA\left(C_o^b - C_o^s\right)\sqrt{D_o/\pi t} \qquad (1.41)$$

note, $i - t^{-1/2}$ linear.

Experimental data is tested by plotting i vs $t^{-1/2}$ and comparing the slope with the theoretical. Catalytic (higher slope than diffusion) and slow preceding chemical reactions (lower slope than expected) can be detected by this method.

With the opposite assumption, $\lambda t^{1/2} < 1$, equation (1.38) becomes

$$\frac{i}{A} = I\left(1 - \frac{2\lambda t^{1/2}}{\pi^{1/2}}\right) \qquad (1.42)$$

which means that I can be measured by plotting i vs $t^{1/2}$ and extrapolating to $t=0$. The cross over from $i \propto t^{-1/2}$ to $i \propto t^{1/2}$ is discussed in the literature[23]. When the electrochemical reaction is very slow $\lambda t^{1/2} \ll 1$ then

$$\frac{i}{A} = I \tag{1.43}$$

and the transient is a constant current.

1.5.3. Linear Potential Sweep

The fact that the whole potential range can be scanned in a single experiment makes the method of linear potential sweep a very useful technique. The method is most easily interpreted in the single sweep mode, the first cycle of the potential profile. It is sometimes advantageous however, to observe the current due to continuous potential cycling, for example, the theory for continuous cycling to observe stationary state currents is more complex than for a single sweep and is rarely calculated.

Two main types of processes have been identified.

(i) Electron transfer with diffusion in solution.

(ii) Electron transfer with adsorption.

Only type (i) will be considered here, the maximum current i_p, and potential E_p, can be measured as a function of sweep rate and bulk concentration of reactant, to measure the kinetics. The relation of the parameters to one another is subject to the reaction scheme. Information about the kinetics is also contained in the foot of the wave. It is often possible to obtain a Tafel slope as a function of sweep rate which should be complementary to the behaviour of i_p, E_p. A third source of information

is the shape of the wave measured by the width of the wave at suitable points. The behaviour of the current on reverse sweep is also important.

The $i-V$ relationship has been formulated for several reaction schemes and these are listed in reference (22).

The simple redox reactions

$$R \rightleftharpoons O + ne$$

respond to a single linear sweep as shown in Figure 1.3. The curve rises sharply as the potential increases, accelerating the reaction until the growing diffusion layer begins to exert control and the current goes down. In the case of metal dissolution the current is usually limited by the formation of a film. The experimental parameters which characterise a peak are height (i_p), peak potential (E_p) and shape. The shape can be denoted by the width at $i_p/2$; this last test is rarely used. A comprehensive review[24] of the expected results for various reaction schemes is given in the literature. The most important and well known results are for a reversible simple redox reaction at a planar electrode where R is absent in the bulk.

$$E_p = E_{1/2} - 1.109\frac{nF}{RT} \tag{1.44}$$

$$i_p = 0.269\, A n^{3/2} C_R^b D_R^{1/2} V^{1/2} \tag{1.45}$$

E_p is independent of sweep rate. A completely irreversible redox charge transfer reaction

$$R \longrightarrow O + ne$$

behaves as

$$E_p = E^\circ + \frac{RT}{\alpha nF}\left[-0.78 + \ln\frac{k_1}{D_R^{1/2}} - \tfrac{1}{2}\ln\left(\frac{\alpha nF}{RT}V\right)\right] \tag{1.46}$$

$$i_p = 0.495\, AnF\left(\frac{\alpha n'F}{RT}\right)^{1/2} D_R^{1/2} C_R^b V^{1/2} \tag{1.47}$$

FIG 1.3 LINEAR POTENTIAL SWEEP CURVE FOR A REDOX REACTION (DIAGRAMMATIC)

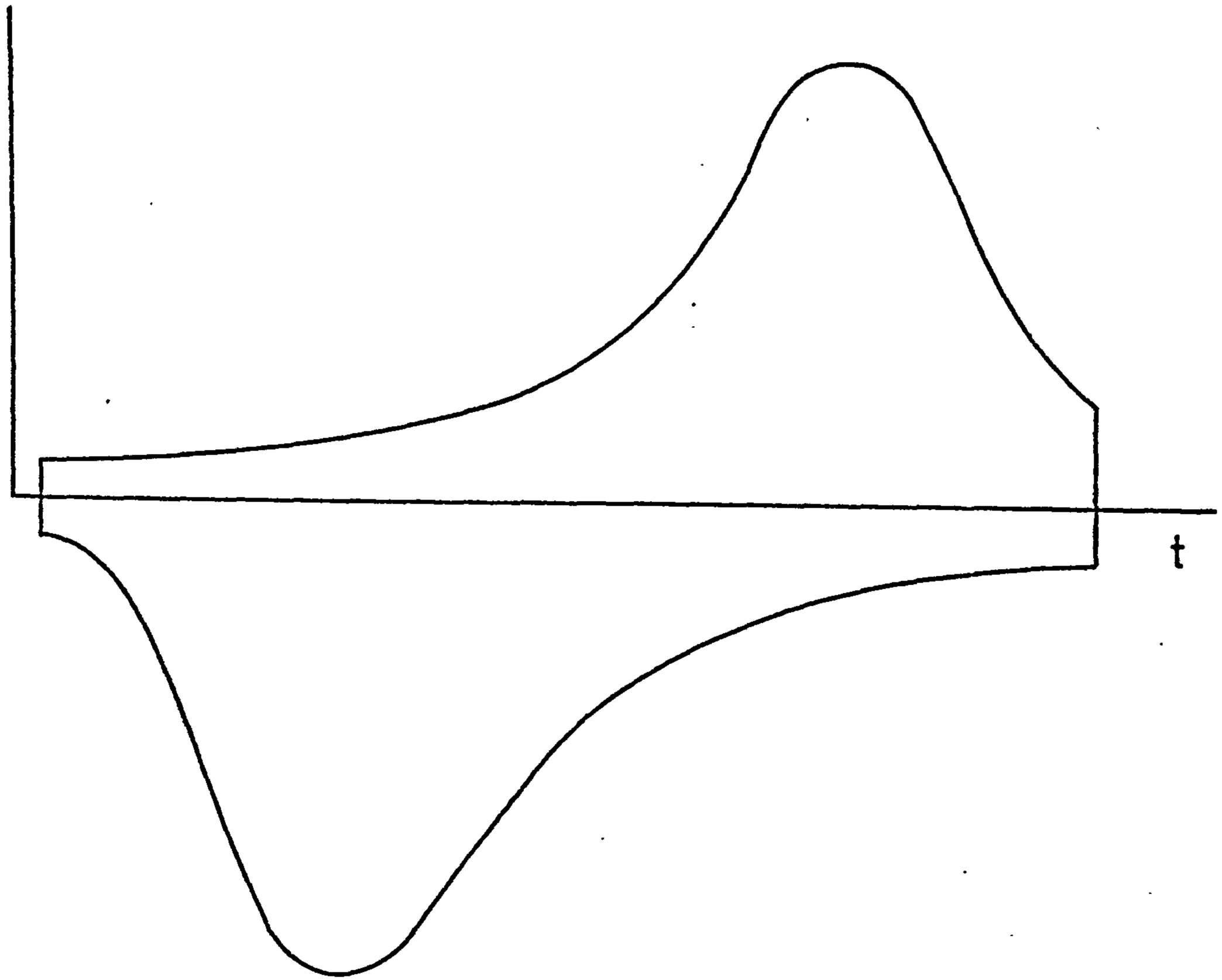

where K_1 is the reaction constant at the normal hydrogen reversible potential. i is proportional to $V^{1/2}$ as before. E_p depends now on sweep rate, a fact which is used to distinguish the two cases. In essence, plotting E_p against $\log V$ corrects for diffusion, and a Tafel slope is obtained directly. Rewriting equation (1.46) gives

$$\frac{dE_p}{d\log v} = -\frac{b}{2} \qquad (1.48)$$

where b is the Tafel slope.

The reversible and totally irreversible limiting cases can usually be attained in a practical system by adjusting the sweep rate and conditions.

1.5.4. The Rotating Disc Electrode

The rotating disc is a powerful tool in electrochemistry[25,26]. The electrode system, shown diagrammatically (Figure 1.4) is rotated at a strictly controlled and measurable angular velocity, the current or potential control is exercised at the electrode-solution interface according to the desired experimental scheme. At these electrodes there exists a diffusion layer thickness independent of time and radial distance from the axis of revolution, with a well designed electrode. The diffusion layer thickness depends on the angular velocity of revolution in a manner predicted by the theory. In principle, stationary measurements can be made by controlling the potential or current, usually the potentiostatic version is used.

Only the steady state for a simple electrode reaction will be discussed here. The treatment of more complicated reaction schemes and

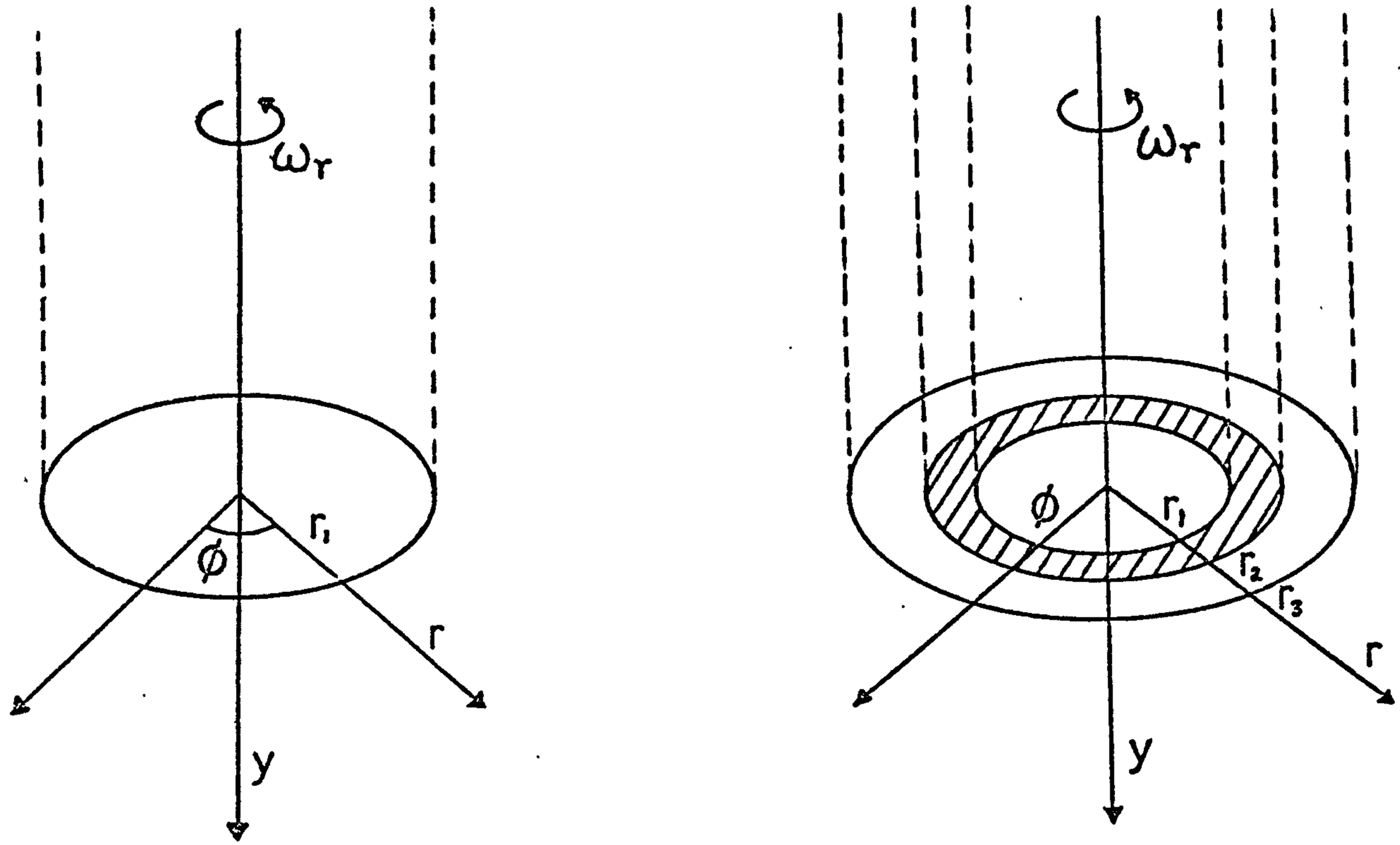

Fig 1.4 Rotating disc assembly (a) simple rotating disc showing usual co-ordinate system; (b) rotating ring-disc.

non-steady state behaviour can be found in the literature[22].

Steady state at the rotating disc

The electron transfer reaction for the case of a redox reaction,

$$R \underset{k_b}{\overset{k_f}{\rightleftharpoons}} O + ne$$

as before leads to a relation between current and potential at various rotation speeds by the following route: from equation (1.2)

$$i = nFA\left(k_f C_R^s - k_b C_o^s\right) \tag{1.49}$$

also equation (1.4) shows that the diffusion flux at $x=0$ is given by

$$i = \frac{nFAD_o\left(C_o^s - C_o^b\right)}{\delta} = \frac{\left(C_R^s - C_R^b\right)nFAD_R}{\delta} \tag{1.50}$$

In the stationary state the concentration gradient must be linear as given by equation (1.50). Elimination of the surface concentrations between equations (1.49) and (1.50) gives

$$\frac{1}{i} = \frac{1}{nFA\left(k_f C_R^b - k_b C_o^b\right)} + \frac{\delta\left(\frac{k_b}{D_o} - \frac{k_f}{D_R}\right)}{nFA\left(k_f C_R^b - k_b C_o^b\right)} \tag{1.51}$$

Substituting the value of the diffusion layer thickness calculated from the hydrodynamics[25,26]

$$\delta = 1.62 D^{1/3} \nu^{1/6} \omega_R^{-1/2} \tag{1.52}$$

then

$$\frac{1}{i} = \frac{1}{I} + \frac{K}{\omega_R^{1/2}} \tag{1.53}$$

where K is a constant dependent only on potential and I is the current corrected for diffusion. The intercept of $1/i$ versus $1/\omega^{1/2}$ gives I which, when measured as a function of potential, gives the Tafel slope.

If the electron transfer is perfectly reversible then equation (1.51) becomes, with $K_f \to \infty$, $K_b \to \infty$

$$\frac{1}{i} = \frac{\delta}{nF} \frac{\left(\frac{K_b}{K_f D_o} - \frac{K_f}{D_R}\right)}{\left(C_R^b - \frac{K_b}{K_f} C_o^b\right)} \tag{1.54}$$

K_b/K_f is independent of the kinetics, that is, of K_a and α .

From equations (1.11), (1.12)

$$\frac{K_b}{K_f} = \exp \frac{-nF(E-E^o)}{RT} \tag{1.55}$$

Exactly the same expression can be derived by substituting in equations (1.49), (1.50) the Nernst equation for the surface concentrations. In contrast to equation (1.53), equation (1.54) has the form

$$\frac{1}{i} = \frac{K'}{\omega_R^{1/2}} \tag{1.56}$$

The graph $1/i$ versus $1/\omega_R^{1/2}$ goes through the origin for all potentials. For anodic reactions $1/i$ is positive.

At high potentials both equations (1.54) and (1.56) predict a maximum current, the diffusion current given by

$$-i_d = \frac{nFAC_o^b D_o}{\delta} \tag{1.57}$$

$$= \frac{nFAC_o^b D_o \omega_R^{1/2}}{1.62 D^{1/3} \nu^{1/6}} \tag{1.58}$$

The diffusion current is invariably tested in practice according to this equation.

So far in this section we have assumed that a uniform current distribution exists at the surface. Newman[27,28] has shown by considering the effects of charge transfer resistance, and concentration polarization that this is not so. However if the condition

$$\frac{di}{d\eta} < 0{\cdot}36\, r K_\infty \qquad (1.59)$$

(where r is the disc radius and K_∞ is the specific conductivity of the solution)

is obeyed the complications of a non-uniform current distribution can be ignored.

1.5.5. The Rotating Ring-Disc Electrode

The R.R.D.E. was first developed by Frumkin and Nekrasov[29] in 1959, and used in the detection of unstable intermediates in electrode reactions. The electrode consists (Figure 1.4) of a central disc electrode surrounded by a concentric ring electrode, there being an insulating spacer between them. The potential and current at each of the two electrodes can be independently controlled. On rotation, solution-soluble species are transported from the disc to the surrounding ring electrode and in order to describe this process quantitatively, the collection efficiency N must be defined. An approximate solution to the problem was found by Ivanov and Levich[30] and a more exact analytical expression was subsequently derived by Albery and Bruckenstein[31,32].

Suppose the reaction at the disc electrode is

$$A + n_D e \longrightarrow B$$

where B is formed in solution. At the ring electrode, the potential is set at a value at which all the species B, which reaches the ring surface, is converted to X. The ring electrode reaction is

$$B \pm n_R e \longrightarrow X$$

(where, + sign for reduction, - sign for oxidation). However, some of B will escape into bulk solution and will not be reduced or oxidised at the ring electrode. Thus, the ring current (i_R) will only be a fraction of the disc current (i_D)

$$N = \frac{i_R}{i_D} \cdot \frac{n_D}{n_R} \qquad (1.60)$$

This expression has a negative sign if the disc and ring reactions are in opposite directions. A simple example of the use of the R.R.D.E. is one in which X is the same as A and so $n_D = n_R = n$. We now have

$$A + ne \longrightarrow B \qquad \text{disc}$$

$$B - ne \longrightarrow A \qquad \text{ring}$$

and $N = -i_R / i_D$

A rotating ring-disc system is characterized by the three radii

r_1 radius of disc electrode

r_2 inner radius of ring electrode

r_3 outer radius of ring electrode.

and the mass transport problem is solved by dividing the solution into three zones[30] each having their own boundary conditions.

$$0 \leqslant r \leqslant r_1$$

$$r_1 < r < r_2$$

$$r_2 \leqslant r \leqslant r_3$$

Using the relevant boundary conditions for each zone and the appropriate differential equation, Albery and Bruckenstein[31,32] have given the mathematical solution to the mass transport problem. The resulting collection efficiency can be calculated from a knowledge of the three radii and values for N have been tabulated[32] for electrodes with certain common radius ratios (r_1/r_2 and r_2/r_3). Experimental collection efficiencies, determined with various redox couples and electrodes, are in excellent agreement with the predicted theoretical values.

Recently, Bard and Prater[33] have adapted the numerical method of the digital simulation technique developed by Feldberg[34,35] to the R.R.D.E. This technique involves dividing the solution below the electrode into "boxes" and the concentration of reacting species at time intervals Δt , is estimated in each box, taking into account diffusion, convection and the electrochemical reactions. Iteration is continued until a steady-state is obtained, the concentration in each box becoming constant with time - a computer program was developed for this iteration process. The values for N obtained by this method are in good agreement with the analytical values.

The theory for the R.R.D.E. has been extended by Albery, Bruckenstein and co-workers in a long series of publications beginning in 1966. These cover such topics as transient currents, first and second order reaction of the generated species, diffusion layer titration curves

and radial transport times (with limitations on the detection of electrode intermediates undergoing homogeneous reactions).

1.5.6. Ancillary techniques

So far the techniques discussed have been concerned exclusively with electrochemical parameters and their interpretation. In the past few years there has been a trend for development of methods that investigate the structure of the electrode. Methods in this field that are relevant to this thesis will be discussed here.

Scanning Electron Microscopy

Development in the last few years of the scanning electron microscope[36,37,38] has made available a valuable instrument for association with electrochemical studies.

The principle of the instrument is as follows. A primary beam of electrons from a heated tungsten filament is focussed into a fine probe and made to scan in a raster on the surface of interest, which may be the specimen as received or, if an insulator, i.e. hydroxide or salt, subjected to an even metal shadowing prior to positioning in the microscope. The electrons liberated from the specimen by the probe are detected by a scintillator - photomultiplier system. In the so-called emissive mode low energy, secondary electrons are collected, in the reflective mode high energy primary electrons are collected. The resulting signals are used to modulate the brightness of a cathode-ray tube screen which is scanned in synchronism with the electron probe scanning the specimen. Secondary electrons are mainly used and details of deeply re-entrant holes are readily available. For similar magnifications the depth of focus is of

the order of three hundred times that of a light microscope and resolution of 200 Å is readily realisable. The working magnification range can be put at fourteen times to seventy thousand times. Other modes of operation are also available with additional instrumentation. Thus luminescence, detectable by measuring the optical emission, semi-conductor properties from absorption and conductivity and chemical identification from x-ray emission are all possible from appropriate specimens. These various operating modes are shown diagrammatically in Figure (1.5).

The most important development in the use of the scanning electron microscope has been the development of energy dispersion x-ray analysis[39,41].

The scanning beam is of very low current, about 10^{-12} A, thus the total level of x-ray excitation is low. Nevertheless the energy spectrum can be analysed and recorded and analysis is rapidly carried out in order to determine the elements lying in or near the electrode surface. Three methods are available; the first by using the stationary beam located on a point chosen from the displayed image of the surface in order to select areas of chemical interest. The second to scan the surface in order to give an overall analysis. Finally, to display the distribution of elements by recording, by beam modulation, the location of the material of interest in the scan of the surface at a chosen magnification. Elements of as low an atomic weight as fluorine, even oxygen under certain conditions,can be detected and, no complications with crystallinity arise.

FIG 1.5 OPERATING MODES FOR A SCANNING ELECTRON MICROSCOPE

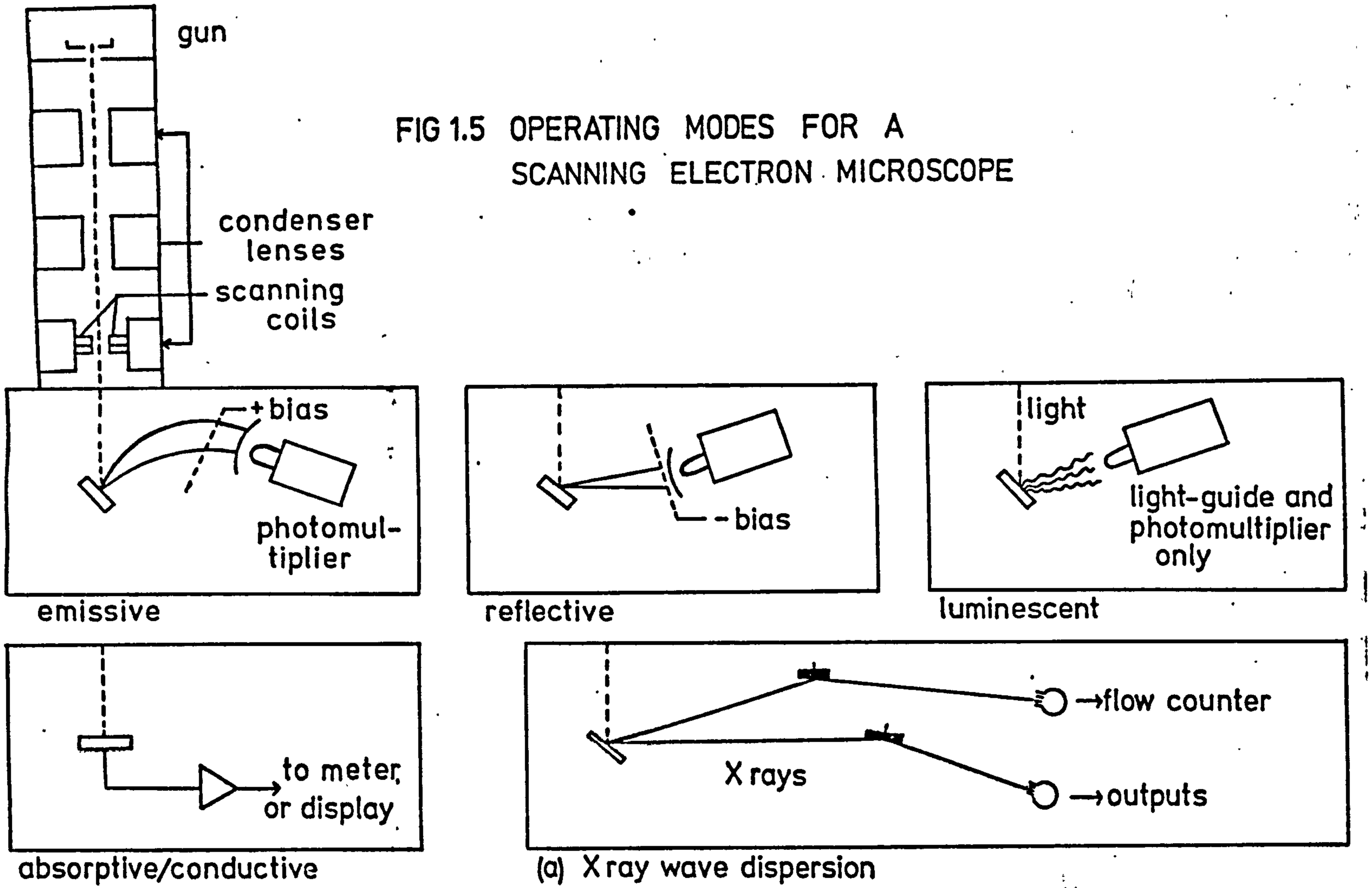

REFERENCES

1. DELAHAY, P. "Double Layer and Electrode Kinetics". Interscience, New York (1965).

2. GRAHAME, D.C. Chem. Rev. 41, 441 (1947).

3. PARSONS, R. "Modern Aspects of Electrochemistry", No. 1. (Ed., J. O'M Bockris), Butterworths, London (1952).

4. BARLOW, Jr, C.A., MACDONALD, R., and ROSS, J. In "Advances in Electrochemistry and Electrochemical Engineering", Vol. 6. (Ed., P. Delahay), Interscience, New York (1966).

5. PAYNE, R. In "Advances in Electrochemistry and Electrochemical Engineering", Vol. 7 (Ed., P. Delahay), Interscience New York (1970).

6. "Physical Chemistry" (Eds., H. Eyring, D. Henderson and W. Jost), Vols. 9A, 9B. Academic Press, London and New York (1970).

7. FRUMKIN, A.N. and DAMASKIN, B.B. In "Modern Aspects of Electrochemistry" (Ed., J. O'M. Bockris), Butterworths, London (1964).

8. FRUMKIN, A.N. Disc. Far. Soc., 1, 57 (1947).

9. PARSONS, R. Surf. Sci. 2, 418 (1964).

10. SLUYTERS, J.H. Rec. Trav. Chim. 79, 1092 (1960).

11. DE LEVIE, R. In "Advances in Electrochemistry and Electrochemical Engineering", Vol.6 (Eds., P. Delahay and C.W. Tobias), Interscience, New York (1967).

12. GILES, R.D. and HARRISON, J.A. J. Electroanal. Chem. 24, 399 (1970).

13. MARCUS, R.A. J. Chem. Phys. 43, 679 (1965).

14. RANDLES, J.E.B. Can. J. Chem. 37, 238 (1959).

15. GERISCHER, H., VIELSTICH, W. Z. physik. Chem. (N.F.) 3, 16 (1955) 4, 10 (1955).

16. BROWN, E.R., SMITH, D.E., and BOOMAN, G.L. Anal. Chem. 40, 1411 (1968).

17. BROWN, O.R. Electrochim. Acta 13, 317 (1968).

18. Operational Amplifiers Symposium, Anal. Chem. 35, 1770 (1963).

19. GOOLSBY, A.D., and SAURYER, D.T. Anal. Chem. 39, 411 (1967).

20. BRAND, M.J.D., and FLEET, B. Chem. in Britain 557 (1970).

21. FRUMKIN, A.N. In "Advances in Electrochemistry and Electrochemical Engineering", Vol. 3, p.287. Interscience, New York (1963).

22. THIRSK, H.R., HARRISON, J.A. "A guide to the Study of Electrode Kinetics". Academic Press, London (1972).

23. OLDHAM, K.B. and OSTERYOUNG, R.A. J. Electroanal. Chem. 11, 397 (1966).

24. NICHOLSON, R.S. and SHAIN, I. Anal. Chem. 36, 706 (1964).

25. LEVICH, V.G. "Physicochemical Hydrodynamics", Prentice-Hall, New York (1962).

26. RIDDIFORD, E.C. "Advances in Electrochemistry and Electrochemical Engineering", Vol. 4, Interscience, New York (1966).

27. NEWMAN, J. J. Electrochem. Soc. 113, 501 (1966).

28. NEWMAN, J. J. Electrochem. Soc. 113, 1235 (1966).

29. FRUMKIN, A.N., and NEKRASOV, L.N. Dokl. Akad. Nauk. S.S.S.R. 126, 115 (1959).

30. IVANOV, Y.B. and LEVICH, V.G. Dokl. Akad. Nauk. S.S.S.R. 126, 1029 (1959).

31. ALBERY, W.J. Trans. Far. Soc. 62, 1915 (1966).

32. ALBERY, W.J., and BRUCKENSTEIN, S. Trans. Far. Soc. 62, 1920 (1966).

33. BARD, A.J. and PRATER, K.B. J. Electrochem. Soc. 117, 207, 335 (1970).

34. FELDBERG, S.W., and AUERBACH, C. Anal. Chem. 36, 505 (1964).

35. FELDBERG, S.W. "Electronalytical Chemistry" A.J. Bard Ed., Vol.3., Marcel Dekker (1969).

36. EVERHART, T.E., and HAYLES, T.L. Scientific American, January 1972.

37. THORNTON, P.R. "Scanning Electron Microscopy", Chapman and Hall Ltd. London (1968).

38. OATLEY, C.W., NIXON, W.C. and PEASE, R.F.W. "Advances in Electronics and Electron Physics". Vol. 21. 181-247 (1965).

39. REUTER, W. Surf. Sci. 25, 80 (1971).

40. National Bureau of Standards Special Publication 298 (198).

CHAPTER 2.

THE ANODIC BEHAVIOUR OF METALS

2.1. Introduction

In this chapter it is hoped to outline the present understanding of the anodic processes which can occur at the metal electrolyte interface.

Modern technology is dependent on the use of non-noble metals and if it were not for the passive state, which provides corrosion protection, the use of such metals would not be viable. A knowledge of metal dissolution and passivating films is invaluable in the study of battery systems.

The first half of this chapter will deal with passivation phenomena and the remainder with characteristics of active and passive states.

2.2. Passivation Phenomena

2.2.1. Introduction

Passivation is a phenomenon observed when a metal is immersed in a solution and is characterised by a decrease in the anodic current density as the potential is made more noble[1].

Although passivity is a general phenomenon and applies to all metals, the discussion of the experimental findings as well as theoretical considerations is often focused on iron, for which the difference between the active and passive states is especially pronounced. If the electrode is oxidised potentiostatically, a current-potential curve of the type shown schematically in Figure (2.1) is obtained.

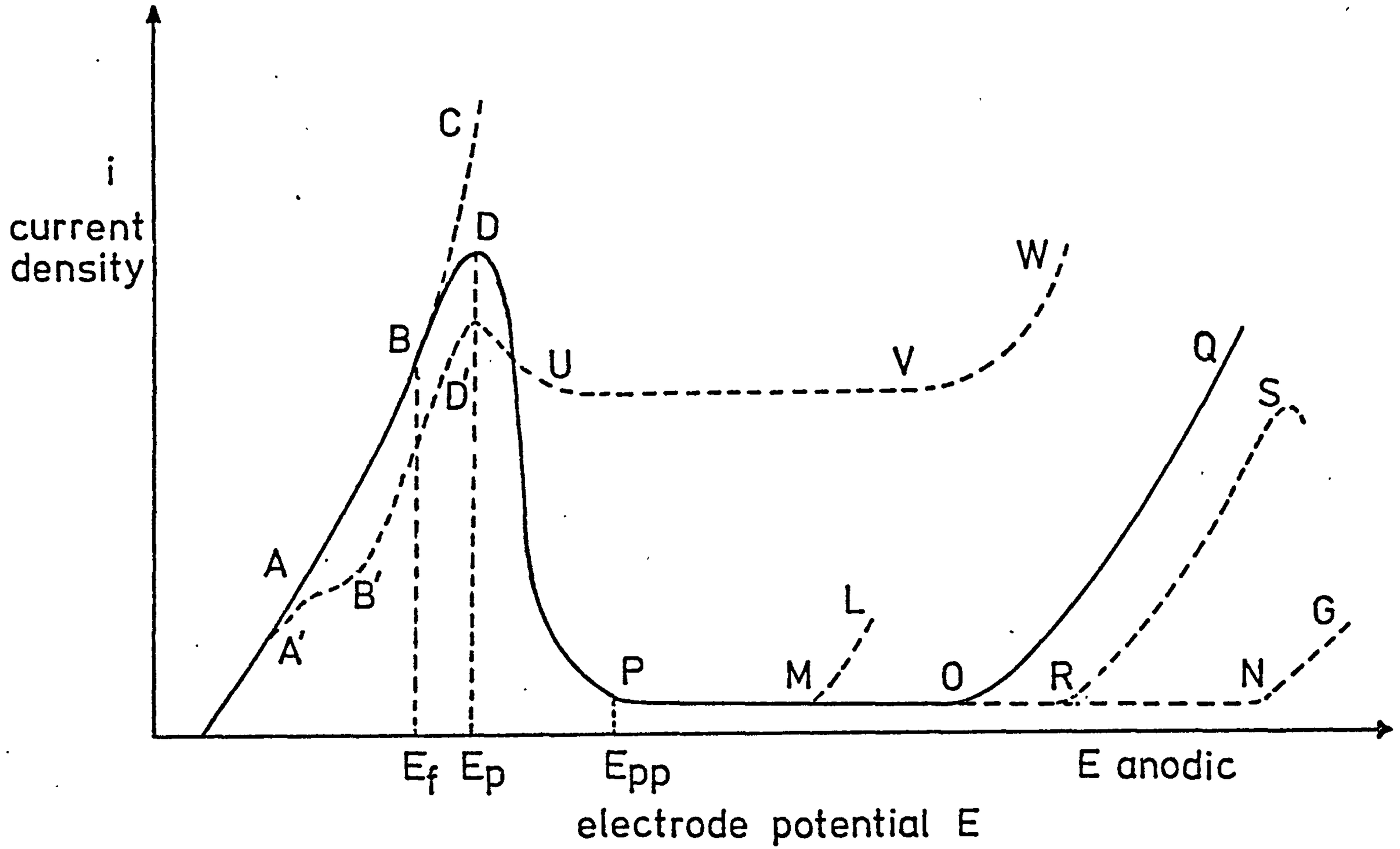

FIG 2.1 SCHEMATIC REPRESENTATION OF THE ANODIC PROCESSES ON METALS

Figure (2.1) is the schematic representation of the anodic processes on metals. Curve ABDPOQ: typical active, passive, and transpassive i-E curve for metal in water (Fe, Ni); curve ABC: free dissolution (Fe in alkali); curve ABDML: i-E curve in the presence of active anions, with possible salt formation in the active region (Fe in chloride solution); curve ABDPRS: active, passive, and transpassive behaviour of metals that may dissolve in transpassive region as high valency cations, with possible appearance of secondary passivity (Cr); curve ABDUVW or A'B'D'UVW: i-E curve for metals forming less protective film (Cu, Zn) or iron in electropolishing solutions; curve ABDPNG: i-E curve for metals with low electron conductivity, with oxide growth possible at high potentials (Al, Ti, Ta).

In the active state metal ions go into the solution

$$M \longrightarrow M^{2+} + 2e \qquad (2.1)$$

undergoing hydration or as a complex ion. At still higher potentials the polarisation curve deviates from simple logarithmic dependence (Tafel equation - see Chapter 1) because the dissolution is hindered by another anodic process, that is, the formation of a protective film[2] through a reaction of the type

$$M + H_2O \longrightarrow M\text{-}O + 2H^+ + 2e \qquad (2.2)$$

At the passivation potential E_p a limiting passivation current i_p is reached. With further increase in potential the rate of metal dissolution is decreased due to increased hinderance by the passivation process, which

evidently terminates at E_{pp}. Thereafter the dissolution rate (i.e., corrosion rate) is independent of potential. The increase in current at some higher potential is determined by the overpotential of oxygen discharge (or the presence of some oxidation-reduction system). The region is termed "transpassive".

The name "Flade potential", E_f, has a variety of connotations. Many investigators, following Flade's original definition, assign this name to the potential at which an already passivated metal begins to lose passivity[3,4,5]. Some authors, however, prefer to assign this term to the passivation potential E_p[6] at which the current is maximal or even to E_{pp}, the potential of "complete passivity"[7]. According to Tomashov and Charnova[1], E_f is the thermodynamic potential at which the formation of a metal oxide becomes possible.

The transition from active to passive behaviour which occurs in Figure 1.1 between B and P can only be described if it consists of at least two individual systems coupled together. This transition is discussed in more detail by Hoar[8] and Brusic[9].

The reaction by which a free electrode surface diminishes, that is, film formation, may not occur below a certain potential E_f, the standard electrochemical potential for the reaction. Thus points AB below E_f belong to another, separate reaction, such as free dissolution. Also the current at the potential $E > E_f$ may be only partly due to the film-forming reaction and partly due to metal dissolution, hydrogen evolution, and similar reactions; thus points above E_f will be a result of the competition between reactions that diminish a, the area of bare electrode surface, and reactions that either do not change a or enlarge it.

2.2.2. Passivation Processes

The investigation of the nature of the oxidised state introduced two schools of thought; those supporting the adsorption theory and those supporting the oxide-film theory of passivity.

Passivation Theories

Adsorption Theory

The adsorption theory has been developed by Uhlig et al[3,10-15], Frumkin et al[16], Kabanov et al[17-19], and Kolotyrkin[20]. According to Kolotyrkin[20] passivity is described as a specific case of the widespread phenomenon of the change in the kinetics of an electrode reaction due to the activated adsorption of the oxygen of water. The basic anodic processes described in this theory, even in the passive potential region, are direct dissolution of the metal as one and the competitive adsorption of anions as another.

In Uhlig's earlier theory, one of the factors determining passivation (and chemisorption) is the ratio of the work function to the enthalpy of sublimation, ΔH_s. If this ratio is less than unity, conditions are favourable to passivation because the electron would escape more readily than the atom, favouring the chemisorption of substances like oxygen. A passive film is composed, then, from chemisorbed atomic and molecular oxygen (supplemented perhaps by OH and H_2O). The formation of chemical bonds satisfies the surface affinities of the metal without metal atoms leaving their lattice site. Later this model was discussed by Uhlig[15] in the light of the results reported by Germer and MacRae[21-23]. These studies (L.E.E.D) show that when oxygen atoms (ions) are chemisorbed, a specific number of metal atoms enter the approximate plane of adsorbed

oxygen atoms to form a very stable structure of negative oxygen ions and positive metal ions.

It is argued that on typical transition metals (Ni, W, Cr, Ti, Ta) the formation of such a layer (i.e., $M{\cdot}O{\cdot}O_2$) proceeds with more favourable free energy of formation than the oxide formation, as they have unfilled d electron energy levels leading to the formation of strong chemical bonds between oxygen and the metal. These are the metals that typically exhibit passivity. For non-transition metals with filled d levels, e.g. Cu, Zn, the heats of oxygen adsorption are expected to be lower, and the formation of oxides is more favourable. Such metals do not exhibit thin-film passivity.

The impedance work of Armstrong and Henderson[24], on chromium in sulphuric acid, led them to suggest that the primary cause of passivation was formation of a layer of oxygen species adsorbed onto the surface of the electrode. Similar behaviour was shown by nickel[25], titanium[26] and iron[27].

The adsorption theory however, falls down on some points.

1. If Kolotyrkins[20] theory applies one would expect a logarithmic increase in the current at potentials below E_p, a very sharp peak, a logarithmic decrease until E_{pp} is reached, and the presence of the adsorbed film in dimensions smaller than monomolecular ones even at high passive potentials. This is in disagreement with experimental evidence.

2. A chemisorbed film of $M{\cdot}O{\cdot}O_2$ composition in the electrolyte is not very likely since: most metals Cr[28,29], Ti[28,29], Fe[31], Ni[30] can be passivated in a deoxygenated solution, i.e. with water oxygen, as long as some water is present in the solution. In such solutions, the formation of molecular oxygen at low cathodic potentials is impossible,

and without its presence estimates of film thickness[31] at E_{pp} would exceed reasonable limits for the adsorbed monolayer of oxygen ions.

3. If the adsorbed layer has a structure that contains both metal and oxygen ions, assuming 0.5 mC/cm^2 corresponds to the monolayer of O^{2-} ions if each metal ion adsorbs one oxygen ion, the resulting passivating film is several layers thick - that is, a thin oxide is more likely than an adsorbed multilayer of O^{2-}.

4. Factors that favour adsorption may also favour the formation of oxides.

The Oxide-Film Theory

The oxide-film theory describes the state of improved corrosion resistance through the formation of a protective film on the metal substrate; this consists of the reaction products of the metal with its environment. Such a film is a definite new phase, even if it is as thin as a single monolayer[32] or thick enough to be stripped away from the surface and examined separately[33]. Electron diffraction[31,32,34,35] and ellipsometric[36-42] studies give the experimental evidence for the theory.

Controversy exists on the potential at which the film forms, its thickness, the mechanism of formation and most important, the cause of passivity. The essential concept of the passivation process is however, connected with the change of the properties (chemical or physical of the primary film at a certain potential).

Sato and Okamota[43,44] have studied the i-E curve for nickel in acid solution and have calculated the passivation potential as a potential for NiO/Ni_3O_4 transition. This was in fair agreement with the experimentally observed value. Because anodic dissolutions at active

potentials proceed at a high rate, Sato and Okamoto have suggested that the primary film forms by a dissolution-precipitation mechanism, (see later) although no direct experimental evidence was offered. Bockris, Reddy, and Rao[36] have studied the passivation of nickel in acid solution by a combination of electrochemical methods and in situ ellipsometry. In their view the primary oxide is relatively thick ($\sim$60 Å), is formed by the precipitation, is poorly conducting, and is transformed into well-conducting, nonstoichiometric NiO. This transformation is thought to be the essential step in the passivation process.

This theory, however, is not generally accepted. As pointed out by Hoar[45], some of the best passivating films, as those on aluminium or tantalum, are poor electron conductors, whereas many poorly passivating films, such as CuO or PbO_2, are excellent electron conductors. Also more recent work[46] on the passivation of a nickel electrode using a R.D.E. method suggests a solid state mechanism (see later) rather than a dissolution-precipitation mechanism. The ellipsometric data of Bockris et al may be in error due to continuous electrode roughening in the active potential region[39].

De Gromoboy and Shreir[47] found that their observed "passivation potentials" (determined from anodic charging curves) corresponded closely with the potentials calculated for $Ni \rightarrow NiO$, $Ni \rightarrow Ni_3O_4$, $Ni \rightarrow Ni_2O_3$ and $Ni \rightarrow NiO_2$. Similarly Arnold and Vetter[48] suggest the direct formation of NiO at the electrode. From the anodic charging curves these authors have concluded that the film reaches a monomolecular dimension at the potential of complete passivity.

This and many other similar hypotheses can be said to form the monolayer oxide theories. Here the onset of passivity is due to the

formation of a single phase, an oxide, which is very thin in this potential region (at E_p , $\theta < 1$) and grows to a monolayer at E_{pp} [19,45, 48,49,50-55]. Its formation is a potential-dependent reaction involving the direct oxidation of the metal by the discharge of water, which, once thermodynamically possible, is suggested to be kinetically easier in its crucial primary stage than is metal dissolution. However, metal or oxide dissolution can still be simultaneous electrode processes[47,50-53]. The decrease in the anodic current is described as a result of a decrease in film-free area caused by film formation and its influence on the kinetics of the anodic reaction.

It is appropriate here to describe the dissolution-precipitation process (D.P.) and solid state processes (S.S.) of passivation.

(a) The D.P. mechanism, in which the metal dissolves until a critical concentration C^* is reached in the vicinity of the electrode where a precipitate is formed which blocks the metal surface, preventing further dissolution (C^* represents a supersaturated solution). This model for passivation implies that two-dimensional films will not be formed since the nuclei formed in solution must be three-dimensional. Among the early theories to explain passivity, Müller[56] was one of the first to suggest that the initial stages of anodic film formation involved this process. The D.P. mechanism is thought to operate in calomel formation on mercury[54, 57], the passivation of zinc and cadmium in alkaline solution as well as the formation of pre-passive films on nickel[36,58,59]. In light of conclusions drawn on the work on nickel, cadmium and mercury must be viewed with caution[60,61].

(b) The S.S. mechanism, in which anions (these may derive from the solvent e.g. O^{2-}) react directly with the metal to form a passivating film,

without metal cations entering the solution. Thus, it must be assumed that for a D.P. model, the film is formed from nuclei which are precipitated outside the double layer otherwise, the two mechanisms are indistinguishable.

The S.S. mechanism occurs in parallel with a metal dissolution reaction. When a certain anodic potential E^* is exceeded a film begins to form on the metal surface through the direct action of an anion on the metal. This potential E^* will generally be more positive than the thermodynamically reversible potential for the formation of the phase, because of nucleation or crystallisation overpotential. At short times this film is non-uniform, consisting of discrete nuclei which may be two- or three-dimensional in nature. At longer times these nuclei coalesce to form a continuous film varying in thickness from one monolayer to several thousand monolayers. The $i-t$ and $\eta-t$ transients which result from the different geometries of solid state reactions in the absence of metal dissolution are summarised elsewhere[62,63].

The most suitable type of experiment to distinguish D.P. from S.A. mechanisms is the rotating disc method using potentiostatic control[64-66]. For irreversible metal dissolution, the steady state i-E curve will be independent of rotation speed for a S.S. mechanism, whilst for a D.P. mechanism one can predict a considerable dependence on the rotation speed (since an increase in rotation speed will decrease the surface concentration of metal cations). The current at which precipitation is initiated is

$$i = \frac{nFD^{2/3}C^*\omega_D^{1/2}}{1.61\,\nu^{1/6}} \qquad (2.3)$$

and the potential at which this occurs is given by the Tafel equation.

However, when metal dissolution is reversible, the i-E curve will be rotation speed dependent for both mechanisms[67]. The distinction between D.P. and S.S. mechanisms in this case is given by the shift in the potential of the active-passive transition which is observed for the former mechanism, but not the latter. Armstrong and Harrison[66] have considered the case of a D.P. reaction occurring at a rotating disc electrode, using the Nernst diffusion layer approximation. In the first instance, equations describing the situation have been solved for a critical nucleus of two molecules by both an approximate analytical and a numerical method. The two solutions give results in good agreement, and a generalisation of the treatment to consider nuclei made up of n molecules has been suggested. The data obtained from this work predicts that precipitation will occur only at the electrode surface and that the current or potential at which passivation occurs will be a sensitive function of the diffusion layer thickness - and thus the rotation speed of the electrode.

Rotating ring-disc experiments can readily indicate the presence of solution-soluble species which are formed at the disc electrode, provided the concentration of these species is not too low. However, the method will not reveal whether these species are a precursor of a precipitate or whether they are formed in a parallel dissolution reaction. This consideration was not made in recent investigations of the passivation of Cadmium[68] and silver[69] electrodes in alkaline solution using the ring-disc technique.

The a.c. impedance technique has been used[70] in a study of the passivation of thallium amalgam in chloride solutions and has indicated successive monolayer formation, with inhibition of dissolution only after a three-dimensional phase has formed; this occurs only after at least two successive monolayers have been completed. Since the D.P. model for

passivity can lead only to three-dimensional film formation, such observations offer strong support for a S.S. mechanism.

As pointed out by a number of authors[2,45,71,72] on the initial passivations the oxide-film and adsorption theories do not contradict but supplement one another. In looking at the primary act of passivation as the formation of a tightly held monolayer containing oxide or hydroxide anions and metal cations, Hoar[45] concurs with supporters of both theories. In the formation of such a film, adsorption may, however, play an important role[73]. Adsorption is the first stage of the process; in an oxygen atmosphere molecular oxygen is adsorbed, dissociated, and chemisorbed, whereas in an aqueous solution, water molecules or OH^- will be adsorbed and chemisorbed. The second stage is the intrusion of metal ions from the lattice into the adsorbed layer, which in the third stage may grow in the third dimension. With time and potential (at $E > E_{pp}$) oxide growth is a function of the film's ionic and electronic conductivity. The thickness of the film will then be further responsible for the retardation of the anodic processes, both growth of the oxide and anodic dissolution, since the ions have to pass through the protective film. Thus, one may speak of a combined oxide-film-adsorption theory of passivity[2].

2.3. Characteristics of Active and Passive States

2.3.1. Introduction

As far as the electrode material is concerned, both anodic dissolution in its simplest formulation

$$M \longrightarrow M^{n+} + ne \qquad (2.4)$$

and anodic film formation by a reaction of the type

$$M + \frac{n}{2} H_2O \longrightarrow MO_{n/2} + n H^+ + n e \qquad (2.5)$$

are dissolution processes.

A more realistic formulation for ordinary aqueous corrosion conditions is

$$M + X H_2O \longrightarrow M^{n+} X H_2O + ne \qquad (2.6)$$

This latter case (equation 2.6) requires less energy than that required for the removal of the metal from the lattice as a bare cation M^{n+}; this is due to the large negative free energy of hydration.

Similarly water molecules in the double layer at a metal surface under anodic conditions - that is, at potentials more positive than the potential of zero charge (p.z.c.), tend to orientate with their oxygen toward the metal, presenting the possibility of the following reactions:

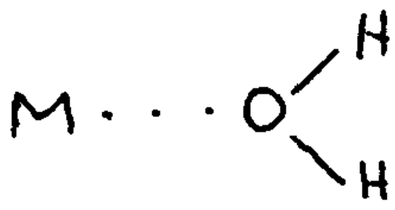

$$\longrightarrow M\text{-}OH + H^+ + e \qquad (2.7)$$

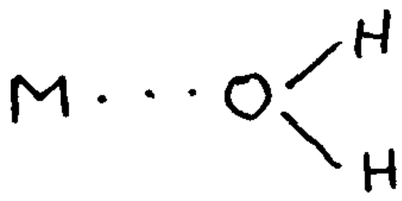

$$\longrightarrow M\text{-}O + 2H^+ + 2e \qquad (2.8)$$

Again the formation of a surface monolayer of "solid" hydroxide or oxide requires a much smaller energy because of the large negative free energy for cation association with surrounding oxide ions.

Which of the two processes prevails - the formation of the solvated ions (equation 2.6), i.e. dissolution with an appreciable rate,

or the formation of the solid film (equations 2.7, 2.8) which may or may not slow down the dissolution - depends on the potential, the composition of the solvent, the specimen geometry and microstructure and, to a great extent, on the properties of the solid film. The last, if it forms, separates the reacting substances, and further reaction is possible only if some of the reacting species can diffuse through the layer. Thus, the reaction depends on its thermodynamic stability, crystal structure, thickness, conductivity, phase-boundary reactions, and diffusion and transport processes to and from the boundary. All strongly influence the kinetics of thermodynamically possible reactions.

2.3.2. Metal Dissolution

(a) Active Dissolution

Active dissolution occurs with the majority of metals, when they are cautiously made the anode in a solution in which they can form readily soluble products. This applies even for noble metals, such as palladium or silver in orthophosphoric acid[74].

The following experimental observations have been made:

1. The lattice cations immediately concerned are those from sites of high reactivity, such as kink sites, as indicated by the non-random dissolution of the metal surface to produce crystallographic facets.

The importance of the effect of the crystallographic features of the metal lattice on electrochemical phase change, or electrocrystallisation in general, has long been recognised. Models following from vapour deposition studies have indicated that the surface features shown in Figure 2.2 are likely to be present on a metal surface - these are (1) kinks, (2) step lines,

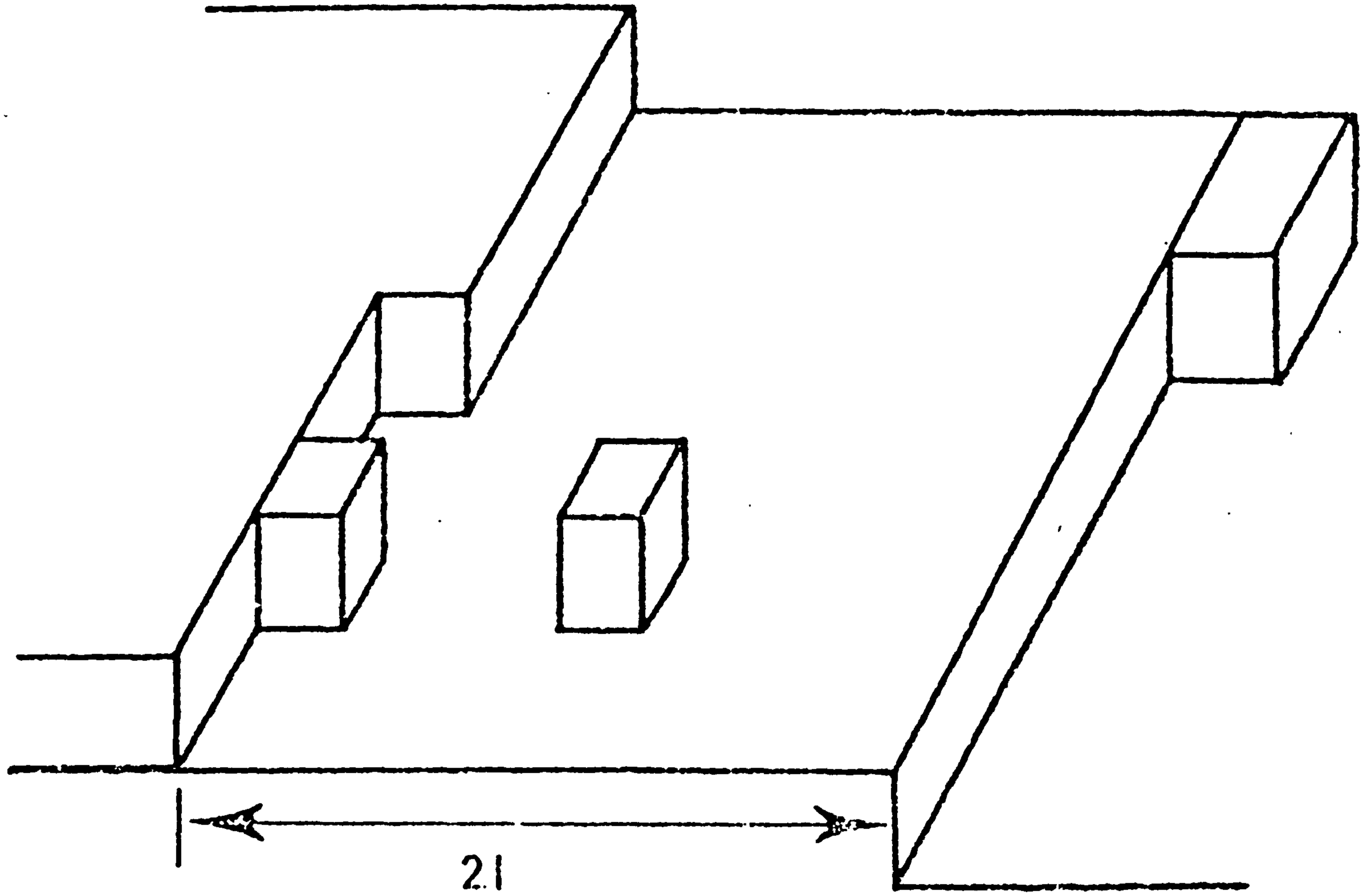

FIG. 2.2 Features present on a real metal surface.

and (3) adsorbed molecules. The step lines which are one atom high could be part of a screw dislocation, a front formed by the interaction of two screw dislocations or the edge of a two-dimensional nucleus formed on an originally flat, low index crystal plane. The active sites of dissolution may be self-perpetuating, as in screw dislocations, or may be nucleated on the surface and diffuse to the active sites by a two-dimensional mechanism, resulting in layer-by-layer dissolution. Thus, an overall picture of the dissolution process is one in which the lattice dissolves preferentially at the step lines. This occurs either by two-dimensional surface diffusion to adatom positions on the surface or by direct dissolution at the step lines. A detailed analysis of the adatom model has been given by Harrison and Thirsk[63].

2. Dissolution rates on low index planes are normally slower than those on high index planes[75], although in the potential region where the film-formation process becomes possible the opposite may be true[76].

3. The process may involve the intermediate formation of lower valence cations, as in the dissolution of copper[77], anodic dissolution of beryllium in anhydrous ~~anhydrous~~ media[78], or the dissolution of indium[79,80] and bismuth[79].

4. The dissolution may involve the heterogeneous disproportionation reaction of the low-valency intermediate, as shown for the anodisation of indium, concentrated indium amalgams and bismuth amalgam in very concentrated solution[79].

5. The intervention of anions occurs in the process,as shown for the dissolution of iron[52,53,81-83], nickel[28,30], and other metals.

These are complicated factors determining, to a greater or lesser extent, the kinetics and mechanism of anodic dissolution. The net rate at which ions are removed from the crystal is given by the Tafel equation.

Using the exchange current density, i_o, as the indicator, Piontelli[84] has made a useful empirical classification of metals, later modified by Vermilyea[85] which is given in Table 1. According to this, iron, cobalt, nickel, and the transition metals in general exhibit a very sluggish dissolution reaction. Hoar[73] has recently argued that this may be a function of the incomplete d-band in nickel and other transition metals, which may hinder the separation of metal cations and electrons in the lattice, i.e. metal dissolution. Therefore, an easy passivation of those metals may occur not as a result of altered adsorption properties as argued by the adsorption passivation theory, but as a result of a slow dissolution, thus making it easier for the metal → metal-oxide potential to be reached[73].

(b) Breakdown of the film: Activation

Partial or complete breakdown of passivity, with the onset of a high dissolution rate is brought about by any process that leads to (a) partial or complete removal of the passivating film or (b) its structural change, as observed during the electrolytic breakdown of passive films on aluminium, titanium, and tantalum[86].

In aqueous solution film removal may be effected through electrochemical reduction or oxidation, chemical dissolution, mechanical disruption, and especially by the presence of active anions (chlorides). These may either encourage the activation of the "weak" sites in the film (mechanical flaws, inclusions etc.) or introduce new ones. When using

the galvanostatic technique depassivation is usually occurring when the potential suddenly falls to a value slightly more noble than that required for passivation, i.e. the activation or Flade potential.

Work on iron-chromium alloys[76] has shown, using transmission electron microscopy, that activation initiates at discrete points on the electrode surface, these points becoming clear etch figures. The influence of active anions on film breakdown, and therefore on increased metal dissolution, is still a subject of much discussion[45]. This phenomenon has been studied on stainless steel[87], aluminium[88], zirconium[89], magnesium[90], and nickel, cobalt, titanium, tantalum, as well as iron[45,91-94].

2.3.3. Thermodynamics of the Active-Passive Transition

The factors that determine whether an anode in aqueous solution is active, passive, or brightening are (a) the metal-solution potential difference[45,7,95], and (b) the anion/water ratio[45].

(a) The Metal-Solution Potential Difference

The metal-solution potential difference, combined with the influence of pH, determines whether the formation of hydrated cations (equation 2.1) or oxide formation (equation 2.2) is the thermodynamically prevailing possibility. Pourbaix[95] has collected together, such thermodynamic data, in graphical form giving the domains of thermodynamic stability for a variety of compounds in potential-pH diagrams. In order that oxide formation may proceed, the anode potential must be at least as high as that for oxide or hydroxide formation from the metal and water in the particular solution.

If the oxide forms as a monolayer, the problem arises of the validity of applying data obtained on bulk oxides. Some experimental evidence does indicate that for many metal-oxide systems the free energy of formation of the first monolayer is indeed close to that observed for the bulk phase[96], and hence no appreciable difference in the reversible potential should be expected. On the other hand, Vermilyea[97] has shown that, if the first monolayer forms by two-dimensional nucleation, the potential of the two-dimensional film formation may be lower than that expected from the thermodynamics, the actual potential being dependent on the relative values for the interfacial energies between metal-film, film-solution, and metal-solution.

At higher pH and potentials a higher oxide phase, often more passive may be formed. At lower pH hydrated cations are stable. However, metals with low exchange-current densities for the dissolution reaction (see Table 1) can still form, at high potential, products that according to the diagram would only be present at lower potentials. Which product predominates is now dependent on the kinetics. Consequently, as already discussed, relatively easy passivation may occur for metals having a sluggish dissolution reaction. In neutral and slightly alkaline solutions passivation occurs readily for nearly all metals through the formation of stable oxides. Some metals, such as tin and especially tantalum and molybdenum, form stable oxides (i.e. passivate even at low pH values). At very high potentials metals may form oxides that can partially redissolve as hydrolysed ions, such as CrO_4^{2-} or FeO_4^{2-} and in the transpassive potential region corrosion may be expected, with possible occurrence of secondary passivity.

(b) The Anion/Water Ratio

Hoar[45] extended the Pourbaix diagram to illustrate the joint influence of the measurable anode potential and the anion/water ratio. At a low $[X^-]/[H_2O]$ ratio (where $[X^-]$, and $[H_2O]$ represent the concentrations of anions and water respectively) the electrode may behave according to the Pourbaix diagram, showing regions of active, passive (sometimes having more than one oxide with passivating properties), and transpassive behaviour. At higher $[X^-]/[H_2O]$ ratios the electrode brightens, this becoming more likely at higher potentials.

2.3.4. Properties of Passivating Films

1. Thickness

Film thickness increases with both time and electrode potential, and depends inversely on the corrosion current and the electron conductivity of the film. There is some experimental evidence that the thickness varies from monomolecular dimensions in the active potential region up to dimensions of several hundred angstroms, but mostly up to dimensions of less than 100 Å in the passive potential region[31,34,39].

2. Composition and Structure

Several methods, such as anodic or cathodic charging curves, microchemical analysis, ellipsometry, electron (and x-ray) diffraction, Mössbauer spectroscopy and scanning electron microscopy have been used to determine the composition and structure of passivating films. Since such films are rarely elementary quite some controversy exists as to the exact nature of the films. Iron is a good example; roughly speaking there are two schools of thought.

Nagayama and Cohen[31,34], Foley et al[98], and Heusler[99] suggest that the passivating film is essentially Fe_2O_3 with some Fe_3O_4 immediately next to the iron surface, i.e.

$$Fe \mid Fe_3O_4 \mid Fe_2O_3$$

This structure is thermodynamically the most stable system[6,8,100].

However, Brusic[9] using combined electrochemical and ellipsometric methods (in situ) could not detect the presence of Fe_3O_4 and suggested that $Fe(OH)_2$ is the initial passivating film.

Oxides formed at low potential, on aluminium, tantalum and titanium are non-crystalline whereas those formed at higher potentials are crystalline[86,101].

Fleischmann and Thirsk[32] have determined the composition of very thin films, practically monomolecular, such as $Cd(OH)_2$ on cadmium amalgam and ZnO on zinc. However, the determination of the composition of the initial film on metals, formed in the active potential region, as well as many other parameters of its characterisation, requires much more data.

3. Conductivity

(a) Electronic Conductivity

Passive layers on iron, nickel, chromium and other metals are reported[4,6,45,102] to have a good electron (or hole) conductivity. Measurement of the resistance of the passive film on iron formed in nitric acid indicates $R_{film} < 0.1$ ohm. cm^{-2}, i.e. if the thickness is about 100 Å, the conductivity σ is about 10^{-5} ohm^{-1} cm^{-1}[103]. This value is

in agreement with the value measured on epitaxially grown single crystals of $\gamma-Fe_2O_3$ [104], where, at room temperature, the conductivity was determined as being between 3×10^{-8} and 5×10^{-3} ohm^{-1} cm^{-1}, depending on the addition of foreign atoms or departure from stoichiometry. The latter plays a particularly important role in thin anodic films. Oxide films on aluminium and tantalum do not show the ability to evolve oxygen i.e. they are poor electron conductors, but they are able to sustain fairly large electric fields and grow to considerable thickness through ionic movement. An intermediate behaviour is shown by the oxides of tin and titanium, on which oxygen evolution and film thickening can both occur.

(b) Ionic Conductivity and Film Growth

Ionic conductivity occurs predominantly through the movement of defects in the lattice[102] and depends on the concentration gradient and on the electric field strength. The potential gradient (i.e. the field E) is assumed to reduce the height of the energy barrier for the ions moving with the field

$$i = const.\, n.\, exp\left(-\frac{u-\alpha n e a E}{kT}\right) \qquad (2.9)$$

and to increase the barrier for the ions moving against the field

$$i = const\left(N+a\frac{\partial N}{\partial x}\right) exp\left[-\frac{u+(1-\alpha) n e a E}{kT}\right] \qquad (2.10)$$

where N is the number of mobile ions per unit volume, a is the jump distance ($\sim$ lattice constant), x is the distance through the oxide, u is the chemical activation energy, k is the Boltzmann constant, and e the electronic charge. With very strong electric fields, of the order

of 10^6 to 10^7 V/cm (typical of oxide films on most metals), the influence of the reverse current can usually be neglected[105]. Hence according to Verwey[106], Mott[107,108] and Cabrera[109,110] the overall current shows an exponential dependence on the field:

$$i = k_0 \exp\left(\xi \frac{V}{L}\right) \tag{2.11}$$

with $\xi = \frac{\alpha n a F}{RT}$, L being the film thickness.

Expression (2.11) is the fundamental equation for high-field ionic conductivity and is a key equation in the theory of anodic film growth. It is, however, modified in detail according to what is considered to be the rate-determining step in ionic movement.

According to the model of Verwey[106], the limiting factor is the rate at which ions move from one interstitial position to another. The concentration of mobile species is large and has a value corresponding to electroneutrality, that is, the value that would exist in the bulk oxide. The system is under internal (not interfacial control).

In the model of Mott and Cabrera[107-110] the crossing of the first barrier, which metal ions have to surmount to enter the oxide, is considered to be the rate-determining step; i.e. the current is under interfacial control when the film is very thin:

$$i = \text{const}\ N' \exp\left(-\frac{u_1 - \alpha n e a' E}{kT}\right) \tag{2.12}$$

where N' is the concentration of atoms on the metal surface and a' is the distance from an equilibrium site in the metal to an equilibrium site in the oxide film.

Dewald[111] and Young[112] have extended the above models to include the effects of space charge due to ions in transit; both the number of mobile species and the field are treated as a function of distance. The system is under internal-interface control; i.e. the rate-determining step is either in the bulk or at the metal surface, depending on conditions, giving rather complicated significance to the Tafel Slope. Young[112,113] has suggested on empirical grounds that the activation energy is a non-linear function of the electric field.

Christov and Ikonopisov[114] have modified the model of Young[112] and postulate that the activation energy, as a function of electric field potential, includes a non-linear term:

$$E_{ac} = \mu - a\mathcal{E} + b\mathcal{E}^2, \qquad (2.13)$$

which not only lowers the barrier but also shifts the equilibrium position of the barrier. Barrier parameters calculated by this model are in agreement with experimental data.

Bean, Fisher and Vermilyea[115] have postulated that the high field strength not only influences the migration of ions but is also the driving force for the production of Frenkel defects; i.e. it lowers the activation energy needed to pull an ion out of a lattice into an interstitial position.

Dignam[116] suggested that the non-linear relationship between the activation energy and the field can be accounted for by a model in which the field-independent component of the potential-energy function, for the displacement of a mobile charged species, is assumed to resemble

a Morse function.

In an investigation of the conduction properties of valve-metal-oxide systems Dignam[117] developed a theory of co-operative ion transport. Thus the "amorphous" oxide is considered to be composed of very small crystallites, and ion transfer through such a dielectric medium is thought to be influenced by the effective, rather than the external, field. The co-operative-ion-transport phenomena arise then as a result of the time-dependent polarisation properties of the amorphous oxide film. The comparison of these theories with experimental results gives a better agreement[118,119] than the earlier theories[8,111,113,115]. Furthermore, another advantage of Dignam's theories is that both anionic and cationic charge transport, in certain valve-metal oxides, are taken into account.

Equations for high-field ionic conductivity were originally derived for the oxidation of valve metals, of which tantalum is a typical example. With these metals an oxide film is nearly always present, and the growth kinetics can be studied in sufficient detail to give a valid test of the growth theories.

The experimental data for the growth of thin films on other metals, formed either by low-temperature oxidation in an oxygen atmosphere or by anodic oxidation in solution, are very sparse and even more controversial.

For the growth of the thin, passive films on iron, for example, high-field-assisted ionic migration has been suggested[39,42,120,121] as the growth-determining factor. Alternatively, field-assisted place exchange of the cations and anions in the film[122,123] or some such similar mechanism has been proposed[9].

TABLE 1.

PIONTELLI'S CLASSIFICATION FOR THE ELECTRODEPOSITION OF METALS

Normal metals ($i_o \approx 10\text{-}10^{-3}$ A/cm^2)	Intermediate ($i_o \approx 10^{-3}\text{-}10^{-8}$ A/cm^2)	Sluggish ($i_o \approx 10^{-8}\text{-}10^{-15}$ A/cm^2)
Lead	Copper	Iron
Tin	Zinc	Cobalt
Mercury	Bismuth	Nickel
Thallium	Antimony	Transition metals
Cadmium		Noble metals
Silver		

REFERENCES

1. WAGNER, C. — Corrosion Sci., 5, 751 (1965).

2. TOMASHOV, N.D. and CHERNOVA, G.P. — Passivity and Protection of Metals Against Corrosion Plenum Press, New York, 1967.

3. UHLIG, H.H. and KING P.F. — J. Electrochem. Soc., 106, 1 (1959).

4. WEIL, K.G. — Z. Elektrochem., 59, 711 (1955).

5. FRANCK, U.F. — Z. Naturforsch., 4A, 378 (1949).

6. VETTER, K.J. — Electrochemical Kinetics Theoretical and Experimental Aspects (trans. by Scripta Technica), Academic Press, New York, 1967.

7. WEST, J.M. — Electrodeposition and Corrosion Processes, Van Nostrand, New York, (1965).

8. HOAR, T.P. — "Modern Aspects of Electrochemistry" Vol. 2 J. O'M Bockris Editor, Butterworths, London (1959).

9. BRUSIC, V. — "Oxides and Oxide Films" Vol. 1. J.W. Diggle, Editor, Marcel Dekker (1972).

10. UHLIG, H.H. — Ann. N.Y. Acad. Sci., 58, 843 (1954).

11. UHLIG, H.H. — Z. Elektrochem., 62, 626 (1958).

12. FELLER, H.G. and UHLIG, H.H. — J. Electrochem. Soc., 107, 864 (1960).

13. FOROULIS, Z.A. and UHLIG, H.H. — J. Electrochem. Soc., 111, 13 (1964).

14. MANSFELD, F. and UHLIG, H.H. — J. Electrochem. Soc., 115, 900 (1968); Corrosion Sci., 9, 377 (1969).

15. UHLIG, H.H. Corrosion Sci., 7, 325 (1967).

16. FRUMKIN, A.N., BAGOTSKI, V.S., IOFA, Z.A., and KABANOV, B.V. "Kinetics of Electrode Processes" (Eng. transl.), 1967, available from Clearinghouse for Federal Scientific and Technical Information, accession No. TT 7000987.

17. KABANOV, B.N., and LEIKIS, D.I. Z. Elektrochem., 62, 660 (1958).

18. POPOVA, T.J., BAGOTSKY, V.S.,and KABANOV, B.N. Zh. Fiz. Khim., 36, 1432 (1962).

19. KABANOV, B.N. In discussion on paper by Bockris, J.O'M., Reddy,A.K.N. and Rao, B., J. Electrochem. Soc., 113, 1142 (1966).

20. KOLOTYRKIN, Ya.M. Z. Elektrochem., 62, 664 (1958).

21. GERMER, L. and MACRAE, A. J. Appl. Phys., 33, 2923 (1962).

22. MACRAE, A. Science 139, 379 (1963).

23. MACRAE, A. Surface Sci., 1, 319 (1964).

24. ARMSTRONG, R.D. HENDERSON, M. and THIRSK, H.R. J. Electroanal. Chem., 35, 119 (1972).

25. ARMSTRONG, R.D. and HENDERSON, M. J. Electroanal. Chem., 39, 222 (1972).

26. ARMSTRONG, R.D. and FIRMAN, R.E. J. Electroanal. Chem., 34, 391 (1972).

27. ARMSTRONG, R.D. and BAURHOO, I. J. Electroanal. Chem., 40, 325 (1972).

28. TOMASHOV, N.D. and VERSHININA, Z.P. Electrochim. Acta, 15, 501 (1970).

29. KOLOTYRKIN, Ya.M. and KOSSYI, G.G. — Zashch. Metal, 1, 272 (1965).

30. SCHWABE, K. and SCHMIDT, W. — Corros. Sci. 10, 143, (1970).

31. NAGAYAMA, N. and COHEN, M. — J. Electrochem. Soc., 109, 781, (1962).

32. FLEISCHMANN, M. and THIRSK, H.R. — J. Electrochem. Soc., 110, 688, (1963).

33. EVANS, U.R. — Z. Elektrochem., 62, 619, (1958).

34. NAGAYAMA, N. and COHEN, M. — J. Electrochem. Soc., 110, 670, (1963).

35. TOMASHOV, N.D. and MODESTOVA, V.N. — Tr. Inst. Fiz. Khim. Akad. Nauk S.S.S.R., No.5, 75, Moscow, 1955; Chem. Abstr., 50 11138 (1965).

36. BOCKRIS, J.O'M., REDDY, A.K.N. and RAO, B. — J. Electrochem. Soc., 113 1133 (1966).

37. KRUGER, J. — J. Electrochem. Soc., 108, 504 (1961).

38. KRUGER, J. — Corrosion, 22, 88 (1966).

39. KRUGER, J. and CALVERT, J.P. — J. Electrochem. Soc., 114, 43 (1967).

40. ORD, J.L. — J. Electrochem. Soc., 113, 213 (1966).

41. ORD, J.L. and DE SMET, D.J. — J. Electrochem. Soc., 113, 1258, (1966). J. Electrochem. Soc., 116, 762, (1969).

42. ORD, J.L. and HO, F.C. — J. Electrochem. Soc., 118, 46 (1971).

43. SATO, N. and OKAMOTO, M. — J. Electrochem. Soc., 110, 605 (1963).

44. SATO, N. and OKAMOTO, M. — J. Electrochem. Soc., 111, 197 (1964).

45. HOAR, T.P. — Corrosion Sci., 7, 341 (1967).

46. EBERSBACH, U. SCHWABE, K. and KONIG, P. — Electrochim. Acta 14, 773 (1969).

47. DE GROMOBOY, T.S. and SHREIR, L.L. — Electrochim. Acta, 11, 895, (1966).

48. ARNOLD, K. and VETTER, K.J. — Z. Elektrochem., 64, 407 (1960).

49. DAVIES, D.E. and BARKER, W. — Corrosion, 20, 47t (1964).

50. SCHWABE, K. — Electrochim. Acta, 3, 186 (1960).

51. EBERSBACH, U., SCHWABE, K. and RITTER, K. — Electrochim. Acta, 12, 927 (1967).

52. SCHWABE, K. — Proc. 3rd Intern. Congr. Metallic Corrosion, Mir, Moscow, 1968.

53. SCHWABE, K. — Corros. Week, Manifestation Cent. Fed. Corros. 41st (1968) (T. Farkas, ed.) Akad. Kiado Budapest, 1970. p.739.

54. DEVANATHAN, M.A.V. and LAKSHMANAN, S. — Electrochim. Acta, 13, 667 (1968).

55. MUELLER, W.A. — J. Electrochem. Soc., 107, 157 (1960).

56. MULLER, W.J. — Z. Elektrochem. 33, 401 (1927). Trans. Far. Soc. 27, 737 (1931). "Die Bedeckungstheorie der Passivitat der Metalle und Ihre Experimentalle Begrundung". Verlag Chemie, Berlin (1933).

57. BOCKRIS, J.O'M, DEVANATHAN, M.A.V. and REDDY, A.K.N. — Proc. Roy. Soc. A279 327 (1964)

58. REDDY, A.K.N. and RAO, B. — Canad. J. Chem. 47, 2687 (1969).

59. REDDY, A.K.N., RAO, B., and BOCKRIS, J.O'M. — J. Chem. Phys. 42, 2246 (1965).

60. ARMSTRONG, R.D. — J. Electroanal. Chem. 28, 221 (1970).

61. REDDY, A.K.N. — J. Electroanal. Chem. 28, 217 (1970).

62. ARMSTRONG, R.D. and HARRISON, J.A. — J. Electrochem. Soc. 116, 328 (1969).

63. HARRISON, J.A. and THIRSK, H.R. — Electroanal. Chem. Vol. 5, (ed. A.J.Bard), Dekker, New York (1971).

64. ARMSTRONG, R.D. HARRISON, J.A. and THIRSK, H.R. — Corr. Sci. 10, 679 (1970).

65. ARMSTRONG, R.D. — Corr. Sci. 11 693 (1971).

66. ARMSTRONG, R.D. and HARRISON, J.A. — J. Electroanal. Chem. 36, 79 (1972).

67. ARMSTRONG, R.D. and BULMAN, G.M. — J. Electroanal. Chem. 25, 121 (1970).

68. OKINAKA, Y. — J. Electrochem. Soc. 117, 289 (1970).

69. MILLER, B. — J. Electrochem. Soc. 117, 491 (1970).

70. ARMSTRONG, R.D. RACE, W.P. and THIRSK, H.R. — J. Electroanal. Chem. 23, 351 (1969).

71. NOVAKOVSKY, V.M. — Electrochim. Acta, 10, 353 (1965).

72. NOVAKOVSKY, V.M. and LIKHACHEV, M.A. — Electrochim. Acta, 12, 267 (1967).

73. HOAR, T.P. — J. Electrochem. Soc., 117, 17C (1970).

74. APPLEBY, A.J. — J. Electrochem. Soc., 117, 1373 (1970).

75. DESPIC, A.R., RAICHEFF, R. and BOCKRIS, J.O'M. — J. Chem. Phys., 49, 926 (1968).

76. PICKERING, H.W. and FRANKENTHAL, R.P. — J. Electrochem. Soc., 112, 761 (1965).

77. MATTSSON, E. and BOCKRIS, J.O'M. — Trans. Faraday Soc., 55, 1586 (1959).

78. AIDA, H., EPELBOIN, I. and GARREAU, M. — J. Electrochem. Soc., 118, 243 (1971).

79. LOSEV, V.V. — Electrochim. Acta, 15, 1095 (1970).

80. ARMSTRONG, R.D., SUTTIE, A.B. and THIRSK, H.R. — Electrochim. Acta, 13, 1 (1968).

81. BOCKRIS, J.O'M., DESPIC, A. and DRAZIC, D. — Electrochim. Acta, 4, 325 (1961).

82. HEUSLER, K.E. — Z. Elektrochem., 62, 582 (1958).

83. HOAR, T.P. and HURLEN, T. — in Proc. 8th Meeting C.I.T.C.E., Madrid (1956), Butterworths, London, 1958, p.445.

84. PIONTELLI, R. — International Committee on Electrochemical Thermodynamics and Kinetics, Vol. 11, 1950, p.136.

85. VERMILYEA, D.A. — in Advances in Electrochemistry and Electrochemical Engineering. Ed. Delahay, P., Vol. 3, Interscience, New York, 1963.

86. YAHALOM, J. and ZAHAIR, J. — Electrochim. Acta, 15, 1429 (1970).

87. WILDE, B.E. and WILLIAMS, E. — J. Electrochem. Soc., 117, 775 (1970).

88. KAESCHE, H. — Z. Phys. Chem., NF, 34, 87 (1962).

89. KOLOTYRKIN, Ya. M. and GILMAN, V.A. — Dokl. Akad. Nauk. S.S.S.R., 137, 642 (1961).

90. KOKULINA, D.V. and KABANOV, B.N. — Dokl. Akad. Nauk. S.S.S.R., 112, 692 (1957).

91. ENGEL, H.J. and STOLICA, N.D. — Z. Phys. Chem., 215, 167 (1960).

92. HOAR, T.P., MEARS, D.C. and ROTHWELL, G.P. — Corrosion Sci., 5, 279 (1965).

93. HOAR, T.P. and MEARS, D.C. — Proc. Royal Soc. (London), A294, 486 (1966).

94. BREITER, M.W. — Electrochim. Acta, 15, 1195 (1970).

95. POURBAIX, M. — Atlas of Electrochemical Equilibria in Aqueous Solutions, Pergamon Press, New York, 1966.

96. BRENNAN, D., HAYWARD, D.O. and TRAPNELL, B.M.W. — Proc. Royal Society (London), A256, 81 (1960).

97. VERMILYEA, D.A. — in Advances in Electrochemistry and Electrochemical Engineering. (P. Delahay, Ed.,), Vol. 3, Interscience, New York, 1963.

98. FOLEY, C.L., KRUGER, J. and BECHTOLDT, C.J. — J. Electrochem. Soc., 114, 994 (1967).

99. HEUSLER, K.E. — Z. Electrochem., 66, 177 (1962).

100. GOHR, H. and LANGE, E. — Naturwissenchaften, 43, 12 (1965).

101. TOMASHOV, N.D., AL'TOVSKII, R.M. and KUSHNEREV, M.Ya. — Dokl. Akad. Nauk S.S.S.R., 141, 913 (1961).

102. HAUFFE, K. — Oxidation of Metals, Plenum Press, New York, 1965.

103. VETTER, K.J. — Z. Elektrochem., 55, 274 (1951).

104. TAKEI, H. and CHIBA, S. — J. Phys. Soc. Japan, 21, 1255 (1966).

105. YOUNG, L. — Anodic Oxide Films, Academic Press, London and New York, 1961.

106. VERWEY, E.J.W. — Physica, 2, 1059 (1935).

107. MOTT, N.F. — Trans. Faraday Soc., 43, 429 (1947).

108. MOTT, N.F. — J. Chem. Phys., 44, 172 (1947).

109. CABRERA, N. and MOTT, N.F. — Rep. Progr. Phys., 12, 163 (1948-49).

110. CABRERA, N. — Phil. Mag., 40, 175 (1949).

111. DEWALD, J.F. — J. Electrochem. Soc., 102, 1 (1955).

112. YOUNG, L. — Proc. Royal Soc. (London), A258, 496 (1960).

113. YOUNG, L. — J. Electrochem. Soc., 110, 589 (1963).

114. CHRISTOV, S.G. and IKONOPISOV, S. — J. Electrochem. Soc., 116, 56 (1969).

115. BEAN, C.P., FISHER, J.C. and VERMILYEA, D.A. — Phys. Rev., 101, 551 (1956).

116. DIGNAM, M.J. — Can. J. Chem., 42, 1155 (1964).

117. DIGNAM, M.J. — J. Electrochem. Soc., 112, 722 (1965).

118. DIGNAM, M.J. — J. Electrochem. Soc., 112, 729 (1965).

119. DIGNAM, M.J. and GOAD, D. — J. Electrochem. Soc., 113, 381 (1966).

120. MOSHTEV, R.V. — Z. Elektrochem., 71, 1079 (1967).

121. MOSHTEV, R.V. — Electrochim. Acta, 15, 657 (1970).

122. SATO, N. and COHEN, M. — J. Electrochem. Soc., 111, 512 (1964).

123. SATO, N. and COHEN, M. J. Electrochem. Soc., 111, 519 (1964).

CHAPTER 3.

SOLUTION FILLED POROUS ELECTRODES

3.1. Introduction

Much theoretical work has been done on porous electrodes because of their practical importance in batteries and fuel cells. The i-E relationship of a porous electrode is different to that of a non-porous one. Although the active surface area is increased considerably the effectiveness is offset due to transport of current or reacting species into the porous body being limited. Nevertheless porous electrodes can operate at overpotentials much lower than those associated with a solid electrode supporting the same current.

In this chapter it will be assumed that the electrode surface is macroscopically flat, and physically and chemically homogeneous so that only geometric effects will be important.

3.2. Fundamental Equations for Single-Pore Models

It is possible to simplify calculation of the current and potential distribution in a pore by considering the pore to be one-dimensional with electrolyte and electrode resistance uniformly distributed throughout its entire length. The electrode is composed of such pores identical and non-interconnected.

This simple model was used by Daniel-Bek[1]. He treated the cases of linear and exponential current i-E relations, with finite resistances of both solution and metal phase. Frumkin[2] modified this

model by introducing average potentials to take into account the curvature of the equipotential surfaces within the pores. He extended Daniel-Bek's treatment to an Erdey-Gruz and Volmer[3] type equation, with transfer coefficient $\alpha = \frac{1}{2}$. Ksenzhek and Stender[4] also took into consideration the non-faradaic current necessary to charge the double layer. They derived expressions for transient and a.c. response in cases where double-layer charging is the primary process.

A single pore of uniform cross section, homogeneously filled with electrolyte can be represented by the equivalent circuit (Figure 3.1). Here the impedance Z of the electrolyte-electrode interface is, in general, a function of potential, reactant concentrations, and time. Figure 3.2 depicts an infinitesimally small section dx of this model, where E is the potential, i the current, x the direction along the pore axis, R the ohmic resistance of the electrolyte solution inside the pore (measured per unit pore length), and Z the generalized (i.e., possibly potential- and time-dependent) impedance of the electrolyte-electrode interface, taken per unit pore length. If R and Z are independent of x, which implies that mass transport can be neglected, then we can write

$$\frac{d^2E}{dx^2} - \frac{R}{Z}E = 0 \qquad (3.1)$$

$$\frac{d^2i}{dx^2} - \frac{R}{Z}i = 0 \qquad (3.2)$$

since Figure 3.2 shows that $dE = -iRdx$ and $di = -E\frac{dx}{Z}$. In the more general case, where R and Z are functions of x, we can rewrite equations (3.1) and (3.2) as

$$\frac{d^2E}{dx^2} - \frac{d\ln R}{dx}\frac{dE}{dx} - \frac{R}{Z}E = 0 \qquad (3.3)$$

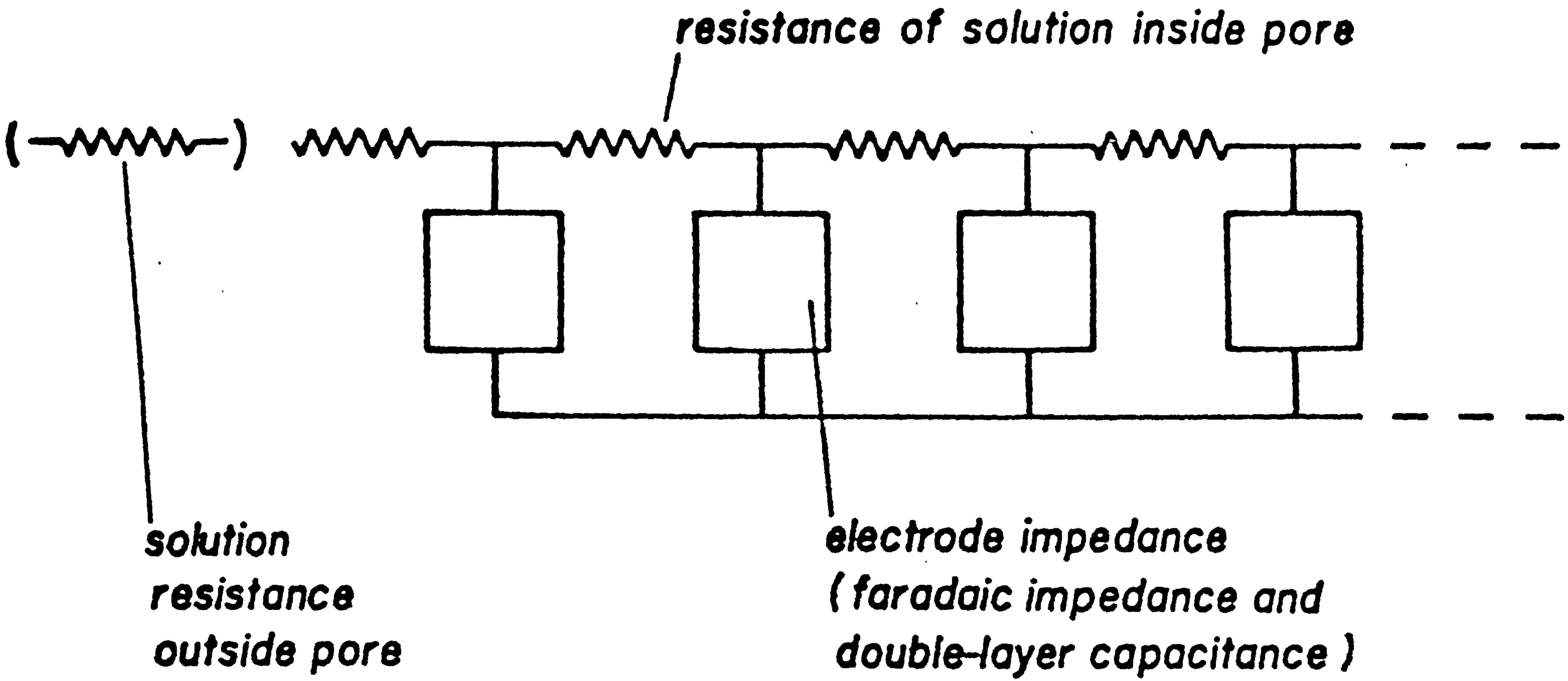

Fig. 3.1 The equivalent circuit of a pore.

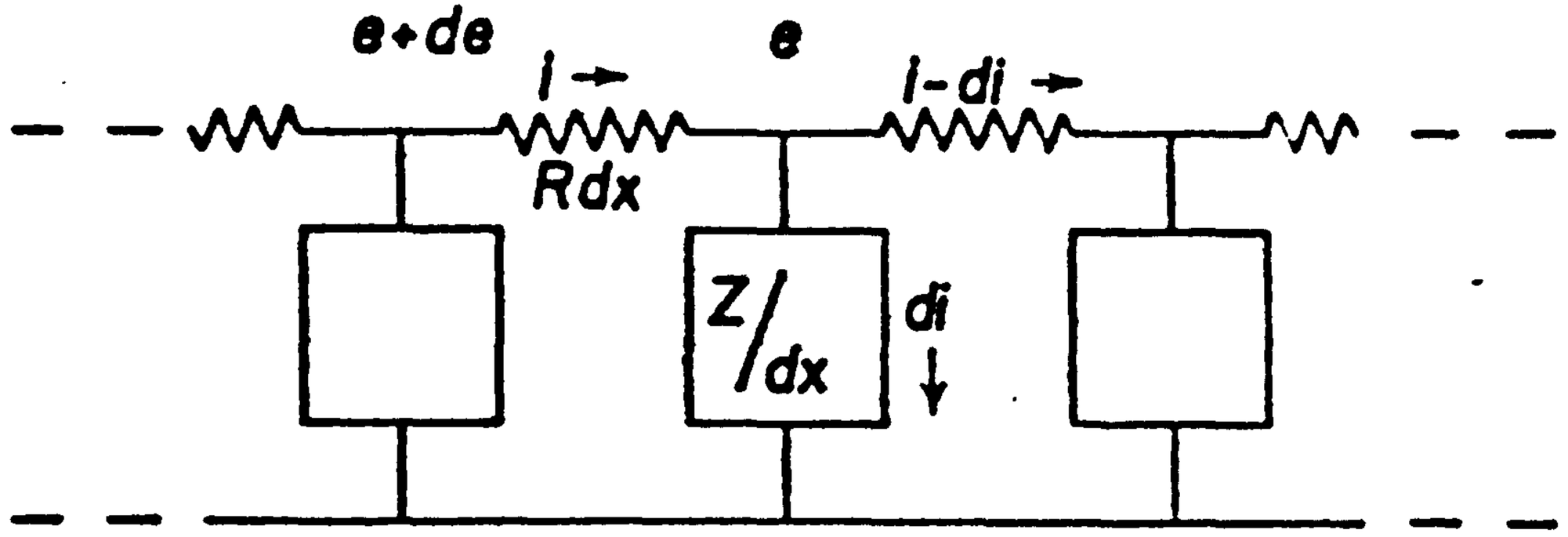

Fig. 3.2 A small section dx of the equivalent circuit of a pore. (e) Potential, (i) current, (x) distance along pore axis, (R) solution resistance per unit pore length, (Z) electrode impedance per unit pore length.

$$\frac{d^2i}{dx^2} + \frac{d\ln Z}{dx}\frac{di}{dx} - \frac{R}{Z}i = 0 \qquad (3.4)$$

The situation when Z is a function of x corresponds to the case where the concentrations of reactants and products vary with the depth into the pore and, unless there is a large excess of supporting electrolyte, R will change correspondingly.

Equations (3.1) to (3.4) assume that the resistance of the electrode material is small compared with R. If the resistances are similar, then the equivalent circuit will change. De Levie[5] has given equations corresponding to equations (3.1) to (3.4) for this case.

3.3. Charge Transfer Control

(a) Linearized i-E characteristics

In this case potentials are measured with respect to the equilibrium potential of the system and $Z = R_{ct}$ which is independent of potential and time. For a pore of length l, assuming the effect of the bottom end of the pore is negligible and for a constant potential E_o at the open end we can write

$$x = 0 \qquad E = E_o \qquad (3.5)$$

$$x = l \qquad \frac{dE}{dx} = 0 \qquad (3.6)$$

$$E = E_o \frac{\cosh(\rho x - \rho l)}{\cosh \rho l} \qquad (3.7)$$

where

$$\rho = \left(\frac{R}{R_{ct}}\right)^{1/2} \qquad (3.8)$$

The total current $i_{x=0}$ entering the pore at $x=0$ follows from equation 3.1 as

$$i_{x=0} = -\frac{1}{R}\left(\frac{dE}{dx}\right)_{x=0} = \frac{\rho E_0}{R} \tanh \rho l \qquad (3.9)$$

and the pore behaves as a resistance

$$E_0/i_{x=0} = (R R_{ct})^{1/2} \operatorname{cotanh} \rho l \qquad (3.10)$$

Although this treatment is limited two important points are brought to light.

1. For a porous electrode the current is inversely proportional to $(R R_{ct})^{1/2}$, whereas the current at a flat electrode is inversely proportional to R_{ct}.

2. The contribution of the electrode surface deep inside the pore (for $\rho l \gg 1$) is negligible, $1/\rho = \left(R_{ct}/R\right)^{1/2}$ being a characteristic "penetration depth". If $\rho l \gg 1$ then the pore behaves as a semi-infinite one and equations (3.7) and (3.9) become

$$E = E_0 \exp\left[-\rho x\right] \qquad (3.11)$$

and

$$i_{x=0} = \rho E_0/R \qquad (3.12)$$

It is often possible to calculate R , thus for a cylindrical pore of radius a , filled with a solution of specific conductance K , then we can write,

$$\frac{1}{R} = \pi a^2 K \tag{3.13}$$

R_{ct} can be written in terms of the exchange current density as,

$$\frac{1}{R_{ct}} = 2\pi a n f i_o \tag{3.14}$$

where f is $\frac{F}{RT}$ (R in this case is the gas constant) and i_o is the exchange current density. Hence the penetration depth is

$$\frac{1}{\rho} = \left(\frac{aK}{2nfi_o}\right)^{1/2} \tag{3.15}$$

This penetration depth decreases with K and pore radius a and increases with increasing i_o.

A linear i-E relation may be represented in terms of a resistance network and Euler[6,7,8] has used this method in an attempt to simulate the behaviour of a porous electrode. The simple linear i-E approach is useful in that it allows an estimate of when the curvature of equipotential surfaces within the pore can justifiably be neglected. Frumkin[2], Winsel[9] and Drossbach[10] have attempted rigorous analytical solutions for the circular, cylindrical pore and a simplified treatment has been given by De Levie[5]. The overall electrical response of the one-dimensional model agrees with that of the more complicated model to within 5% if $a\rho \ll 0.5$. The penetration depth must be at least equal to the diameter of the pore for the one-dimensional model to apply.

(b) <u>More General i-E Characteristics</u>

Daniel-Bek[1] also considered the Tafel[11] type relationship

$$i = i_o \exp[\alpha n f \epsilon] \qquad \text{anodic} \tag{3.16}$$

$$-i = i_o \exp[(\alpha-1)nf\epsilon] \qquad \text{cathodic} \qquad (3.17)$$

where i is the current density, and other symbols are as before, (ϵ is measured with respect to the equilibrium potential. Equations (3.16) and (3.17) are mathematically equivalent. Consider equation (3.16) for a cylindrical pore

$$E/Z = 2\pi a i_o \exp[\alpha nf\epsilon] \qquad (3.18)$$

which inserted into equation (3.1) and using equations (3.13) and (3.15), yields

$$\frac{d^2E}{dx^2} - \frac{\rho^2}{nf} \exp[\alpha nf\epsilon] = 0 \qquad (3.19)$$

Using the boundary condition equation (3.6) gives

$$\frac{dE}{dx} = -\left(\frac{2}{\alpha}\right)^{1/2} \frac{\rho}{nf} [\exp(\alpha nf\epsilon) - \exp(\alpha nf E_\ell)]^{1/2} \qquad (3.20)$$

since

$$\frac{d}{dz}\left(\frac{dy}{dz}\right)^2 = 2\frac{dy}{dz}\frac{d^2y}{dz^2} \qquad (3.21)$$

where E_ℓ is the potential at the bottom of the pore. Thus we can write

$$i_{x=0} = -1/R \left(\frac{dE}{dx}\right)_{x=0} \qquad (3.22)$$

$$= \left(\frac{4\pi^2 a^3 K i_o}{\alpha nf}\right)^{1/2} [\exp(\alpha nf\epsilon_o) - \exp(\alpha nf E_\ell)]^{1/2} \qquad (3.23)$$

and a Tafel slope is predicted as,

$$\frac{d\ln i_{x=0}}{dE_0} = \frac{\frac{1}{2}\alpha nf}{1-\exp[\alpha nf(E_\ell - E_0)]} \tag{3.24}$$

Consequently, for semi-infinite pores, where $E_\ell = 0$, the observed Tafel slope is $\frac{1}{2}\alpha nf$ or just half that at a flat but otherwise identical electrode.

A more general i-E relation considers both anodic and cathodic components, i.e. combines equations (3.16) and (3.17) into

$$i = i_0\left[\exp(\alpha nfE) - \exp[(\alpha-1)nfE]\right] \tag{3.25}$$

from which follows

$$\frac{d^2E}{dx^2} - \frac{\rho^2}{nf}\left[\exp(\alpha nfE) - \exp[(\alpha-1)nfE]\right] = 0 \tag{3.26}$$

This equation has been solved by Frumkin[2], Ksenzhek[12], Winsel[9] and Posey[13], for $\alpha = \frac{1}{2}$ and the solution takes the form

$$\frac{d^2E}{dx^2} - \frac{2\rho^2}{nf}\sinh \tfrac{1}{2} nfE = 0 \tag{3.27}$$

from which we obtain for a finite pore,

$$\frac{dE}{dx} = -\frac{2^{3/2}\rho}{nf}\left[\cosh \tfrac{1}{2}nfE - \cosh \tfrac{1}{2}nfE_\ell\right]^{1/2} \tag{3.28}$$

for $\frac{1}{2}nfE \gg 1$ this approaches equation (3.20). Furthermore,

$$i_{x=0} = -\frac{1}{R}\left(\frac{dE}{dx}\right)_{x=0}$$

$$= \left(\frac{8\pi^2 a^3 K i_0}{nf}\right)^{1/2}\left[\cosh \tfrac{1}{2}nfE_0 - \cosh \tfrac{1}{2}nfE_\ell\right]^{1/2} \tag{3.29}$$

All the derived equations have their simplest forms for the case of the semi-infinite pore. The larger fraction of the current flows in the region $0 \leq x \leq 1/\rho$ and thus, for practical cases, electrodes with pore lengths near to $1/\rho$ are more economical[9,12,14].

3.4. Mass Transfer Control

In the foregoing it has been assumed that the concentration of reactants and products are constant throughout the pore, as may virtually be the case with either a very slow electrode reaction or forced flow of electrolyte through the porous electrode. Ksenzhek[15], Austin and Lerner, and Euler have treated the problem of longitudinal axial diffusion of either the oxidised or reduced species or both.

The simplest case is when the current is limited by diffusion of a single species, and $nf\epsilon \gg 1$ (anodic reaction) or $nf\epsilon \ll -1$ (cathodic reaction). If the solution contains an excess of an inert electrolyte any potential drop effects can be neglected. Equations analogous to (3.1) and (3.2) can be written by replacing the electrolyte resistance with $1/D'$, where D' is the effective diffusion coefficient of the species and is given by

$$D' = \pi a^2 n F D \tag{3.30}$$

F is the Faraday and D the diffusion coefficient.

Z' the ratio of interfacial concentration and current replaces Z and is written as

$$\frac{1}{Z'} = \frac{E}{C^* Z} = \left(\frac{2\pi a i_o}{C^*}\right) \exp(\alpha n f E) \tag{3.31}$$

where C^* is the bulk concentration outside the porous electrode.

The current at the mouth of the pore can be calculated[5] as,

$$i_{x=0} = -D'\left(\frac{dc}{dx}\right)_{x=0}$$

$$= \rho C_{x=0} D' \tanh \rho l \qquad (3.32)$$

The semi-infinite pore, with $\rho l \gg 1$, gives a Tafel slope of

$$\frac{d \ln i_{x=0}}{dE} = \tfrac{1}{2} \alpha n f E \qquad (3.33)$$

and thus either charge transfer or diffusion limited operation of a porous electrode give rise to similar Tafel slopes.

Since ρ is a function of $i_{x=0}$ and $C_{x=0}$ then the characteristic penetration depth will also depend on these variables. The concentration at the opening of the pore, $C_{x=0}$, will be different from the bulk concentration C^*. If we assume a diffusion layer, outside the pores, of thickness δ, then the current at the mouth of the pore is given by

$$i_{x=0} = \frac{\pi a^2 n F D}{\delta}\left(C^* - C_{x=0}\right) \qquad (3.34)$$

and equation (3.32) can be modified to give

$$i_{x=0} = \frac{\rho C^* D' \tanh \rho l}{(1 + \rho \delta \tanh \rho l)} \qquad (3.35)$$

As $E \rightarrow \infty$, $\rho \rightarrow \infty$ and $i_{x=0}$ approaches the limiting current given by equation (3.34) with $C_{x=0} = 0$. The diffusion limited current is thus the same as that for a flat electrode of identical external

surface area, since both are determined by the mass transport in the diffusion layer outside the electrode.

Austin and Lerner[16] have treated the case of a porous electrode and a reaction $X \rightleftharpoons Y + ne$. X and Y are reactants and products that have different diffusion coefficients. The solution was given as[16]

$$i_{x=0} = \frac{2\pi a i_o}{\rho}\left[\frac{C_{x=0,X}}{C_X^*}\exp\alpha nfE - \frac{C_{x=0,Y}}{C_Y^*}\exp[(\alpha-1)nfE]\right]\tanh\rho l \qquad (3.36)$$

where $C_{x=0,X}$ and $C_{x=0,Y}$ are the concentrations of the reduced and oxidised species, respectively at the orifice of the pore.

The penetration depth has a maximum at an overpotential given by

$$E = \frac{1}{nf}\ln\frac{(1-\alpha)C_X^* D_X}{\alpha C_Y^* D_Y} \qquad (3.37)$$

which is at or near the standard potential of the redox system. Equation (3.36) approaches equation (3.32) for $nfE \gg 1$ or $nfE \ll -1$.

The derivation above neglects any effects due to a finite solution resistance and Austin[18] has considered this case for K remaining constant. However the resulting equations are complicated even for the simplest of cases.

The above theories for the treatment of porous electrodes consider only a few simple cases. Real porous electrodes will show more complicated behaviour. A number of points should be mentioned.

1. Real systems will involve double layer effects and more complex reaction mechanisms.

2. The electrode material itself is not always inert but may participate in the electrode reaction, e.g. lead-acid batteries, thus causing the geometry of the pores to change as a function of time and local current

density.

3. In the latter case, the assumption that K is constant is not always applicable, since in the case of silver-cadmium batteries hydroxyl ions of the base electrolyte, KOH, are reactants.

However, the preceding theories have indicated the main features of the steady-state behaviour of solution filled porous electrodes, and the reasons for the peculiar behaviour of such electrodes can be understood.

3.5. Transient Response

(a) Double layer charging

So far in this chapter we have been concerned with the steady-state at a single pore. The attainment of this steady-state may take as long[19] as 10^4 sec. Ksenzhek and Stender[4,20] considered the time dependence of the current necessary to charge the double layer for a galvanostatic pulse. For sufficiently small charges of potential, so that the double layer capacitance C is effectively constant, they arrived at the equation for a current pulse of amplitude $i_{x=0}$ at a semi-infinitely deep pore,

$$E_o = 2 i_{x=0} R \left(\frac{t}{\pi RC}\right)^{1/2} \qquad (3.38)$$

De Levie[21] similarly calculated the response to a potentiostatic pulse

$$i_{x=0} = E_o \left(\frac{C}{\pi Rt}\right)^{1/2} \qquad (3.39)$$

The potentials E_o used in equations (3.38) and (3.39) are referred to the initial potential rather than the equilibrium potential, since this

analysis assumes there is no interference from electrode reactions. These equations show that the double-layer charging of a pore is a time-dependent process with a characteristic time constant of the order of $\chi^2 RC$. The charging process travels down the pore and reaches different depths, χ, at different times.

Posey and Morozumi[22] treated the transient response of pores of finite length in great detail. For short times after the application of the pulse, the results of Posey and Morozumi reduce to equations (3.38) and (3.39). However, as soon as the charging wave reaches the bottom end of the pore, deviations from the simple semi-infinite behaviour become apparent. The analysis in the latter case is rather complex.

Ksenzhek[23,24] have solved the case of an electrode with double-layer charging in parallel with an independent, slow, electrode reaction. The $E-t$ curves (galvanostatic method) calculated for pores of a finite depth were similar to those for pores of infinite depth and in the limiting case a very shallow pore would behave virtually as a flat electrode.

(b) Diffusion

If the rate of electrode reaction is greater than or near to the rate of mass transfer, the latter must be considered. Ksenzhek[15] has shown that the double-layer charging process is a much faster process than axial diffusion and suggests that the two processes can be considered separately with the potential and current uniformly distributed throughout the pore at the onset of diffusion at $t=0$. Fick's second law for the longitudinal diffusion of a single species can be written as

$$\frac{1}{D}\frac{\partial c}{\partial t} = \frac{\partial^2 c}{\partial x^2} - \frac{c}{D'z'} \qquad (3.40)$$

where $2'$ is no longer a constant but depends on potential and any effects due to the ohmic resistance of the solution have been neglected. Ksenzhek[24] solved equation (3.40) for short times after a galvanostatic pulse is applied. The potential increases linearly with time, with a slope proportional to the applied current and inversely proportional to the concentration C. Experimental charging curves[25] for the oxidation of H_2 on porous Ni showed double-layer charging followed by a much slower drift of potential due to hydrogen depletion in the pores according to equation (3.40). The observed potential-time relation was in close agreement with Ksenzhek's calculation[24].

Winsel in an extensive treatment of the transient response of lead-acid storage battery electrodes with limited electroactive material proposed that the active material near the mouth of the pore would react first and the process shift inwards until the whole electrode material was used up. The analysis was presented for operation under both galvanostatic and potentiostatic.

3.6. Impedance Measurements

The impedance technique is an alternative to the pulse method for studying time dependent processes.

The mathematics for the impedance of a porous electrode is simplified if small amplitudes of the applied voltage are used, allowing the rate equation to be linearised.

For an alternating voltage of frequency ω and amplitude E_0 at the mouth of the pore, the pore exhibits an impedance,

$$Z_0 = \frac{E_0}{i_{x=0}} = (RZ)^{1/2} \operatorname{cotanh} pl \qquad (3.41)$$

where Z is the interfacial impedance.

For the semi-infinite pore simplification $\rho l \gg 1$, so that $\text{Cotanh}\,\rho l \approx 1$. In this case the phase angle of the pore impedance Z_o is half that of the interfacial impedance Z. This interfacial impedance is the impedance one would measure if the electrode was flat rather than porous. The absolute magnitude of Z_o is proportional to the square root[26] of Z. Thus the impedance of a semi-infinite pore can be correlated with that of the corresponding flat plate, the absolute magnitude is squared and the phase angle doubled. The phase angle of the pore impedance is a function of the pore depth and, if an electrode contains deep and shallow pores, the former will usually contribute most to the total electrode impedance.

Ksenzhek[4,20] has analysed impedance measurements on porous electrodes and shows when double-layer charging is the only process the impedance of a pore is given by,

$$Z_o = (1-j)\left(\frac{R}{2\omega C}\right)^{1/2} \text{cotanh}\,(1+j)l\left(\frac{\omega RC}{2}\right)^{1/2} \qquad (3.42)$$

When the pore bahves as semi-infinite the cotanh term can be dropped and the pore behaves like a Warburg impedance[27], with a 45^o phase shift between potential and current. The characteristic ρ is given by

$$\rho = (1+j)\left(\frac{\omega RC}{2}\right)^{1/2} \qquad (3.43)$$

and increases with ω. Even a shallow pore will tend to behave as if semi-infinitely deep at sufficiently high values of ω.

For the case of double-layer charging in parallel with a slow electrode reaction, the a.c. admittance of the electrode is given by,

$$\frac{1}{Z} = \frac{1}{R_{ct}} + j\omega C \tag{3.44}$$

and the impedance,

$$Z = \frac{R\left(1 - j\omega R_{ct} C\right)}{1 + \left(\omega R_{ct} C\right)^2} \tag{3.45}$$

The charge transfer resistance is given by,

$$\frac{1}{R_{ct}} = 2\Pi a f i_o n\left[\alpha \exp(\alpha n f E) - (\alpha - 1)\exp[(\alpha - 1) n f E]\right] \tag{3.46}$$

Equation (3.45) traces out a semicircle in the complex impedance plane and the impedance of a semi-infinite pore traces out a lemniscate as ω varies.

Winsel[9] treated the case of diffusion control by assuming that the radial diffusion in a pore could be described in terms of semi-infinite linear diffusion equations. The impedance can then be described by a Warburg impedance. This is proportional to $\omega^{-1/2}$ and shows a phase angle of -45°. A semi-infinite pore should exhibit an impedance, Z_o, proportional to $\omega^{-1/4}$ and with a phase angle of -22.5°. De Levie[26] has presented experimental verification of these predictions and also discusses the limits of application of the semi-infinite diffusion model for the radial diffusion inside the pore. The Warburg impedance could be used for pores with radii $\geqslant 30\mu m$ but significant deviations would arise at low frequencies for pores with a $< 10\mu m$.

Equation (3.41) requires that Z is independent of x and for diffusion controlled processes this would not be true. Z would vary with x (and possibly with t) since it would contain the concentrations of

the electroactive species. The error introduced by this simplification is small since the variations due to axial diffusion are on a different scale with respect to both x and t and, to a first approximation the concentration can be considered uniform over the limited depth penetrated by the a.c. signal.

The faradaic impedance is only important at applied d.c. potentials close to the equilibrium potential of the reaction and Z_o approaches pure double-layer behaviour (phase angle of 45^o) for large overpotentials.

3.7. Continuum Models

The mathematical treatment so far has considered that the electrodes are made up of combinations of single pores with no crosslinkages. The total current of the electrodes was taken as the sum of the contributions for each individual pore. This approach is useful in that it allows prediction of electrode performance as a function of pore size distribution and the error introduced by disregarding cross-links is small[26]. The method falls down if the electrode has a distribution of pore sizes, and in real cases this is so since electrodes are generally made by sintering a metal powder. The resulting matrix being not easily described by simple pore diameters. These problems may be overcome if the electrode is described by two continua, one the electrode matrix and the other the solution filling all the unoccupied space within the matrix. This approach was introduced by Newman and Tobias[28] and modified by Grens and Tobias[19] and Micka[29]. The flux of the particles is given by

$$J = -\left(f/F\right) c D \, \mathrm{grad}\, \tilde{\mu} \qquad (3.47)$$

where grad$\tilde{\mu}$, the electrochemical potential gradient is the true driving force. The electrochemical potential can be split in the usual way into a chemical and electrical part thus

$$\text{grad}\tilde{\mu} = \left(\frac{F}{f}\right)\text{grad}\ln c + zF\,\text{grad}\phi \qquad (3.48)$$

where z is the charge on the particle and gradϕ is the total electric field. The equation becomes

$$J = -D\,\text{grad}c - zfcD\,\text{grad}\phi + cv \qquad (3.49)$$

The cv term is added to allow the solution to move, with velocity v, with respect to the chosen reference point. The conservation of matter within the solution requires that

$$\frac{\partial c}{\partial t} = -\text{div}J - \frac{1}{nF}\,\text{div}\,I. \qquad (3.50)$$

The div$J$ term represents the mass transport in the solution and $\frac{1}{nF}$ div$I$, the generation or removal of a given substance by an electrode reaction. Since charge must also be conserved, we have

$$\text{div}\,I_1 + \text{div}\,I_2 = 0 \qquad (3.51)$$

provided that any double-layer effects are neglected. Furthermore, we have within the phases.

$$i_1 = \sum zFJ$$
$$i_2 = -K_2\,\text{grad}\,\phi_2 \qquad (3.52)$$

where K_2 is the conductivity of the electrode matrix.

If we now specify a current-potential-concentration relation at the interface between the two phases, we have equations describing the complete electrode in perfectly general terms. The equations are difficult to apply but Tobias[19,28] has discussed the solutions using certain simplifications.

REFERENCES

1. DANIEL'-BEK, V.S. — Zh. Fiz. Khim., 22, 697 (1948).
2. FRUMKIN, A.N. — Zh. Fiz. Khim., 23, 1477 (1949).
3. ERDEY-GRUZ, T. and VOLMER, M. — Z. Physik, Chem., 150, 203 (1930).
4. KSENZHEK, O.S. and STENDER, V.V. — Dokl. Akad. Nauk S.S.S.R., 106, 487 (1956).
5. DE LEVIE, R. — "Advances in Electrochem. and Electrochem. Eng." Vol. 6 Interscience, New York, (1967).
6. EULER, J. — Naturwiss., 45, 537 (1958).
7. EULER, J. and NONNENMACHER, W. — Electrochim. Acta, 2, 268 (1960)
8. EULER, J. — Electrochim. Acta, 7, 205 (1962).
9. WINSEL, A. — Z. Elektrochem., 66, 287 (1962).
10. DROSSBACH, P. — Z. Elektrochem., 56, 599 (1952).
11. TAFEL, J. — Z. Physik. Chem., 50, 641 (1905).
12. KSENZHEK, O.S. — Zh. Fiz. Khim., 36, 633 (1962).
13. POSEY, F.A. — J. Electrochem. Soc., 111, 10 (1964).
14. DANIEL'-BEK, V.S. — Elektrochim., 1, 1319 (1965).
15. KSENZHEK, O.S. — Zh. Fiz. Khim. 36, 243 (1962).
16. AUSTIN, L.G. and LERNER, H. — Electrochim. Acta, 9, 1469 (1964).
17. EULER, J. — Electrochim. Acta, 8, 409 (1963).
18. AUSTIN, L.G. — Trans. Faraday Soc., 60, 1319 (1964).
19. GRENS, E.A. and TOBIAS, C.W. — Z. Elektrochem., 68, 236 (1964).

20. KSENZHEK, O.S. and STENDER, V.V. — Zh. Fiz. Khim., 31, 117 (1957).

21. DE LEVIE, R. — Electrochim. Acta, 8, 751 (1963).

22. POSEY, F.A. and MOROZUMI, T. — J. Electrochem. Soc., 113, 176 (1966).

23. KSENZHEK, O.S. — Zh. Fiz. Khim., 37, 2007 (1963).

24. KSENZHEK, O.S. — Zh. Fiz. Khim., 38, 1846 (1964).

25. KSENZHEK, O.S. and KALINOVSKII, E.A. — Zh. Prikl. Khim. 37, 541 (1964).

26. DE LEVIE, R. — Electrochim. Acta, 9, 1231 (1964).

27. WARBURG, E. — Ann. Phys., 67, 493 (1899).

28. NEWMAN, J.S. and TOBIAS, C.W. — J. Electrochem. Soc., 109, 1183 (1962).

29. MICKA, K. — Coll. Czech. Chem. Commun., 29, 1998 (1964).

CHAPTER 4.

BATTERIES AND FUEL CELLS

4.1. Introduction

There are many uses for electricity which call for a portable power source, and, to meet these requirements a wide range of primary and secondary batteries have been developed.

The best known batteries are probably,

(i) The 'dry' cells used in lighting appliances.

(ii) The lead-acid storage batteries used primarily for the starting, lighting and ignition (s.l.i.) of internal combustion engined vehicles, particularly motor cars.

During recent years, however, there has been a considerable increase in the use of "cordless power appliances" which use different kinds of primary and secondary batteries. These range from tiny medical devices e.g. heart pacers to many consumer products e.g. transistor radios, electric shavers, etc. The use of batteries for electric traction is an expanding field e.g. submarines, motor cars, and is becoming more important as the worlds oil supplies run out. Storage batteries are also used as stationary sources of power for switch operation, and emergency lighting.

Fuel cells are a more recent form of power source. They have not yet been used commercially, due to their high cost, but they have found application as the inboard electrical power source on the Apollo space vehicles.

4.2. Definitions and Basic Principles

A battery is an assembly of voltaic cells which, as with fuel cells convert the energy evolved during certain chemical reactions into low-voltage direct current. Voltaic cells contain three major components: a positive electrode or cathode, a negative electrode or anode, and an electrolyte. All three are involved in the electrochemical reactions that take place during discharge, and, in secondary cells, during recharge. In general, the term 'primary' is reserved for cells which can be discharged only once, and the chemical compounds cannot be regenerated by recharging. In 'secondary' cells, however, the whole of the capacity which has been drawn from the cell on discharge may be replaced by passing a direct current through the cell in the reverse direction. This cycle of discharge-recharge can, in the commonest examples of lead-acid and nickel-cadmium alkaline batteries, be repeated several hundred times.

Most of the cathodes are metallic oxides, though some chlorides also function as cathodes. Anodes are metals, such as lead, zinc, cadmium or iron. The electrochemical reactions of discharge and charge are combined oxidation-reduction processes - oxidation reactions occurring at the anode, reduction reactions at the cathode.

The cathode reactions can be summarised by the following equations in acid electrolyte

$$M_x^c O_y + H^+ + 2e \rightleftharpoons M_x^c O_{y-1} + OH^- \qquad (4.1)$$

in alkaline electrolyte

$$M_x^c O_y + H_2O + 2e \rightleftharpoons M_x^c O_{y-1} + 2OH^- \qquad (4.2)$$

where M^c denotes cathode metal. The metals of these oxides exhibit more

than one valency and pass readily from a higher to a lower valency state. Silver and copper oxides may be reduced to the metal during the discharge process. To ensure that the electrolyte/metal oxide interface is maintained at a steady potential during discharge the metal oxide has to be a good electronic conductor. Brenet[1] has shown that oxides with good semiconductive properties have many lattice defects and hence vacant electron sites. Once a potential gradient has been set up in the active materials, electrons will flow freely through it. For most of these oxides, however, the electronic conductivity is of a different order from that of the metals themselves. The specific resistivity of metals ranges from $1.6 \times 10^{-6} \Omega$cm for silver to about $22 \times 10^{-6} \Omega$cm for lead. For lead dioxide (a component of the cathodes in lead-acid cells), the figure is about 400 times that of metallic lead. In general, the products of discharge reactions have a low electrical conductivity. Hence, in practical cells, the active material of both the cathode and anode is generally incorporated in a metallic mesh or grid, the members of which are distributed throughout the mass, so as to keep the internal resistance of the electrodes to a minimum.

The anode reaction for a metal M^a can be summarised by the following reaction,
in an alkaline electrolyte

$$M^a + 2OH^- \rightleftharpoons M^a(OH)_2 + 2e \qquad (4.3)$$

To perform its function efficiently, the electrolyte must have a high ionic conductivity. Two factors are involved,

(i) the concentration of ions must be high,

(ii) the ions should have a high mobility.

In practical cells, the physical migration of bulky ions to and away from the electrical double layer on the surface of the electrodes raises problems of mass transport; a factor also directly related to the viscosity of the electrolyte. Ohm's law applies inside the cell, as well as in the external circuit. The voltage loss is controlled by keeping the thickness of the electrolyte layer between the electrodes to a minimum, and compatible with the stoichiometry of the chemical reactions concerned. Solutions in water, particularly those of strong mineral acids and caustic alkalis, fulfil many of the above mentioned requirements, and, since they can be used at ambient temperatures, they form by far the most common group of electrolytes.

Common aqueous electrolytes (H_2SO_4, KOH) have a maximum conductivity at concentrations between 5 and 8 normal. Water has a high relative permittivity indicating a high degree of ionic conductivity; it ionises by the equilibrium reaction,

$$H_2O \rightleftharpoons H^+ + OH^-$$

Since the hydrogen ion H^+ is a prime reductant and the hydroxyl ion OH^- is an active oxidant, water presents an ideal solvent for an electrochemical redox reaction. Molten salts also possess some of these required characteristics and are used in some voltaic systems. Recently some non-aqueous electrolytes have been suggested for use with metals such as lithium, but their electrical resistance limits their applicability. Some solid electrolytes have been suggested[2,3], of these β-alumina and silver rubidium iodide look the most promising.

4.3. Electrode Potentials

On consulting any table of standard electrode potentials one can

see that the alkali metals lithium and potassium appear at the top of the negative end of the series with potentials around - 3.0 V, the noble metals platinum (+ 1.2 V) and gold (+ 1.4 V) and the halogen gases chlorine (+ 1.36 V) and fluorine (+ 2.85 V) are at the positive end. The overall voltage of a voltaic cell is given by the difference between the potentials of the two electrodes. It is obviously an advantage to use a couple with potentials as widely spaced as possible in the electrochemical series; hence the efforts to use lithium and fluorine, for which the theoretical cell voltage would be around 6 V.

4.4. Kinetic aspects of electrode reactions

The standard reversible potentials of electrodes only apply under conditions of equilibrium. When an externally imposed current flows (discharge, or charge) in the system, the balance is disturbed. The reactions then become irreversible, energy changes take place and the electrode potentials change from their equilibrium values by an amount referred to as the overvoltage. Since the function of galvanic cells is to supply energy (measured in watt-hours) or power (measured in watts) to do useful work, the current/voltage relationships are of prime importance. Various factors impede the free course of the electrode reactions and the rate at which they take place. These factors are referred to collectively as polarisation, and, may be divided into three broad categories.

(a) Activation overvoltage: energy required to start the electron-transfer reaction.

(b) Concentration overvoltage: arising from problems of mass transport due to changes in concentration of the reacting species in the electrodes and the electrolyte. This factor is countered by diffusion.

(c) Resistance overvoltage: this is caused by changes in concentration of the electrolyte and also by the formation on the surface of the electrodes of solid reaction products with a higher electrical resistance than that of the substrate of active material.

(b) and (c) are of particular importance in lead-acid and alkaline storage batteries, since the products of the discharge in both these systems are insoluble in the electrolyte and have a high electrical resistance. To overcome these problems, the active materials of both cathodes and anodes are made in a highly porous state, and in alkaline cells, special substances are added to improve their electrical conductivity. The high degree of reversibility of these systems is due to the insolubility of the reaction products.

4.5. Non Electrochemical Criteria

So far only electrochemical properties have been discussed for power sources. Other desirable properties for a 'good' power source are low weight and small size. Hence we need,

(i) High energy density

$$= \int \frac{V \cdot I \cdot dt}{\text{total mass}} \quad \left(W.hr.kg^{-1} \right)$$

This is governed by

(a) High voltage that is independent of I and t

(b) lightweight components, electrodes of low equivalent weight.

(ii) High volumetric energy density

$$= \int \frac{V \cdot I \cdot dt}{\text{total volume}} \quad \left(W.hr.\,dm^{-3} \right)$$

Obviously the case, separator, terminal contacts etc. have to be included in (i) and (ii). Shelf-life i.e. the time that a battery can be stored

on open circuit without significant self discharge, and for secondary batteries, cycle life are important criteria in battery performance. In fuel cells the operating life is often limited due to the catalyst being poisoned by impurities in the gases.

4.6. Primary Cells and Batteries[4,5,6]

The Leclanché type cell is the most widely used primary cell; technical improvements in this primary power source have been enormous over the last twenty years. The development of the transistor, with the resultant miniaturisation of equipment and reduction in power requirement, has given considerable impetus to the production of primary batteries. Most of the recent developments in the primary cell field have been in the direction of miniaturisation of batteries, and in the production of batteries to operate the many appliances which can now be made in portable form. Many types of primary cell have appeared in commercial form, but only a few of these have gained any major commercial significance. Others have found application in specialised fields.

Table I summarises primary batteries and lists some of their properties. Table II lists a few of the more well known cell reactions.

4.6.1. Leclanché dry cells

These cells are manufactured in a variety of shapes and sizes depending on their application.

In the cylindrical type the +ve electrode is a carbon rod and the -ve electrode a high purity zinc can. The active material (high grade manganese dioxide) is mixed with small amounts of acetylene black, to improve its conductivity, and ammonium chloride. This mixture is then

moulded around the +ve electrode. The method of construction and grade of materials is of overriding importance; manufacturers use different techniques, some add extra electrolyte in the form of a gel, others use absorbent paper. Certain materials, such as zinc chloride, mercuric chloride and sometimes chrome inhibitor, are added to the electrolyte to reduce chemical attack on the zinc can, particularly during periods of open circuit at high ambient temperatures. Leak resistant cells have been developed, these are generally made by enclosing the whole cell in a heat-shrunk plastic sleeve.

The electrochemical parameters of the cell are poor,

(i) high internal resistance,

(ii) poor shelf-life.

However, the cell is still of use in low current drain applications. Its major attribute is its low cost.

4.6.2. Alkaline-Manganese Cells

This is a variant of the Leclanché dry cell. The negative electrode is made of finely divided zinc, amalgamated with small amounts of mercury and pressed into the desired shape. The electrolyte is a solution of potassium hydroxide immobilised as a gel. The cell is encased in a thin-walled cylindrical mild-steel container, fitted with gas vents and tightly sealed to prevent leakage of the electrolyte. This cell shows marked improvement in conductivity over the ammonium chloride type. It has approximately twice the capacity and can sustain higher current drains. The low temperature performance is good, and the shelf-life is reasonable. These advantages are, however, offset by its high manufacturing cost.

4.6.3. Mercury-oxide zinc cells

In these cells, mercuric oxide acts as the positive active material, finely divided zinc the oxidisable negative electrode and a solution of potassium hydroxide acts as the electrolyte, generally immobilised as a gel. The construction is similar to that of alkaline Leclanché cells. The open-circuit voltage of the normal cell is 1.34 V, but, on adding manganese dioxide to the +ve active material, this is raised to 1.40 V. The cell has very low standing losses, the open circuit voltage being maintained over long period with a variation of less than 5 mV. On discharge, the cell has a flat voltage curve; an invaluable characteristic where voltage regulation is important. The cells have high energy/volume and energy/weight ratios; the low temperature performance is good. As these cells are expensive they can only be used where the arduous duty can take advantage of their special properties. Hearing aids and cardiac pacemakers are good examples.

4.6.4. Miscellaneous Primary Cells

Copper chloride/magnesium/sea water (or potassium chloride) cells

The low density of magnesium metal has encouraged the development of these cells for special applications such as meteorological equipment. These cells are 'one-shot' or 'reserve' types and they cannot be recharged. As the standing losses are high, once the cells have been primed, the electrolyte is held in reserve and added just before use. The cathodes are prepared from pressed or molten copper chloride, the anodes from thin magnesium sheet, and absorbent paper is used as the separators. The chloride ions released from the cathode reduce polarisation of the magnesium anode by magnesium hydroxide formed during the discharge. The

batteries are primed by immersion in sea water. In fresh water, the separators are impregnated with potassium chloride solution and thoroughly dried before assembly. The voltage on discharge ranges from about 1.5 V to 1.1 V per cell, and they operate on low current drains.

Silver chloride/magnesium/sea water cells

These cells are capable of giving high outputs at high rates of discharge, and have been extensively used for the propulsion of electric torpedoes. Operational voltages are about 1.58 - 1.50 V, and these assemblies can be safely stored for long periods in the dry unprimed condition. Table I: contains the energy densities; the brackets indicate the densities in the unprimed condition.

Other 'reserve' cells for special applications include lead dioxide/magnesium cells and lead dioxide/zinc sulphuric acid cells.

4.7. Secondary Batteries[4,5]

Secondary batteries differ from primary batteries only in their ability to be recharged. In theory electrode reactions are reversible, but in most practical cases secondary reactions and, or physical changes occur when a current is taken from a cell, so that the passage of a reverse current does not restore the cell to its original condition. There are a few systems in which this does occur, and these are the basis of commercial secondary batteries.

Batteries of secondary cells are often called storage batteries or accumulators. The first storage battery was introduced by Plante in 1859. It was of the lead-acid type. The commercial application of such batteries was not developed until the last twenty years of the nineteenth

century, when recharging systems became available. In addition to the lead-acid system, other systems have been developed on a commercial scale, the most important of them being the nickel-cadmium cell, the nickel-iron cell and the silver-zinc cell. Table III summarises some secondary batteries and Table IV lists a few cell reactions.

4.7.1. Lead-acid Storage Batteries[4,5,7,13]

The lead-acid battery is the main source of portable power in the medium and relatively high output range. The contributory factors can be summarised as follows,

(a) Versatility; it can supply high or low currents over a wide range of temperatures,

(b) good storage characteristics, particularly in the dry charge condition,

(c) high degree of reversibility; it is capable of hundreds of discharge-charge cycles with great reliability,

(d) lead; the basic constituent of the grids has a low melting point. The grids can be easily cast in thin sections and grouped by low-temperature welding,

(e) the metal is cheap when compared with nickel, cadmium or silver used in other voltaic cells.

The use of lead-acid batteries is more than ten times that of its nearest rival the nickel-cadmium battery and considerable changes have been made during the past twenty-five years with s.l.i. batteries. Most obvious has been the improved cranking ability of automobile batteries, which is achieved by the use of thinner, more porous separators, thinner

and more numerous plates; more efficient active materials, and better design of the electrical system.

Manufacturing processes

The electrodes or plates for s.l.i. batteries are made by the Faure process, in which the active materials are prepared from lead oxide in the form of a stiff paste with sulphuric acid and water. The paste for - ve grids differs from the paste for + ve's in that it contains additives (barium sulphate, lignin compounds and carbon). Generally this is pressed into the grids by automatic machines. In the subsequent processes the positive active material is converted to lead dioxide and the negative to spongey lead. This can be carried out by passing a charge through the plates when they are immersed in dilute sulphuric acid - "tank formed". Alternatively the plates, seasoned and dried after pasting, may be assembled in their final containers, which are then filled with acid of about 30% concentration, and the whole battery is 'one-shot formed' by a charge.

The metallic grids not only support the active materials physically, but they also serve as current collectors and conduct the electrons either into or away from the electrochemical reactions. For various reasons, the choice of metals for the grids is strictly limited. Lead is about the only metal able to withstand the highly corrosive conditions in the cell. For many types of service, however, lead is too weak, and its strength and hardness are improved by the addition of alloying constituents, such as antimony, arsenic and tin. During the discharge-charge cycle, antimony is leached out of the positive-grid alloy, and is deposited on the negative plate. Antimony considerably

lowers the hydrogen overpotential on lead, and hydrogen gas is evolved. This reaction continues during periods of open circuit, and is the main cause of the standing losses observed in s.l.i. batteries. Attempts have been made to eliminate antimony altogether. Lead-calcium alloy has been used in maintenance free batteries but difficulties arise in the casting of the alloys and adhesion of paste to the grids. Dispersion strengthened lead and plastic materials have been used to produce grids with improved mechanical properties but neither of these proved satisfactory.

After pasting, the castings are generally surface dried and left to season for periods of up to 72 hours in a very humid atmosphere. This promotes the growth of prismatic crystals, which, in turn, cause rigid interlocking of the active material. X-ray analysis indicates that the preferred chemical compound causing this structural change is the tribasic sulphate $3PbO\ PbSO_4\ H_2O$. Antimony which causes the deleterious effects noted on the negative plate, appears to help in encouraging the growth of prismatic crystalline formations[7], which play a valuable part in ensuring a good cycling life of positive plates.

Positive and negative plates grouped in parallel arrays are separated by non-conducting separators. To reduce the internal resistance, the interval between the plates is kept to a minimum. Water produced at the positive plate during discharge dilutes the acid in the vicinity of this electrode. In order that the acid at this plate can circulate well it is customary to profile the separator with ribs on this side. The main requirements for separators are,

(a) mechanical strength suitable to withstand stresses during assembly,

(b) resistance to oxidation under the severe conditions of service,

(c) a microporous structure with an overall porosity of at least 50% to permit free diffusion of the electrolyte and to give a low electrical resistance.

Separators used are made from various rubbers, p.v.c., polythene, glass wool, terylene and wood pulp.

The battery containers were once made from bituminous pitch, but now they tend to be made from polypropylene, giving considerable weight reductions.

Performance

The open circuit voltage of a cell varies between 2.05 V and 2.15 V depending on the concentration of electrolyte and temperature. Polarisation reduces the voltage when the cell is on load, and the drop in voltage increases with increasing discharge current, this is caused by mass transfer effects increasing the solution resistance and formation of non-conducting lead sulphate decreasing the electrolyte-electrode interface. The $PbSO_4$ also tends to block the pores of the active material, reducing the area of contact between it and the electrolyte.

The capacity of the battery will depend on the amount of active material present. Not all the active material can react during the discharge, because the voltage falls below the accepted minimum long before the electrochemical reactions are complete. Cells for s.l.i. applications are designed with thin plates of large surface area so the maximum amount of active material is utilised.

Temperature has a very marked effect on the capacity of a battery. This is thought to be due to "polarisation"effects[8]. This is, however, a complex phenomenon and no satisfactory explanation has been given.

During the first stage of charge lead sulphate is reconverted to lead dioxide and lead. High currents, particularly towards the end of charge when the cell voltage increases, can lead to high temperatures, which are detrimental and should be avoided. After a certain time, the efficiency of charge acceptance begins to fall, because most of the active material is then covered with layers of lead dioxide or lead. A growing proportion of the current is now involved in electrolysis of the water in the electrolyte causing "gassing". Some overcharge is necessary, and the gassing helps to unify the concentration of electrolyte. Excessive overcharge, however, causes anodic corrosion of the positive grid and loss of water through electrolysis and evaporation if the temperature rises unduly. Vigorous gassing also tends to disrupt the surface of the active materials. Voltage regulators are therefore included in s.l.i. charging circuits.

Batteries for electric traction

Traction batteries differ from s.l.i. batteries in that they have to undergo 'deep' cycling and be capable of withstanding approximately 1,500 of these cycles. Hence, the pasted plates are thicker and more robust than their s.l.i. counterparts. The positive active material is usually held in position with a well matted glass-fibre retainer or some other suitable material. Many types of construction are used, the two most important being flat and tubular positive plate types.

4.7.2. Alkaline storage batteries[4,5]

Alkaline and lead-acid batteries share the various services which call for a portable power source with a high degree of reliability and a long cycle life. Two main systems have been developed, namely, the nickel-iron cell and the nickel-cadmium cell.

Alkaline batteries are used in a variety of applications; e.g. standby power, signalling, engine starting and as sealed or maintenance-free cells in cordless electrical appliances of different types. Their outstanding features are a good cycle life, good performance under adverse temperature conditions (e.g. below - 40°C where lead-acid batteries could not be used), almost complete freedom from maintenance (when sealed), robustness, low standing losses, and, in the case of sintered plate cells, stable voltage characteristics and high power densities at high rates of discharge. Their main disadvantage lies in the high cost, due largely to the costly raw materials nickel and cadmium. As with other battery systems, the manufacturing cost is a major component of the total cost.

Pocket plate nickel-cadmium cells

Two types have been developed, referred to as normal resistance and low-resistance types. These are aimed at producing, on the one hand, the maximum capacity at medium currents, and, on the other hand, the maximum current for relatively short periods. Cells of the low-rate type have relatively thick plates; low-resistance cells have thinner plates.

The cells are robust in construction with tightly packed elements, generally in strong steel containers, and can be used for a

variety of applications. They are particularly effective at low temperatures; the standing losses are low and the cells are not seriously affected by overdischarging or, in fact reversal. The production costs are the lowest of all types of alkaline cells.

Tubular nickel-iron cells

Batteries of this type are used for deep cycling service (e.g. electric traction) as well as for standby applications. The chief advantages lie in the robust construction and long life. The chief disadvantages are that the energy density is only moderate on both a weight and volume basis, the low-temperature performance is poor and the rate of standing loss is appreciably higher than that of nickel-cadmium cells. In addition, the charge characteristics are not so favourable, and larger amounts of overcharge are, in general, necessary. Although iron is a cheaper raw material than cadmium, the basic manufacturing costs for tubular cells are higher than for pocket-type cells.

Sintered-plate cells

In this type of assembly, the conducting grids are made of sintered nickel, generally supported on a fine woven metal screen or thin perforated metal sheet. The positive and negative active materials are uniformly dispersed throughout the sintered matrices. This gives three special advantages. First, the plates can be accurately made in extremely thin sections. Secondly, as the active materials are in close contact with the grid metal, the internal resistance does not increase as rapidly towards the end of the discharge as in other types, and,

thirdly, the plates can be very closely spaced, thereby reducing the IR drop due to the electrolyte. Sintered plate cells are generally assembled with thin separators made of woven or felted fabric in materials such as nylon or cellulose fibre.

For the above reasons, cells with thin sintered plates have excellent high-rate performance, particularly at low temperatures, and they are used wherever this service is required e.g. on aircraft, military vehicles. They can be charged at high rates and at low temperatures. The standing losses are higher than those for nickel-cadmium pocket-type cells, but the cells can be left in a discharged condition without significant deterioration. One particular disadvantage of sintered-plate cells is their cost, which is appreciably higher than that of pocket-type cells, and this naturally limits their application.

Sealed sintered-plate cells

The discovery that alkaline cells of this type could be hermetically sealed opened the way to some interesting applications. The principle depends on the provision of an excess of negative active material; during the final stage of recharge, this absorbs the oxygen as it is released from the positive plates. Since some of the negative material remains unreduced by this process, no hydrogen is evolved. At reasonably low charging rates the process can be carried on indefinitely, and, since water is being reformed as rapidly as it is electrolysed, the cell components remain in a more or less invariant state. To get the best results with this process, a minimum of electrolyte must be used, and the capacity of these cells is therefore somewhat less than the capacity of cells of equivalent size with free electrolyte. Cells have been widely

applied in circumstances where electrolyte spray must be completely avoided and where maintenance, in the form of topping up with water, must be reduced to a minimum. For this purpose, a wide range of small cells, both of the rectilinear and button type, has been developed.

4.8. Silver-oxide Cells

Two couples having silver oxide cathode depolarisers are of interest: one has zinc anodes and the other has cadmium anodes.

4.8.1. Silver oxide/Zinc cells[14]

Cells of this type have energy and power densities at least four times that of conventional storage batteries. As primary single-shot batteries, they have been widely used for torpedo propulsion. Secondary rechargeable batteries have been used for submarines, where a limited number of cycles were required. The positive active material consists of silver oxide, generally made by anodising a porous sintered-silver compact, in which is embedded a conducting mesh or screen. The negative active material comprises porous spongey zinc, generally formed from a paste made from zinc oxide and retained in an open-mesh grid. The electrolyte is potassium hydroxide of similar concentration to that used in conventional alkaline storage batteries, and cellulose film is used as the separator.

The discharge reactions at the positive electrode take place in two stages:

(a) $2AgO + H_2O + 2e \underset{\text{charge}}{\overset{\text{discharge}}{\rightleftharpoons}} Ag_2O + 2OH^-$ $\quad E^\circ = 0.57V$

(b) $Ag_2O + H_2O + 2e \rightleftharpoons 2Ag + 2OH^-$ $\quad E^\circ = 0.344V$

At the negative electrode

$$Zn + 2OH^- \rightleftharpoons Zn(OH)_2 + 2e \qquad E^\circ = -1.245\ V$$

and overall

$$2AgO + Zn + H_2O \rightleftharpoons Ag_2O + Zn(OH)_2 \quad E^\circ = 1.815\ V$$

$$Ag_2O + Zn + H_2O \rightleftharpoons 2Ag + Zn(OH)_2 \quad E^\circ = 1.589\ V.$$

The formation of the higher oxide and reaction (a) is limited as far as possible, as this leads to a 2-step discharge with a higher voltage plateau in the early stages. To overcome this difficulty, the cells are sometimes given a short initial discharge at a high rate, after which constant voltage levels are obtained.

Unfortunately, replating of the zinc, which is partially soluble in the electrolyte, does not proceed uniformly, and short circuits tend to develop after a limited number of cycles, particularly if deep discharges are given. For this reason overcharging is strictly controlled. In spite of its high output, the high cost of silver and its limited reversibility, rules out the use of this battery for most commercial applications.

4.8.2. Silver oxide/Cadmium cells

Potassium hydroxide is also used as the electrolyte in this couple, and the reactions at the negative plate are

$$Cd + 2OH^- \rightleftharpoons Cd(OH)_2 + 2e \quad E^\circ = -0.809\ V$$

The reactions at the positive plate are as given in Section 4.8.1. Because of the difference between the potentials of the zinc and cadmium electrodes, the overall open-circuit voltage of the cell is lower by about 0.4 V. The energy density, however, is still two to three times higher

than that for the conventional storage batteries. As cadmium is practically insoluble in the electrolyte, this couple is capable of many more discharge-charge cycles than the silver-zinc cells. The high cost of cadmium, however, added to that of silver, makes it even less acceptable for commercial applications. The use of cadmium makes it possible to work the cell in the sealed condition, for similar reasons to those which apply to the sealed nickel-cadmium cell. Because of its high energy density and high degree of reversibility, the couple finds uses in small button and cylindrical sealed cells, where the cost of the active materials represents a small proportion of the total production costs.

4.9. High-temperature systems

Practically all the voltaic cells and batteries in present use operate with aqueous electrolyte over the fairly narrow temperature range from - 40°C to + 60°C. Systems have been proposed, which work at considerably higher temperatures.

4.9.1. Sodium sulphur cells

In this couple sulphur takes the place of oxygen as the active material, and, to make it sufficiently reactive, the temperature must be raised to about 350°C. Because of low densities of the active materials and their high electrode potentials, this cell is capable of energy densities of 10 to 12 times greater than those of conventional storage batteries.

The active materials are separated by a thin sintered or fritted diaphragm of beta alumina, doped with small amounts of sodium oxide.

When heated to about 350°C this diaphragm becomes permeable to sodium ions, and, with suitable conductors to convey the electrons into an external circuit, reversible reactions of the following types take place between the molten active materials:

$$2Na \rightleftharpoons 2Na^+ + 2e \qquad S + 2e \rightleftharpoons S^{2-}$$

$$2Na^+ + S^{2-} \rightleftharpoons Na_2S$$

followed by reactions leading to the formation of Na_2S_3 and Na_2S_5. The melting points of these higher sulphides are lower than that of the monosulphide, and the conditions are arranged to produce these. To initiate the electrochemical reaction, the cell must first be heated to around 500°C. It is claimed that the reactions are exothermic, and, once the discharge is started, the temperature is self-sustaining. For intermittent service, insulation would have to be provided which would add to the weight and the bulk of the system. It is claimed that sealed cells have given tens of discharge-charge cycles, but as far as is known, no practical multicell battery has yet been built. Difficulties due to porosity and breakdown of the fritted diaphragm have been reported.

4.9.2. Lithium chlorine cells

Two important physical properties of metals used for anodes are the density and equivalent weight. Both affect the energy and power densities, particularly the latter. A low equivalent weight is favourable to a high energy density. Lithium has the most favourable theoretical energy density of metals used as anodes. Because of its spontaneous reaction with water, it cannot be used with aqueous electrolytes, but experiments have been carried out with a molten salt electrolyte, in

particular lithium chloride,using chlorine as the oxidant. The reversible redox potentials of the electrode reactions are

$$Li \longrightarrow Li^+ + e \qquad E^\circ = -3.05\ V$$

$$\tfrac{1}{2} Cl_2 + e \longrightarrow Cl^- \qquad E^\circ = 1.36\ V$$

with an overall reaction

$$Li^+ + Cl^- \longrightarrow LiCl \qquad E^\circ = 4.41\ V$$

The reversible potential is not reached in practice, but cell voltages well above 2 V and estimated energy densities around 150 Wh/lb have been claimed.

4.10. Cells with Organic Electrolyte

The difficulties in using the reactive alkali metals sodium and lithium with aqueous electrolytes have been mentioned. To overcome this problem, considerable experimental work has been done with organic electrolytes, the most promising being with lithium and a fluoride as positive active material.

Lithium/nickel fluoride cells

Seiger, Lyall and Shair[9] have examined the Li/propylene carbonate/nickel fluoride system. The electrical conductivity of the pure electrolyte was too low for practical purposes, and this had to be raised by the addition of a salt, the most effective of these being the complex potassium hexafluorophosphate. The redox potential of a reaction between Li^+ and F^- ions gives the very favourable value of 6.05 V. This was not achieved in practice, and owing to the high internal resistance, the power density is low.

4.11. Fuel Cells[4,5,6,10]

In recent years vast sums of money were spent, particularly in the U.S.A., in developing working models of fuel cells; this culminated in the production of hydrogen-oxygen fuel batteries for the Gemini, and later the Apollo, lunar spacecraft.

For fuel batteries to be viable for commercial applications, it is generally considered that the capital cost should not exceed £50 - 100 per kilowatt. So far no model produced is within sight of this target. In the early days of this development, the expensive noble-metal catalysts, platinum and palladium, were blamed for the high capital costs. The more economical use of these catalysts and the promise of much cheaper substances for this purpose have shifted the burden of costs to other components, e.g. processes of fabrication, ancillary equipment etc.

The use of air as the oxidant in fuel cells has an obvious advantage, since it eliminates the need to store this component and the initial cost is nil. The use of air, however, has disadvantages. To provide oxygen at the rate required by the electrodes an electrically operated fan is needed; a filter is required to remove dust, and, if an alkaline electrolyte is used, a scrubber is needed to remove CO_2. The high dilution with nitrogen generally depresses the potential of the oxygen electrode by a few per cent.

Hydrogen is a useful fuel; it has a relatively high free energy of oxidation, and, with the appropriate amount of catalyst, hydrogen electrodes can be made with a low degree of polarisation, thus ensuring a favourable cell voltage on discharge. Also, when oxidised, hydrogen produces the harmless product water, and, unlike organic fuels like

methanol, one of the oxidation products of which is CO_2, hydrogen can be used with alkaline electrolyte at ambient temperatures. This simplifies the materials of construction, as common metals can be used to build the electrodes and the cell structures. With the growing understanding of the behaviour of porous, gas-diffusable electrodes made of sintered metal, carbon or plastics and improved methods of distributing the catalysts throughout these substrates and preserving their high activity by wet proofing, considerable economies have been achieved.

One of the main objections to the use of gases like hydrogen and oxygen is that they must be stored and transported in pressurised cylinders or by cryogenic means. Both present problems of size and weight.

Many methods of producing hydrogen from some feedstock in an integrated unit built into the fuel-battery system have been tested. A battery was produced for submarine propulsion where hydrogen was produced in an ammonia cracker. Various manufacturers have described reforming units in which an organic fuel (such as methanol or low grade hydrocarbon) is made to react with steam to produce hydrogen. Exploratory work has also been carried out on methods of storing hydrogen in compounds such as lithium hydride, and F.T. Bacon has studied the problem of the economic storage of hydrogen, but so far no satisfactory method has evolved.

Fuels other than hydrogen

The advantages of a liquid fuel in a concentrated form (e.g. hydrazine hydrate containing 60% of hydrazine, which can be stored in lightweight thin-walled containers at ambient temperatures) are obvious. Hydrazine electrodes have been made with a minimum amount of catalyst and, in some cases, without any catalyst at all and with a minimum degree of

polarisation at current densities around 100 mA/cm^2 at temperatures down to 0^{o}C. Unfortunately, hydrazine is a very expensive fuel, and until some process of manufacture is developed which will provide this attractive fuel at about 10% of its present cost, hydrazine fuel batteries are unlikely to find commercial use.

Heath et al[11] have produced batteries that use gaseous hydrocarbons, and methanol directly, but only in the presence of excessive platinum catalyst. Attempts have been made to use natural gas as a fuel but no satisfactory system has been produced.

Applications

Fuel cells have been used to power industrial trucks. Certain characteristics of fuel batteries give them worthwhile advantages over storage batteries used for this purpose. The process of recharging storage batteries after discharge generally takes periods of 8 hrs. or longer, fuel batteries may be refuelled in minutes. Also, in spite of their immature development, for periods of continuous use longer than about 5 hrs., fuel batteries have a higher energy density (i.e. watt-hours per pound) than storage batteries. Because of all of the ancillary equipment (circulators, evaporators, heat exchangers, control devices etc.) the output per unit of volume of fuel batteries may not be as favourable as that of storage batteries. Fuel cells find application where long endurance, minimum of maintenance, and a reasonably high energy density are required. Hence, they are used in beacons, buoys and repeater stations for television.

4.12. Zinc-air Hybrid Fuel Cells[12]

These systems use metal anodes similar to those used in other voltaic cells and an air (or oxygen) cathode basically similar to that used in certain fuel cells. The usual electrolyte is a solution of potassium hydroxide of concentration similar to that used in alkaline storage batteries. The cells and batteries are made in two forms, in the first, after each discharge, the oxidised zinc electrodes are removed and replaced by new electrodes. These are enclosed in a porous envelope which acts as the separator and contains sufficient solid caustic potash to replenish the electrolyte removed in the discharged plates. The air electrodes will withstand several tens of discharges.

In the second type of rechargeable cell, the zinc electrode is recharged in situ with an auxiliary electrode serving as the positive. To ensure uniform replating of the zinc, the electrolyte is circulated through the cells, and any solid zinc hydroxide formed in solution during the discharge is trapped in a filter in the circulating system. Unfortunately the cycle life of these cells is, as yet, poor. The accessories (pumps, filters, reservoirs, etc.) add to the weight, volume and complexity of the system.

TABLE I.

PRIMARY BATTERIES

SYSTEM + ve	- ve	Electrolyte			O.C.V. (Nominal)	Capacity mA hr	Current mA	Operating Voltage	E.D. Whr/kg (To 0.8 V)	V.E.D. Whr/dm^3	% Capacity after 2 yr at 20°C
MnO_2(c)	Zn(Hg)	NH_4Cl	Cylindrical High-power type	'Dry'	1.5	6000	21	~1.3	80	140	75%
MnO_2(c)	Zn(Hg)	KOH	Cylindrical	'Dry'	1.5	10000	300	~1.2	80	220	>75%
HgO(c)	Zn(Hg)	KOH	Cylindrical	'Dry'	1.35	14000	150	~1.2	100	420	93%
HgO(c)	Cd	KOH		'Dry'	1.15						>95%
Ag_2O(c)	Zn(Hg)	KOH	Button	'Dry'	1.55	100	1.5	~1.5	90	340	90%
Ag_2O(c)	Cd	KOH		'Dry'	1.35						>90%
CuO	Zn(Hg)	NaOH	Plate	Wet	1.1	500A hr	1.5A	~0.65	35	50	
AgCl	Mg	NaCl	Reserve		1.7				(130)	(200)	
CuCl	Mg	NaCl	Reserve	Sealed	1.2				(50)	(50)	
PbO_2	Pb	$NClO_4$	Reserve		1.95						
PbO_2	Zn	H_2SO_4	Reserve		2.2						

TABLE II.

Cell reactions

1) Leclanché

$$2\ MnO_2 + 2\ H_2O + 2\ e = 2\ MnO(OH) + 2\ OH^-$$

$$Zn + 2\ OH^- + 2\ NH_4Cl = Zn(NH_3)_2\ Cl_2 + 2\ H_2O$$

$$2\ MnO_2 + 2\ NH_4Cl + Zn = Zn(NH_3)_2\ Cl_2 + 2\ MnO(OH)$$

---

2) Alkaline manganese

$$2\ MnO_2 + 2\ H_2O + 2\ e = 2\ MnO(OH) + 2\ OH^-$$

$$Zn + 2\ OH^- = Zn(OH)_2 + 2\ e$$

$$2\ MnO_2 + 2\ H_2O + Zn = Zn(OH)_2 + 2\ MnO(OH)$$

---

3) HgO-Zn

$$HgO + H_2O + 2\ e = Hg + 2\ OH^-$$

$$Zn + 2\ OH^- = Zn(OH)_2 + 2\ e$$

$$HgO + H_2O + Zn = Zn(OH)_2 + Hg$$

---

4) CuO-Zn

$$CuO + H_2O + 2\ e = Cu + 2\ OH^-$$

$$Zn + 4\ OH^- = Zn(OH)_4^{2-} + 2\ e$$

$$CuO + H_2O + 2OH^- + Zn = Zn(OH)_4^{2-} + Cu$$

---

5) AgCl-Mg

$$2\ AgCl + 2\ e = Ag + 2\ Cl^-$$

$$Mg = Mg^{++} + 2\ e$$

$$2\ AgCl + Mg = MgCl_2 + Ag$$

SECONDARY BATTERIES

SYSTEM + ve	SYSTEM - ve	Electrolyte			O.C.V.	E.D. Wh/kg	V.E.D. W hr/dm^3	Cycle life >70% discharge	Charge Retention 25°C % Capacity after 6 months	1 month	Shelf-life discharged
PbO_2	Pb	H_2SO_4	Pasted	Vented	2.0	20-30	40-60	200-700	0	70	None
			Planté	Vented	2.0	10	30	1000			
NiOOH	Cd	KOH	Pocket	Vented	1.3	12-23	20-35	500-2000	75		Years
				Sealed		10-23	20-60	200-2000	60		
			Sintered	Vented		19-30	30-60	300-2000	70		
				Sealed		10-27	30-60	200-2000	0	70	
NiOOH	Fe	KOH	Tubular	Vented	1.36	23-30	30-60	2000-4000	0	60	Years
NiOOH	Zn	KOH		Vented		30-55	50-110	100-200	70		Years
AgO	Zn	KOH		Vented	1.8(1.5)	40-105	60-220	10-150	75		Years
				Sealed		40-105	60-220	~80	85		
AgO	Cd	KOH		Vented	1.6(1.3)	30-65	30-150	300-500	90		Years
				Sealed		30-65	30-150	~700	85		
MnO_2	Zn	KOH		Vented	1.5	15	20-40	~50	95		

TABLE IV

Cell reactions

1) Pb-acid

$$PbO_2 + SO_4^{=} + 4\,H^{+} + 2\,e = PbSO_4 + 2\,H_2O$$

$$Pb + SO_4^{=} = PbSO_4 + 2\,e$$

$$PbO_2 + 2\,H_2SO_4 + Pb = 2\,PbSO_4 + 2\,H_2O$$

2) Ni-Cd

$$2\,NiOOH + 2\,H_2O + 2\,e = 2\,Ni(OH)_2 + 2\,OH^{-}$$

$$Cd + 2\,OH^{-} = Cd(OH)_2 + 2\,e$$

$$2\,NiOOH + Cd + 2\,H_2O = 2\,Ni(OH)_2 + Cd(OH)_2$$

3) Ni-Fe

$$2\,NiOOH + 2\,H_2O + 2\,e = 2\,Ni(OH)_2 + 2\,OH^{-}$$

$$Fe + 2\,OH^{-} = Fe(OH)_2 + 2\,e$$

$$2\,NiOOH + Fe + 2\,H_2O = 2\,Ni(OH)_2 + Fe(OH)_2$$

4) Ag-Zn

$$2\,AgO + H_2O + 2\,e = Ag_2O + 2\,OH^{-}$$

$$Ag_2O + H_2O + 2\,e = 2\,Ag + 2\,OH^{-}$$

$$2\,Zn + 4\,OH^{-} = 2\,Zn(OH_2) + 4\,e$$

$$2\,AgO + 2\,Zn + 2\,H_2O = 2\,Ag + 2\,Zn(OH)_2$$

REFERENCES

1. BRENET, J. "Les oxydes metalliques en élèctrochemie", Ind. Chim. Belge, T32, 523 (1967).

2. HEYNE, L. Electrochim. Acta, 15, 1251 (1970).

3. ARMSTRONG, R.D. BULMER, R.S. and DICKINSON, T. J. Phys. Chem. Solids. In press.

4. BARAK, M. J. Inst. Elect. Eng. Rev. 117, 1561 (1970).

5. PALIN, G.R. "Electrochemistry for Technologists", Pergamon Press (1969).

6. The Primary Battery Heise, G.W. and Cahoon, N.C., (Eds) Vol. 1. J. Wiley, New York, (1971).

7. BURBANK, J. SIMON, A.C. and WILLIHNGANZ, E. in "Advances in Electrochemistry and Electrochemical Engineering". Ed. Tobias, C.W. Vol. 8 (1971).

8. BAIKIE, P.E. GILLIBRAND, M.I. and PETERS, K. Electrochim. Acta 17, 839 (1972).

9. SEIGER, H.N., LYALL, A.E. and SHAIR, R.C. 'High energy density lithium-nickel fluoride non-aqueous batteries' in 'Power Sources 2' (1968) Ed. Collins, D.H. (Pergamon 1970) p. 267.

10. BREITER, M.W. "Electrochemical Processes in Fuel Cells". Springer-Verlag Berlin Heidelberg New York (1969).

11. HEATH, C.E., et al "Soluble carbonaceous fuel cell reports 1 - 4" U.S. Army Electronics Laboratories Contracts DA 36-039 AMC-00134(E) 1963-1965.

12. CHODOSH, S.M., JAGID, B. and KATSOULIS, E. 'Zinc-air battery systems', in 'Power Sources 2 1968' Ed. Collins D.H., Pergamon, 1970, p.423.

13. BARNES, S.C. 'Car Batteries' in 'Motor Management' March 1972.

14. Zinc-Silver oxide Batteries. Eds. Fleisher, A., Lander, J.J. Wiley, New York 1971.

CHAPTER 5.

EXPERIMENTAL

5.1. Introduction - Review on the passivation of lead

The passivation of lead has been studied extensively, mainly by workers concerned with the manufacture of lead acid accumulators. Hence, the bulk of work that appears in the literature is orientated in this direction. Much work has been carried out on battery plates, i.e. porous lead and lead dioxide electrodes. The characteristics of these systems are, however, obscured by the additions of carbon, barium sulphate, and organic compounds to the active material. Work on smooth lead and lead alloys has been primarily concerned with the $PbSO_4/PbO_2$ potential region (thick films) since this is the region in which grids break down. Relatively little research has dealt with the $Pb/PbSO_4$ potential region (thin films).

A recent review[1] on lead passivation has appeared in the literature. The main techniques used have been galvanostatic, potentiostatic and optical/electron optical methods. The earlier references are listed in reference (1).

Pavlov and co-workers studied in detail the growth and passivation processes on lead in H_2SO_4[2,3,4]. They established that the lead, upon anodic polarisation, behaved first as a lead sulphate electrode, then as a lead oxide electrode, and finally as a lead dioxide electrode. It was determined after long time of polarisation that, from -956 to -300 mV vs the mercury/mercurous sulphate electrode in $1NH_2SO_4$, the electrode deposit consisted only of $PbSO_4$. In the region from -300 to +900 mV the deposit

contained $PbSO_4$ plus substantial amounts of tetragonal lead oxide near to the electrode. Minor amounts of basic sulphates were also formed along with some orthorhombic PbO. At potentials more positive than +900 mV, the major component of the deposit was α-PbO_2. At potentials more positive than +1200 mV, β-PbO_2 also began to form. The lead dioxide region could not be exactly defined, since it changed with time of oxidation. According to Ruetschi and Angstadt[5] the basic sulphates are formed in the interior of the film where high local pH's exist. The thermodynamics of the system are well known[6]. In a series of papers Maeda[10] studied the growth mechanism of the passive film. He deduced that the lead sulphate film was an ionic conductor, the rate determining process being the outward diffusion of Pb^{2+} ions. Ruetschi[7] has predicted the potential of PbO and α-PbO_2 formation by taking into account the diffusion potential in the $PbSO_4$ film. Measurements have been made on partly discharged Pb-acid battery electrodes using a scanning X-ray microprobe[8,9], and $S(K_\alpha)$ radiation[9]. The observed distribution curves were not readily explained on the conventional theory of current distribution. At high current densities the electrode reaction takes place mainly in the outer layers of the electrode. A very small flow of acid electrolyte through the porous electrode caused intense deformation of the distribution of lead sulphate, markedly reduced the degree of polarisation, and increased the electrode capacity under high current load. The morphology of oxidised Pb electrodes was also investigated by Sterr[9]; Simon et al[11] studied the morphology of the PbO_2 electrode. Ozhiganova and Aguf[12] described a potentiodynamic study of the influence of surface active substances on the operation of the $Pb/PbSO_4$, H_2SO_4 electrode. Other references concerning organic expanders have appeared recently in the literature[13,14,15].

Tarter and Ekler[16] studied the $Pb/PbSO_4$ system using galvanostatic techniques, however their results were difficult to interpret due to the thick films produced.

Baikie[17] et al considered the effect of temperature and current density on the capacity of lead-acid battery plates and found that the effective plate capacity C at $\theta^{o}C$ was related to the current density i by the equation

$$C = \frac{K_o(1+\alpha\theta)}{i^{(n-1)}}$$

where n = 1.4 for both types of plate. Values of the constant K_o and the temperature coefficient α differ for the two electrodes. No explanation on an electrochemical foundation of this equation was given.

It can be seen from the literature that little fundamental research has concerned passivating film on lead. This provided the impetus for this project.

5.2. Instrumentation

Electrochemical measurements reported in this thesis were obtained under conditions of controlled potential at the working electrode. An electronic potentiostat and a wave form generator were used to control the potential profile applied to the working electrode. A block diagram of the circuit used is shown in Figure 5.1. For ring-disc measurements the block diagram of the circuit is shown in Figure 5.2.

5.2.1. Potentiostats

The potentiostat used for controlling the working electrode potential was a commercial instrument manufactured by Chemical Electronics Ltd., (Model TR70/2A). This is a semiconductor instrument with a built

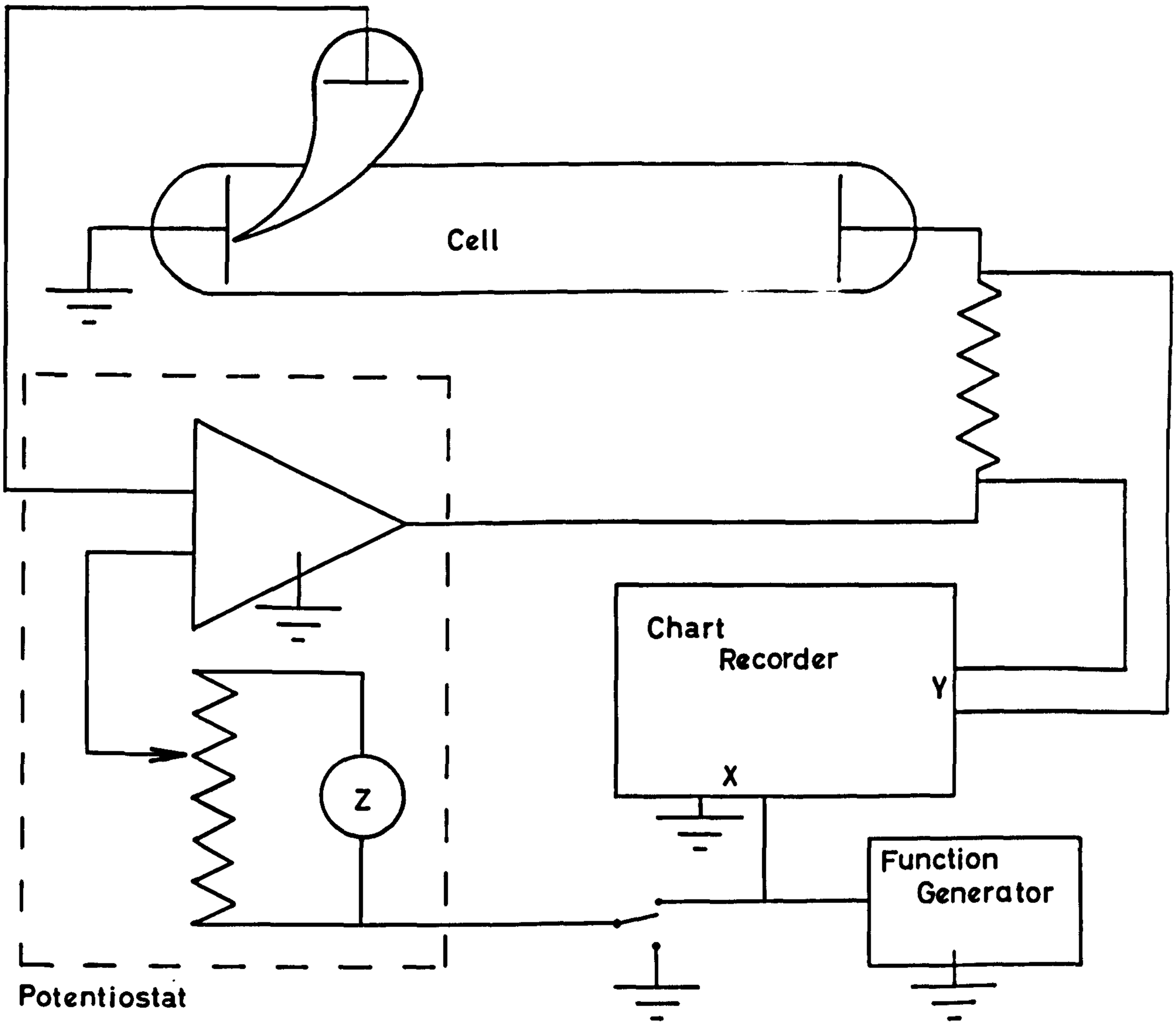

Fig. 5.1 Block diagram of circuit used for R.D.E. experiments

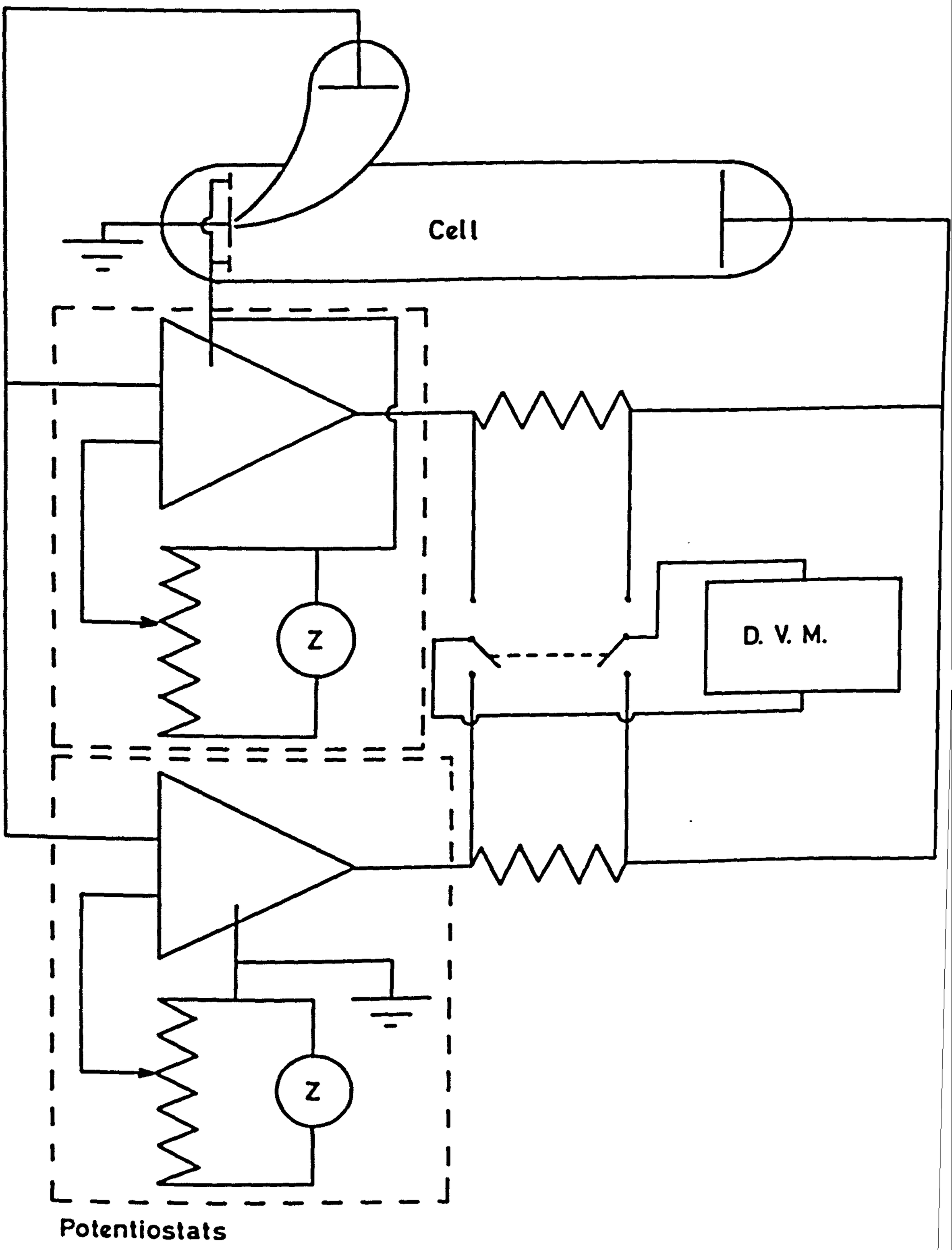

Fig.5.2 Block daigram of circuit used for R.R.D.E.

in zener stabilized reference potential circuit (Z). It has a 3V maximum in the anodic and cathodic sense, total output of 2 amps at 3V and a stabilisation time of 1 to 10μS, when used for supplying potentiostatic pulses. This instrument also had an automatic cut out which operates when the output is overloaded.

For rotating-disc experiments, a second additional potentiostat was required to control the ring electrode potential. This was a smaller solid state instrument specially designed and built in the department around an integrated circuit operational amplifier with a zener-stabilised reference circuit and push-pull transistor output section. This potentiostat had the same potential range as the commercial instrument but a smaller maximum output current.

5.2.2. Function Generator

This was used to supply linear potential sweeps of varying rates and potential pulses for the transient measurements. It was manufactured by Chemical Electronics Ltd., (type RB1) and could supply one or two successive potential steps or continuous linear sweeps of up to 3V in the cathodic sense. The sweeps were continuously variable from 0 to 1000 V/sec. and the cathodic going or returning sweep rates could be separately varied.

5.2.3. Recording and Measuring Equipment

The current flowing through the cell could be read directly from the ammeter incorporated in the potentiostat, or more accurately as the potential drop across a resistor (of known value) placed in series with the subsidiary electrode - this is termed the current measuring resistor.

Accurate monitoring of the current and potential was achieved using a digital voltmeter (Solartron LM 1620).

Current-potential curves from linear sweep measurements were recorded automatically on a Bryans X - Y chart recorder (Type 26000), the output of the function generator being fed simultaneously into the potentiostat and the X-axis of the recorder. At high sweeps (when the response of the chart recorder becomes comparable with the time for one sweep), the current-potential curves were recorded on the Y - X plates of an oscilloscope (Tektronix 503). The curves could be recorded photographically with an oscilloscope camera. Current-time transients from potentiostatic pulse experiments were recorded on a Y - t recorder (Servoscribe) or a Bryans chart recorder fitted with a time-base. For ring-disc experiments, it was necessary to record the ring and disc currents simultaneously as a function of time on a dual-channel recorder (Servoscribe 2). At short times (less than approx. 1 sec.), the current-time transients were recorded on the oscilloscope using the internal time base, in conjunction with the oscilloscope camera. An oscilloscope with dual beam facilities (Tektronix 502A) allowed the simultaneous monitoring of both ring and disc transients when required.

5.2.4. R.D.E. and R.R.D.E. Assemblies

The design of the rotating disc assembly is shown in Figure 5.3. The disc electrode in its teflon holder was fitted on to the steel shaft, contact being made from tbe back of the disc to the shaft via a small metal spring; contact to the external circuit was made through a mercury pool in a cup at the top of the shaft. The electrode was rotated via the shaft, nylon gears and a flexible rubber coupling by the controlled drive unit.

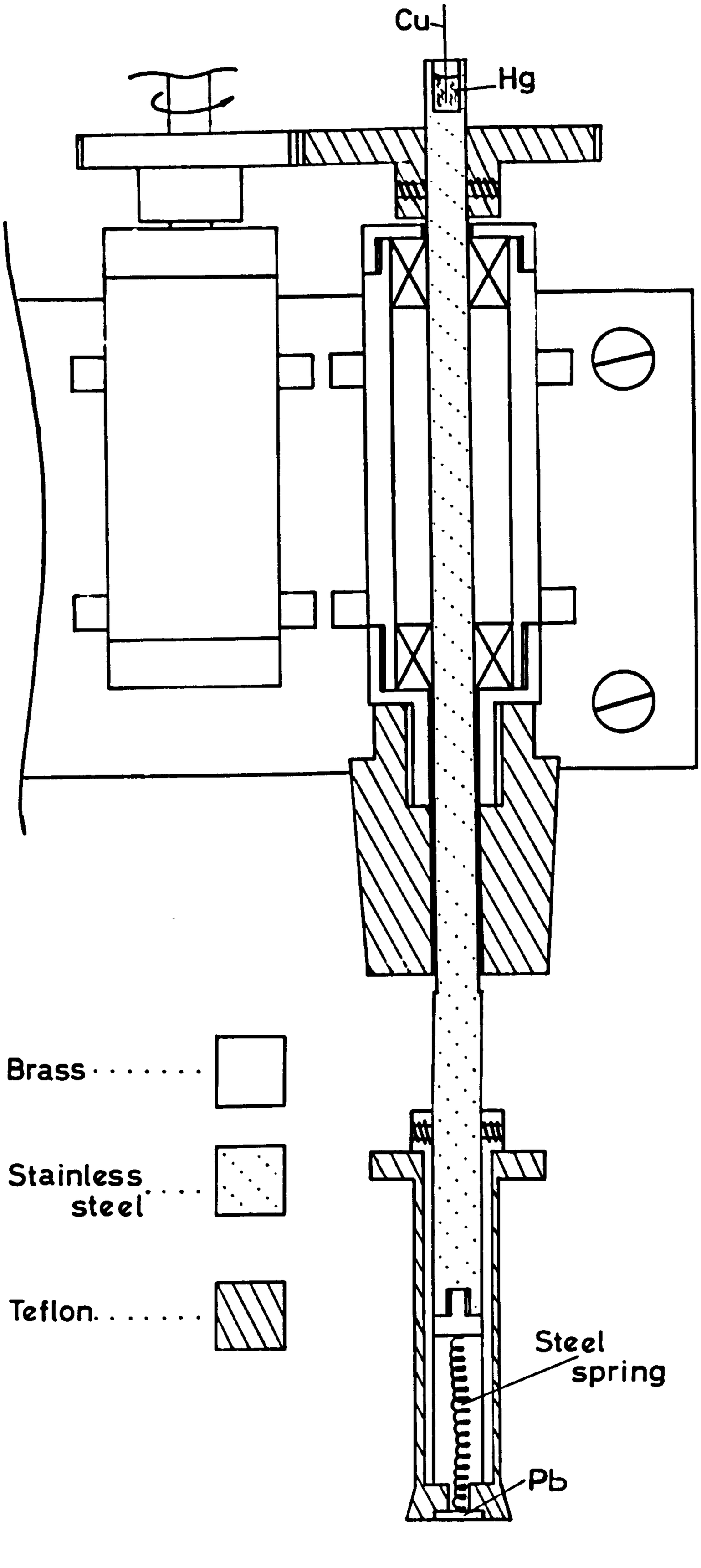

Fig. 5.3 Rotating disc assembly

The design of the rotating ring-disc assembly is shown in Figure 5.4. and was rotated by the same controlled drive unit. Contact to the back of the disc was made via a thin insulated wire which passed, down a central hole, the length of the steel shaft. Again this insulated wire made external contact through a mercury pool in a cup at the top of the shaft - this cup being insulated from the shaft. Electrical contact to the ring electrode was made by sealing the ring with conducting Araldite to a brass sleeve inside the teflon holder. This sleeve then contacts the shaft which makes external contact via a large mercury pool. In this way, using the two mercury pools, it was possible to insulate the ring and disc electrodes from one another while maintaining contact on rotating the assembly.

The controlled drive unit for both assemblies consisted of a motor generator, driven and controlled by a specially designed velodyne servo-amplifier. This was a solid state instrument allowing continuous variation of the rotation speed from zero to 10,000 r.p.m. The rotations were counted by a magnet and reed-switch arrangement, the pulses from which were counted by an Advance Timer (TC 11).

5.3. Electrodes and Solutions

5.3.1. Working Electrodes

Three types of working electrodes were used.

(i) Lead disc electrode

(ii) Lead ring-lead disc electrode

(iii) Lead amalgam spherical electrode.

In all cases the lead was cut from a rod supplied by Koch-Light Laboratories Ltd. (5N purity). The rotating disc electrode is shown in Figure 5.3.

The high purity metal discs (area 0.2 cm^2) were made to be a tight push-fit into the base of the teflon holder and, as a precaution against solution creep or leak, a minimal amount of Araldite expoxy resin was used to seal the discs in their holders. The rotating-ring disc electrode is shown in Figure 5.4. The theoretical collection efficiencies for the electrodes of different dimensions used are quotated with the figures. The spherical lead amalgam electrodes were formed as drops of 0.0421 cm^2 area, on an upturned syringe. The initial amalgam was 0.71% by weight Pb, this was later diluted and the concentrations are quoted when appropriate.

Polishing of solid Pb

Two methods of polishing were used, mechanical polishing and electropolishing, these will be discussed separately. In all cases the ring electrode was mechanically polished.

Mechanical Polishing

The first method of mechanical polishing used involved rubbing the lead disc on various grades of silicon carbide coated paper (S.I.A. Grades 0 $\longrightarrow$ 6). Unfortunately this method tended to leave the surface impregnated with 'lumps'. Examination by use of energy dispersion X-ray analysis (EDAX) revealed that these 'lumps' were in fact particles of silicon carbide lodged in the lead surface (see Figure 5.5).

Figure 5.5. (a) A Stereoscan micrograph (magnification 425) of a silicon carbide polished lead surface.

(b) An X-ray scan of (a) for lead which is shown by the white regions.

Fig. 5.4 Ring-disc electrode assembly

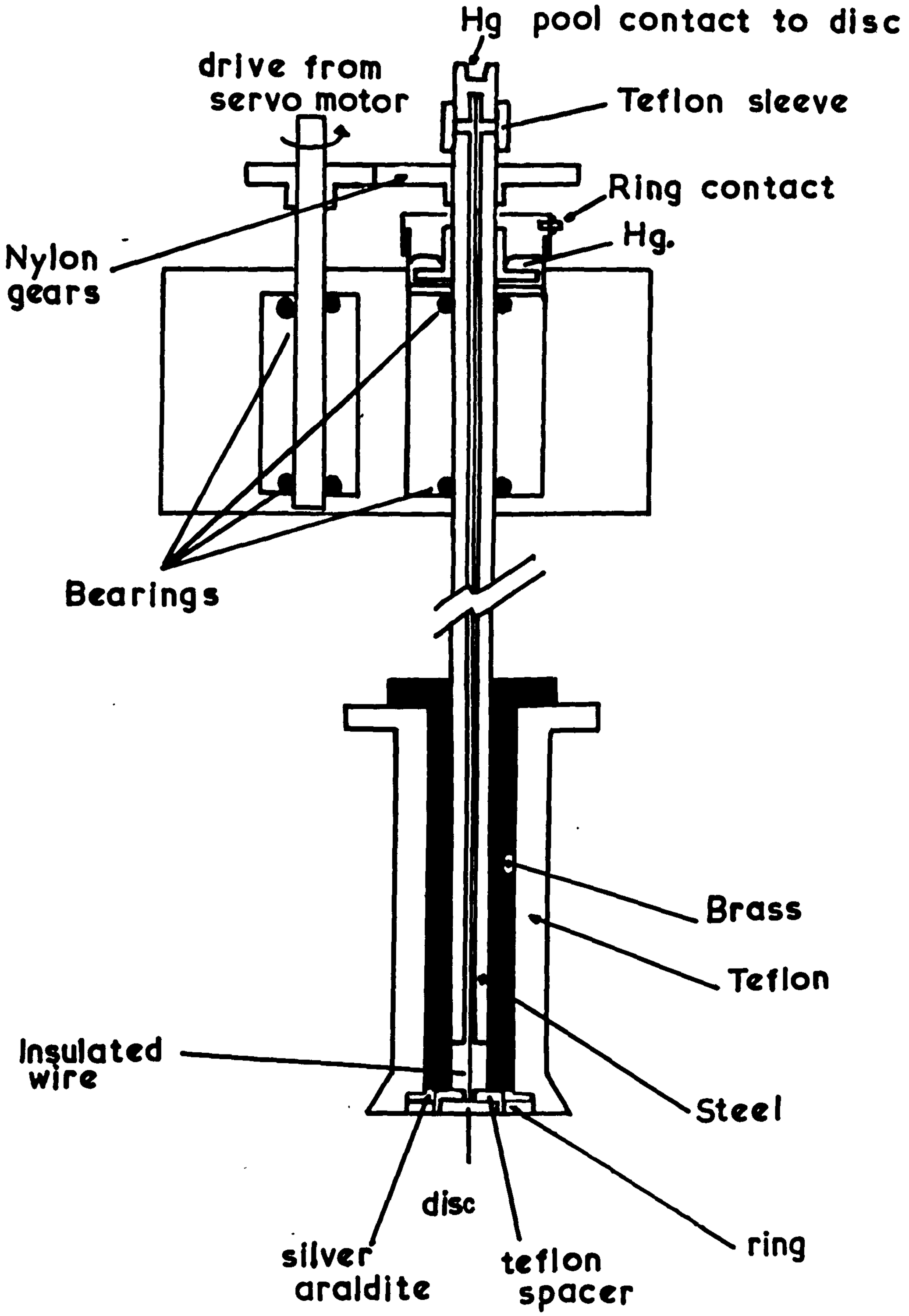

Fig. 5.5a Stereoscan micrograph (X 425)
of a silicon carbide polished
electrode

Fig. 5.5b X-ray scan
Pb excitation

Fig. 5.5c X-ray scan
Si excitation

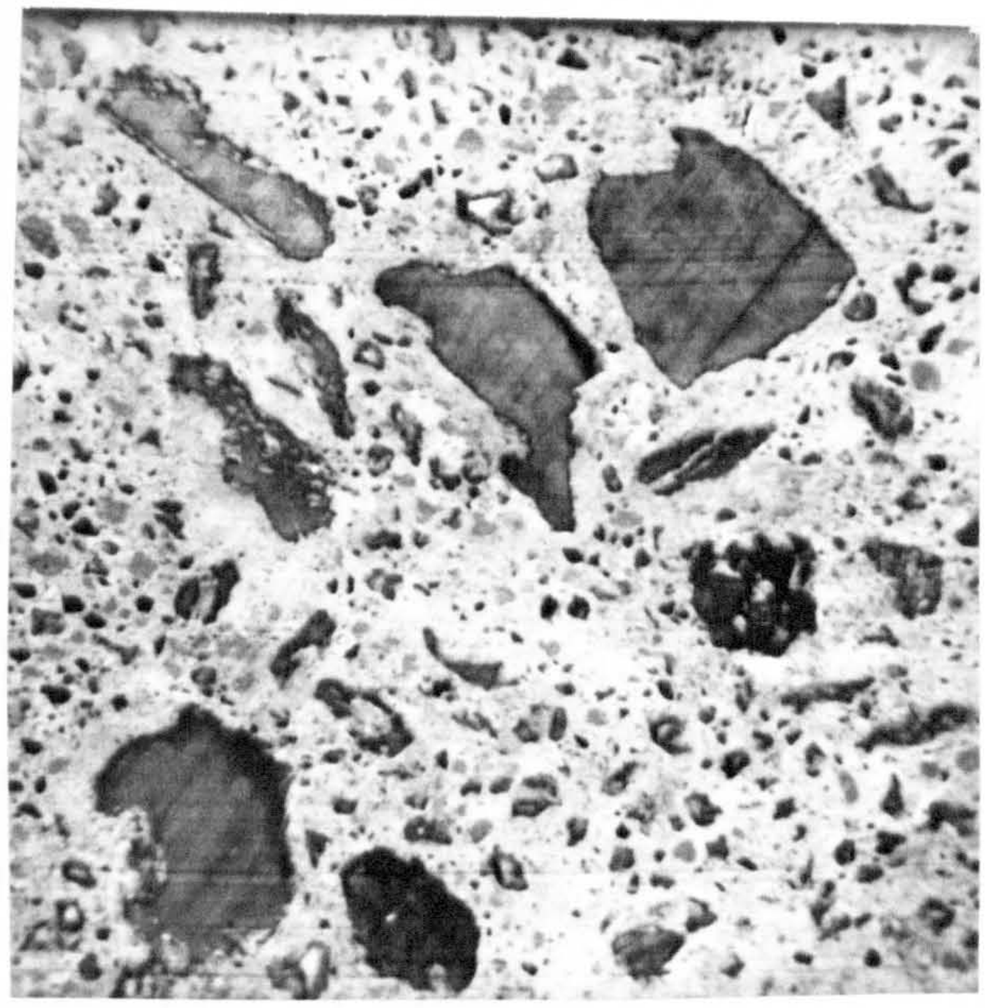

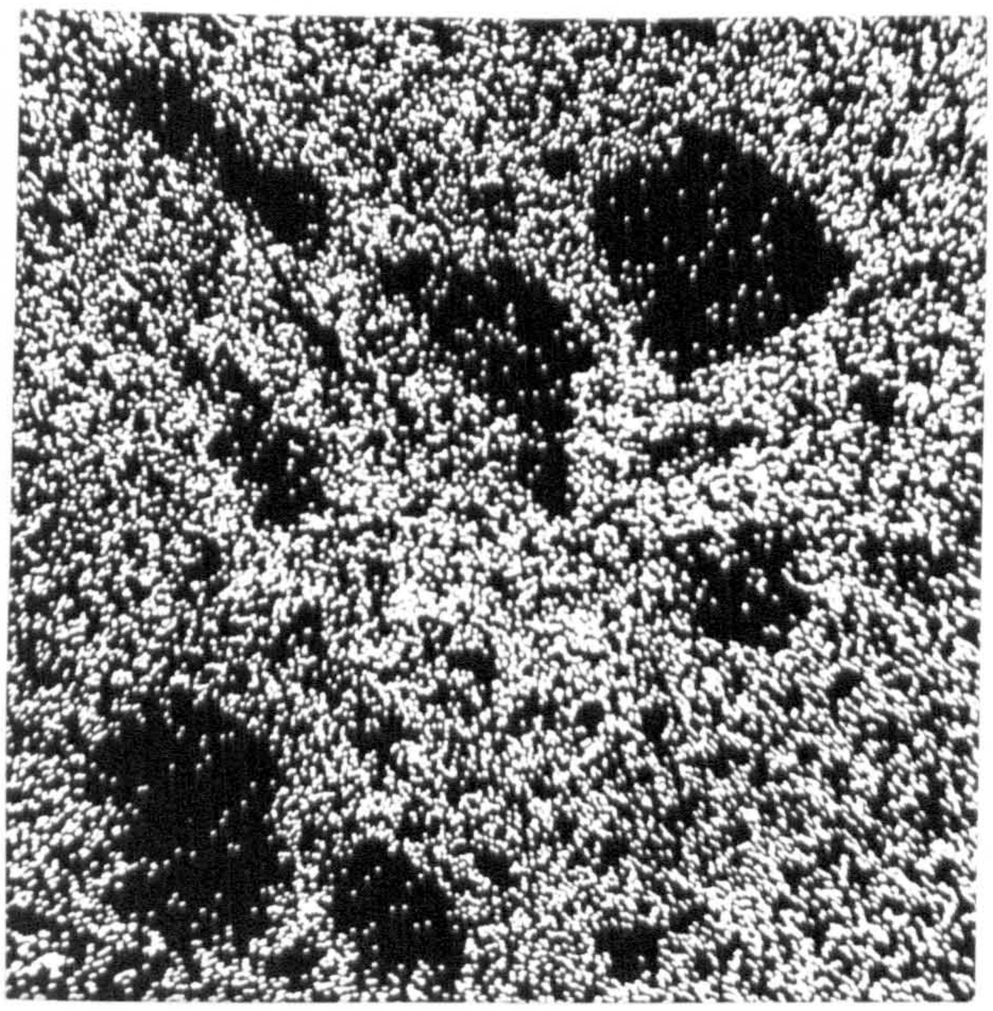

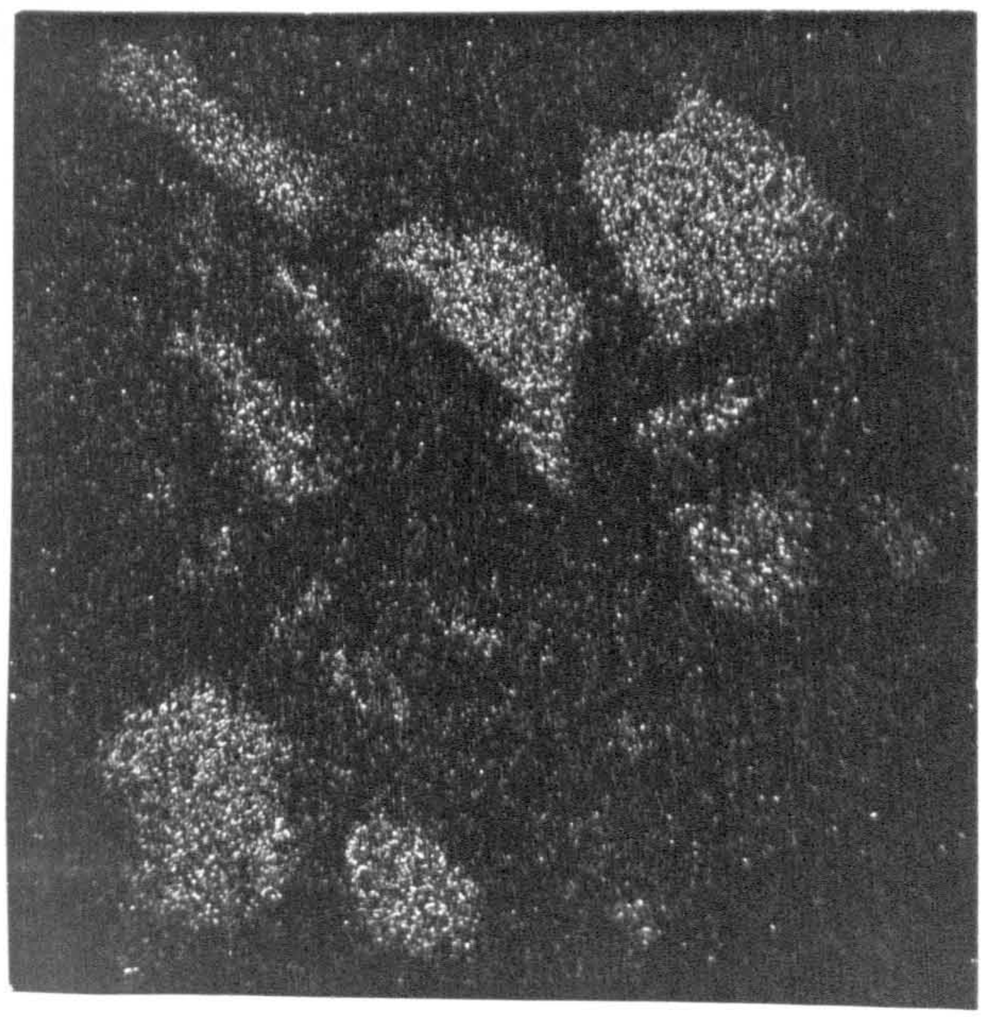

(c) An X-ray scan of (a) for silicon which is shown by the white regions.

These micrographs show conclusively that this method of polishing leaves the surface impregnated with silicon carbide.

A much smoother surface was achieved, if after polishing with silicon carbide paper, the disc was polished with γ -polishing alumina (particle size 1 - 5μm) dispersed in water on a 'Selvyt' cloth placed on a hard, smooth, flat surface. This was a lengthy process but inspection with a microscope showed that the silicon carbide was removed by this treatment.

Electropolishing

Two solutions for electropolishing were used and in both cases 5 amp. cm^{-2} for 10 - 15 seconds gave a good finish.

(a) 40% ammonium fluoroborate and 2% sulphuric acid in water.

The lead was made the anode and a bright platinum sheet was as the cathode.

This solution did not give a surface as smooth as was desired, however the following solution was later found to give a brighter finish.

(b) 50 ml perchloric acid + 200 ml ethyl alcohol + 3 ml ether.

The Pb disc was made the anode and a stainless steel rod was used as the cathode.

Both methods of electropolishing gave similar electrochemical results.

5.3.2. Reference electrodes[18]

$Hg/Hg_2SO_4/H_2SO_4$ reference electrodes were used (for work in

H_2SO_4). The potentials for different sulphuric acid concentrations are summarised in Table I. Data for making these calculations are found in the literature[19,20]. To convert from the E_m scale to the E_h scale in H_2SO_4 676 mV, 662 mV, 650 mV, for 0.1M, 1.0M, 2.0M, respectively were added to potentials E_m measured against Hg/Hg_2SO_4 in the same H_2SO_4 solution.

The Hg/Hg_2Cl_2/sat.NaCl electrode was used for measurements in $NaClO_4$. Conversion of potentials referred to this electrode, to the standard hydrogen scale, E_h, was effected by adding 234 mV plus the junction potential.

In $HClO_4$ the potentials were measured against a hydrogen electrode in the same solution and converted to the E_h scale by subtracting 5.1 mV for 1.0M $HClO_4$ and 66.0 mV for 0.1M $HClO_4$.

5.3.3. Secondary Electrodes

In the cells used for making measurements on solid lead, the secondary electrode consisted of a platinum sheet situated directly beneath the working electrode. For measurements on amalgams the secondary electrode was a platinum wire formed into a helix around the electrode.

5.3.4. Solutions

The solutions used throughout were prepared from Aristar or Analar reagents (B.D.H. Chemicals) and triply-distilled water. This was made by redistilling twice, from an all-glass still, the water obtained from a commercial electric still. The first stage of the all-glass still contained a low concentration of alkaline potassium permanganate to oxidise any volatile organic impurities present. The final triply-distilled

water was collected and stored in pyrex flasks.

The solutions used were:

H_2SO_4 0.1M, 1.0M, 2.0M, 4.7M (B.D.H. Aristar)

$HClO_4$ 0.1M, 1.0M (B.D.H. Aristar)

$NaClO_4$ 0.1M, 1.0M (B.D.H. Analar)

All solutions were deoxygenated with nitrogen (B.O.C. "White Spot") before use. The concentration of SO_4^{2-}, HSO_4^- and H^+ in H_2SO_4 solutions of various strength has been determined by Raman spectroscopy[21]. 1.0M H_2SO_4 has the composition SO_4^{2-} 0.28M, HSO_4^- 0.72M, H^+ 1.28M. The nitrogen was presaturated with the working solution in a dreschel bottle before passage through the cell.

All flasks, bottles and cells used were constructed from pyrex and were thoroughly cleaned with a chromic/sulphuric acid mixture, then rinsed in triply-distilled water before use.

5.4. Electrochemical cells

The cell used for the R.D.E. and R.R.D.E. measurements at 25°C is shown in Figure 5.6. The reference electrode compartment is connected to the main cell by a Luggin capillary, A, and a three-way ground glass tap facilitates the formation of a liquid junction when required. The tip of the Luggin was positioned at approximately 1 mm. below the electrode (disc) centre to minimise the ohmic drop, and was drawn as fine as possible to minimise screening effects. The secondary electrode was a platinum sheet, B.

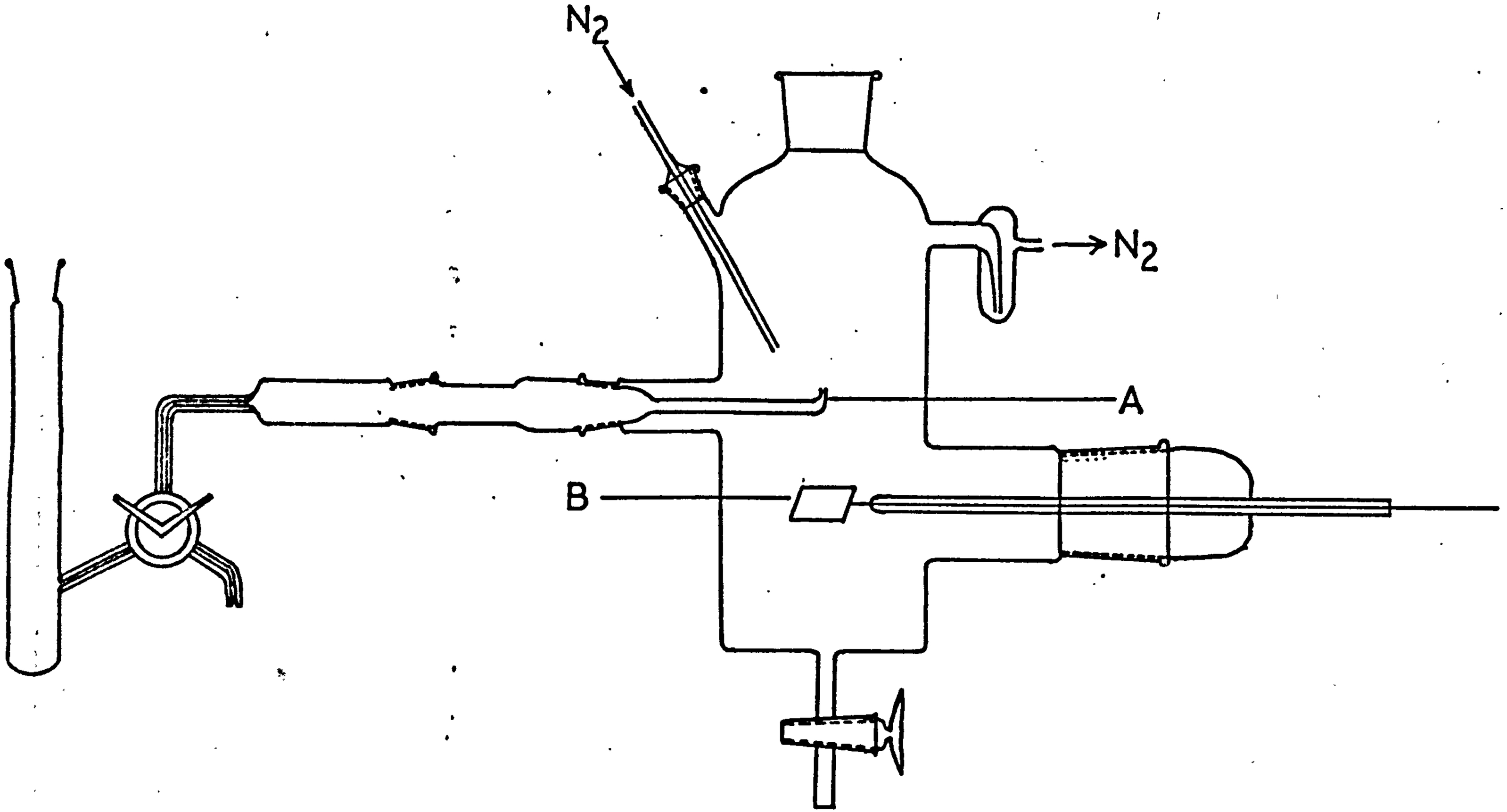

Fig. 5.6 CELL FOR MEASUREMENTS AT ROOM TEMPERATURE

The cell for measurements at low temperatures is shown in Figure 5.7. The cell was designed so that the working solution compartment could be immersed in coolant whilst keeping all ground glass joints clear of the coolant. The reference electrode could be kept at room temperature by being contained outside the bath containing coolant. As before the cell had provision for bubbling nitrogen through the cell.

The cell used for measurements at the lead amalgam electrode is shown in Figure 5.8i. The working electrode consisted of a drop of amalgam formed at the tip of a chamfered vertical capillary. A precision micrometer syringe attached to the lower end of the capillary allowed renewal of the amalgam drop. The area of the drop was calculated from measurements made with a travelling microscope. The relationship is

$$\text{Surface area} = \pi\left(h^2 - r^2\right)$$

where h is the height of the drop and r is the radius of the capillary.

The subsidiary electrode consisted of a helix of platinum wire, concentric with the upturned capillary of the working electrode. The Luggin capillary protruded horizontally through the helix, terminating within a millimeter of the drop. The cell had provision for bubbling nitrogen through the cell solution.

5.5. Liquid Junctions

Liquid junctions were always made at the three way tap, joining the reference electrode compartment and the Luggin capillary, in the following way. The reference compartment was filled with the same solution as in the reference electrode - the three way tap being in position to

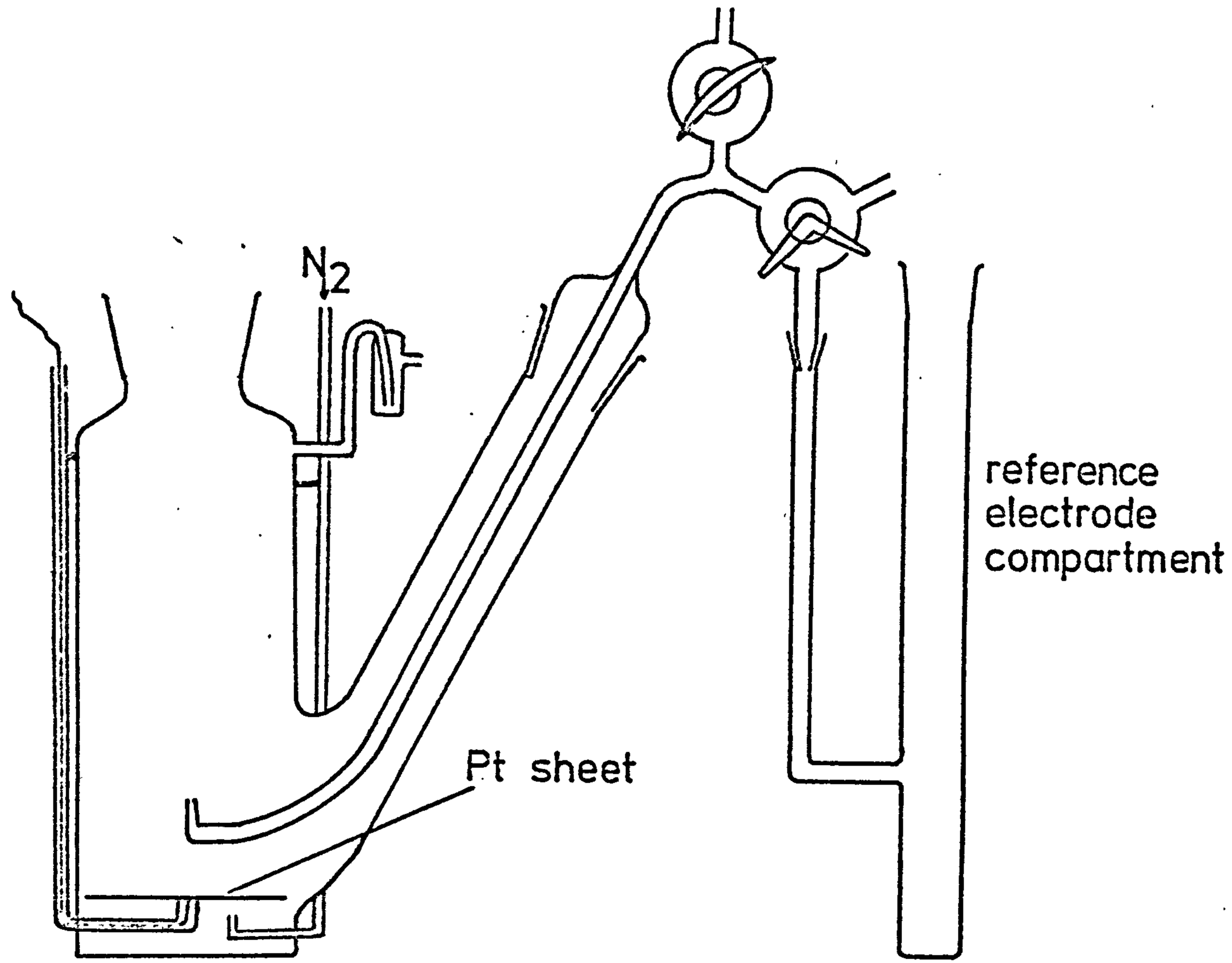

FIG. 5.7 CELL FOR MEASUREMENTS AT LOW TEMPERATURES

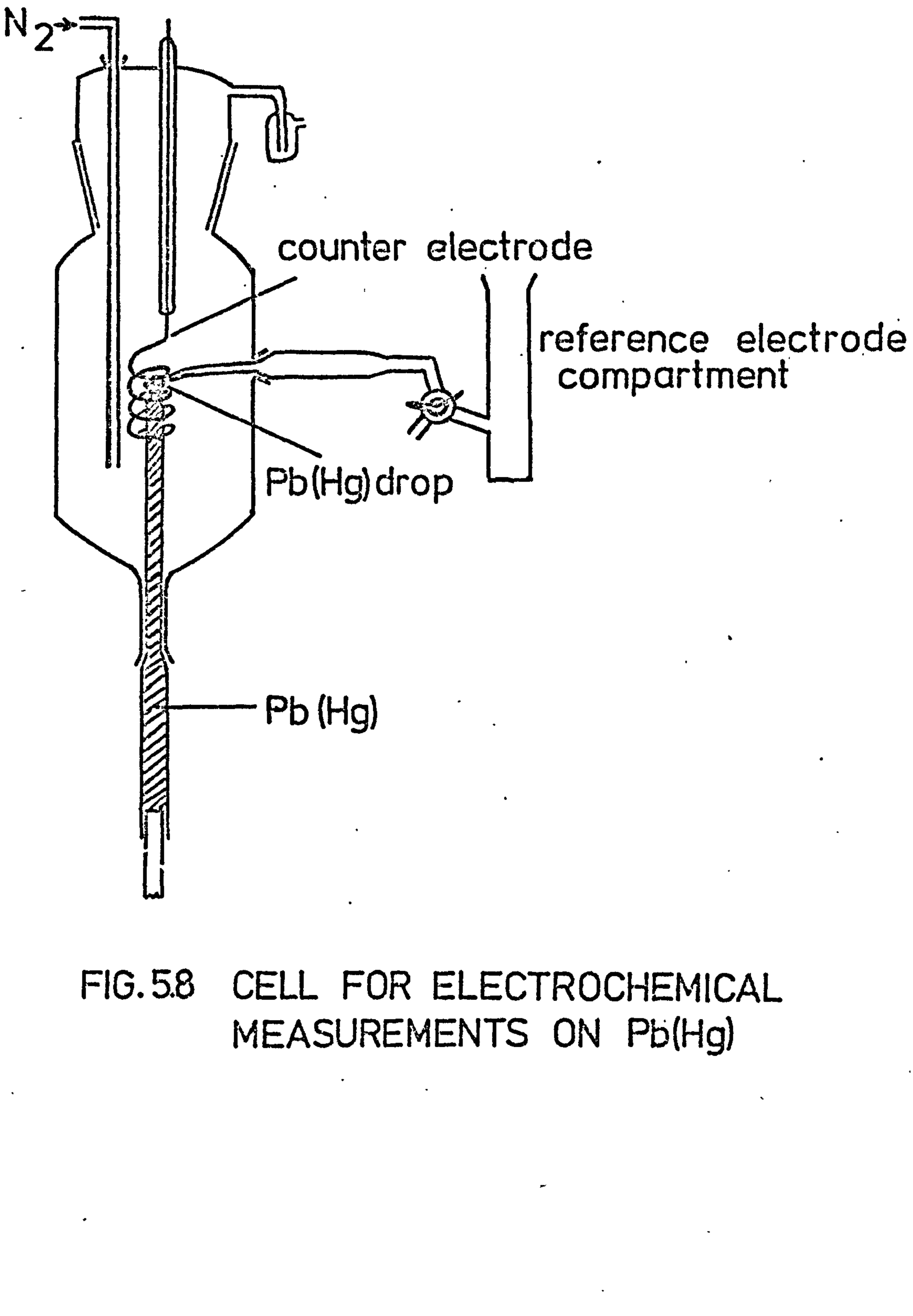

FIG. 5.8 CELL FOR ELECTROCHEMICAL MEASUREMENTS ON Pb(Hg)

joint the reference compartment and the outlet opening. The tap was slightly pulled out to wet the anular space of the tap. Working solution was then sucked in the Luggin capillary by connecting the outlet opening of the tap to a suction device - the tap being in position to connect the Luggin and the outlet opening. After filling the Luggin, the tap was turned in a position such that it joined no two openings directly.

Liquid junction potentials were usually avoided by employing the same solution in the reference electrode as in the working compartment. However, in cases where the working solution was different from that in the reference system, liquid junction potentials were calculated according to Hendersons equation[22]

$$E = \sum \frac{RT}{F} \frac{t_i}{z_i} d \ln a_i$$

where t_i = transport number of species

z_i = the charge of species

a_i = the activity of species

The required ion mobilities were found from Reference 20.

The junction potential was calculated as +13.1 mV for 1M $NaClO_4$ and +25.1 mV for 0.1M $NaClO_4$.

5.6. General

Measurements were made with sulphuric acid at 25°C, 0°C, and -18°C. All other solutions were used at 25°C. The accuracy was within $\pm$ 0.5°C.

Measurements at 0°C were made by immersing the working solution compartment in an ice-bath and allowing sufficient time for the temperature

to stabilise. Measurements at -18°C were effected by circulating a 50% ethanol-water mixture, at approximately -30°C from a refrigerator through a copper coil heat exchanger using a self-primary pump. A similar mixture was contained around the working solution compartment by a well lagged vessel. The copper coil was also immersed in the solution, and with careful control of the flow of coolant through the coil, the working solution could be maintained at -18°C.

TABLE I.

Sulphuric acid concentration			Electrode potential at 25°C	
Moles/litre	Moles/1000g H_2O	pH	Hg/Hg_2SO_4 vs H_2 in the same solution(mV)	Hg/Hg_2SO_4 vs S.T.P. H_2 in pH 0 (mV) (E_m)
.10	0.10	1.03	737	676
1.0	1.04	0.20	674	662
2.0	2.16	-0.06	646.5	650
4.7	4.8	- .56	584	617

REFERENCES

1. BURBANK, J., SIMON, A.C. and WILLIHNGANZ, E. — in "Advances in Electrochemistry and Electrochemical Engineering" Editor Tobias,C.W. Vol. 8. Interscience N.Y.1971

2. PAVLOV, D., POULIEFF, C.N. KLAJA, E. and IORDANOV, N. — J. Electrochem. Soc., 116, 316 (1969)

3. PAVLOV, D. and POPOVA, R. — Electrochim. Acta, 15, 1483 (1970)

4. PAVLOV, D. and IORDANOV, N. — J. Electrochem. Soc., 117, 1103 (1970)

5. RUETSCHI, P. and ANGSTADT, R.T. — J. Electrochem. Soc., 111, 1323 (1964)

6. BARNES, S.C. and MATHIESON, R.T. — in D.H. Collins (Ed.), Batteries Vol.2 Brighton 1964

7. RUETSCHI, P. — J. Electrochem. Soc. 120, 331 (1973)

8. SIMONSSON, D. — J. Electrochem. Soc. 120, 151 (1973)

9. STERR, G. — Electrochim. Acta, 15, 1221 (1970)

10. MAEDA, M. — J. Electrochem. Soc. Japan 25, 197 (1957); Overseas ed; 26, E21, E183 (1958).

11. SIMON, A.C. WALES, C.P. and CAULDER, S.M. — J. Electrochem. Soc., 117, 987 (1970)

12. OZHIGANOVA, N.N. and AGUF, J.A. — Elektrokhimiya, 6, 239, (1970)

13. NIKLAS, H. and JAKOBLIJEVICH — J. Applied Electrochem. 2, 165 (1972)

14. IKARI, S. — U.S. Pat. No. 3,481,785 (1969)

15. PIERSON, J.R.
GURLUSKY, P.
SIMON, A.C. and
CAULDER, S.M.
J. Electrochem. Soc. 117, 1463 (1970)

16. TARTER, E. and
EKLER, K.
Can. J. Chem. 47, 2191 (1969)

17. BAIKIE, P.E.
GILLIBRAND, M.I. and
PETERS, K.
Electrochim. Acta 17, 839 (1972)

18. IVES, D.J.G. and
JANZ, G.J.
"Reference Electrode", Academic Press,
New York (1961)

19. DELAHAY, P.
POURBAIX, M. and
VAN RYSSELBERGHE, P.
J. Electrochem. Soc., 98, 57 (1951)

20. ROBINSON, R.A. and
STOKES, R.H.
'Electrolyte Solutions" Butterworths, London (1968)

21. YOUNG, T.F.
MARANVILLE, L.F.
and SMITH, H.M.
'The Structure of Electrolyte Solutions'
(ed. Hamer, W.J.), Wiley 1959

22. VETTER, K.J.
'Electrochemical Kinetics' (Eng. Trans.) Academic
Press (1967)

Fig. 6.1(a) $PbSO_4$ formed at -850 mV E_m in 1M H_2SO_4 for 5 minutes (X 4,050)

Fig. 6.1(b) $PbSO_4$ remaining after reducing condition of -1200 mV E_m for 3½ hours (X 4,500)

Fig. 6.2(a) Electropolished Pb surface (X 17)

Fig. 6.2(b) Enlarged view of area A in (a) (X 4120)

Fig. 6.2(c) Enlarged view of the more general area (X 4350)

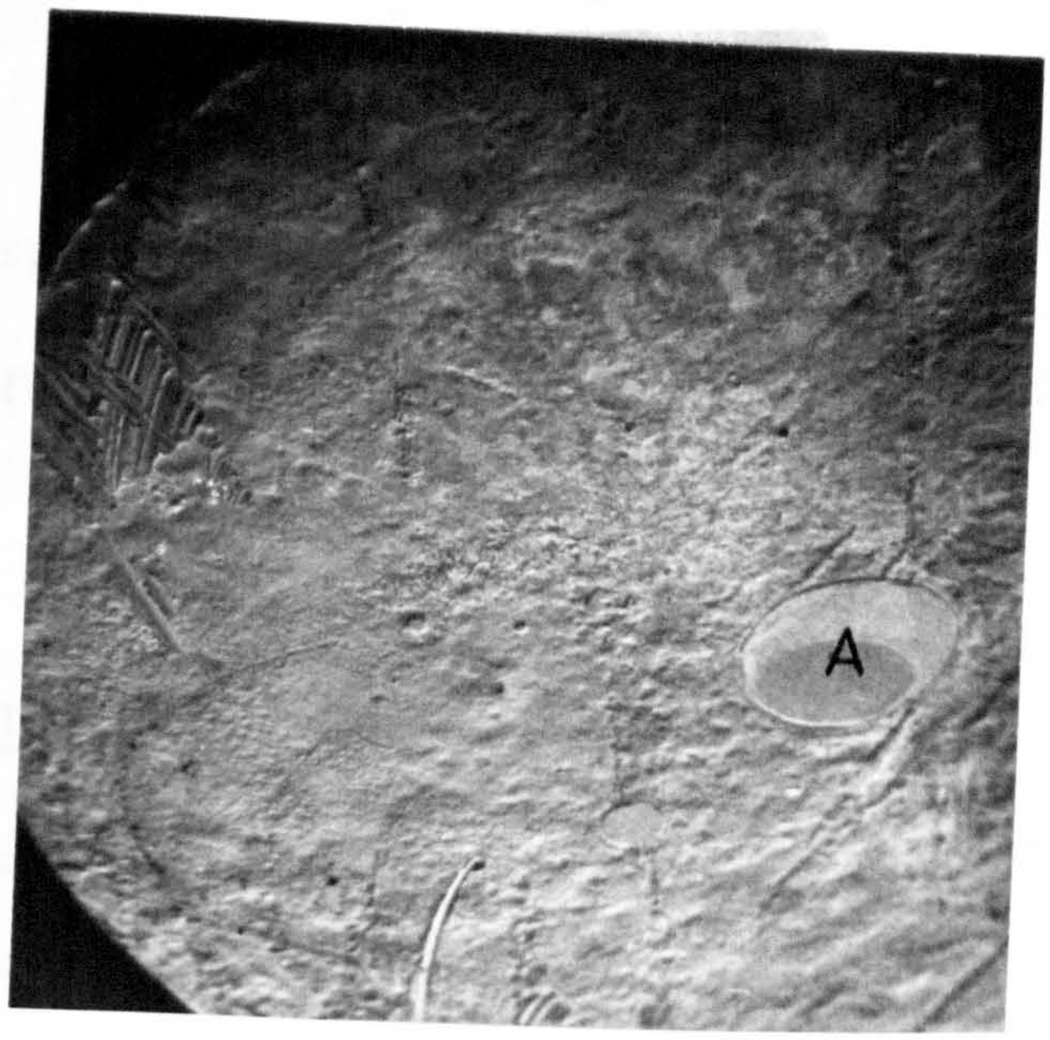
A

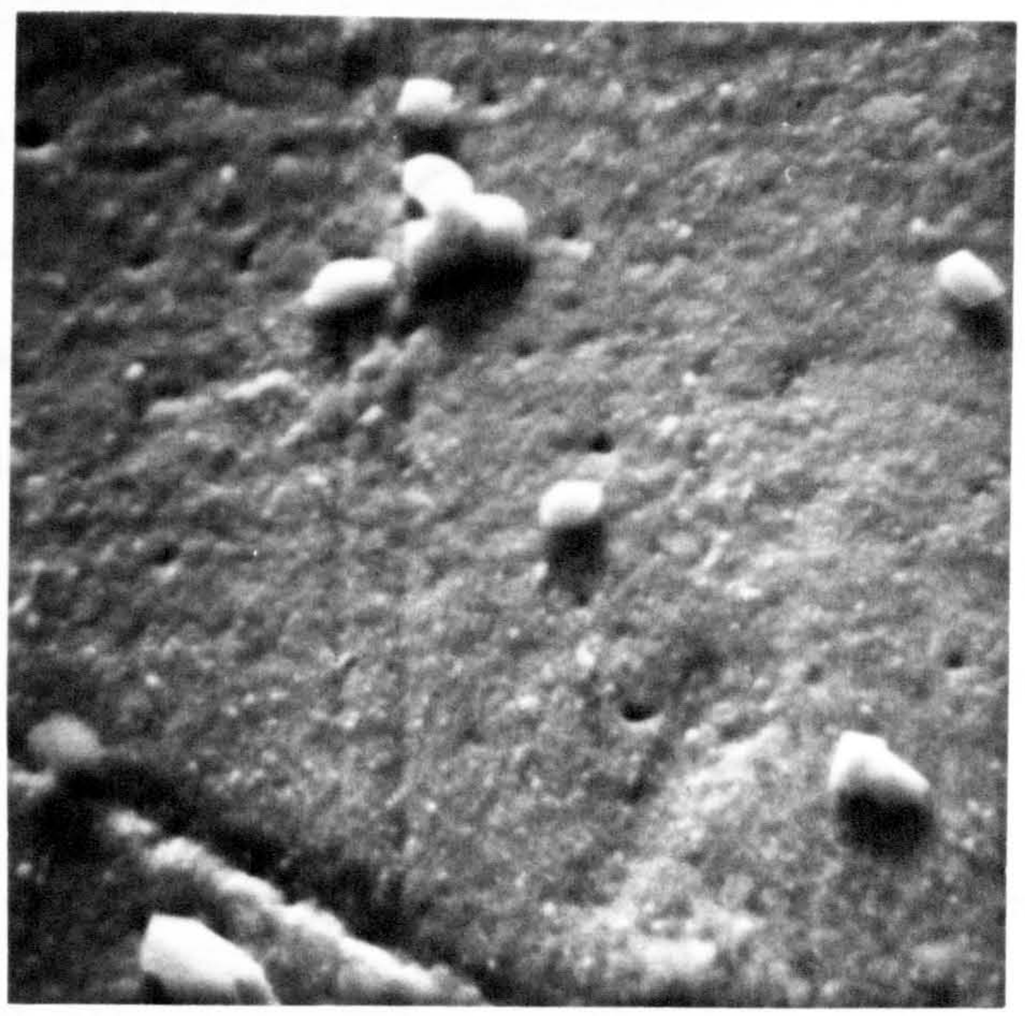

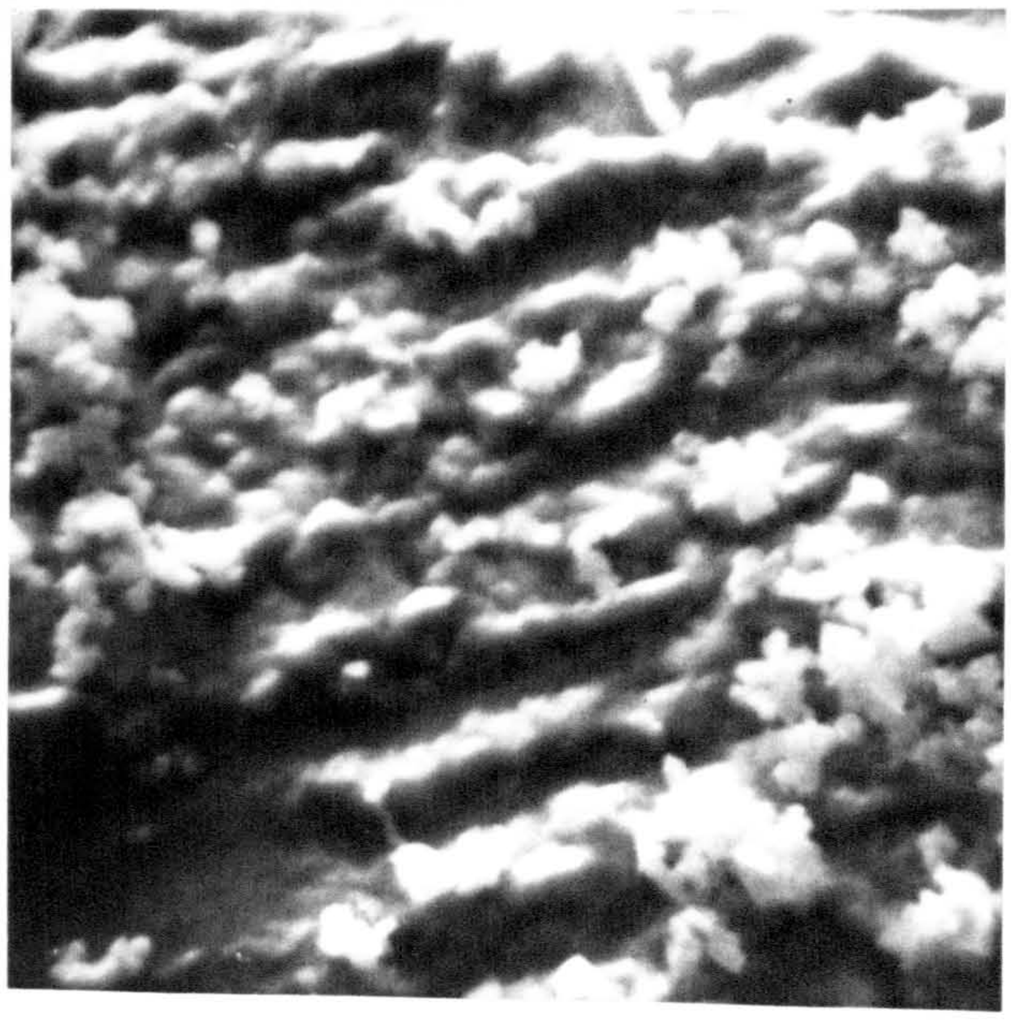

(c) Is an enlarged view of the more general area.

Comparing Figure 6.2(b) and (c) $PbSO_4$ prefers to form on the rougher general area.

6.3. Electrochemical measurements on solid Pb

In this section measurements were made in 1M H_2SO_4 at 25°C unless otherwise stated.

6.3.1. Linear potential sweep measurements

S.E.M. investigation of Pb surfaces has shown differences between electropolishing and mechanically polishing. The difference between the two polished surfaces is also apparent in electrochemical measurements. Figures 6.3, 6.4, 6.5 are foramechanically polished and Figures 6.6, 6.7a,b, for an electropolished Pb disc. The potentials are on the E_m scale. Both sets have a similar potential dependence of the rising portion when log i vs E is plotted Figure 6.8, 6.9. Figure 6.8 for the mechanically polished electrode has a 40 mV slope and Figure 6.9 for the electropolished electrode has a 37 mV Tafel slope. These slopes are lower than expected which is probably due to progress blocking with $PbSO_4$.

The mechanically polished curves, Figures 6.3, 6.4, 6.5 go through a maximum some 100 mV anodic to the reversible $Pb/PbSO_4$ potential, E_m = -969 mV. Some charge is recovered in the cathodic sweep negative to -969 mV, however in the first cycle this is much less than the anodic charge laid down. In the second sweep less anodic charge is formed, see Figure 6.4.

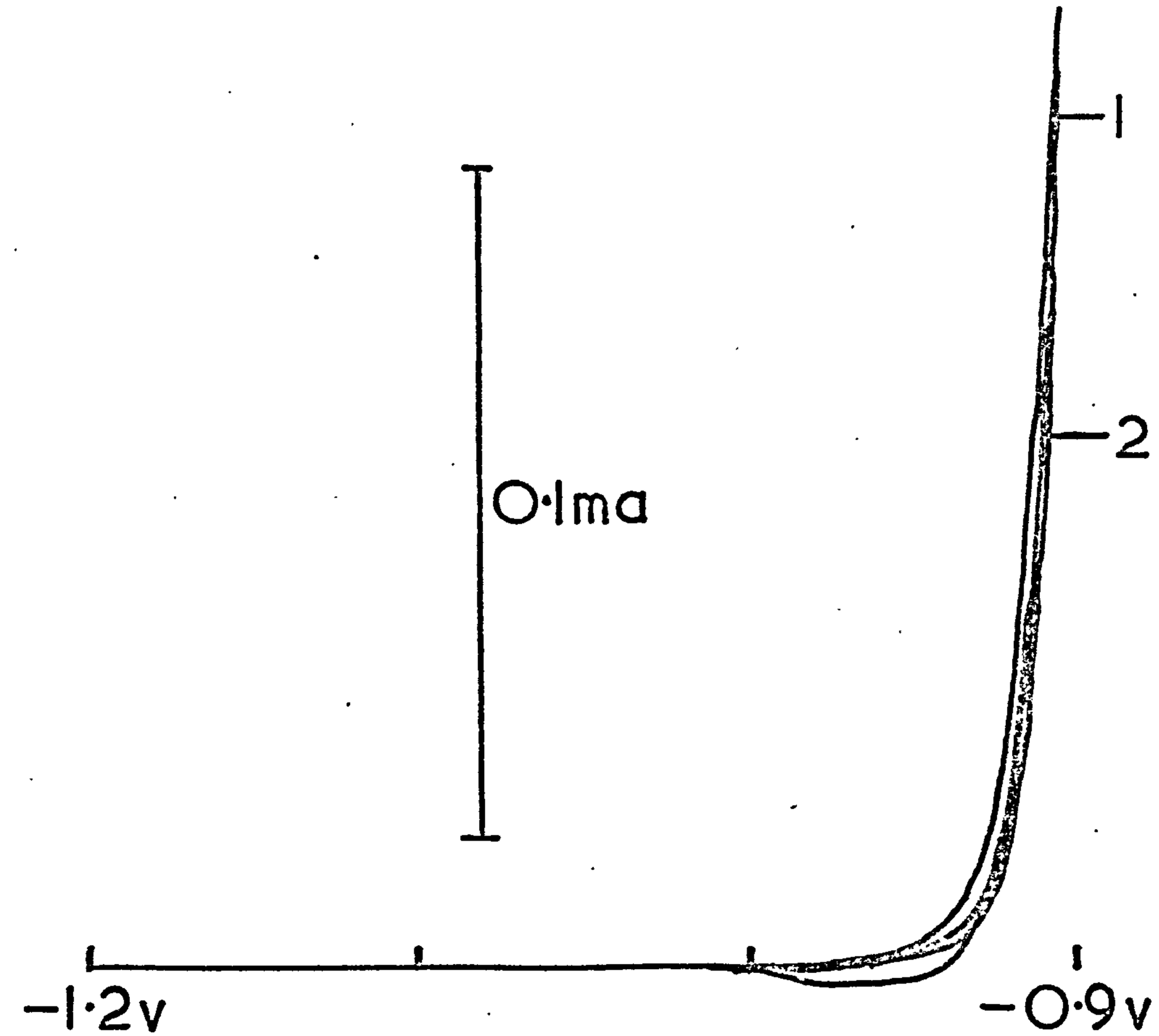

Fig.6.3 i vs E curve of mechanically polished Pb showing rotation speed dependence

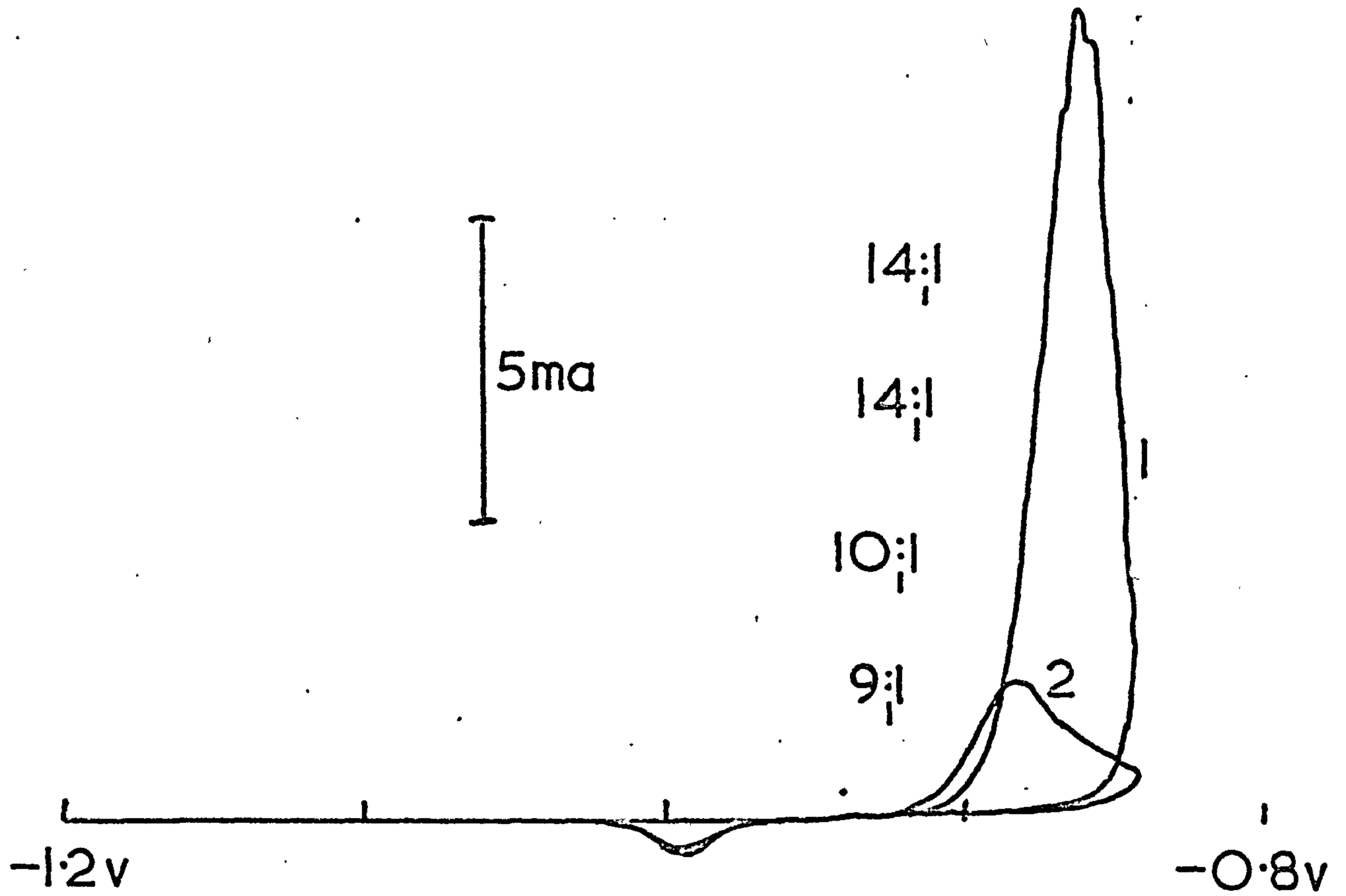

Fig64 I vs E for Mechanically Polished Pb showing 1st and 2nd Sweeps and $Q_A : Q_C$

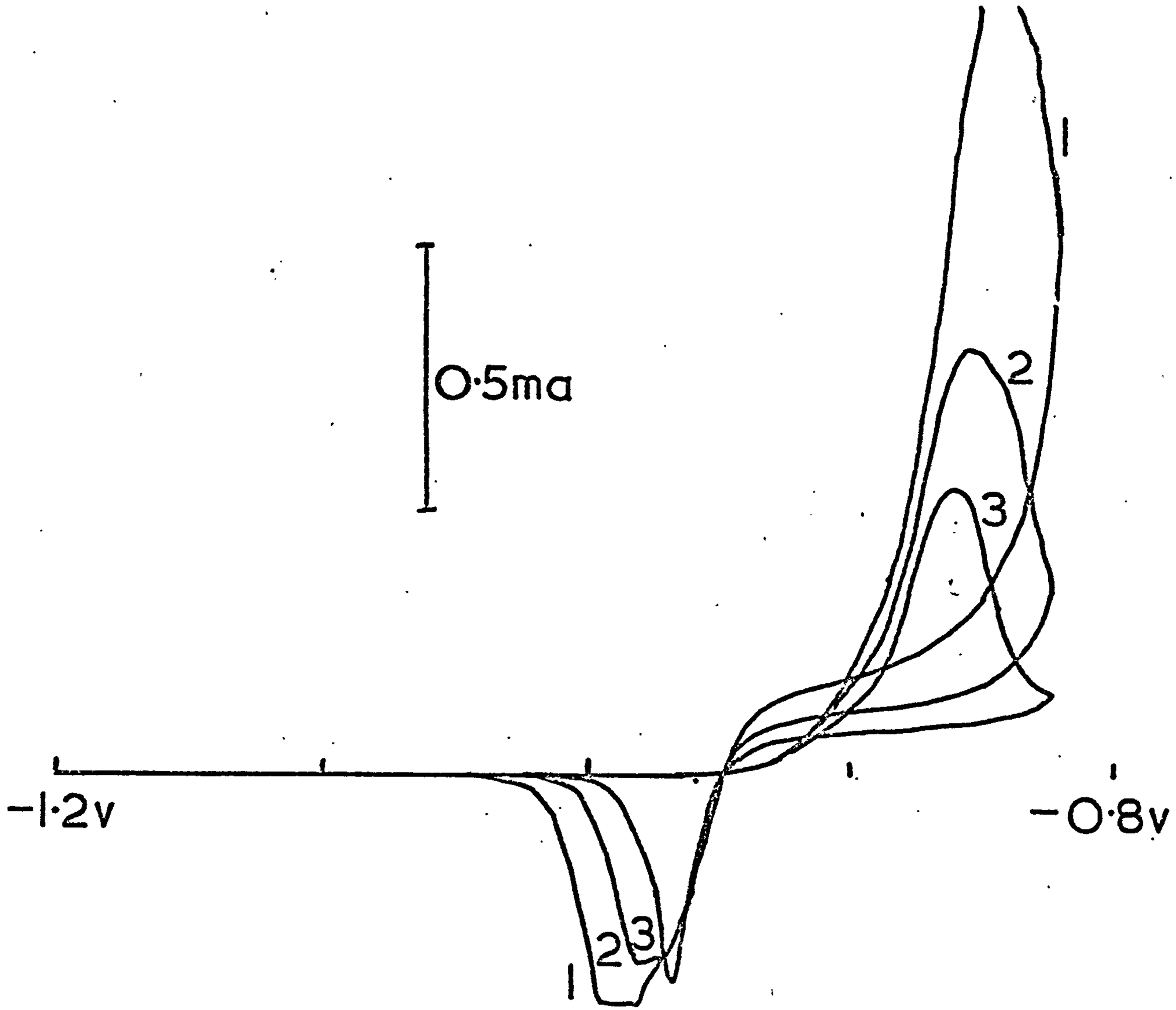

Fig.6.5 i vs E curve showing sweep rate dependence

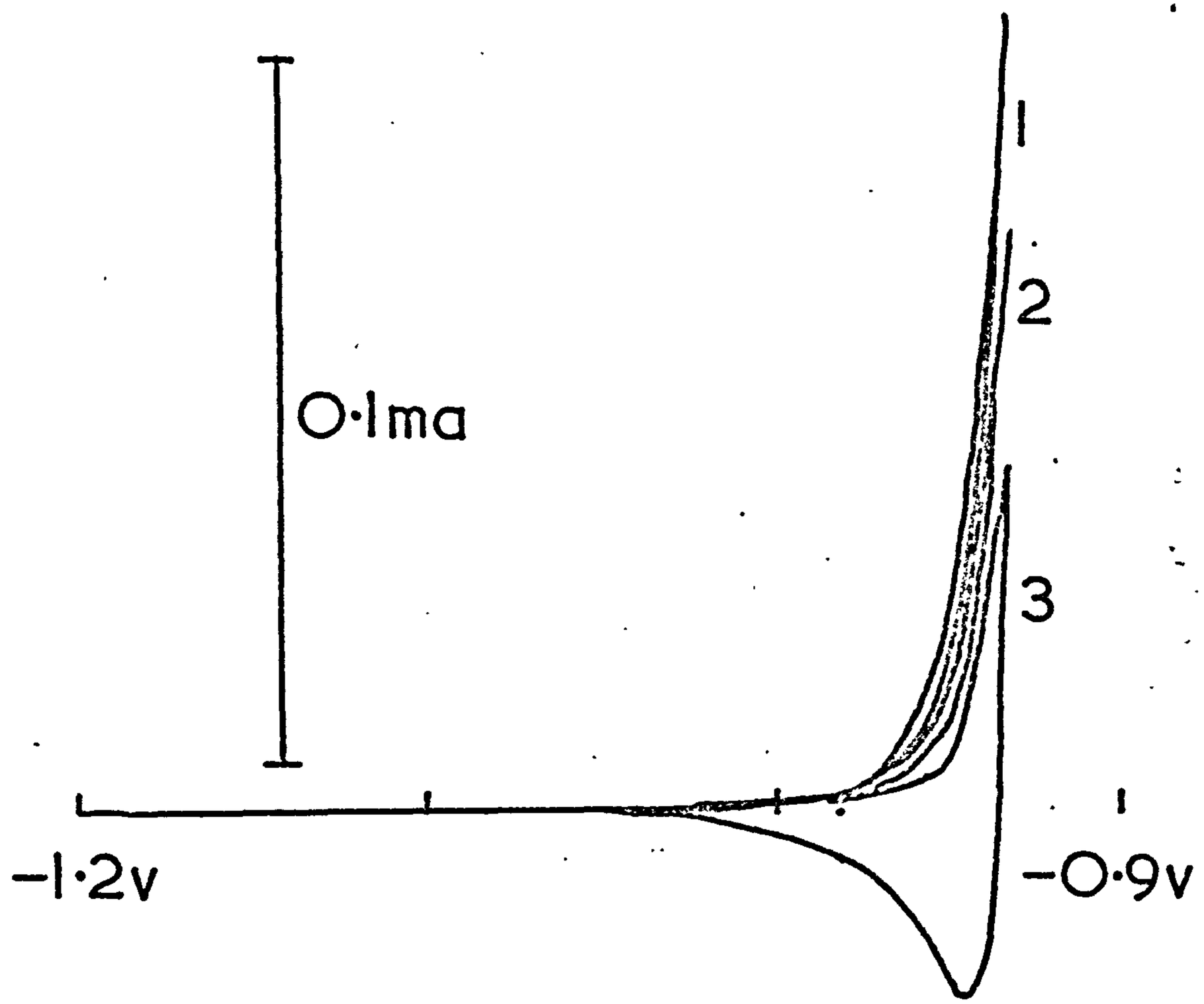

Fig.6.6 i vs E curve of electropolished Pb showing rotation speed dependence

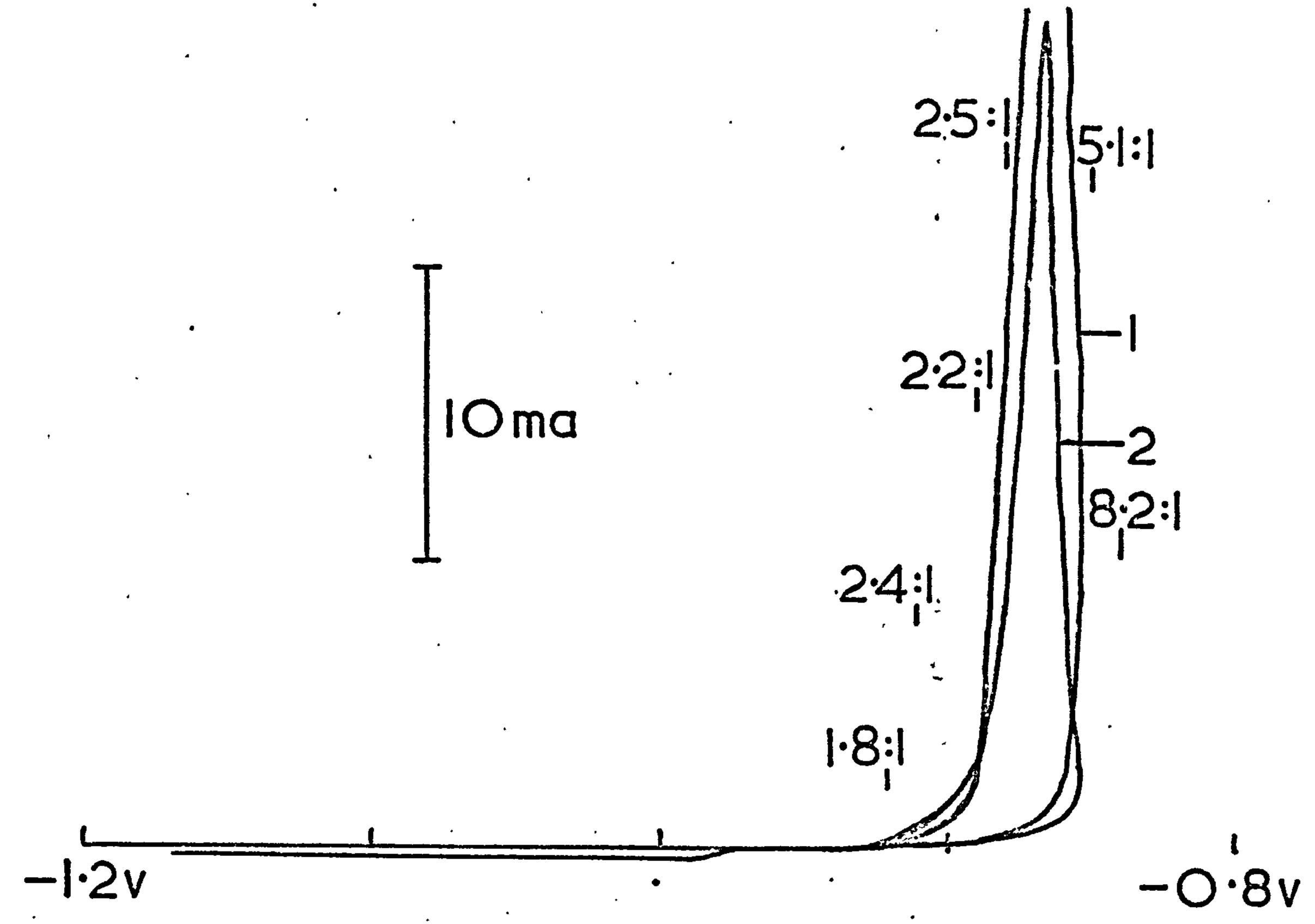

Fig. 6.7a I vs E for Electropolished Pb in IM H_2SO_4 showing rotation speed dependence and $Q_A : Q_C$

Fig. 6.7b I vs E for Electropolished Pb in 1M H_2SO_4
at RDE where ω = a 40rps
b 0 rps
c 64rps

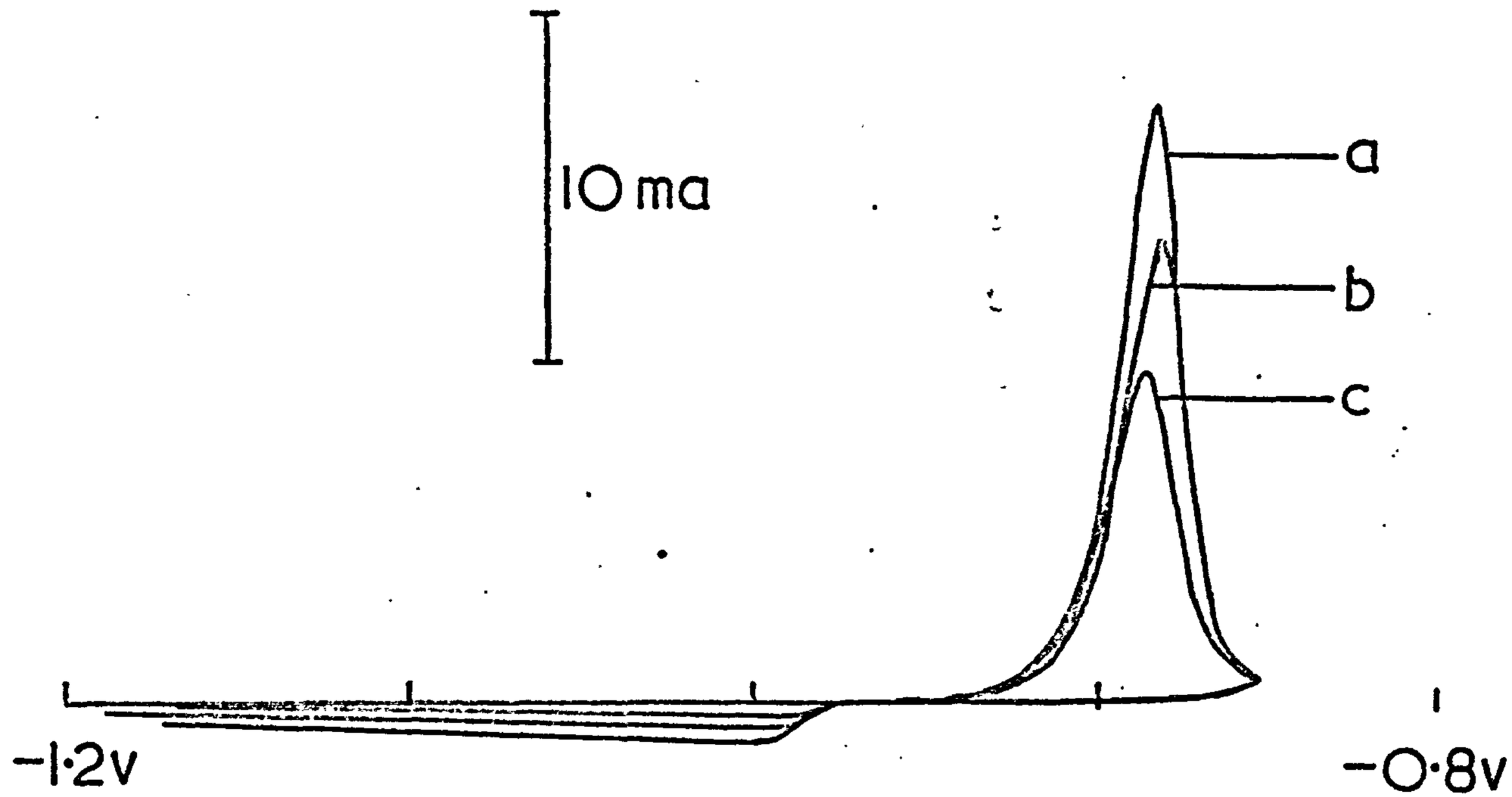

FIG.6.8 LOG CURRENT vs E FOR MECHANICALLY POLISHED Pb FROM SWEEP MEASUREMENTS

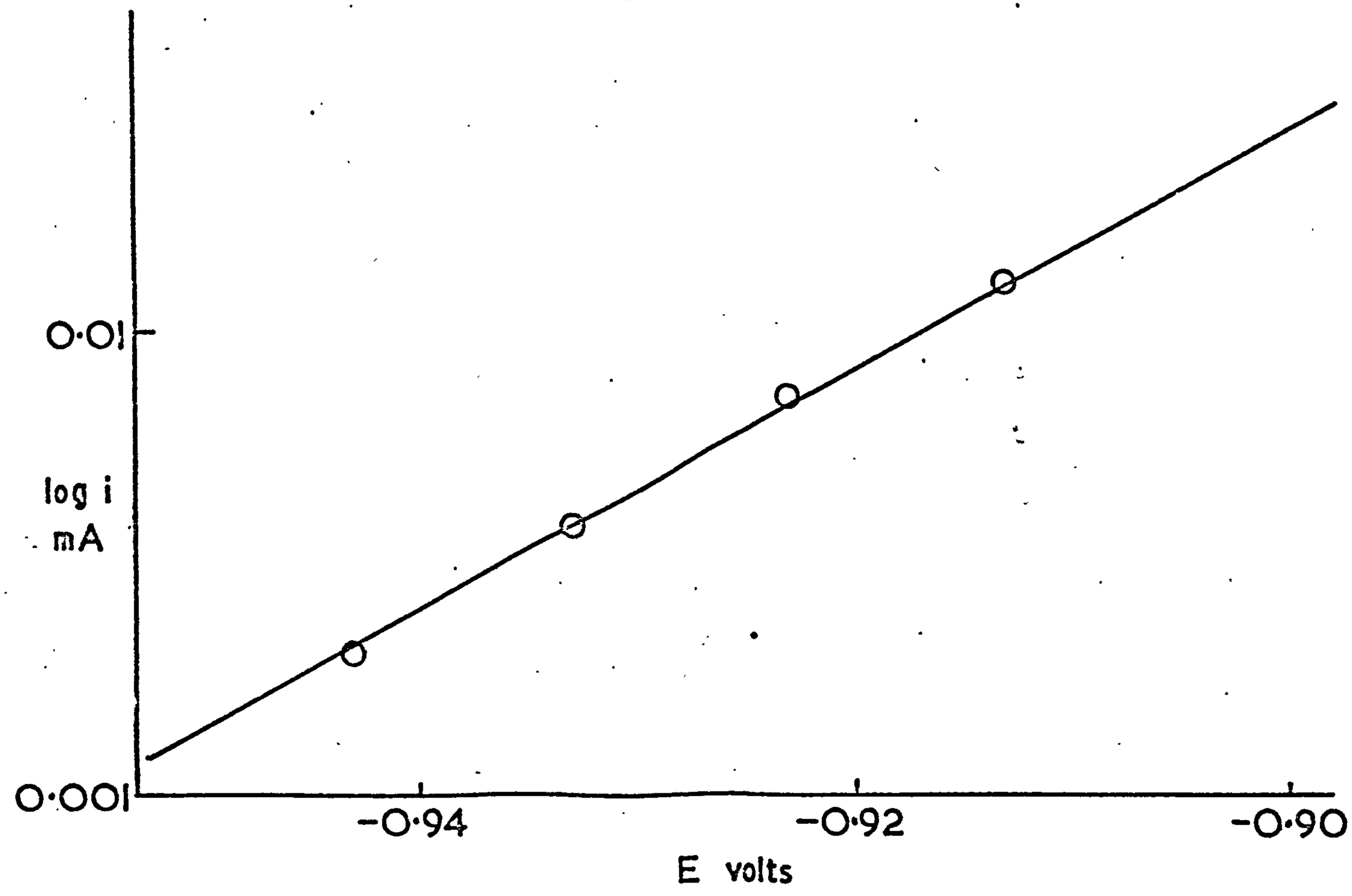

The electropolished curves, Figures 6.6, 6.7a,b, are similar in potential behaviour, but different in some important respects. Figures 6.6 and 6.7b are rotation speed dependent. Figure 6.6 has a cathodic peak which disappears on rotating. Figure 6.7a,b, have only a small cathodic return peak and Figure 6.7a is less sensitive to the number of sweeps than Figure 6.4. It is extremely rotation speed dependent.

6.3.2. Potential Pulse

Figures 6.10, 6.11 show the results for mechanically and electropolished electrodes respectively. The results of Figure 6.10 are typical of a nucleation and growth process. The transients rise linearly with time. An interesting feature is that the charge going into the oxidation is not recovered in the corresponding cathodic transient.

The results of Figure 6.11 fit more closely a diffusion controlled dissolution process. A plot of i vs $t^{-\frac{1}{2}}$, Figure 6.12, shows that the pulse response of Figure 6.11 is completely diffusion controlled at all potentials, according to

$$i = nFAC_o^s \sqrt{\frac{D\epsilon}{\pi t}} \qquad (6.1)$$

The slopes of Figure 6.12 plotted as log i vs E at 5 mS is shown in Figure 6.13. with a 30 mV Tafel slope. The potential dependence of the gradients of Figure 6.10 show a Tafel slope of 25 mV (Figure 6.14), which is reasonably near to 30 mV/decade. This shows that C_o^s increased ten-fold in 30 mV suggesting that the species, O , at concentration C_o^s , is formed in a 2e reversible process. A further test can be made on Figure 6.12.

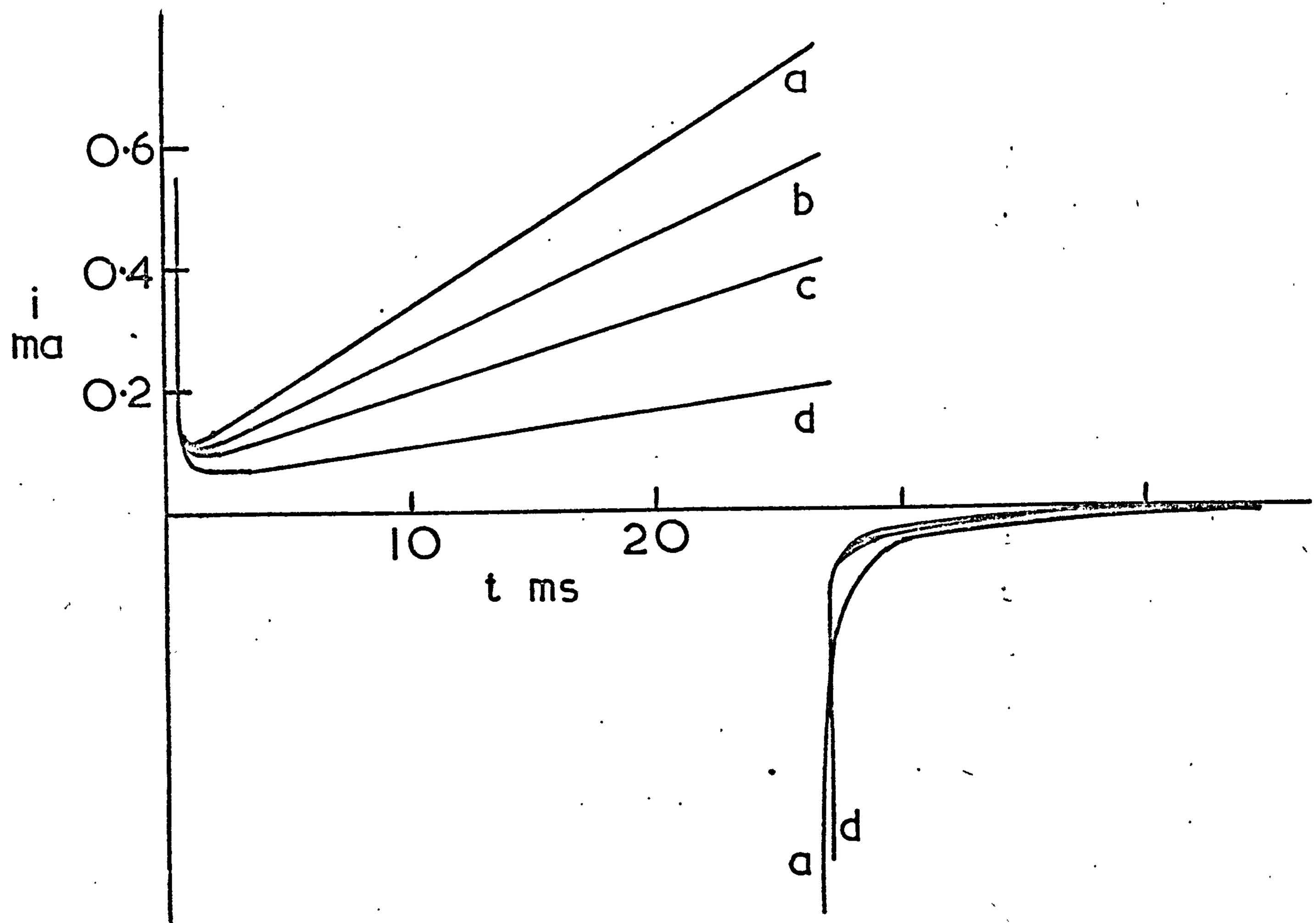

Fig.6.10 Potentiostatic measurements on mechanically polished Pb showing i vs t

Fig.6.11 Potentiostatic measurements on electropolished Pb showing i vs t

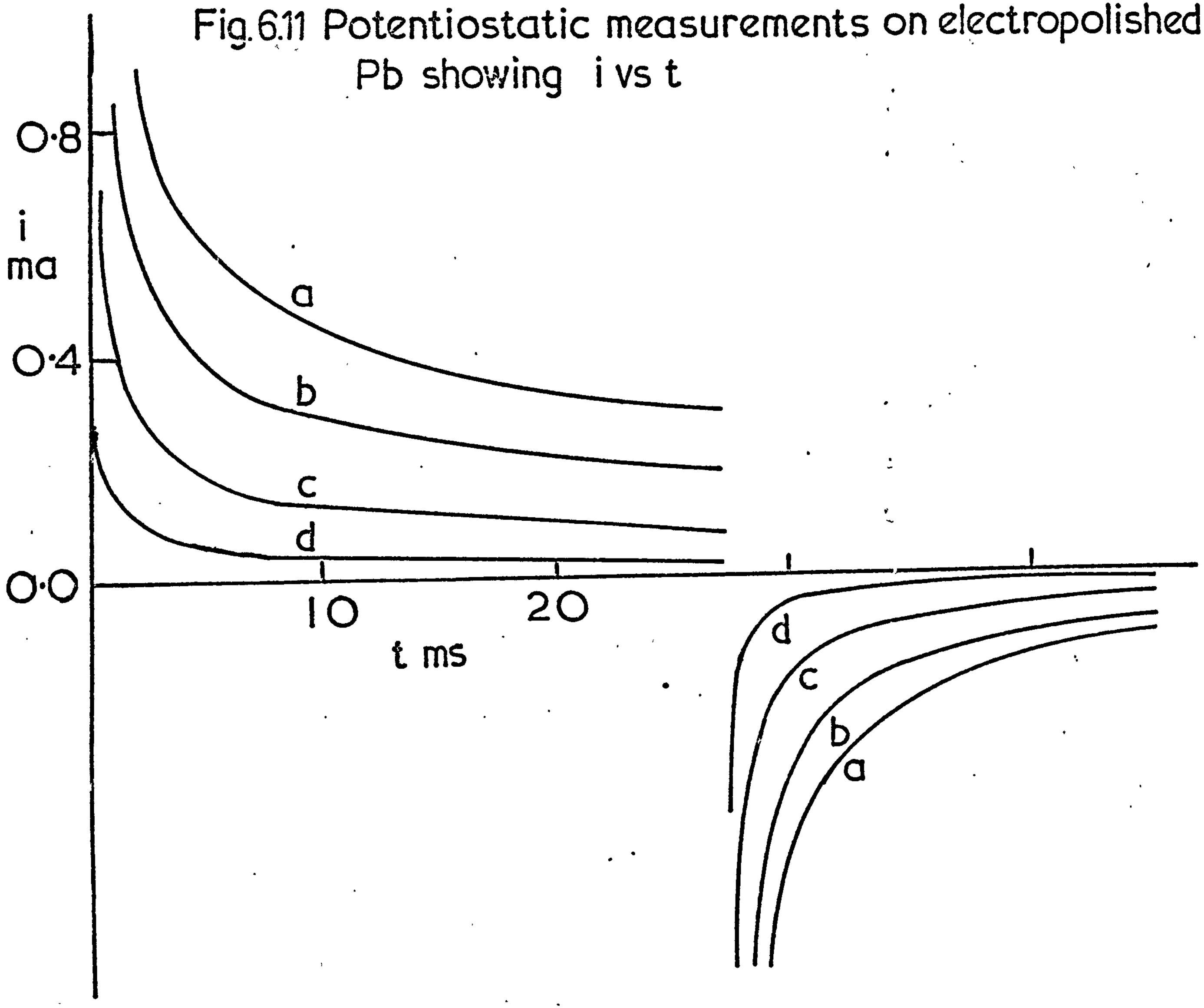

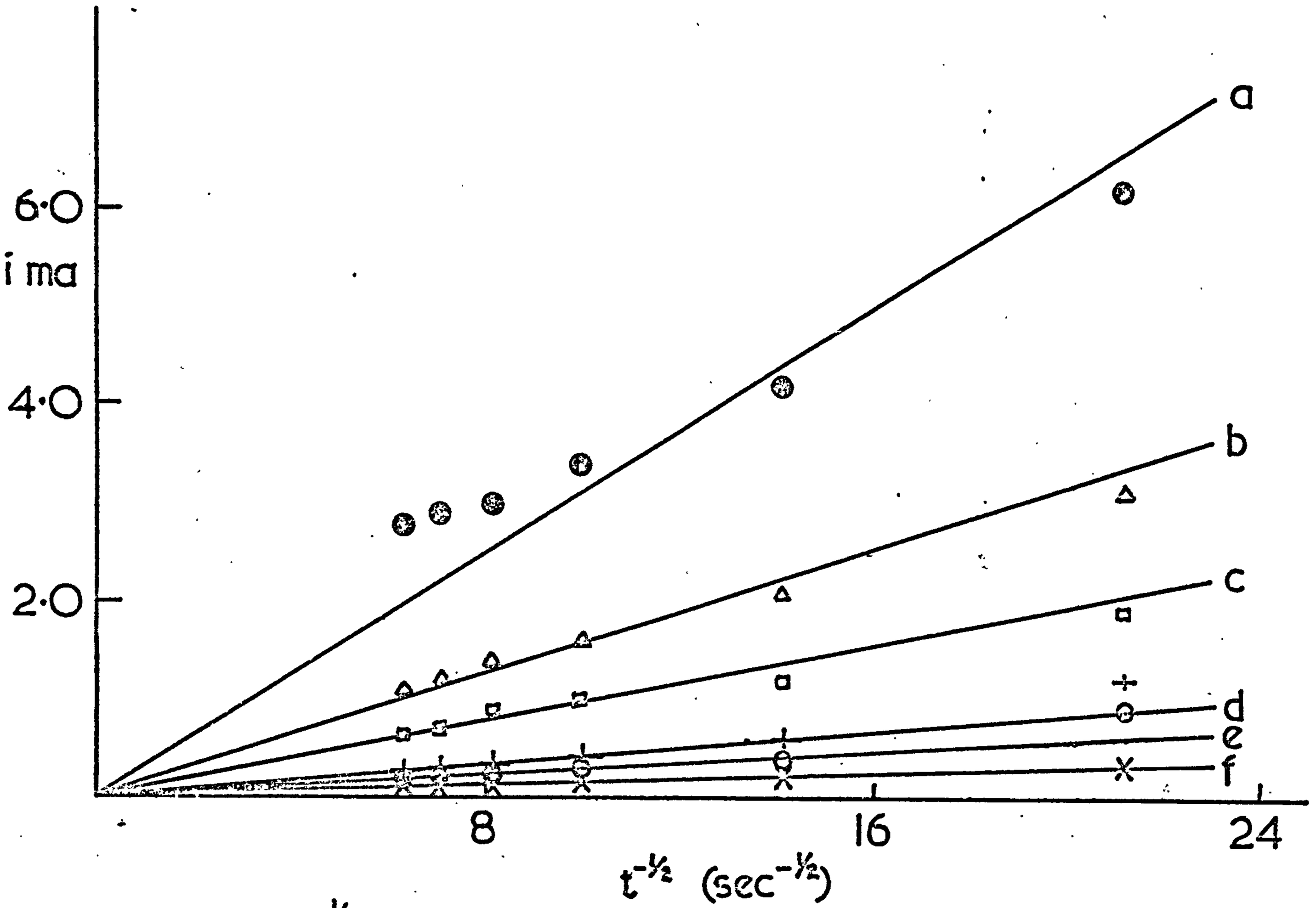

Fig.6.12 i vs $t^{-1/2}$ plot of electropolished Pb taken from potential pulse experiments

Fig. 6.13 Log i vs E for Pb in 1M H_2SO_4

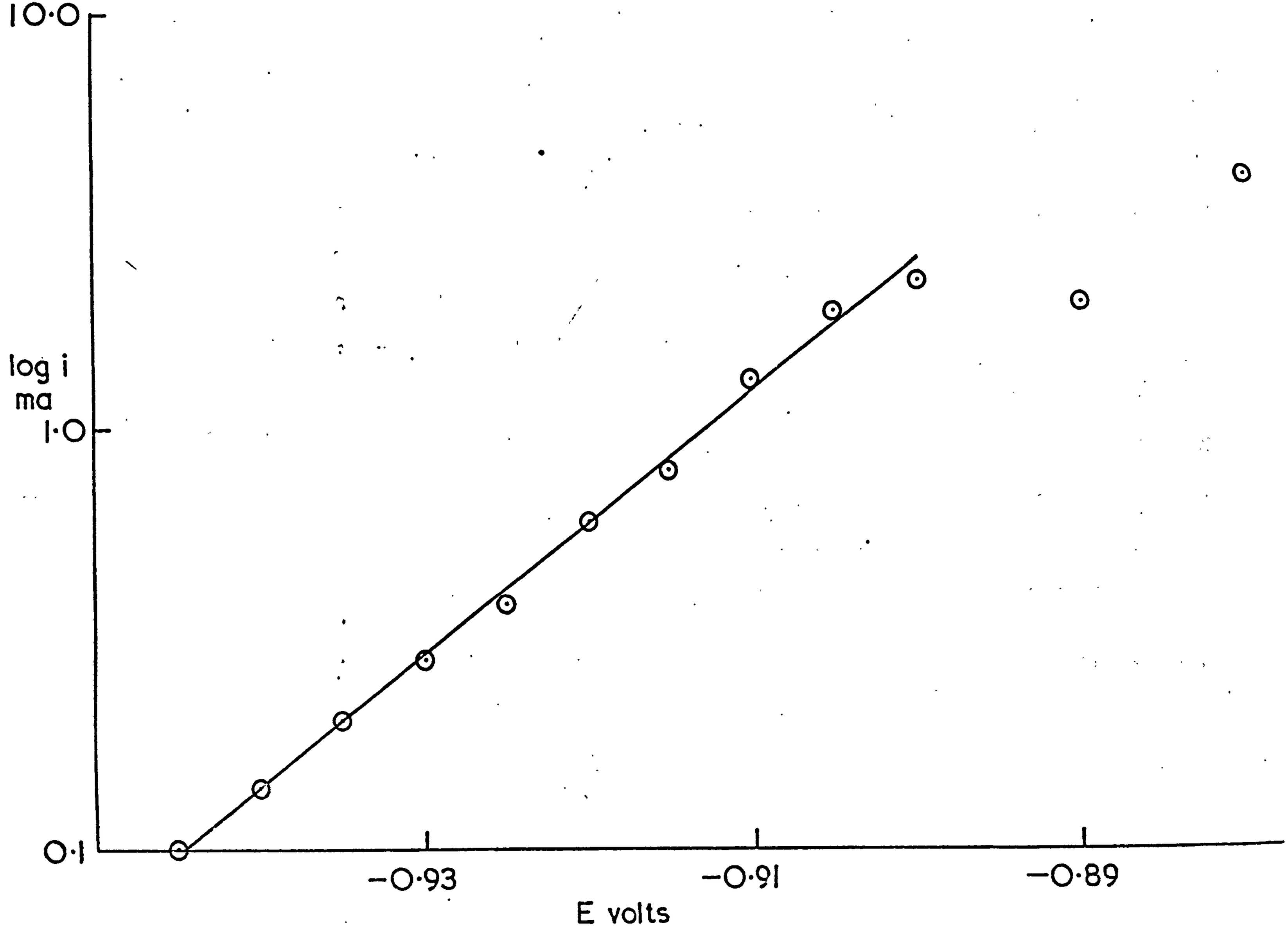

FIG.6.14 LOG CURRENT vs E FOR MECHANICALLY POLISHED Pb

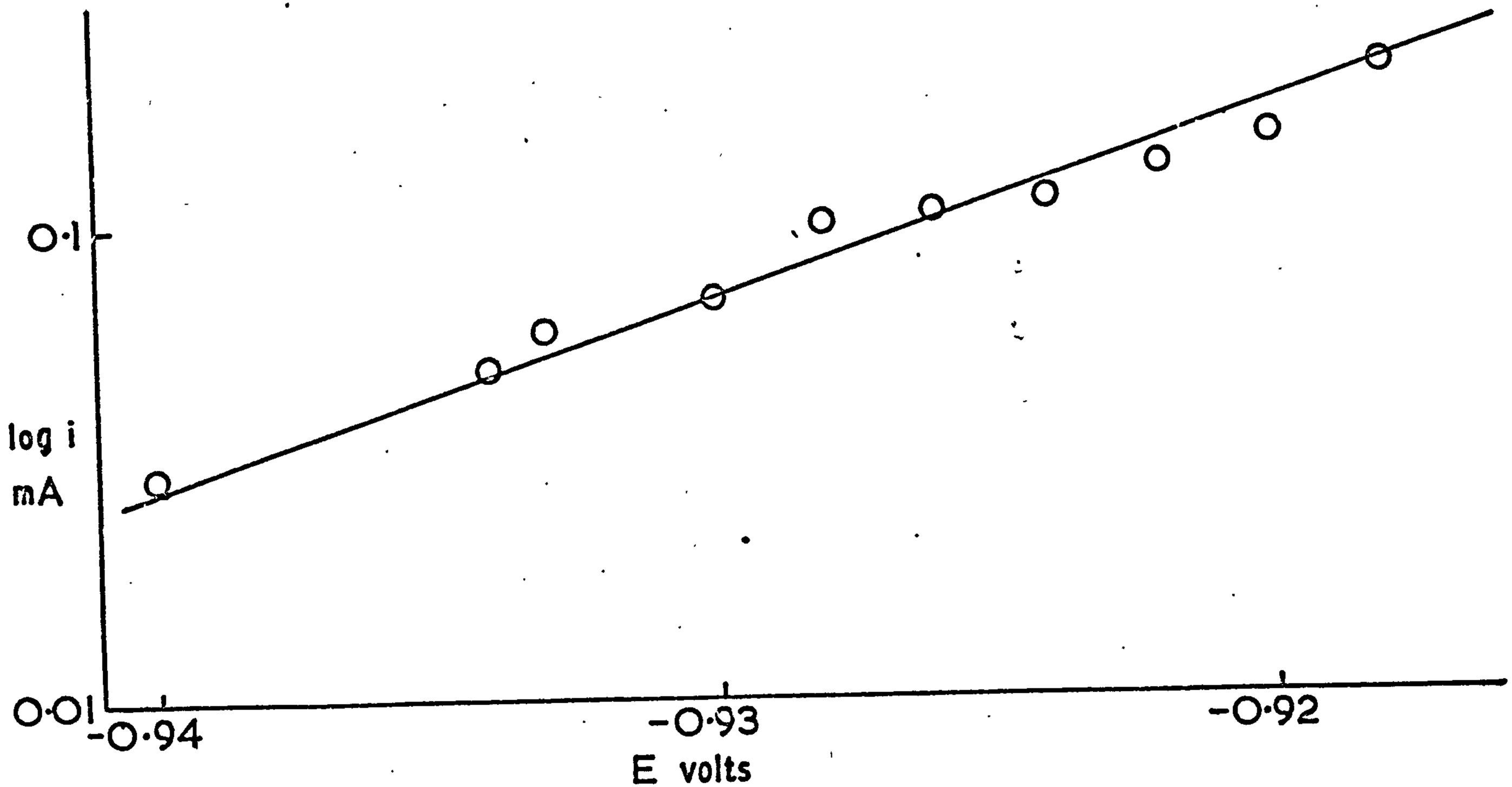

If O is formed reversibly and does not undergo chemical reaction in the diffusion layer the amount of charge passed anodically, Q_a, should be greater than the recovered cathodic charge, Q_c , at equal times of anodic and cathodic polarisation in the ratio[1]

$$\frac{Q_a}{Q_c} = 1.71 \qquad (6.2)$$

A more accurate method is to compare the currents at equal times[2]. The two methods give the same result which is summarised in Figures 6.4 and 6.7. On the mechanically polished surface only a small amount of charge is recovered, and on the electropolished the theoretical amount. Clearly in Figure 6.7 the Pb dissolves freely into solution until the maximum is traversed. This is not the case in Figure 6.4.

The measurements so far suggest that Pb dissolves freely into solution under some conditions. In addition a $PbSO_4$ layer is formed by a solid state reaction which blocks off the Pb surface. The fact that Pb dissolves anodic to the $Pb/PbSO_4$ potential suggests in addition a solution precipitation reaction mechanism for forming $PbSO_4$.

In order to follow these matters in more detail especially at low potentials, rotating disc and ring-disc measurements have been carried out.

6.3.3. Rotating disc at short time

Potentiostatic current-time transients were measured at the rotating Pb disc. Typical results are shown in Figure 6.15. On the diagram are shown the corresponding ring response, which will be considered later. The measurements were carried out by a potentiostatic pulse, 3 seconds long, in order to avoid major dissolution of the Pb disc.

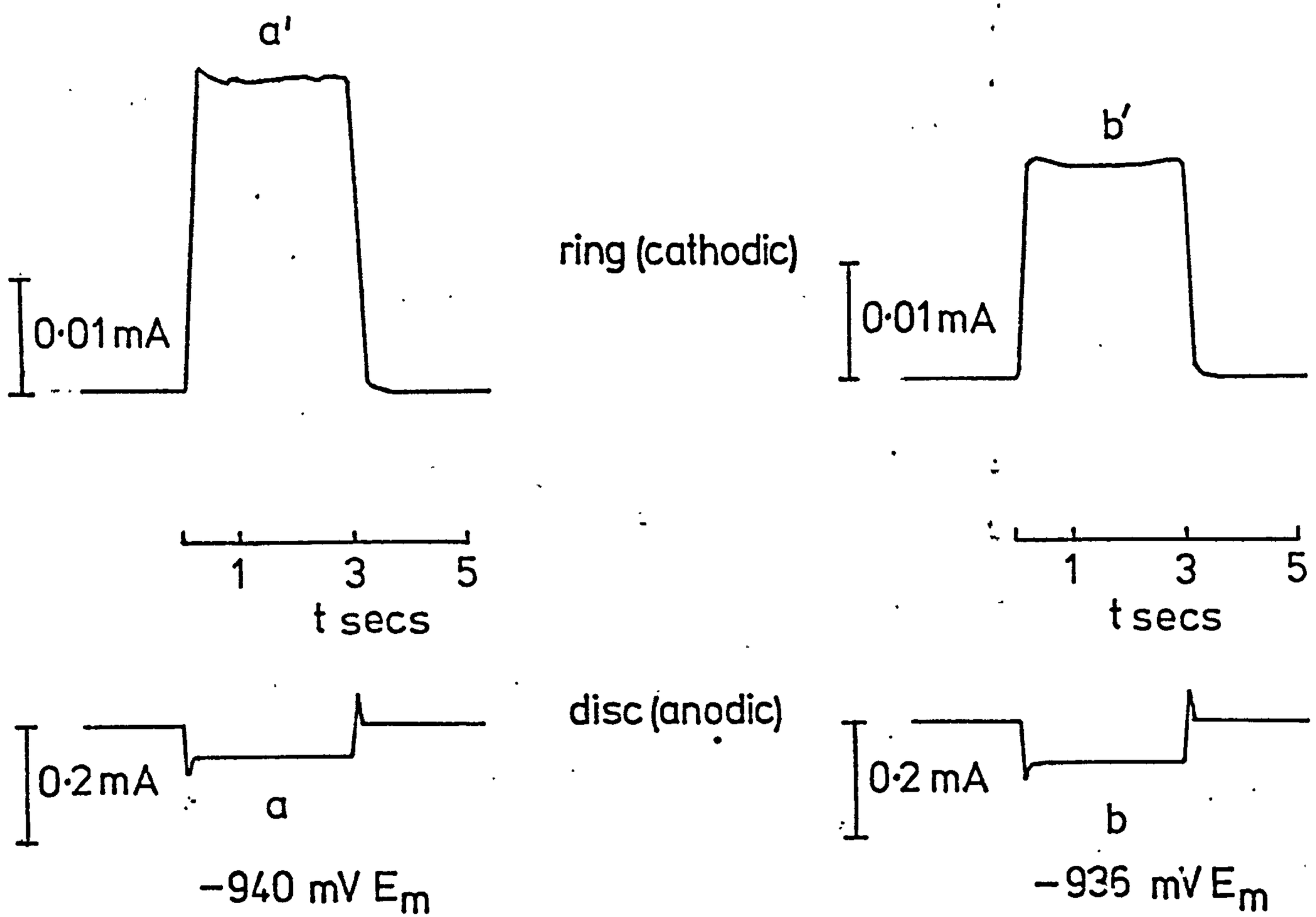

FIG. 6.15 i vs t ON MECHANICALLY POLISHED RING–DISC ELECTRODE, N_{calc} = 0·57, ω = 24 Hz.

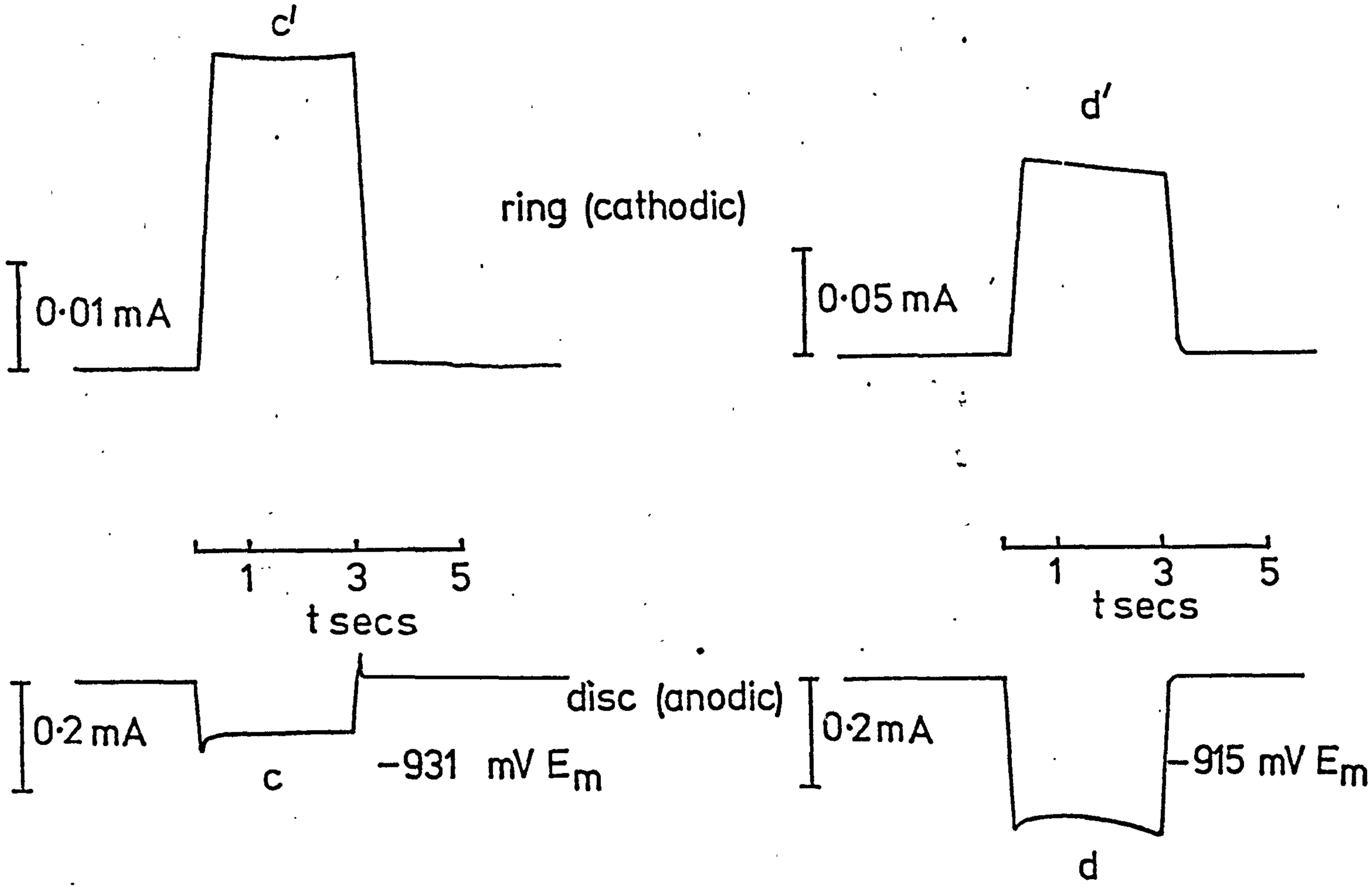

FIG. 6.15 i vs t ON MECHANICALLY POLISHED RING–DISC ELECTRODE, N_{calc} = 0·57, ω = 24Hz.

Longer time transients are more complex and are shown in Figures 6.22 and 6.23. At potentials more cathodic than E_m = -915 mV the current is steady. At potentials more anodic to this potential a rising transient, Figure 6.15d, is observed. However even at potentials well anodic to E_m = -915 mV at short times a flat portion is observed. At potentials cathodic to E_m = -945 mV on the other hand, the current is steady for hours. Figure 6.16 shows the flat current region plotted against potential. The curve is linear up to the point where the rising transient begins to interfere and then the current rises above that expected from more cathodic potentials. Figure 6.17 shows current-voltage curves obtained by plotting the flat portion against potential for various solutions at fairly small overpotentials. The potential scale is now against the standard hydrogen electrode (E_h). Conversions to the standard hydrogen scale, E_h, were effected as described in the previous chapter. The curves have a 30 mV slope and are strongly dependent on the anion. The difference in viscosity between the solutions and its effect on the diffusion coefficient is not sufficient to account for the difference in currents. The rotation speed dependence of the dissolution currents at fixed potential, Figure 6.18, shows typical reversible behaviour. i_D^{-1} vs $\omega^{-\frac{1}{2}}$ is a straight line going through the origin. The accuracy of this plot is not high as shown by the error at the origin.

In order to obtain the most reproducible results, Figure 6.18, a single electrode with one surface treatment must only be used at small overpotentials. Results on different electrodes on different days show a large scatter. The reason for this is the soft nature of Pb. Polishing material sticks in it (as shown by scanning microscope and Edax investigation), and the surface probably ripples and smears. Figure 6.16

FIG. 6.16 TAFEL PLOT i vs E_m, ω = 15 Hz, MECH. POL.

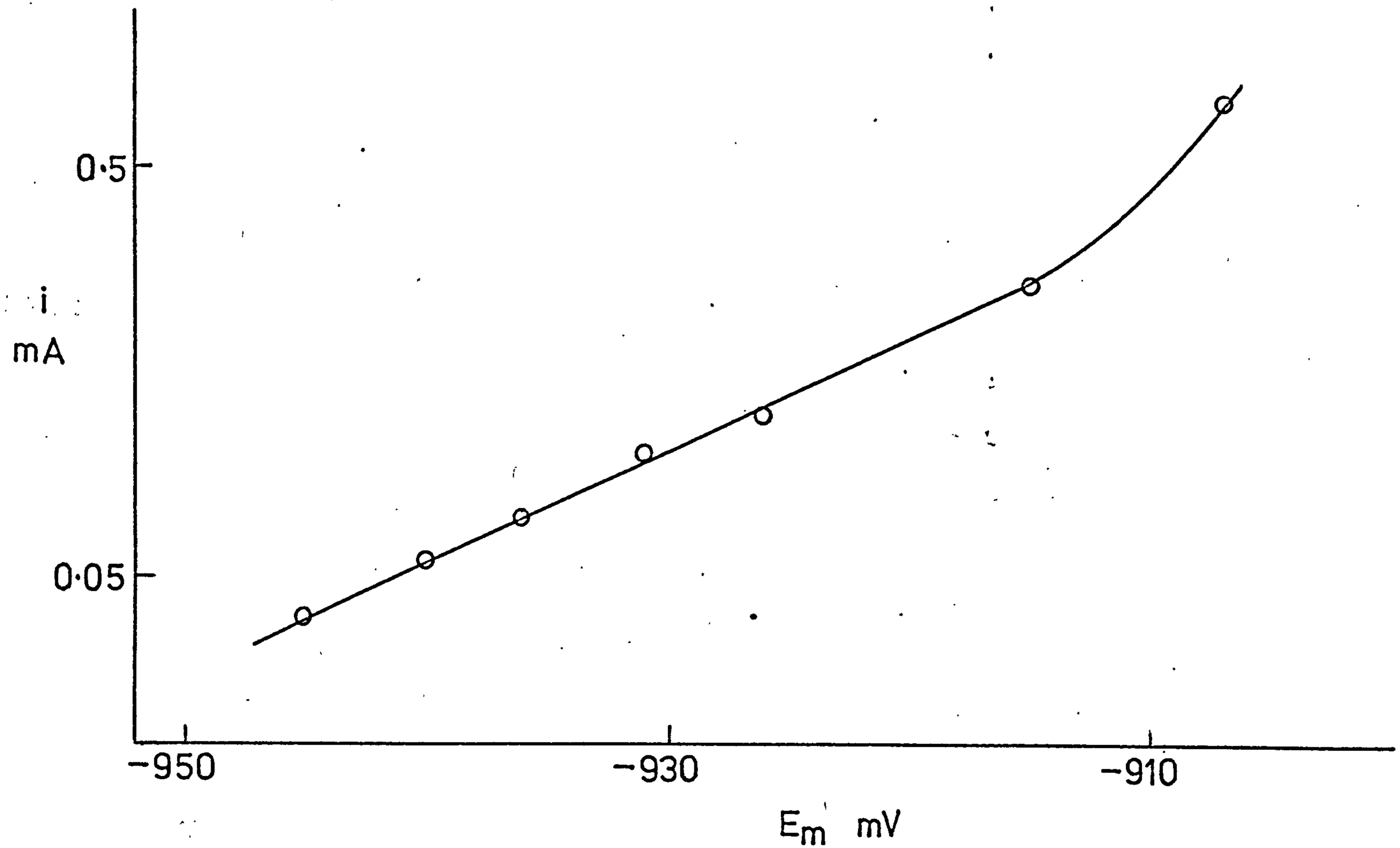

FIG. 6.17 TAFEL PLOT i vs E_h, ω = 15 Hz.

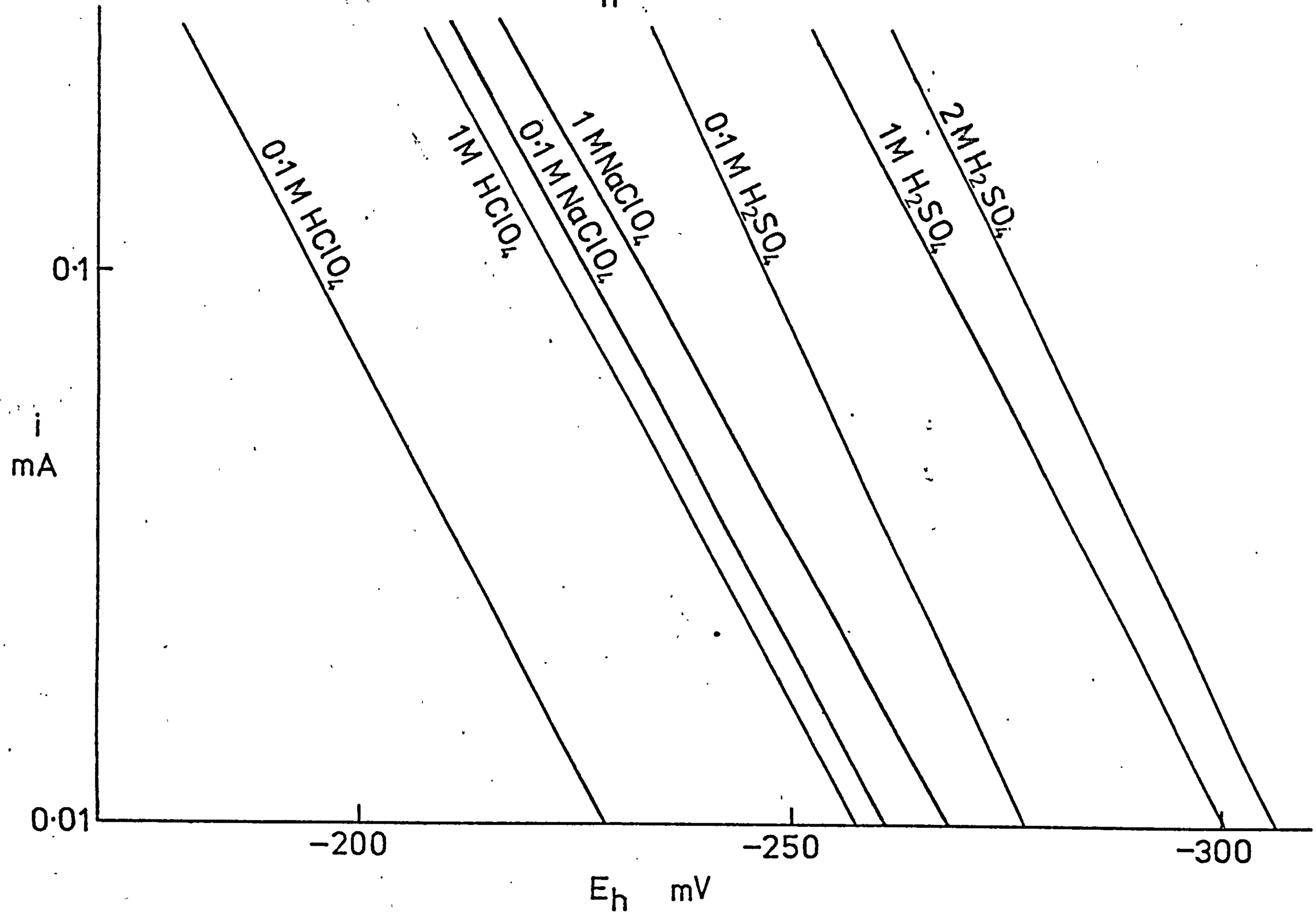

FIG. 6.18 i^{-1} vs $t^{-1/2}$ AT DIFFERENT POTENTIALS.
a −945, b −940, c −935, d −930, mV E_m.
MECHANICALLY POLISHED.

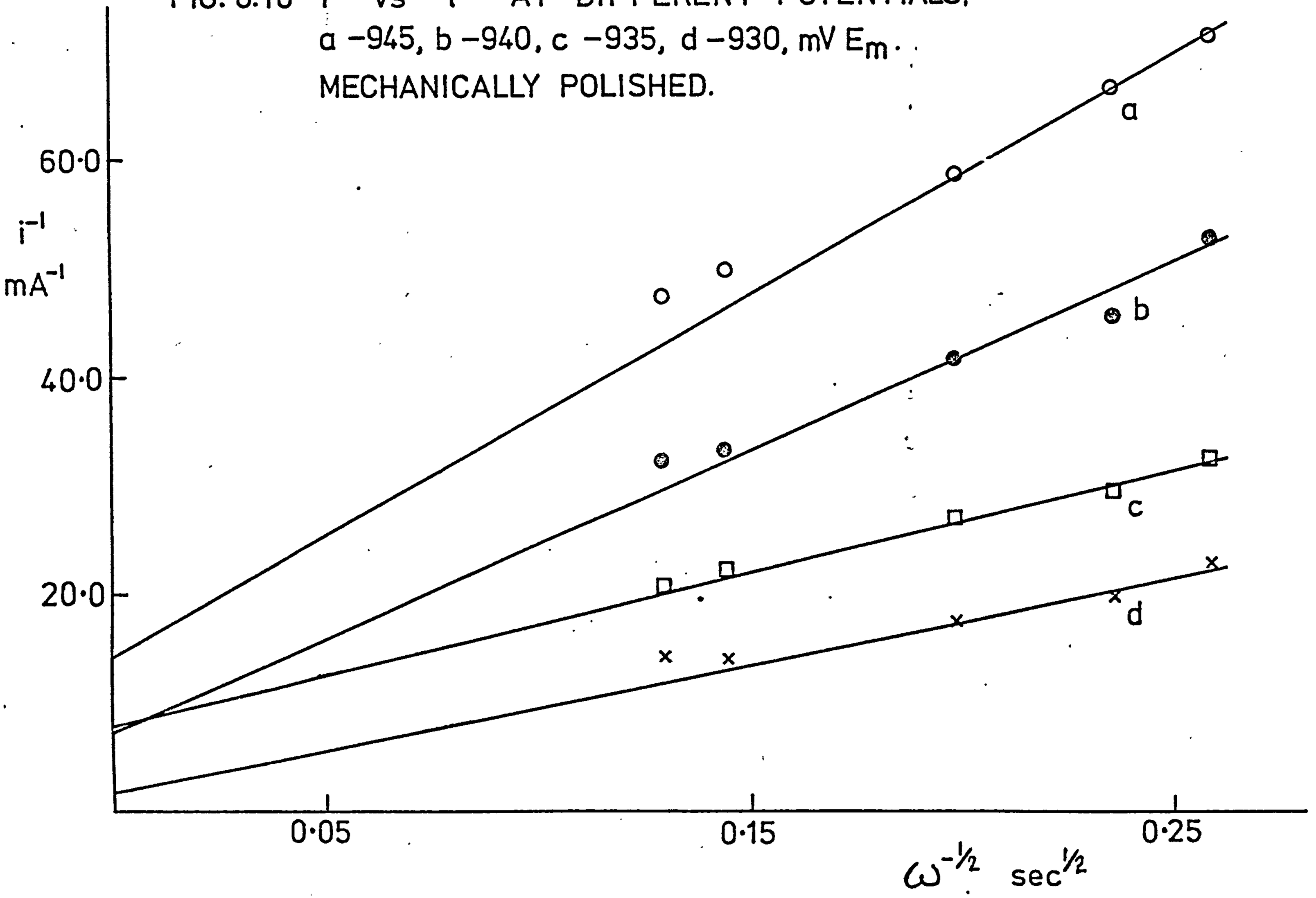

shows that at more anodic potentials some current in addition to a simple dissolution reaction is flowing into the interface.

The curves of Figure 6.17 are compatible with solubility data[3,4,5]. The total soluble Pb species in equilibrium with $PbSO_4$ in 1.0M H_2SO_4 amount[3] to 2.2×10^{-5} M. A similar concentration can be calculated from Figure 6.17. The extrapolated dissolution current at the $Pb/PbSO_4$ potential (E_h = -307 mV) corresponds to a 1.22×10^{-5} M. concentration of Pb^{2+} containing species. The effective diffusion coefficient was assumed to be 9×10^{-5} cm^2 sec^{-1}. The actual value of D was calculated by comparing potentiostatic transients (Figure 6.12) where $i \propto C_o^s D_E^{\frac{1}{2}} t^{-\frac{1}{2}}$ and the rotating disc current at the same potential $i \propto C_o^s D_E^{\frac{2}{3}}$. Effective diffusion coefficients, D_E, calculated in this way are not very accurate and depend somewhat on potential. In 1M H_2SO_4, $D_E = 6 \times 10^{-5}$ cm^2 sec^{-1}, at E_m = -945 mV, and $D_E = 9.5 \times 10^{-5}$ cm^2 sec^{-1} at E_m = - 920 mV.

The disc currents of Figure 6.17 depend on concentration of the anion. This suggests that dissolution proceeds via a complex in addition to the simple ion. For examples at a potential of E_m = -965.3 mV (vs Hg_2SO_4 in 1M H_2SO_4 solution) the concentration of Pb^{2+} calculated from the Nernst equation

$$E = E^\circ + \frac{RT}{nF} \ln a_{Pb^{2+}} \qquad (6.3)$$

is 1.0×10^{-5} M, $PbSO_4$ is 1.9×10^{-5} M ($K_1 = 10^{2.62}$), and $Pb(SO_4)_2^{2-}$ is 5.1×10^{-6}M ($K_2 = 10^{0.85}$)[6,7]. The activity coefficients γ of Pb^{2+} and SO_4^{2-} in 1M H_2SO_4 were assumed equal and were 0.13, calculated by the extended Debye-Huckel equation[8],

$$\log \gamma = \frac{-A |Z^2| \sqrt{I}}{1 + Ba\sqrt{I}}$$

where A and B are constants which involve the absolute temperature and the dielectric constant of the solvent. A was assumed to be 0.5115 and B 0.3291 (Ref. 8). a is the ion size parameter assumed to be equal to 4.5 Å (Ref. 8) and I the ionic strength is assumed equal to 1.56 for 1M H_2SO_4. The ion mobilities are found in Ref.8. It is assumed that the Debye-Huckel equation is appropriate. It is striking that these concentrations are of similar magnitude in the potential region of interest. Figure 6.17 can be interpreted for the reaction

$$M + X - e \begin{cases} \nearrow MX^+ \xrightarrow{D_2} \\ \searrow M^+ \xrightarrow{D_1} \end{cases} \quad \text{with } K_1 \tag{6.4}$$

where the dissolving species are in chemical equilibrium by

$$i = \frac{nFAD_1C_1^s}{\delta_1} + \frac{nFAD_2C_2^s}{\delta_2} \tag{6.5}$$

where

$$\delta_1 = 1.61\,\nu^{1/6} D_1^{1/3} \omega^{-1/2}$$

and C_1^s is the surface concentration of M^+. Equation (6.5) gives

$$i = \frac{nFAC_1^s\left(D_1^{2/3} + D_2^{2/3} K_1 a_x\right)\omega^{1/2}}{1.61\,\nu^{1/6}} \tag{6.6}$$

where $a_{X^-} = \gamma_{X^-} C_{X^-}$ is the activity of the anion in solution. It is assumed that the activity coefficients of MX^+ and M^+ are equal. Figures 6.19 and 6.20 show a plot at fixed potential and fixed ω of i vs a_X for H_2SO_4, $NaClO_4$ and $HClO_4$ according to equation (6.6). The calculated activity coefficient does not change greatly over the concentrations investigated so a plot against concentration has a similar form. The intercept gives D_1 alone if C_1^s is calculated from the Nernst

FIG. 6.19 i vs a_x, E_h = −235 mV. MECH. POL. ω = 15 Hz.
a, x = ClO_4^- IN $HClO_4$
b, x = ClO_4^- IN $NaClO_4$
TAKEN FROM FIG. 6.17.

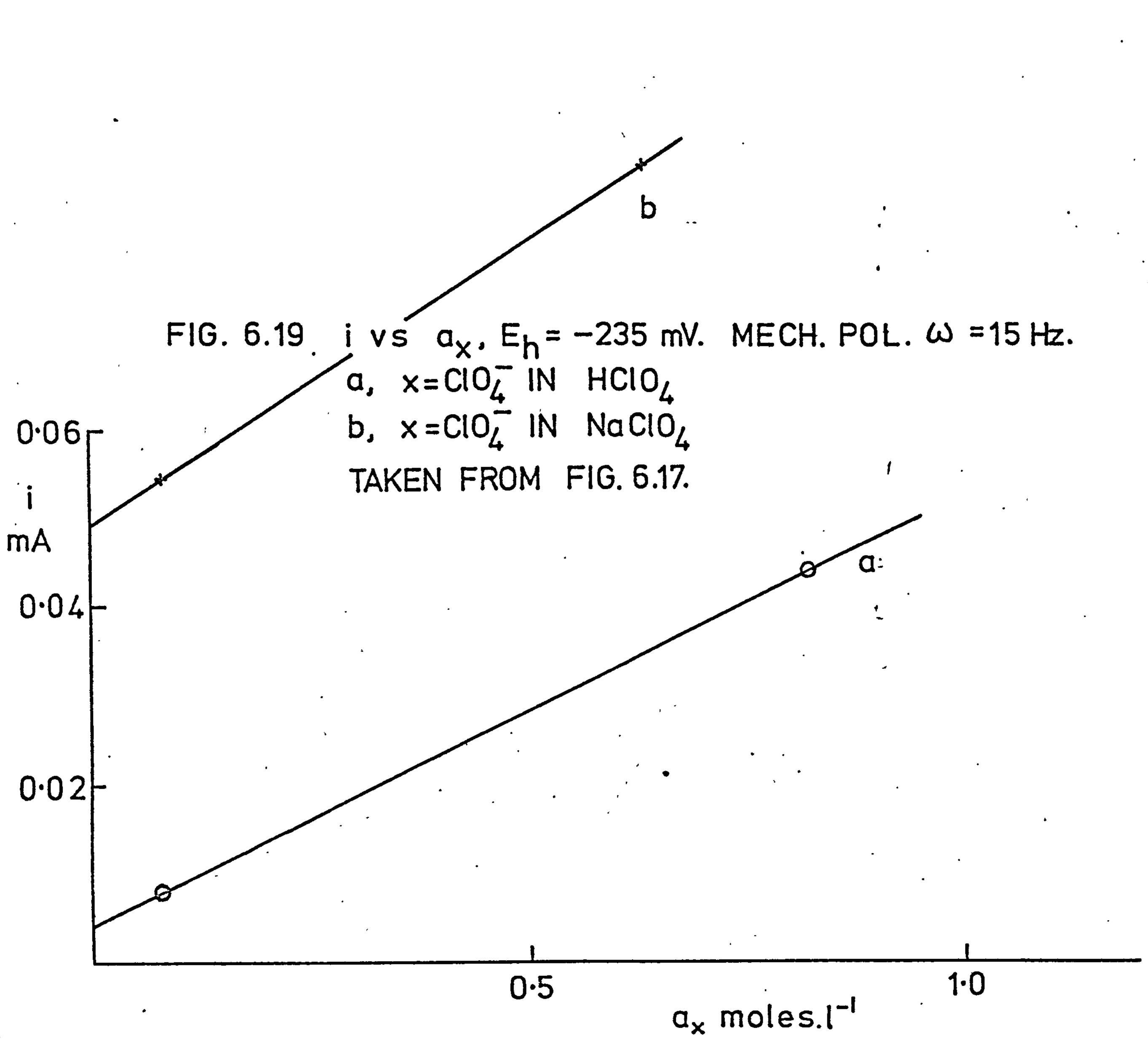

FIG. 6.20 i vs a_x FROM FIG. 6.17 FOR VARIOUS POTENTIALS, x IS $SO_4^=$ IN H_2SO_4 MECH. POL., ω = 15 Hz.

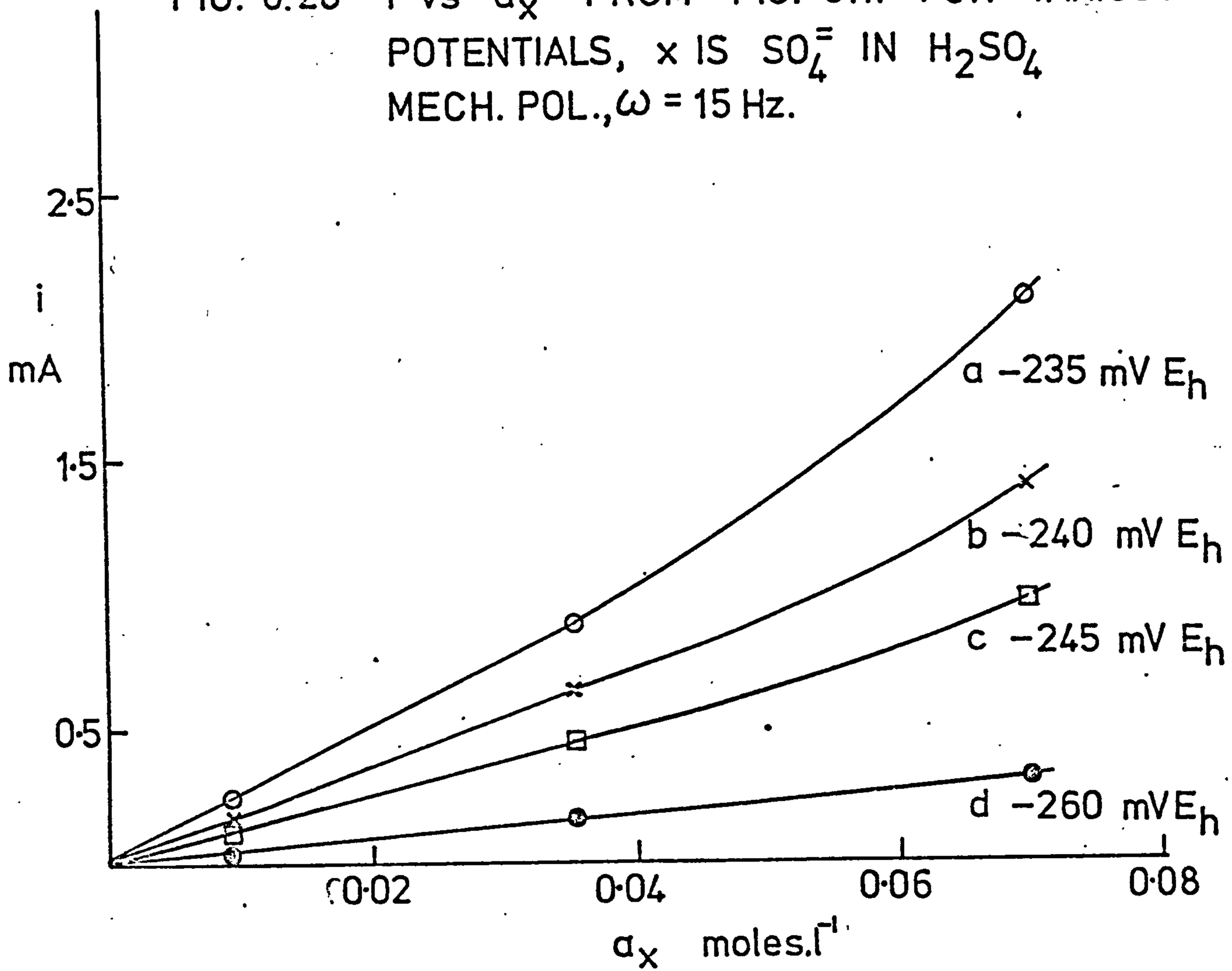

equation using the activity coefficient of 0.13 previously calculated. The points of Figures 6.20 do not lie on straight lines because of the variation of activity a_1, of Pb^{2+}, with ionic strength. A further possibility is that at the higher concentrations $Pb(SO_4)_2^{2-}$ formation begins to be important. It is difficult to decide between these possibilities. A more satisfactory procedure would be to use a large excess of inert electrolyte and plot concentration in Figures 6.19, 6.20 except for the problem of finding a truly inert electrolyte. K_1 can be estimated from the slope and intercept at low concentrations, if D_1 and D_2 are equal. This can be little more than an estimate;

$$(K_1)_{H_2SO_4} = 10^2\ l\,m^{-1}$$

and

$$(K_1)_{NaClO_4} = 0{\cdot}45\ l\,m^{-1}$$

where K_1 is the equilibrium constant for

$$Pb^{2+} + X^- \rightleftharpoons PbX^+ \qquad (6.7)$$

$(K_1)_{H_2SO_4}$ compares favourably with the literature[6] values at zero ionic strength of $K_1 = 10^{2.62}$, $10^{3.7}$, and the latest[7] value of $10^{2.4}$. $(K)_{NaClO_4}$ is not in the literature but it is of the correct order. (Approximate values for other ions at zero ionic strength are[6,7] $(K_1)_{I^-} = 10^{1.92}$, $(K_1)_{Br^-} = 10^2$, $(K_1)_{Cl^-} = 10^{1.92}$, $(K_1)_{F^-} = 10^{0.78}$). A value of $D_1 = 18 \times 10^{-5}\ cm^2\ s^{-1}$, that is for Pb^{2+} ions alone is calculated from the intercept of Figure 6.19 in $NaClO_4$ solution. Measurement of the intercept is not very exact, however it can be seen, Figure 6.20 that

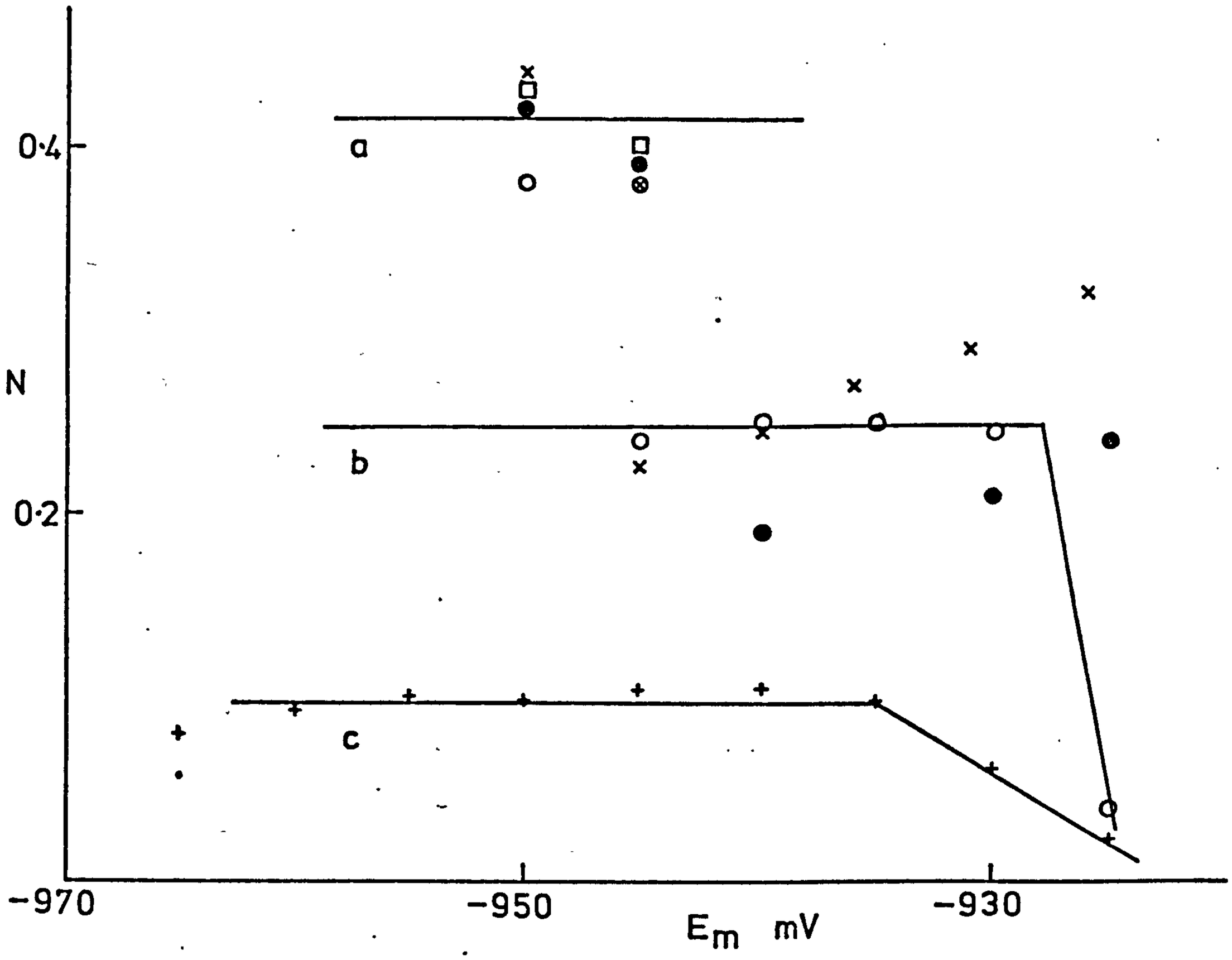

FIG. 6.21 COLLECTION EFFICIENCY, N_{expt} vs E FOR VARIOUS ROTATION SPEEDS. a, FRESHLY MECH: POL. ELECTRODE, N_{calc} = 0·57. (×) 12, (●) 36, (□) 18, (○) 48 Hz. b, MECH. POL. ELECTRODE BUT HAVING BEEN EXPOSED TO POTENTIALS ANODIC TO −935 mV E_m. (×), N_{calc} = 0·57, 24 Hz; (●) N_{calc} = 0·49, 7½ Hz; (○) N_{calc} = 0·45, 15 Hz; c, ELECTROPOLISHED, N_{calc} = 0·48, 15 Hz.

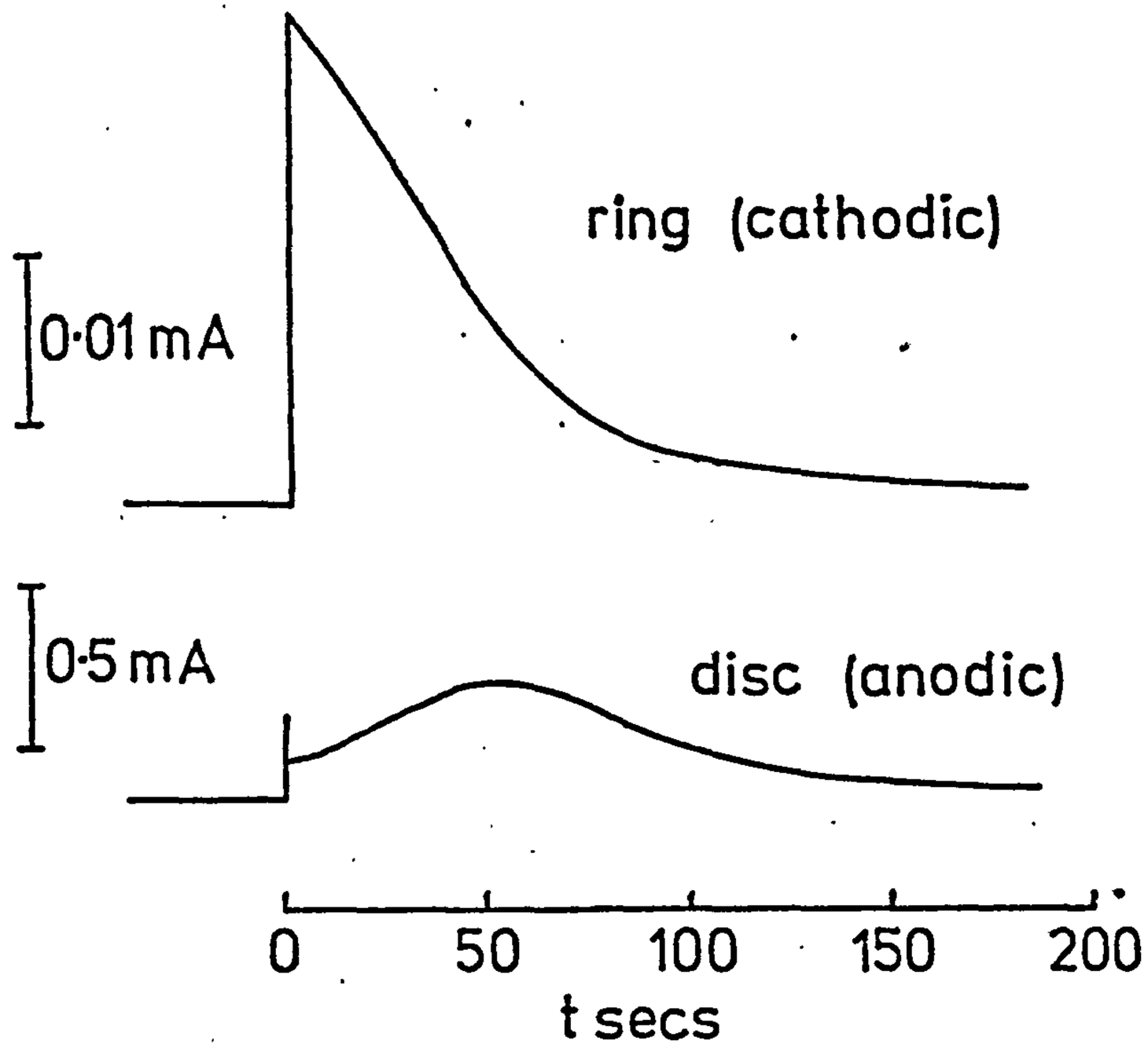

FIG. 6.22a i vs t FOR RING DISC ELECTRODE, $N_{calc} = 0{\cdot}49$.
MECH. POL. $\omega = 7\frac{1}{2}$ Hz, $E_m = -925$ mV.

FIG. 6.22b i vs t FOR Pb DISC
IN 1M H_2SO_4 (UNSTIRRED)

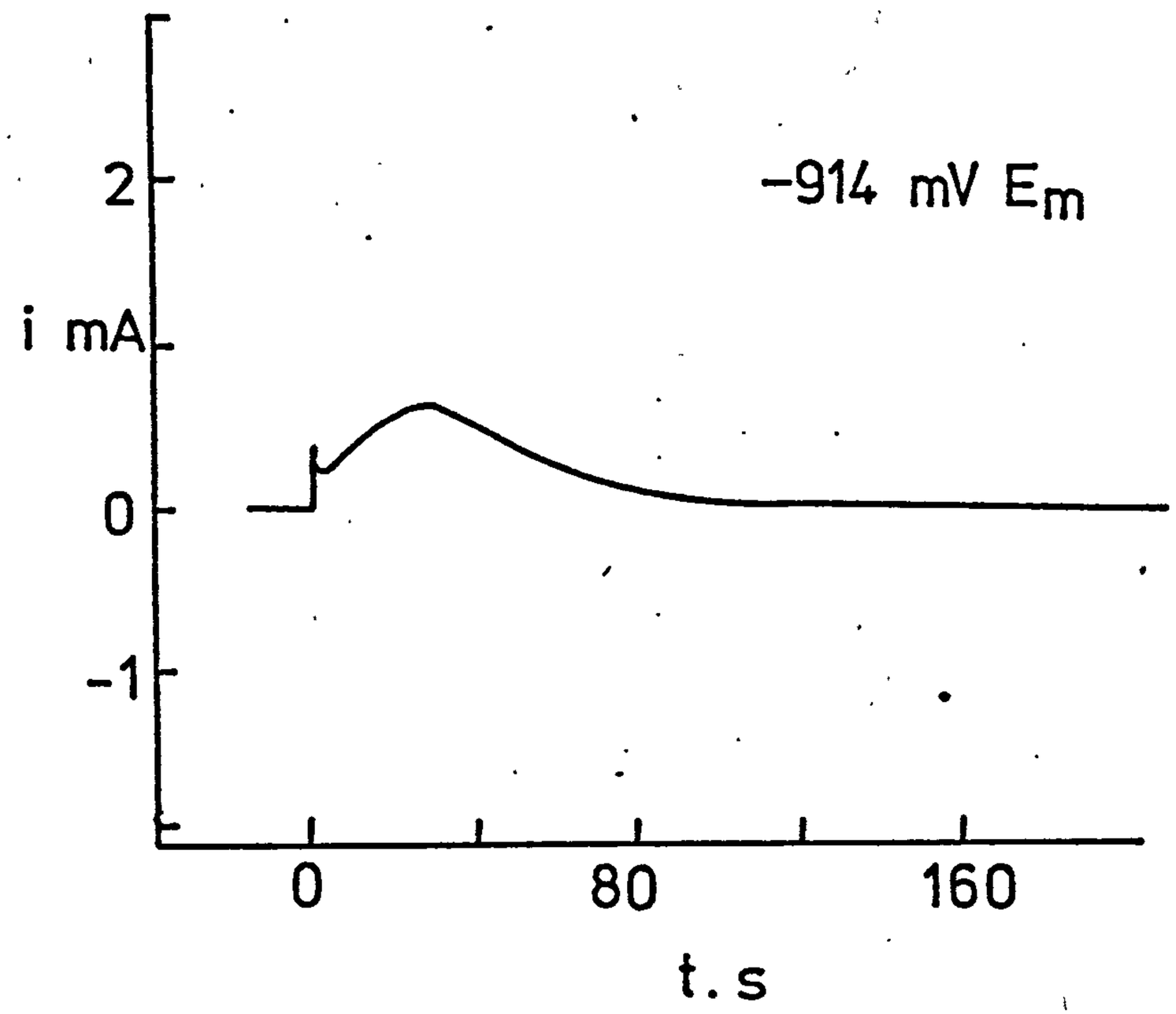

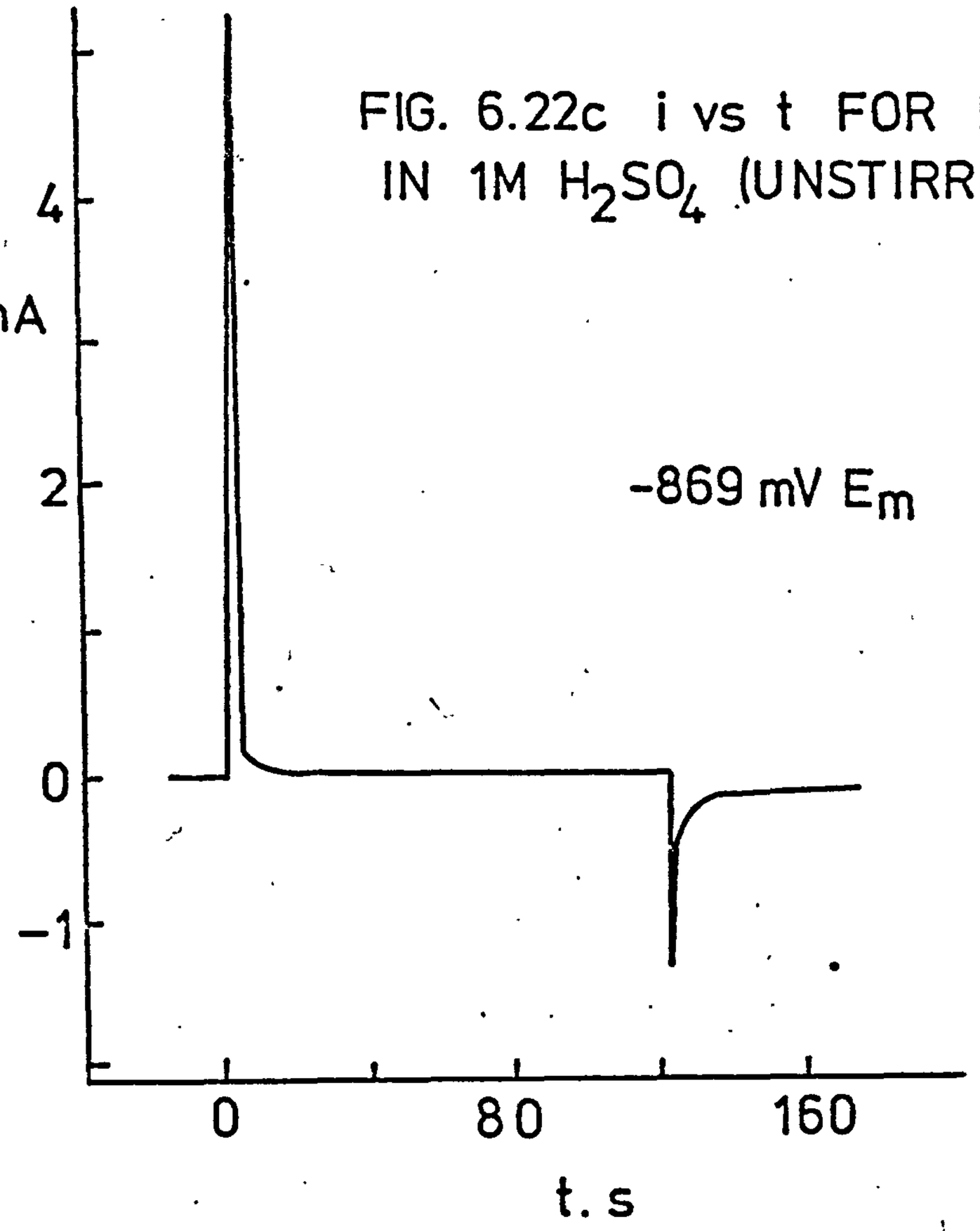

FIG. 6.22c i vs t FOR Pb DISC IN 1M H_2SO_4 (UNSTIRRED)

-869 mV E_m

FIG. 6.23 i vs t TRANSIENTS FOR A STATIONARY MECH. POL. ELECTRODE. E_m: a −928, b −918, c −923 mV.

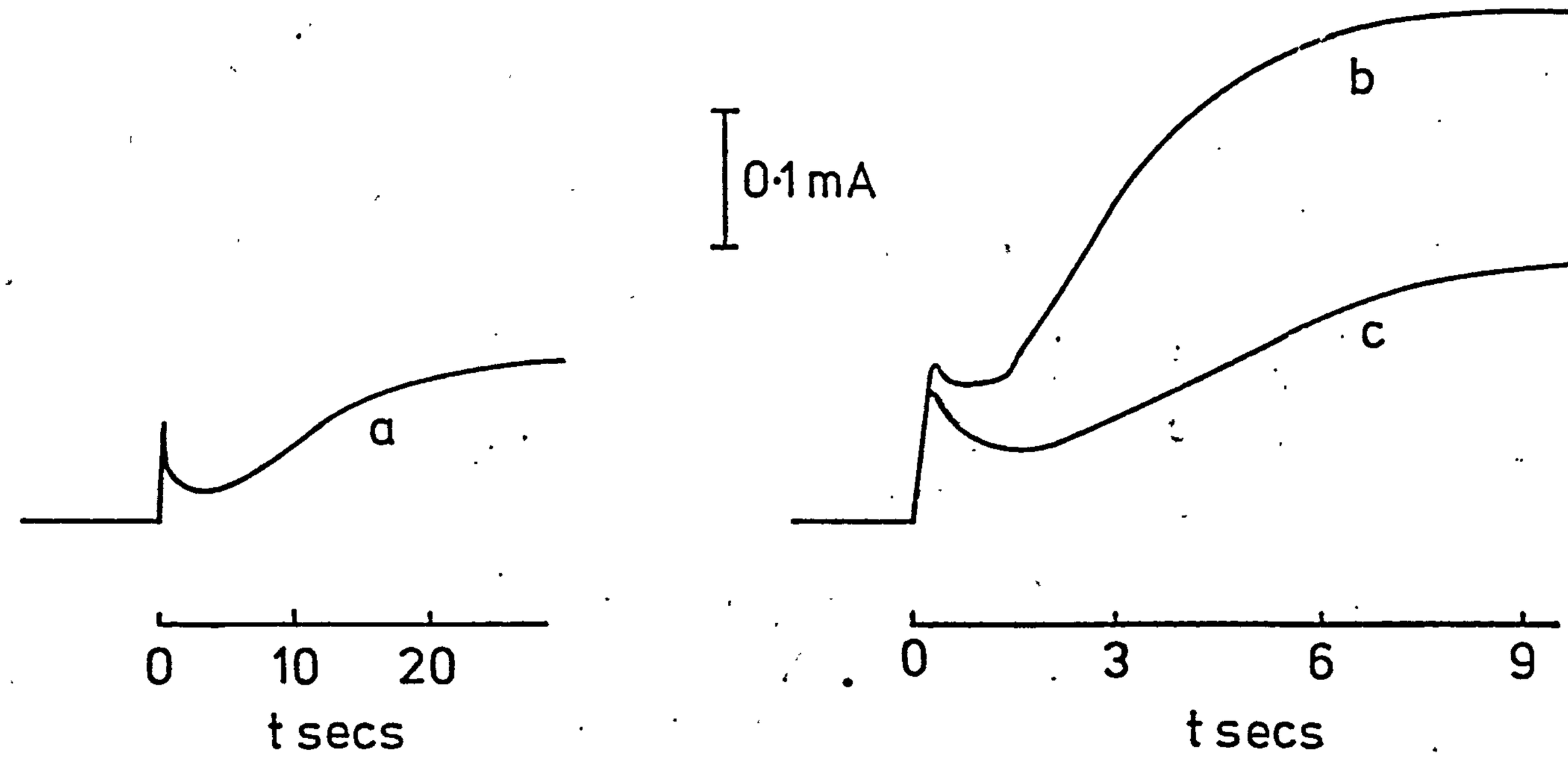

surface preparation of the Pb disc, are of the same overall shape whether the surface is prepared by γ-alumina or electropolishing.

The curves appear to rise as $i \propto t$ although the first part of the curve is obscured by the dissolution reaction. The true dependence is suggested by the corresponding ring response of Figure 6.22a which measures the diminution in free area, not covered by solid nuclei. At short times $i_R \propto (1 - Bt)$, where B is a constant, this is consistent with the models 1, 2, 3, $i_D \propto t$ discussed below. It is not in correspondence with the growth of discreet nuclei, $i_R \propto (1 - B' t^2)$.

The curves fall at long times when the nuclei finally overlap due to thickening of the layer.

6.3.6. Discussion

The potential at which $PbSO_4$ should be formed is E_m = -969 mV, in 1M H_2SO_4, that is E_h = -307 mV. Anodic to this potential the Pb dissolves freely as Pb^{2+} and $PbSO_4$ ions. As shown earlier, potentiostatic transients and sweep measurements agree with this. $PbSO_4$ and Pb^{2+} are precursors in the solution-precipitation of $PbSO_4$ solid. Once - 969 mV has been exceeded, sufficient of these intermediates are present in the diffusion layer to cause solution precipitation. However, the collection efficiency at potentials anodic to -969 mV probably does not show a depletion of species in solution, that is a rotation dependence, so there is no slow reaction in solution which removes the solution soluble ions. In addition, the dissolution disc current before the solid state reaction does not fall markedly with time at the rotating electrode, so it does not seem to be possible, from electrochemical evidence, to say how $PbSO_4$

precipitates. The $PbSO_4$ could precipitate in the neighbourhood of the electrode in a porous layer.

The solid state nucleation growth of a surface film of $PbSO_4$ in 1M H_2SO_4 does not start in any major way until E_m = -940 mV. The expected current-time relations for the slow growth of three dimensional separated nuclei have been reviewed recently and are of the form $i \propto t^{\beta}$. $\beta = 2$ for instantaneous nucleation and $\beta = 3$ for progressive nucleation. In this case something nearer to $i \propto t$ is observed.

A number of reasons are possible for the $i \propto t$ dependence:

(1) The growth is a transport controlled progressive nucleation of nuclei of fixed basal area.

(2) The growth is a transport controlled instantaneous growth of approximately hemispherical nuclei.

(3) The growth is interface controlled but due to the nucleation of areas of the electrode within which nucleation and growth of three dimensional nuclei occurs.

Cases (1) and (2) have been considered previously[10].

Section (3) can be estimated by inserting appropriate values in the growth law

$$i(t) = \int_0^t i(u) \left(\frac{dN}{dt}\right)_{t-u} du \qquad (6.8)$$

It is assumed that the areas are isolated. $\left(\frac{dN}{dt}\right)$ is the nucleation rate of areas and $i(u)$ is the current due to growth of a single area. $i(u)$ has been given for the growth and overlap of pyramidal centres[11]

$$i(u) = \frac{nF\rho}{M} V_2 \left[1 - \exp\left(-\frac{\pi}{\rho^2} N_0 k_1^2 M^2 t^2\right)\right] \qquad (6.9)$$

where there are N_o nuclei in an area. Equation (6.8) now becomes for the rate of appearance of areas

$$\frac{dN}{dt} = A \tag{6.10}$$

then

$$i(t) = \frac{AnF\rho}{M} V_2 t - \int_0^t \exp\left(\frac{-\pi}{\rho^2} N_o k_1^2 M^2 t^2\right) dt \tag{6.11}$$

Equation (6.11) means if one ignores the second term that only the stationary part of equation (6.9) is being considered. Therefore, in spite of the fact that within an area the overall current at small times rises as $i \propto t^2$, overall it rises as $i \propto t$.

In cases (1), (2), (3) the slope $\frac{di}{dt}$ is proportional to the rate of nucleation in (1) and (2) of individual nuclei and in (3) of areas which is therefore given by Figure 6.24a as a function of potential. That case (3) is probably correct is shown by the fact that occasionally $i \propto t^2$ is observed when presumably the nuclei in an area are sufficiently separated. Figure 6.24b shows the situation that may exist on the surface for case (3).

Solution-precipitation mechanism

An analysis of the mechanism for the rotating disc has appeared in the literature[12] based on the reaction scheme

$$M \rightleftharpoons M_1 + ze \tag{6.12}$$

$$M_1 + M_1 \underset{(k_b)_1}{\overset{(k_f)_1}{\rightleftharpoons}} M_2 \tag{6.13}$$

$$M_n + M_1 \rightleftharpoons M_{n+1} \tag{6.14}$$

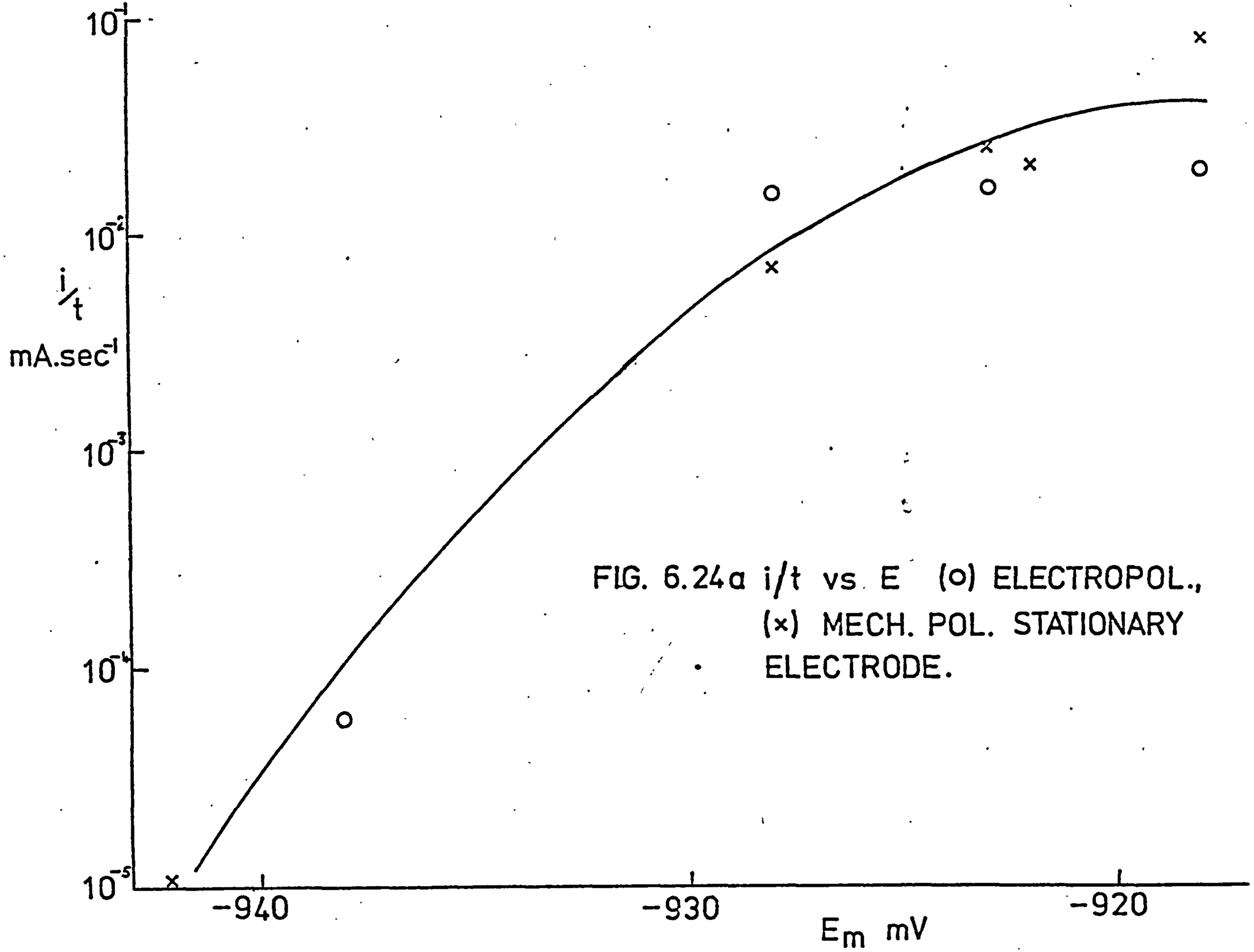

FIG. 6.24a i/t vs E (o) ELECTROPOL., (×) MECH. POL. STATIONARY ELECTRODE.

FIG. 6.24b POSSIBLE SITUATION THAT MAY ARISE ON A LEAD SURFACE

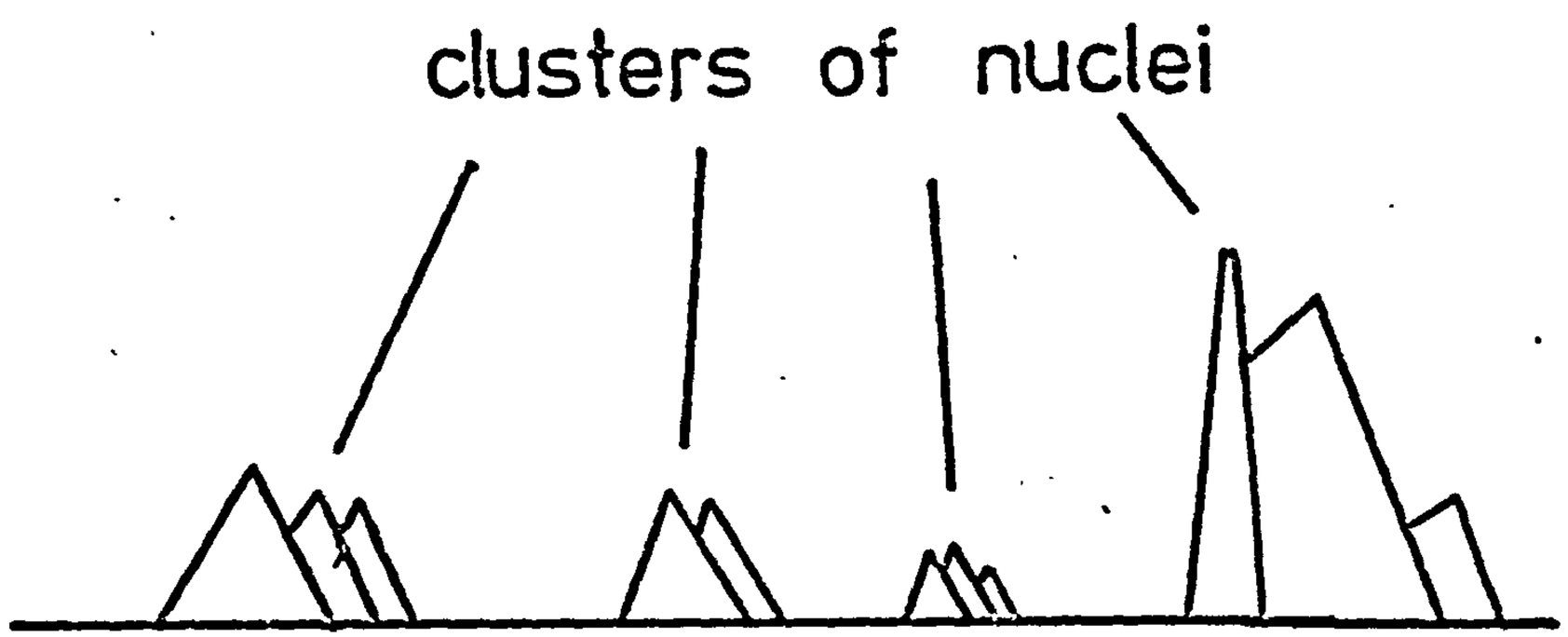

It is predicted that for equation (6.12) reversible at controlled potential and M_2 precipitating, the maximum precipitation should be at x = 0. The potential at which precipitation occurs should depend on rotation speed when

$$\left(\frac{M_1^*(K_f)_1}{D_1}\right)^{1/2}\delta < \left(\frac{(K_b)_1}{D_2}\right)^{1/2}\delta < 1 \qquad (6.15)$$

Neither of these effects seem to be observed for Pb in spite of the fact that substantial dissolution takes place, and it seems possible for solution precipitation to occur. It is possible that the theory which does not take into account the size of the nuclei and their changing diffusion coefficient needs to be refined. A tentative view of the actual situation is shown in Figure 6.25. Figure 6.25 is the situation at one instant in time and shows a distribution of particles of a particular size $(MX)_n$. Once the solubility product of MX has been exceeded the MX, in this case $PbSO_4$, in solution will grow. As it grows the diffusion coefficient decreases due to its increase in size and its chance of escape from the vicinity of the electrode decreases. In Figure 6.25 if the concentration of M^+ corresponding to the solubility product is given by the horizontal dotted line, MX particles will continue to grow up to Y'. The curve labelled $(MX)_n$ will be the concentration distribution of particles of a particular size containing n molecules. Particles will diffuse back to the electrode down the concentration gradient.

6.4. Behaviour of Lead amalgams

6.4.1. Introduction

The essential features of solid Pb oxidation in H_2SO_4 have been

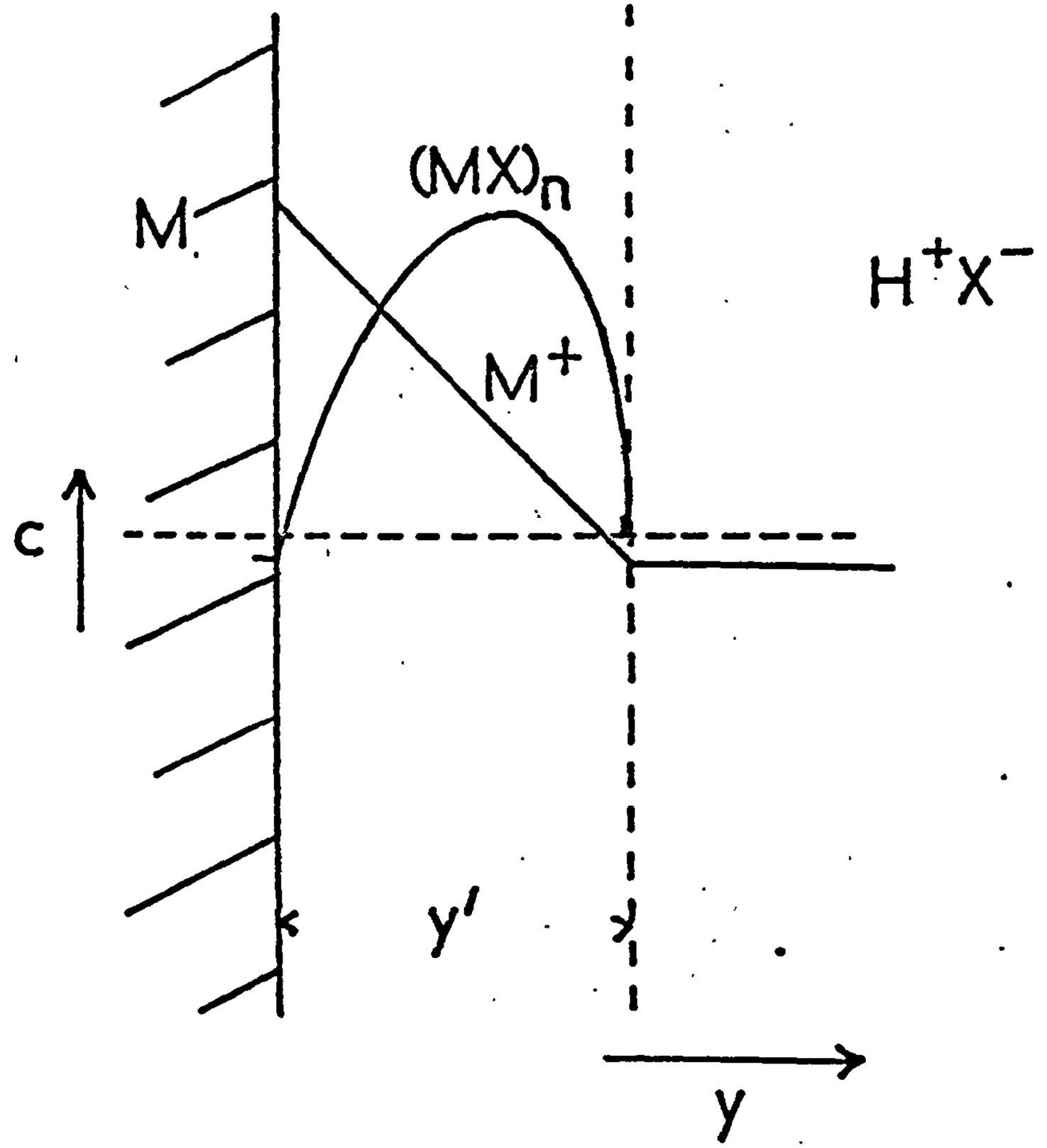

Fig. 6.25 Possible mechanism for a dissolution–precipitation process

investigated in Section 6.3. The purpose of this section is to investigate the behaviour of Pb amalgams under the same conditions. Amalgams were used as these have defect free surfaces, whereas solid lead does not.

Amalgams of four different concentrations were used

Amalgam	α	approx. 0.7% by weight Pb
Amalgam	A	0.289M in Pb
Amalgam	B	2.74×10^{-2}M in Pb
Amalgam	C	6.11×10^{-3}M in Pb

Amalgam α was initially made by direct combination at room temperature, the exact concentration was not determined for this amalgam. Amalgams A, B, and C were made by dilution of α, the exact concentrations were estimated by stripping coulometry. The cell used is described in Chapter 5. Throughout this section 1M H_2SO_4 and Hg/Hg_2SO_4 reference electrodes in the same solution (E_m) were used. The first part of this section concerns measurements on amalgam α, the second part investigates Pb(Hg) dissolution in more detail.

6.4.2. Measurements-amalgam α

Potential sweep

Linear potential sweep measurements are shown as a function of the positive limit in Figure 6.26. Figure 6.26(a) has a typical response expected for a reversible electrochemical process:

$$X + M \rightleftharpoons MX^{2+} + 2e$$ in which MX^{2+} is soluble in solution. A simulated response curve calculated by digital simulation[13] is shown in Figure 6.27. The program used (ALGOL F) is shown in Figure 6.28.

Fig. 6.26 Linear sweeps on Pb(Hg) drop.

$V = 0.3\ V\ s^{-1}$, cathodic end -1200 mV E_m

vs Hg/Hg_2SO_4,

y = 2 mA/division, x = 50 mV/division.

Potential goes anodic left to right.

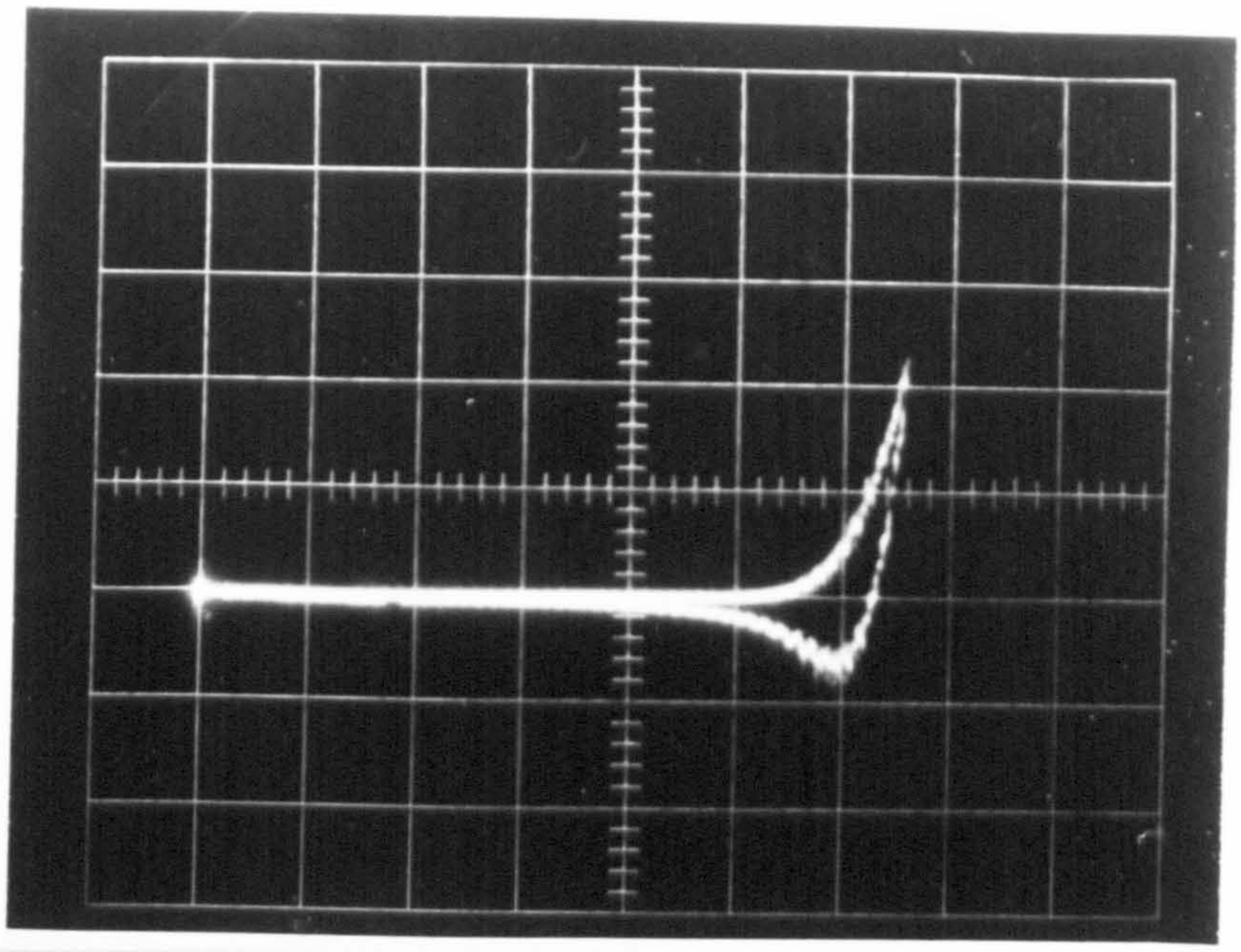

a

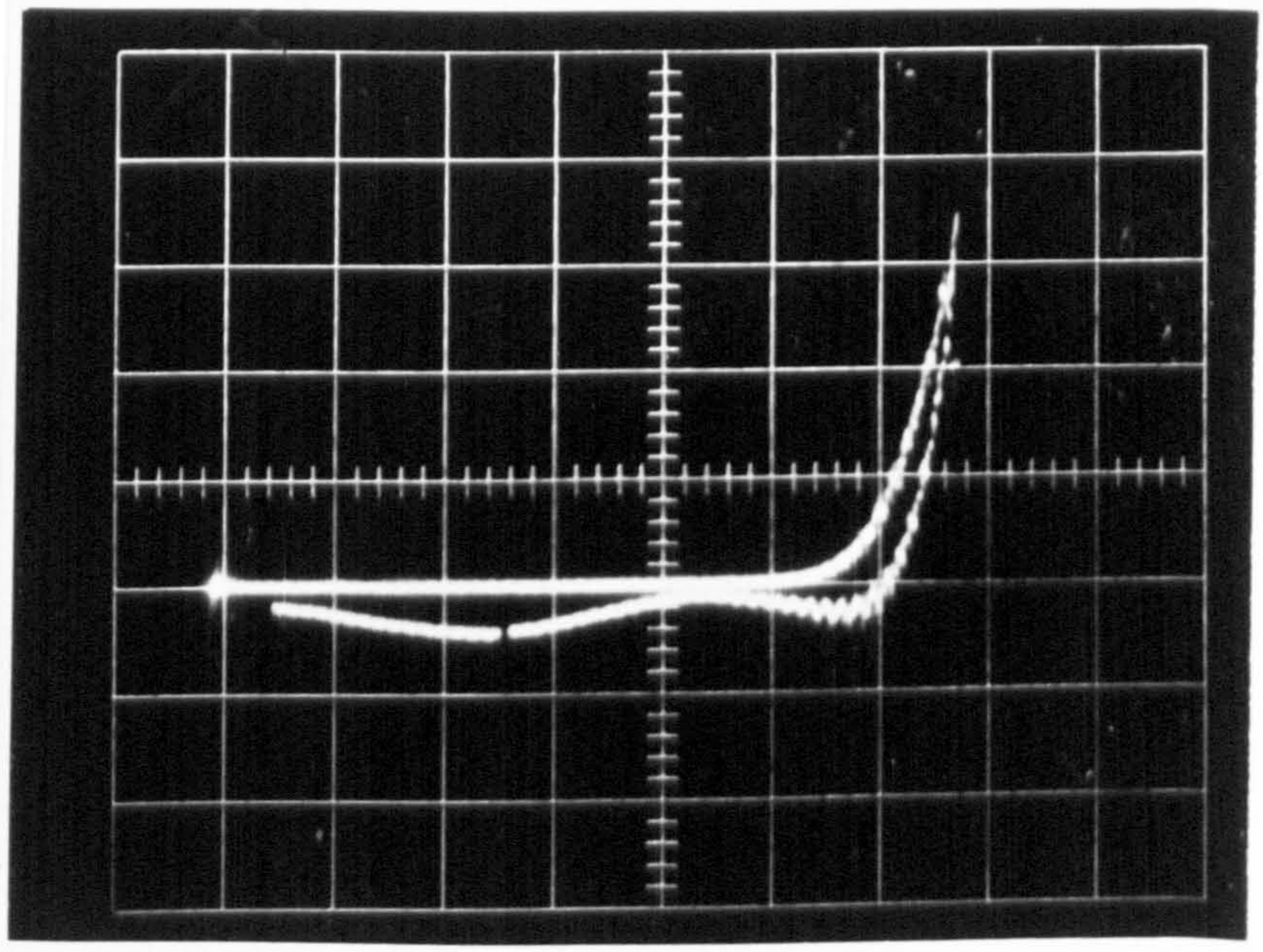

b

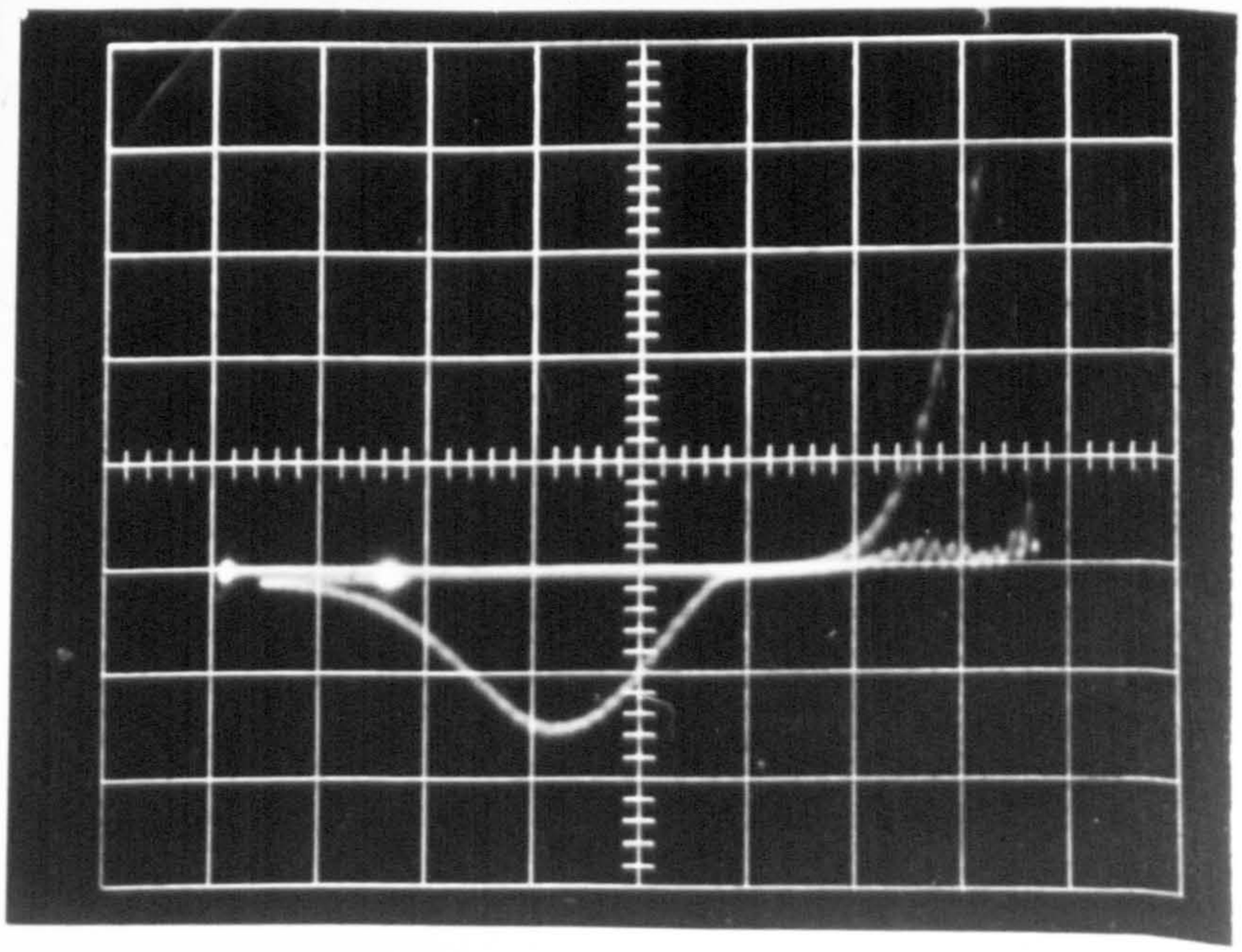

c

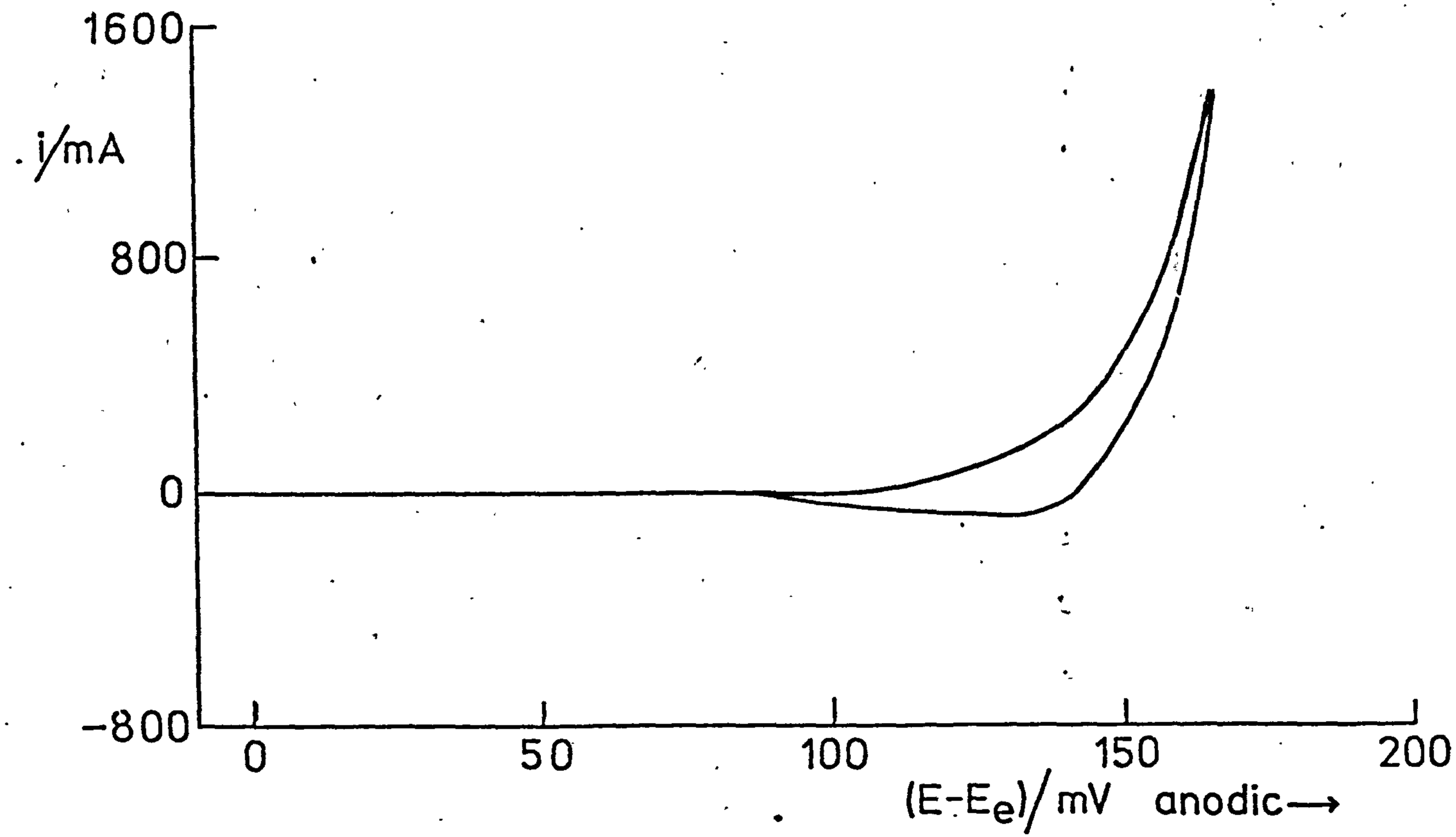

FIG. 6.27 Digital simulation i-E sweep curve for a reversible reaction $M \rightleftharpoons M^{2+} + 2e$. Shape only is significant not the absolute magnitudes. Parameters used: $C^{b}_{M^{2+}} = 10^{-9}$ mol cm^{-3}, $\delta = 10^{-3}$ cm, $\Delta x = 10^{-4}$ cm, $D = 10^{-5}$ cm^2 s^{-1}, $v = 500$ mV s^{-1}, area $= 1$ cm^2, $\Delta t = (\Delta x)^2/6D$, $n = 2$.

FIG. 6.28 COMPUTER PROGRAM ALGOL F

```
'BEGIN'
 'REAL''PROCEDURE'READ(DV);'VALUE'DV;'INTEGER'DV;'CODE';
 'BOOLEAN''PROCEDURE'READBOOLEAN(DVI);'VALUE'DVI;'INTEGER'DVI;'CODE';
 'PROCEDURE'WRITEBOOLEAN(D,B);'VALUE'D,B;'BOOLEAN'B;'INTEGER'D;'CODE';
 'INTEGER''PROCEDURE'FORMAT(S);'STRING'S;'CODE';
 'PROCEDURE'OUTPUT(DV,N);'VALUE'DV,N;'INTEGER'DV;'REAL'N;'CODE';
 'PROCEDURE'WRITE(DV,F,Q);'VALUE'DV,F,Q;'INTEGER'DV,F;'REAL'Q;'CODE';
 'PROCEDURE'WRITETEXT(DV,S);'VALUE'DV;'INTEGER'DV;'STRING'S;'CODE';
 'PROCEDURE'OPEN(DV);'VALUE'DV;'INTEGER'DV;'CODE';
 'PROCEDURE'CLOSE(DV);'VALUE'DV;'INTEGER'DV;'CODE';

'REAL' F,R,TT,ZED,ETA,L,X,TAU,D,T,C,Y,GRAD,ETAR,ZEDAR,FAC;
'INTEGER' F1,F2,Z,N,ZZ;

OPEN(20);OPEN(30);
F:=9.6487'4;
R:=8314.3;

TT:=298.15;
N:=READ(20);
ZED:=READ(20);
ETA:=READ(20);
L:=READ(20);
X:=READ(20);
TAU:=READ(20);
D:=READ(20);
C:=READ(20);
F1:=FORMAT('('10S-D.DDDDDD'-NDC')');
F2:=FORMAT('('10SD.DDDDDD'-ND')');
WRITE TEXT(30,'('''('3C')'SWEEP**FIN**DIFF
'('2C10S')'SEC'('19S')'MA'('2C')''')');
T:=X**2/6.0/D;

ETAR:=ETA*F/R/TT;ZEDAR:=T*ZED*F/R/TT;
'BEGIN' 'REAL' 'ARRAY' U(/0:N/) , V(/0:N/);
'FOR' Y:=0'STEP' 1'UNTIL'N'DO'
     'BEGIN'
     U(/Y/):=0.0;
     V(/Y/):=0.0;
     'END';
'FOR' Y:=0 'STEP' 1'UNTIL' N 'DO'
     'BEGIN'
     U(/Y/):=C*EXP(-ETAR)+C*Y*X/L
          -C*Y*X/L*EXP(-ETAR);
     'END';
```

CONT.

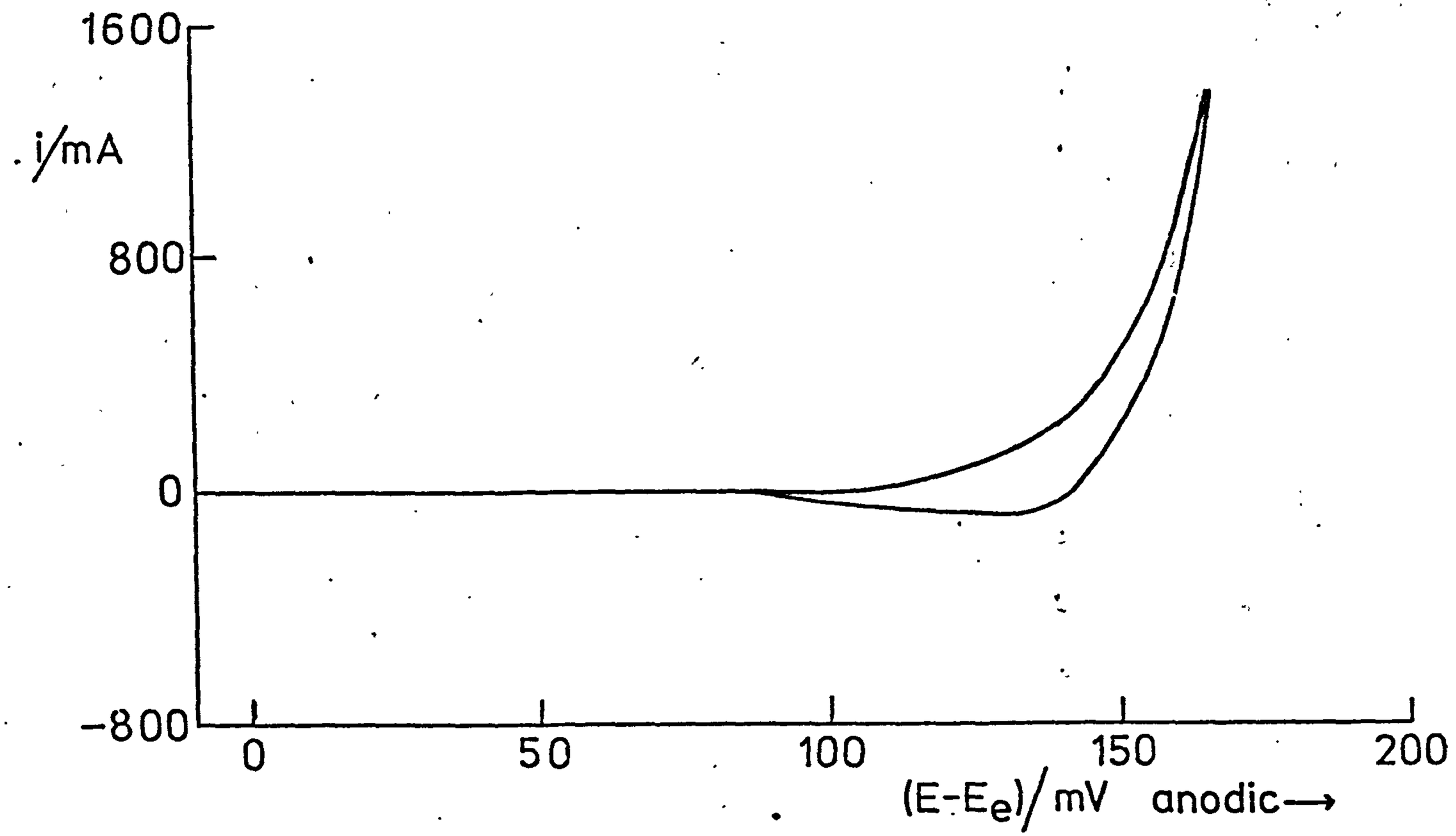

FIG. 6.27 Digital simulation i-E sweep curve for a reversible reaction $M \rightleftharpoons M^{2+} + 2e$. Shape only is significant not the absolute magnitudes. Parameters used: $C^{b}_{M^{2+}} = 10^{-9}$ mol cm^{-3}, $\delta = 10^{-3}$ cm, $\Delta x = 10^{-4}$ cm, $D = 10^{-5}$ cm^2 s^{-1}, $v = 500$ mV s^{-1}, area $= 1$ cm^2, $\Delta t = (\Delta x)^2/6D$, $n = 2$.

FIG. 6.28 COMPUTER PROGRAM ALGOL F

```
'BEGIN'
 'REAL''PROCEDURE'READ(DV);'VALUE'DV;'INTEGER'DV;'CODE';
 'BOOLEAN''PROCEDURE'READBOOLEAN(DVI);'VALUE'DVI;'INTEGER'DVI;'CODE';
 'PROCEDURE'WRITEBOOLEAN(D,B);'VALUE'D,B;'BOOLEAN'B;'INTEGER'D;'CODE'
 'INTEGER''PROCEDURE'FORMAT(S);'STRING'S;'CODE';
 'PROCEDURE'OUTPUT(DV,N);'VALUE'DV,N;'INTEGER'DV;'REAL'N;'CODE';
 'PROCEDURE'WRITE(DV,F,Q);'VALUE'DV,F,Q;'INTEGER'DV,F;'REAL'Q;'CODE';
 'PROCEDURE'WRITETEXT(DV,S);'VALUE'DV;'INTEGER'DV;'STRING'S;'CODE';
 'PROCEDURE'OPEN(DV);'VALUE'DV;'INTEGER'DV;'CODE';
 'PROCEDURE'CLOSE(DV);'VALUE'DV;'INTEGER'DV;'CODE';

'REAL' F,R,TT,ZED,ETA,L,X,TAU,D,T,C,Y,GRAD,ETAR,ZEDAR,FAC;
'INTEGER' F1,F2,Z,N,ZZ;

OPEN(20);OPEN(30);
F:=9.6487'4;
R:=8314.3;

TT:=298.15;
N:=READ(20);
ZED:=READ(20);
ETA:=READ(20);
L:=READ(20);
X:=READ(20);
TAU:=READ(20);
D:=READ(20);
C:=READ(20);
F1:=FORMAT('('10S-D.DDDDDD'-NDC')');
F2:=FORMAT('('10SD.DDDDDD'-ND')');
WRITE TEXT(30,'('''('3C')'SWEEP**FIN**DIFF
'('2C10S')'SEC'('19S')'MA'('2C')'')');
T:=X**2/6.0/D;

ETAR:=ETA*F/R/TT;ZEDAR:=T*ZED*F/R/TT;
'BEGIN' 'REAL' 'ARRAY' U(/0:N/) , V(/0:N/);
'FOR' Y:=0'STEP' 1'UNTIL'N'DO'
     'BEGIN'
     U(/Y/):=0.0;
     V(/Y/):=0.0;
     'END';
'FOR' Y:=0 'STEP' 1'UNTIL' N 'DO'
     'BEGIN'
     U(/Y/):=C*EXP(-ETAR)+C*Y*X/L
          -C*Y*X/L*EXP(-ETAR);
     'END';
```

CONT.

```
FAC:=D*F*1'3/X;
GRAD:=(U(/0/)-U(/1/))*FAC;
WRITE(30,F2,T);
WRITE(30,F1,GRAD);
V(/N/):=C;
Z:=1;
SKIP:'FOR' Y:=1'STEP'1'UNTIL' N-1 'DO'
     'BEGIN'
     V(/Y/):=1/6.0*(U(/Y-1/)+4*U(/Y/)+U(/Y+1/));
     'END';
V(/0/):=C*EXP(-ETAR+ZEDAR*Z);
'IF' Z'/'100*100=Z 'THEN'    'BEGIN'
GRAD:=(V(/0/)-V(/1/))*FAC;
WRITE(30,F2,Z*T);
WRITE(30,F1,GRAD);    'END';
'FOR' Y:=0'STEP'1'UNTIL' N 'DO'
     'BEGIN'
     U(/Y/):=V(/Y/);
     'END';
Z:=Z+1;
'IF' Z*T<=TAU 'THEN' 'GOTO' SKIP;
GRAD:=(V(/0/)-V(/1/))*FAC;
WRITE(30,F2,(Z-1)*T); WRITE(30,F1,GRAD);
```

```
Z:=Z-2;ZZ:=Z+2;
JUMP:'FOR' Y:=1 'STEP' 1 'UNTIL' N-1 'DO'
     'BEGIN'
          V(/Y/):=1/6.0*(U(/Y-1/)+4*U(/Y/)+U(/Y+1/));
     'END';
V(/0/):=C*EXP(-ETAR+ZEDAR*Z);
'IF' Z'/'100*100=Z 'THEN'
     'BEGIN'
       GRAD:=(V(/0/)-V(/1/))*FAC;
          WRITE(30,F2,ZZ*T);
          WRITE(30,F1,GRAD);
     'END';
'FOR' Y:=0 'STEP' 1 'UNTIL' N 'DO'
     'BEGIN'
          U(/Y/):=V(/Y/);
     'END';
Z:=Z-1; ZZ:=ZZ+1;
'IF' Z*T>=0'THEN' 'GOTO' JUMP;
GRAD:=(V(/0/)-V(/1/))*FAC;
WRITE(30,F2,(ZZ-1)*T);
WRITE(30,F1,GRAD);
CLOSE(20); CLOSE(30);
'END';
```

No effort has been made to compare experiment and theory because the nature of MX^{2+} is not known exactly. The response is however characteristic.

As the anodic limit is raised (Figure 6.26(b)) a second peak is observed on the return. This is certainly due to the reduction of a solid layer of $PbSO_4$. At passivation in the anodic direction Figure 6.26(c)) only the reduction of solid $PbSO_4$ is observed. The amount of solid $PbSO_4$ (Figure 6.26(c)) needed to passivate completely, judged by the cathodic reduction peak, is 24 mC cm^{-2}.

Figure 6.29 shows consecutive sweeps. As the solid $PbSO_4$ layer, which is shown by reduction b, grows, the amount of the reversibly formed product MX^{2+} is reduced (reduction peak a). This shows that MX^{2+} is dissolving in the spaces between the $PbSO_4$ nuclei. The solid $PbSO_4$ grows either by a precipitation or a solid state reaction in which three dimensional nuclei are formed.

Further measurements involved polarising the drop for 1 minute at the anodic end and sweeping cathodically. This technique showed both the reduction of MX^{2+} and the solid $PbSO_4$ (Figures 6.30(a), 6.30(b)). The critical potential for nucleation of the solid layer is -910 mV. Polarising at potentials cathodic to this and then sweeping cathodically only produced peaks due to the reduction of MX^{2+} and not $PbSO_4$.

Potential Pulse

Figure 6.31 is a typical response to a potential pulse. Plots of i vs $t^{-\frac{1}{2}}$ were straight lines going through the origin (Figures 6.32 and 6.33) and had a $\sim$ 30 mV/decade slope, indicating a 2e reversible process. Rising transients, indicating the solid state process were not observed.

Fig. 6.29 Consecutive linear sweeps on Pb(Hg) drop.
$V = 0.3\ V\ s^{-1}$, cathodic end -1200 mV vs Hg/Hg_2SO_4,
y = 2 mA/division, x = 50 mV/division. As reduction
peak (a) decreases the corresponding peak (b) increases.
Potential goes anodic left to right.

Fig. 6.31 Typical response to potential pulse. Pulse from -1200 mV
pulse to -906 mV, y = 0.2 mA/division, x = 0.2 ms/division.

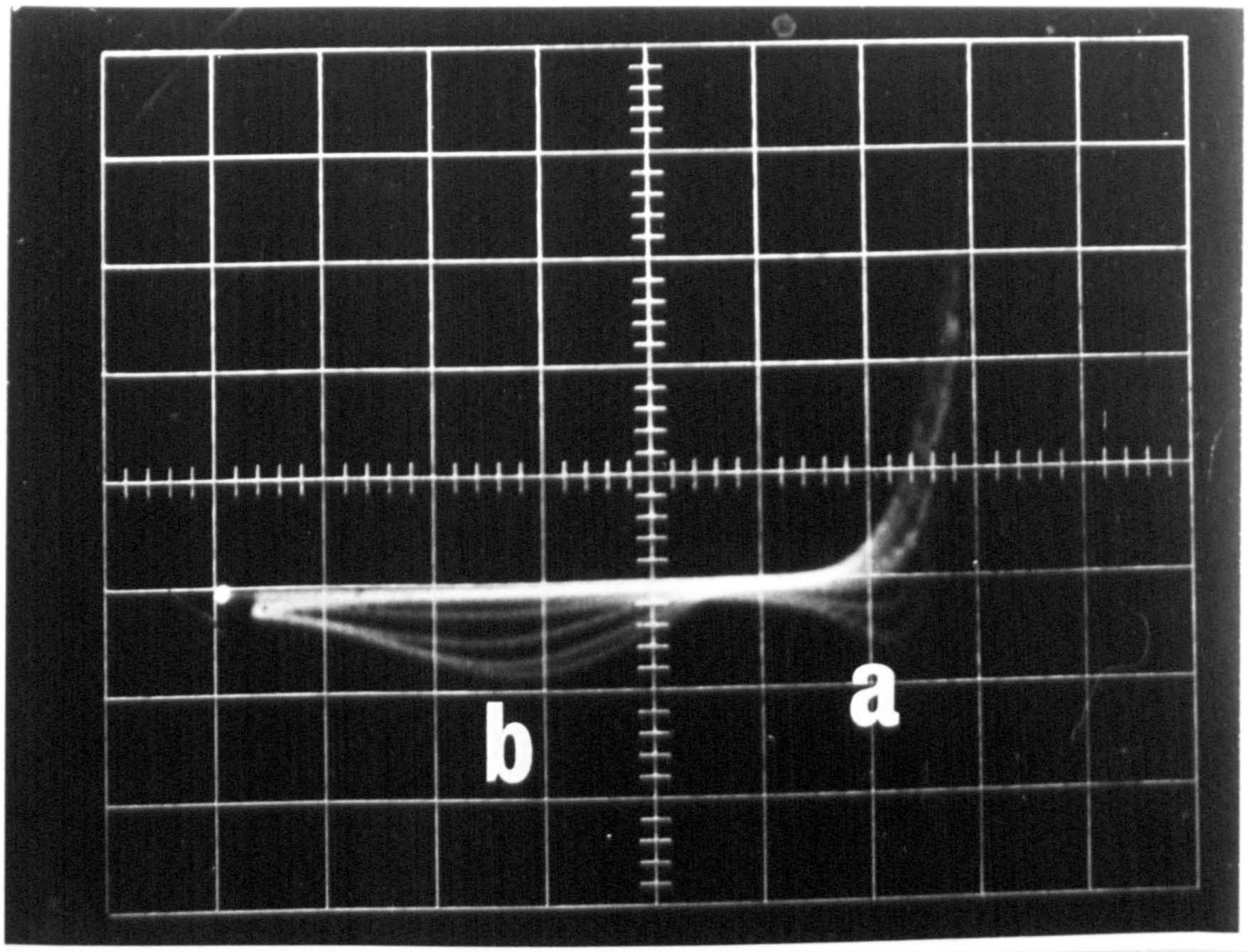
b
a

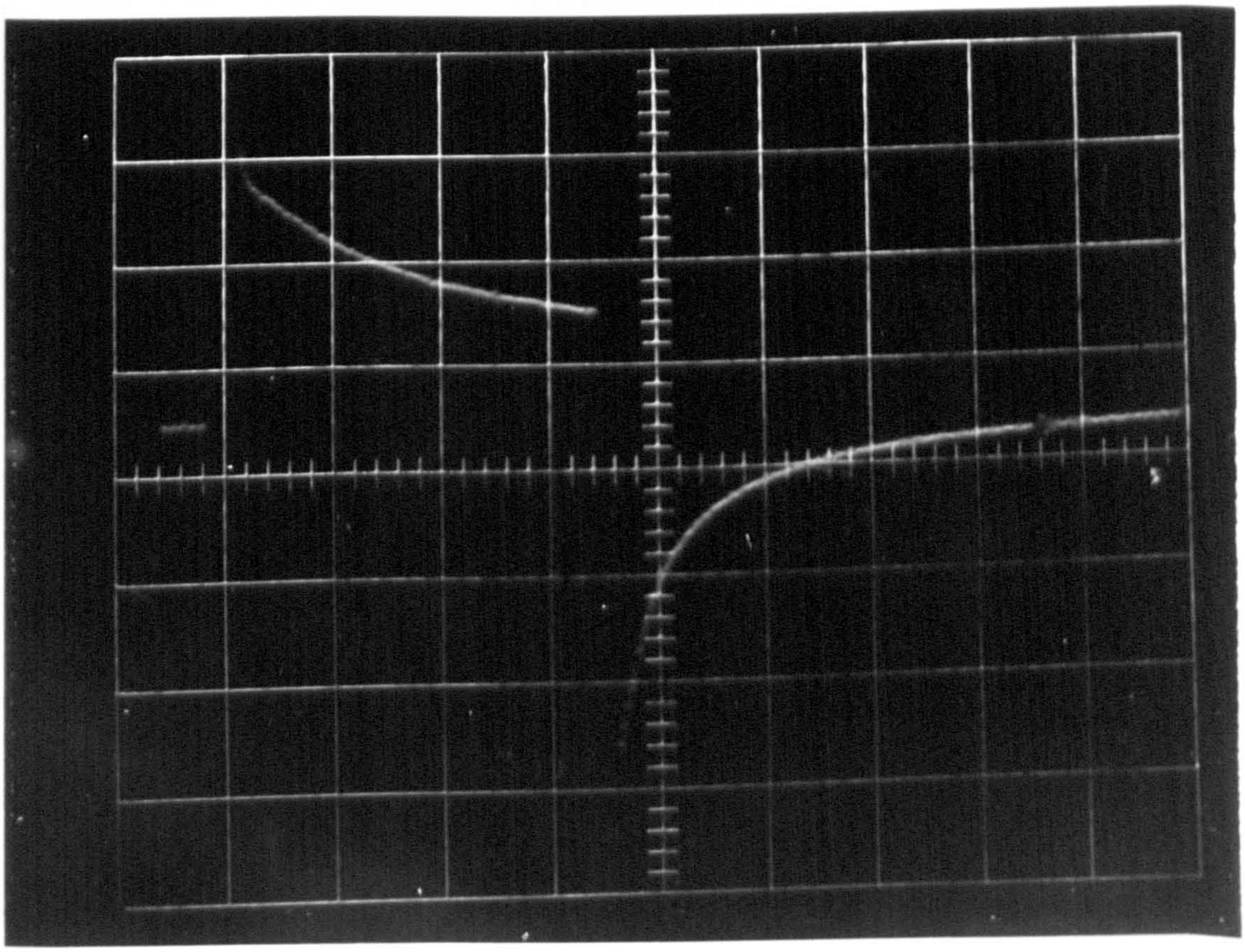

Fig. 6.30 Linear sweep on Pb(Hg). $V = 10\ V\ s^{-1}$, y = 0.5 mA/division, x = 50 mV/division, (a) anodic end -902 mV, (b) anodic end -907 mV, anodic end on right.

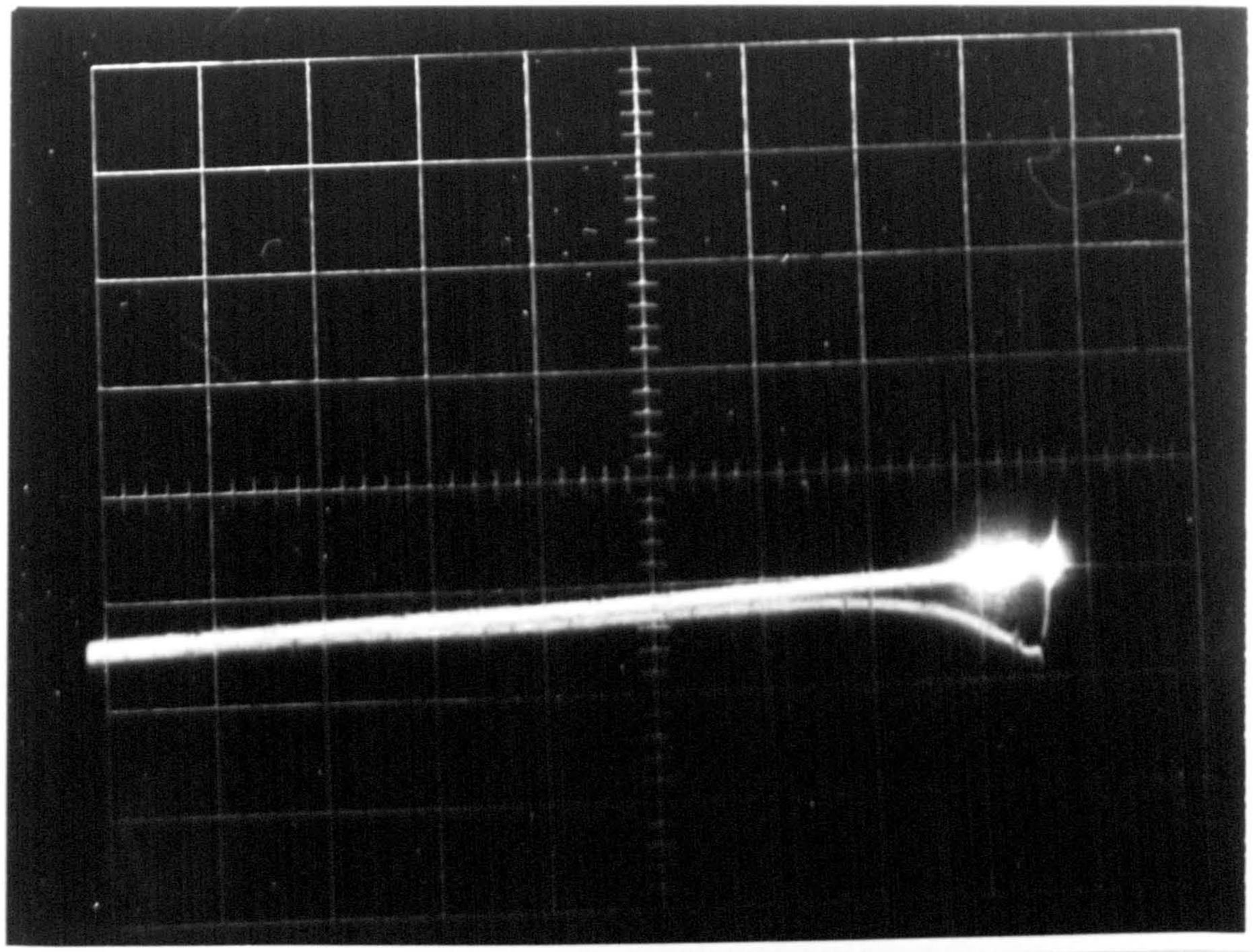

a

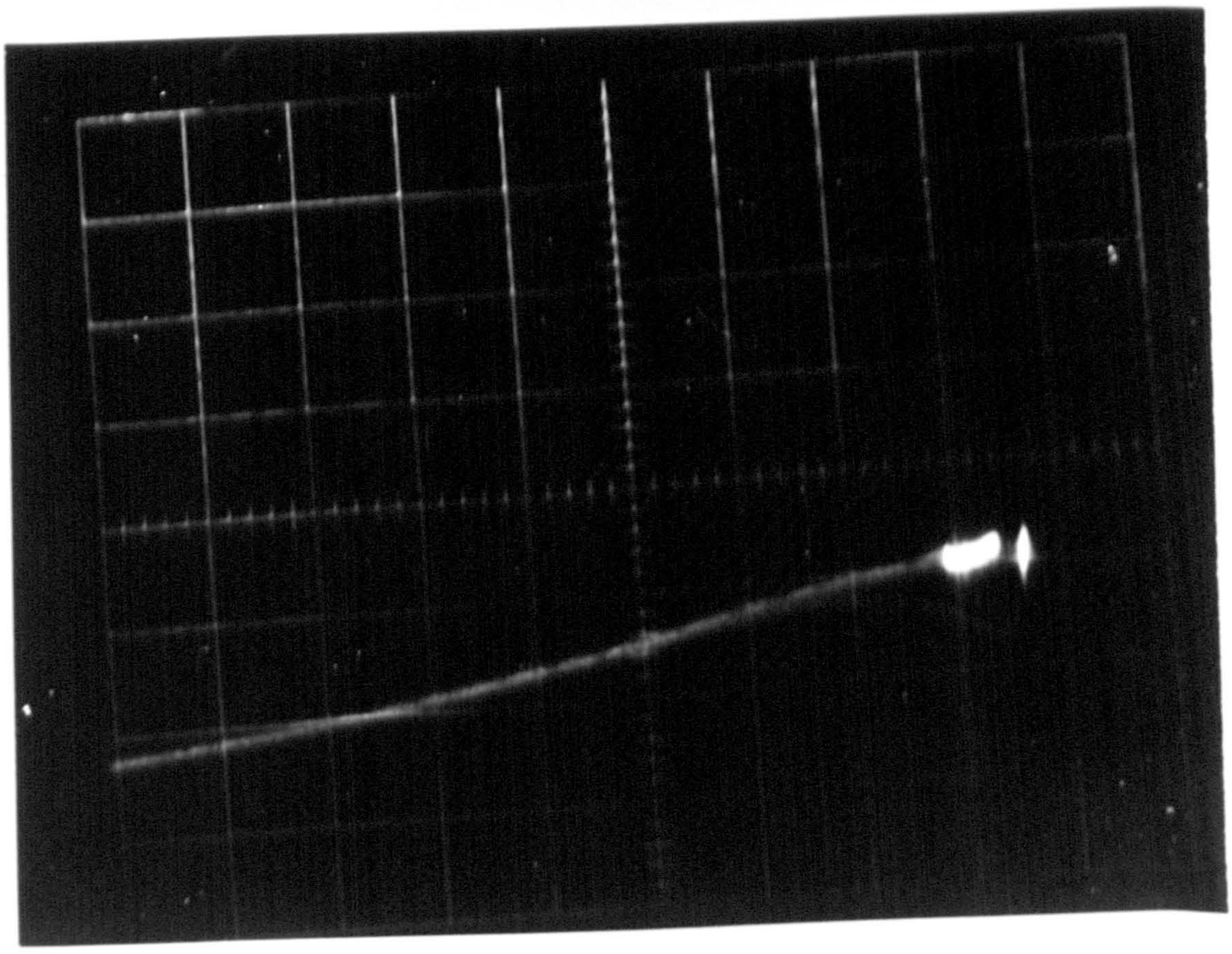

b

FIG. 6.32 i vs $t^{-1/2}$ FOR Pb(Hg)

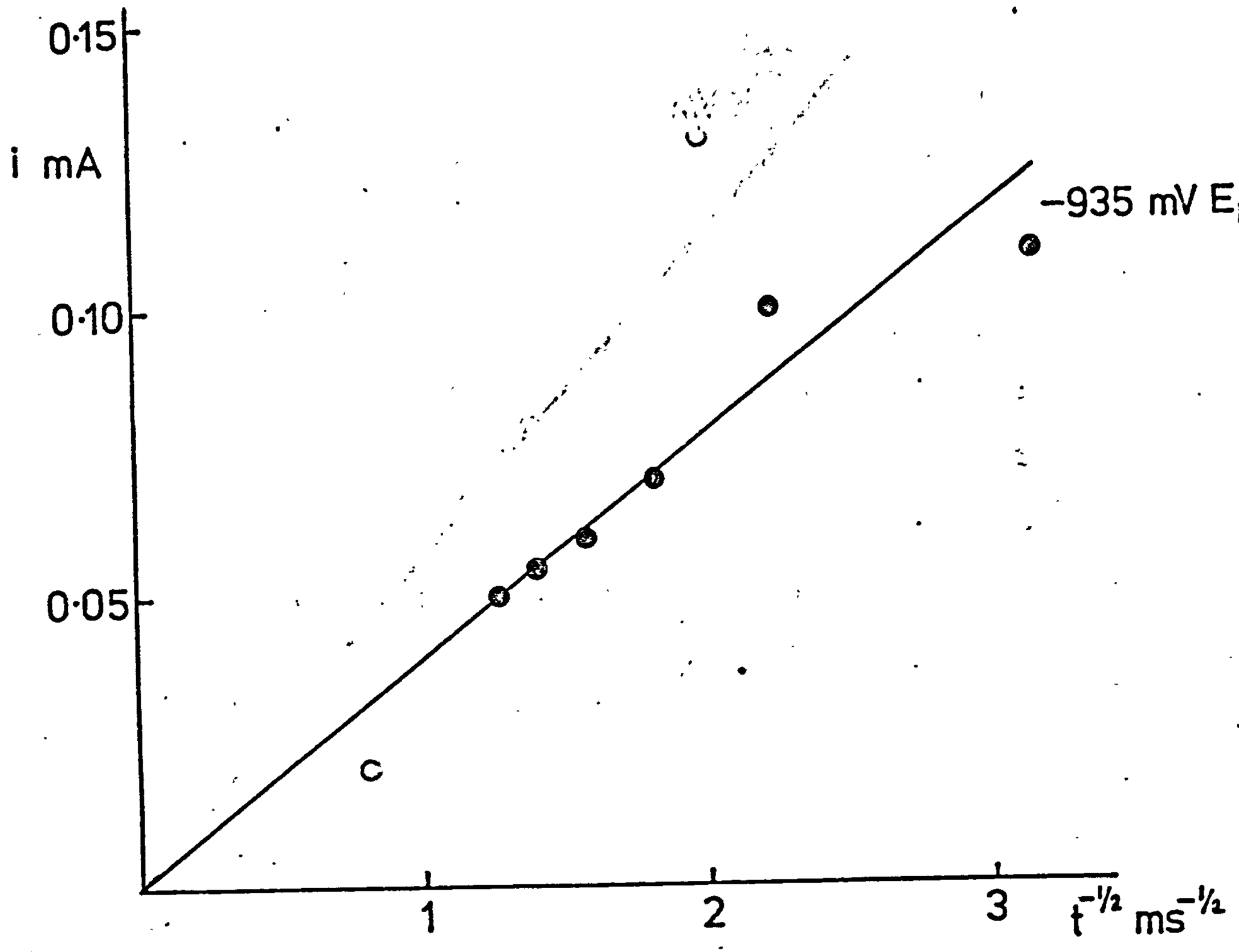

FIG. 6.33 i vs $t^{-1/2}$ FOR Pb(Hg)

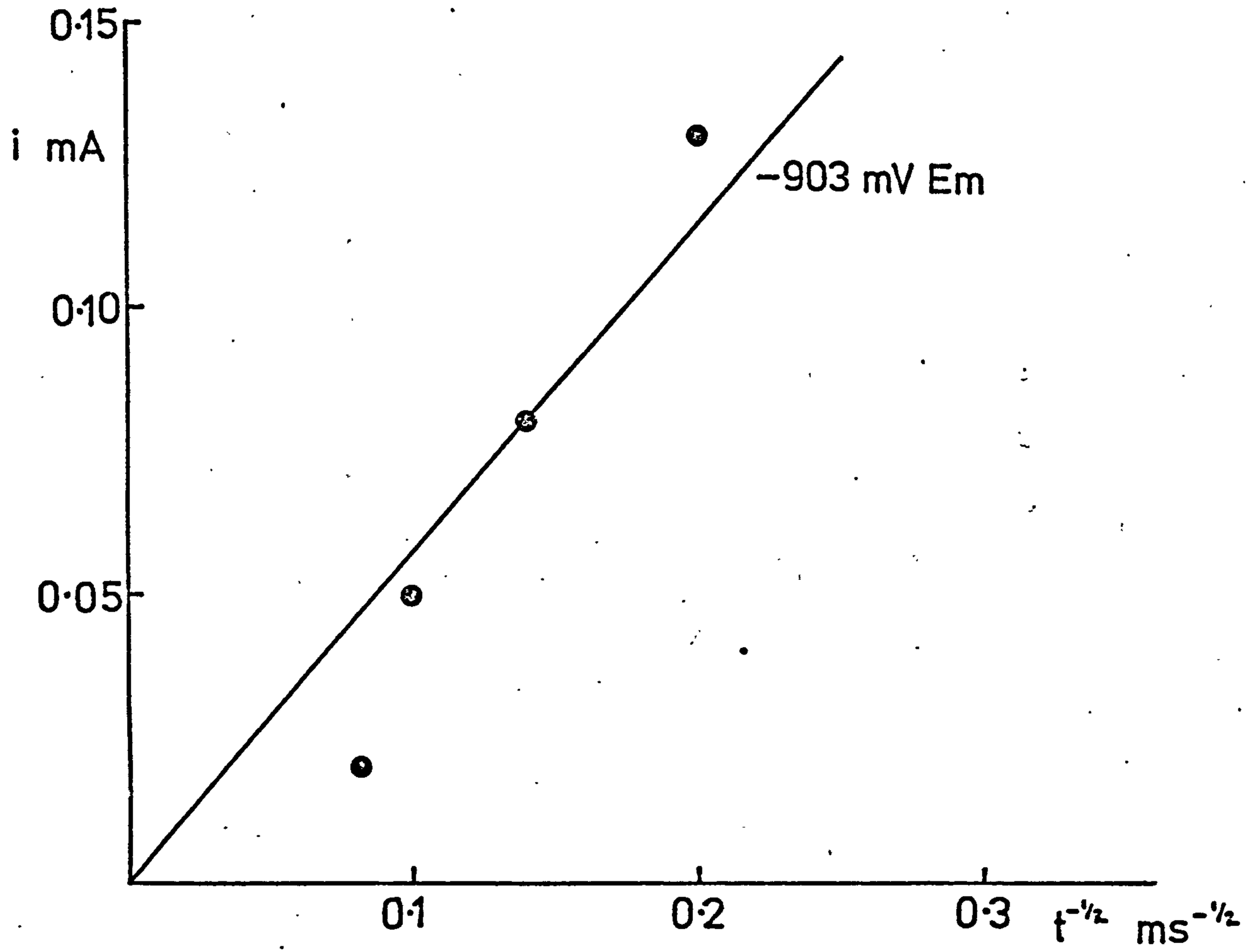

This is probably due to the solid state reaction, which is observed on solid Pb, being the minor process in the presence of major dissolution.

In order to investigate the anodic behaviour of Pb/(Hg) amalgams A, B and C which have a known Pb concentration were used.

6.4.3. Measurements - amalgams A, B, C.

Linear Potential Sweep

A series of curves at different sweep rates and for different amalgams are shown in Figures 6.34, 6.35, 6.36. The curves start from -1.2 V E_m and are single shot.

Graphs of i_p vs $V^{\frac{1}{2}}$ are shown in Figures 6.37(a) and 6.37(b) for the amalgams B and C. The curves are expected to analyse as a reversible two electron dissolution with the limiting step the diffusion of Pb in the Hg. The appropriate equation for i_p is

$$i_p = 3.67 \times 10^5 \, n^{3/2} A \, C^b D^{1/2} v^{1/2} \qquad (6.16)$$

where i_p = peak current amperes

n = number of electrons involved

A = area of electrode (cm^2)

C^b = bulk concentration (mole cm^{-3})

D = diffusion coefficient (cm^2 s^{-1})

V = sweep rate (volt s^{-1})

D has been measured independently[14] as 1.25×10^{-5} cm^2 s^{-1}. It is not possible to analyse the sweep curves of amalgam A due to interference from oscillations. The oscillations point to inhibition by a solid film of $PbSO_4$. Also at such high currents ohmic distortion of the potential is certain. A reverse

FIG. 6.34 POTENTIAL SWEEP ON AMALGAM A IN 1M H_2SO_4
$v = 0{\cdot}03\ V.s^{-1}$

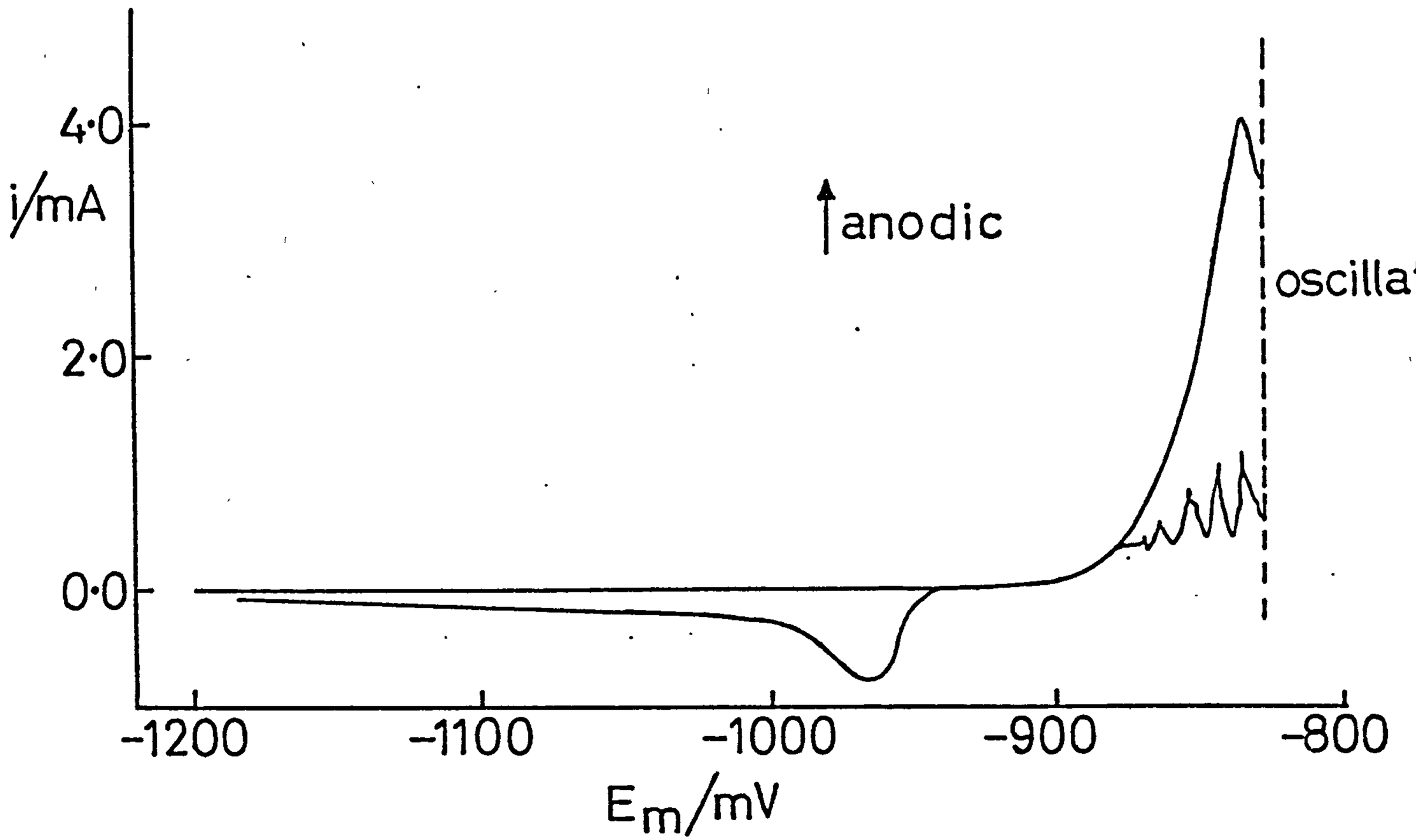

FIG. 6.35 POTENTIAL SWEEP ON AMALGAM B IN 1M H_2SO_4
$v = 0{\cdot}03\ V.s^{-1}$

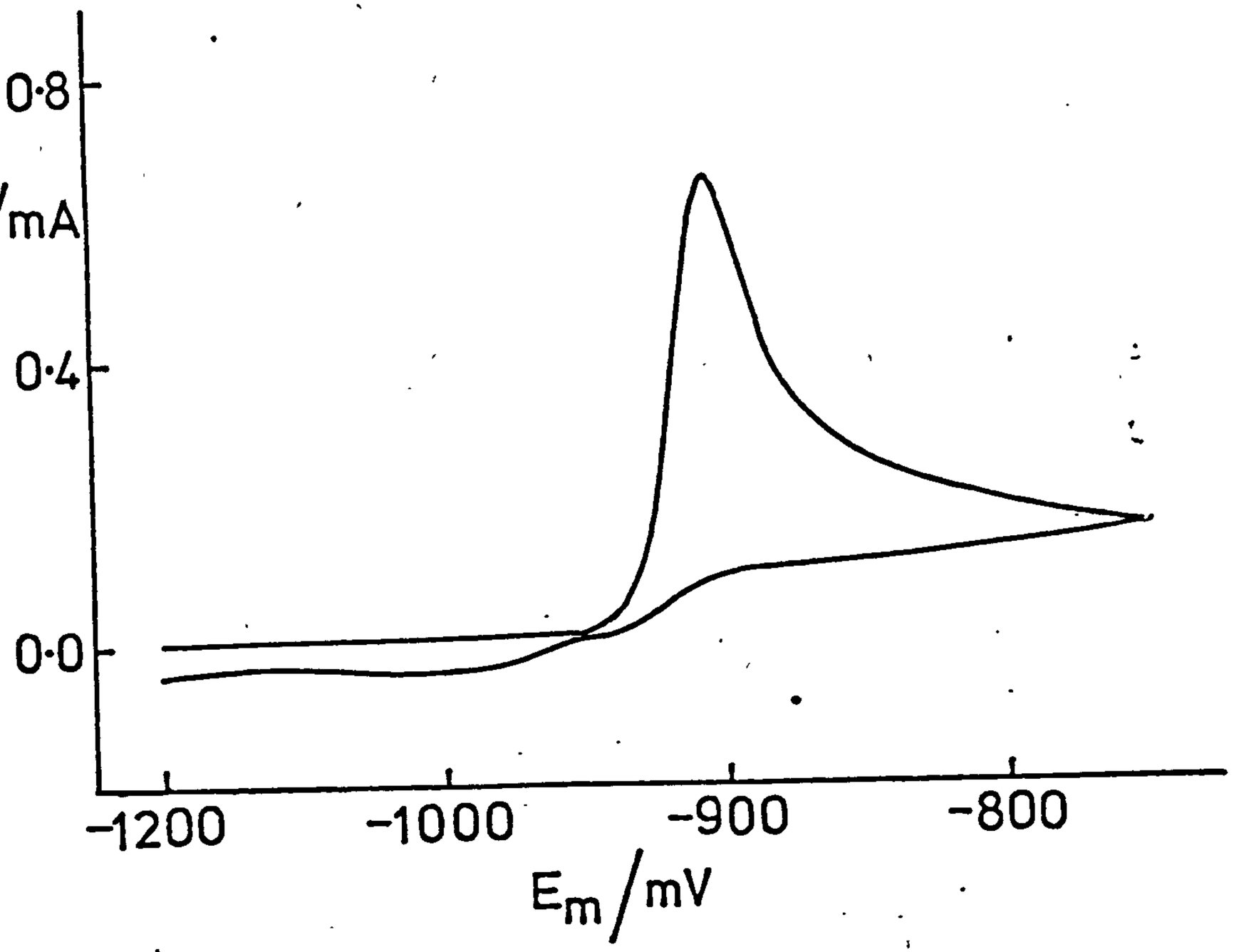

FIG. 6. 36a POTENTIAL SWEEP ON AMALGAM C IN 1M H_2SO_4
$v = 0{\cdot}03\ Vs^{-1}$

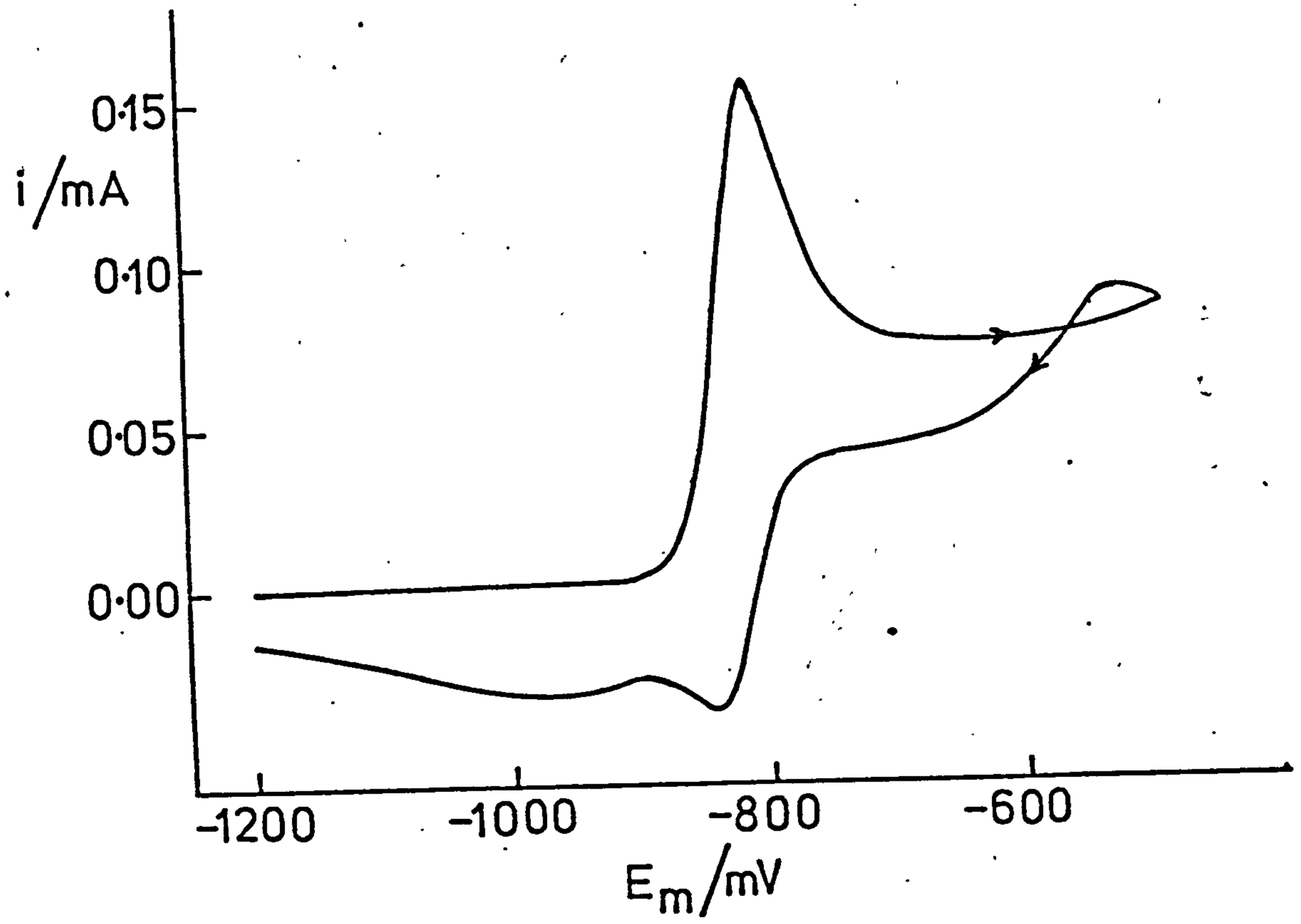

Fig. 6.36. Potential sweep on Amalgam C in 1M H_2SO_4

(b) $v = 1\ V\ s^{-1}$

Y axis, 0.5 mA/division

X axis, 100 mV/division

Cathodic end -1200 mV E_m

(c) $v = 3.2\ V\ s^{-1}$

Y axis, 0.5 mA/division

X axis, 100 mV/division

Cathodic end -1200 mV E_m

(d) $v = 10\ V\ s^{-1}$

Y axis, 1 mA/division

X axis, 100 mV/division

Cathodic end -1200 mV E_m

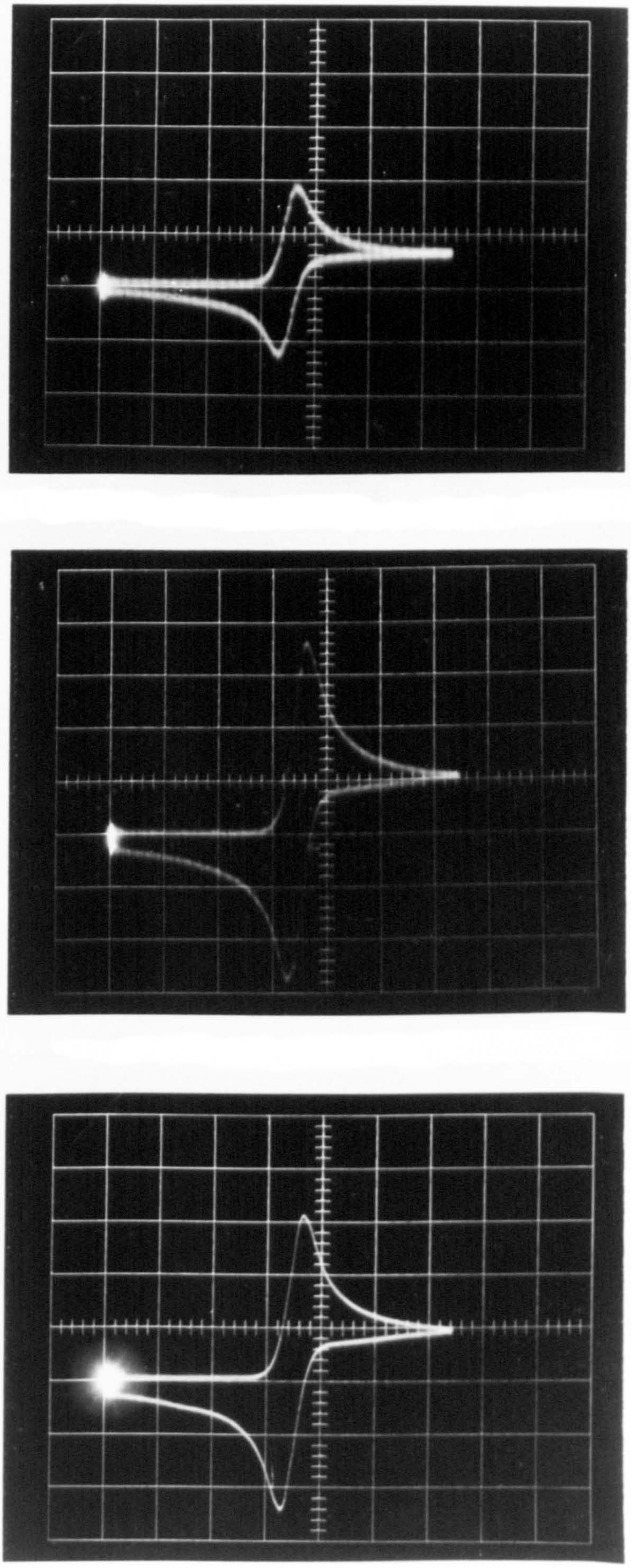

FIG. 6.37a i_p vs $v^{1/2}$ FOR AMALGAM B IN $1M\ H_2SO_4$

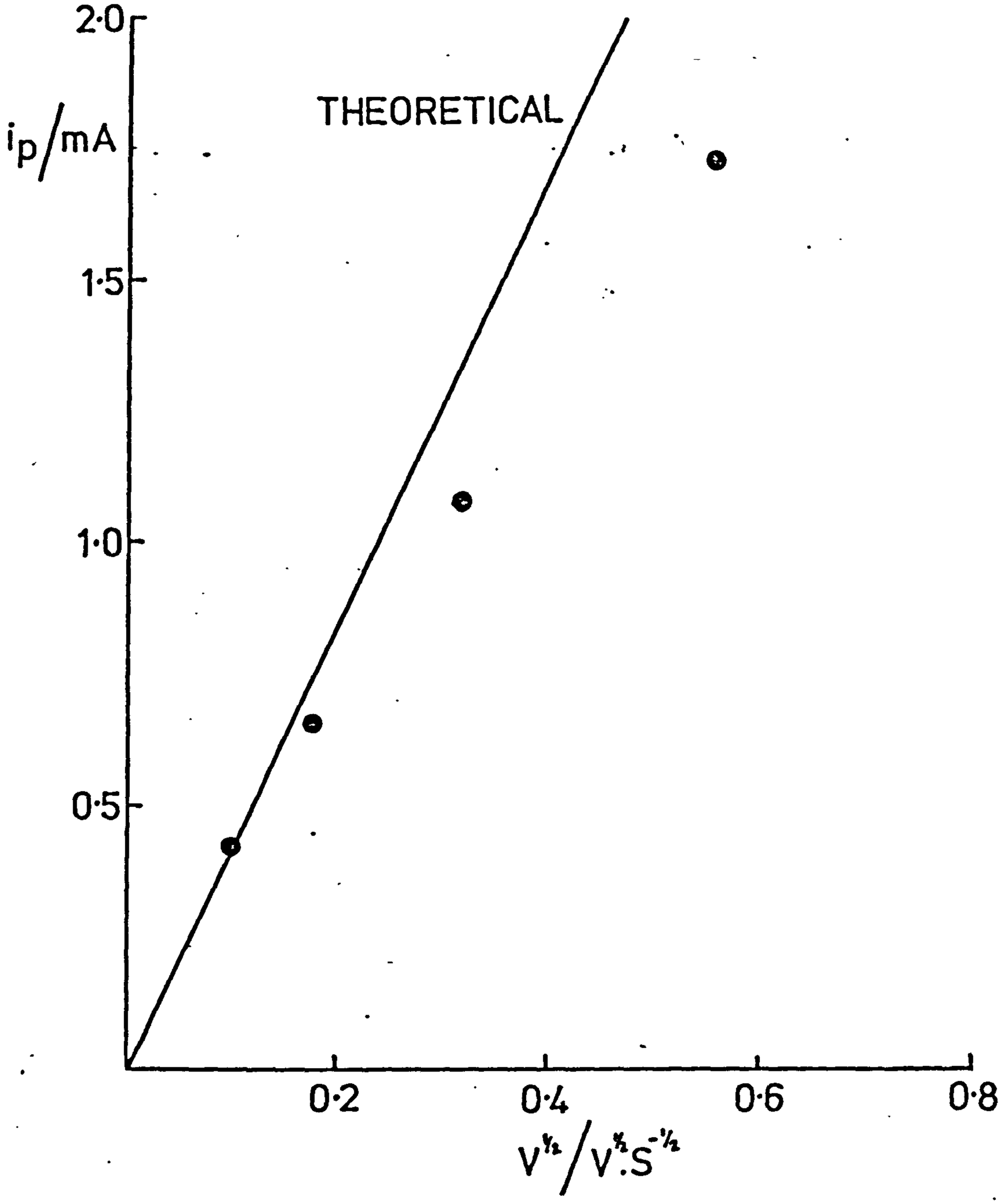

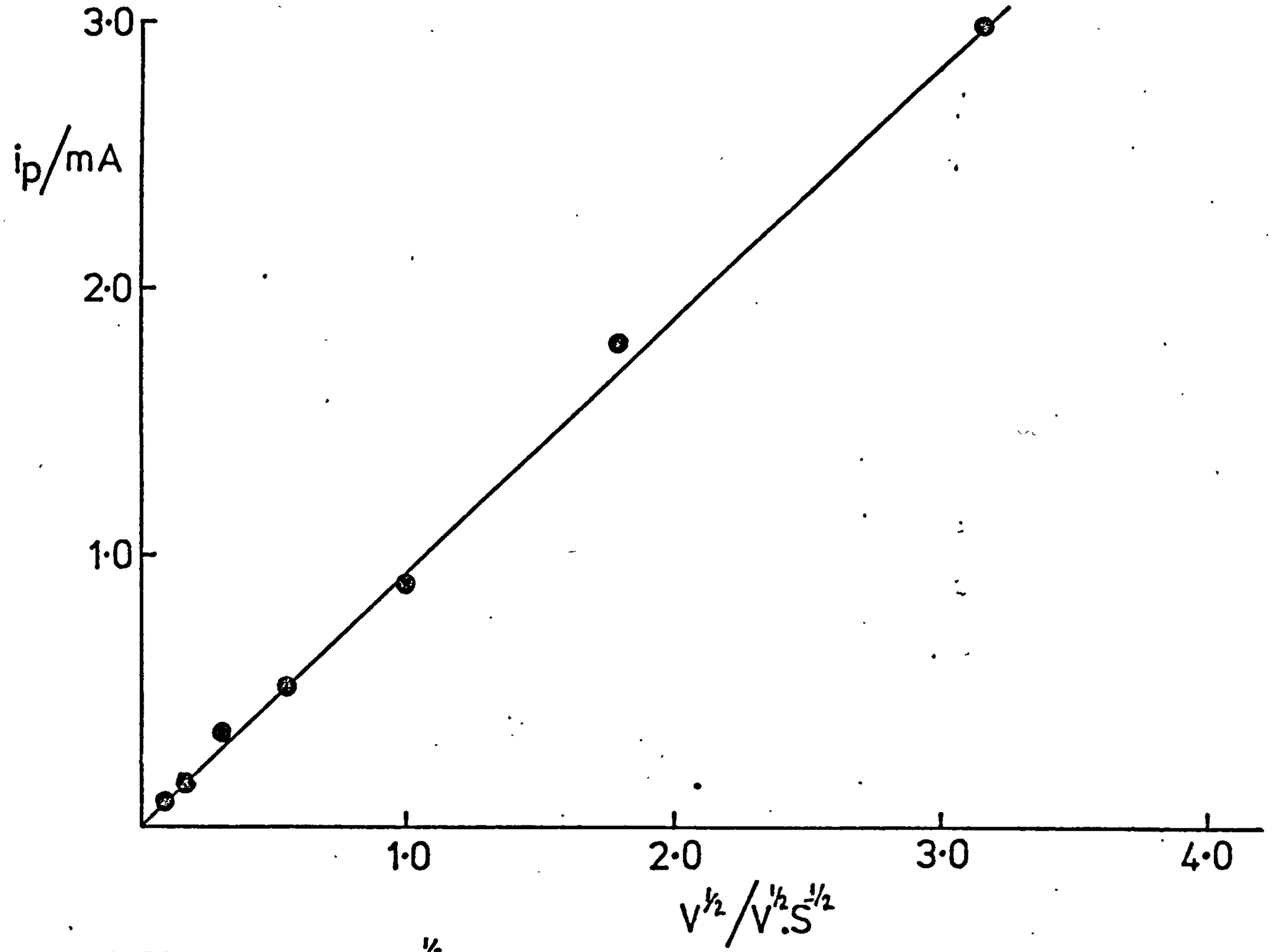

FIG. 6.37b i_p vs $V^{1/2}$ FOR AMALGAM C IN 1M H_2SO_4

cathodic peak is observed which corresponds to the reduction of solid $PbSO_4$.

Amalgam B has a reasonable fit to i_p vs $V^{\frac{1}{2}}$, Figure 6.37(a). However, the current after the maximum for the curve in Figure 6.35 when plotted as i vs $t^{-\frac{1}{2}}$, Figure 6.38, is higher than expected. This shows that initiation of a solid reaction takes place after the maximum. This is a well known result and is due to the fact that if the nuclei of the solid phase are separated by a distance greater than the diffusion layer then a greater surface area than the geometric area is offered to the flux. That this is the correct explanation is reinforced in Figure 6.38, as the current increases with decreasing sweep rate showing that the surface area is increasing with time. Only the reduction of the solid is observed. Ohmic effects preclude an exact analysis. This is shown clearly in Figure 6.37(a) where the experimental points lie on the predicted straight line at low currents but bend off at higher currents.

Amalgam C gives a good fit to equation (6.16) for all sweep rates Figure 6.37(b). At low sweep rates the nucleation and growth of solid $PbSO_4$ appears clearly as an hysteresis. Two peaks appear on reversing the potential due to the reversible reduction of the soluble species and to the reduction of the solid. i vs $t^{-\frac{1}{2}}$ is higher than the theoretical indicating solid growth soon after the maximum. At faster sweep rates the formation and reduction of solid $PbSO_4$ disappear.

The dissolution reaction at the foot of the wave is first order in Pb concentration (by comparing A and B) as expected for a reversible reaction.

FIG. 6.38 i vs $t^{-1/2}$ FOR AMALGAM B IN $1M\ H_2SO_4$

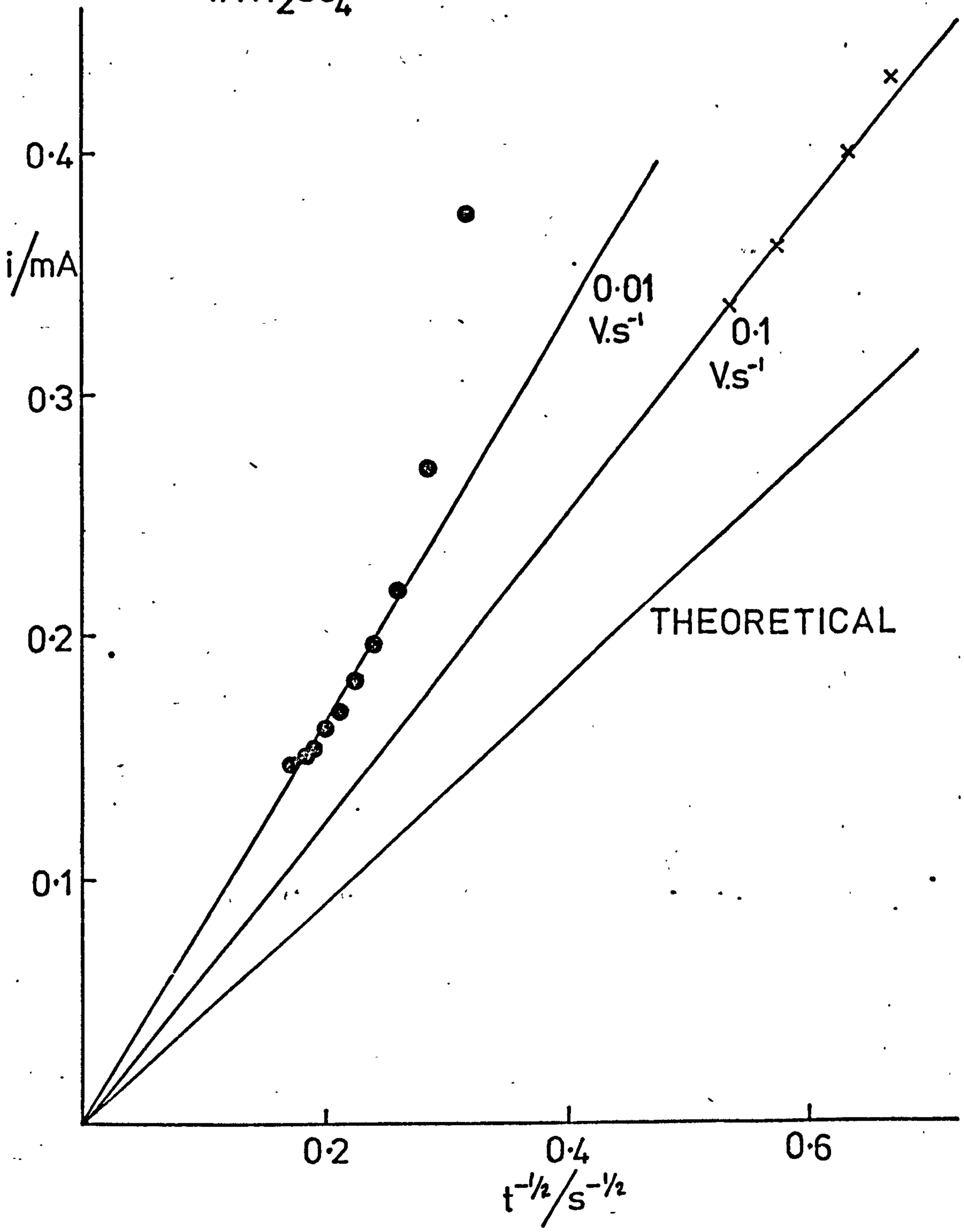

These results substantiate the previously suggested reaction mechanism in which Pb dissolves as Pb^{2+} containing species in parallel with $PbSO_4$.

6.5. The effect of Organic Additives

Lead acid battery manufacturers add various lignin based organic compounds to the negative plate paste. The exact role of these additives is unknown. The purpose of this section is to investigate the effect these additives have on the dissolution of Pb(Hg) and solid Pb in 1M H_2SO_4. 1M H_2SO_4 was saturated with the organic ('Van Dyke Brown') and filtered through sintered glass. A saturated solution is denoted as S. Saturated solutions diluted χ times with 1M H_2SO_4 are denoted S/χ. 'Van Dyke Brown' is a well known lead battery negative plate additive. It is a large complex molecule of the lignin type with an open lattice structure. The exact structure is unknown.

Lead amalgams

The effect of saturating the electrolyte with a lignin based additive is shown in Figure 6.39a,b,c,d, which were measured under identical conditions to Figure 6.36. The peak due to the reduction of soluble Pb almost vanishes and a peak due to the reduction of solid $PbSO_4$ appears. The anodic peak heights are about the same but shifted to more anodic potentials. Slower sweeps Figure 6.39(a) show that the soluble Pb peak disappears completely. No electro-crystallisation reaction is observed.

E_p shifts with v instead of being independent of v without the organic. The shift in potential is characteristic of an irreversible reaction. The Tafel slope measured at the foot of the wave and by E_p shift with v is in the region of 30 - 40 mV. Figure 6.40 demonstrates

FIG. 6.39a POTENTIAL SWEEP ON AMALGAM C IN 1M H_2SO_4 SATURATED WITH ORGANIC ADDITIVE (S). $v = 0{\cdot}03\ V.s^{-1}$

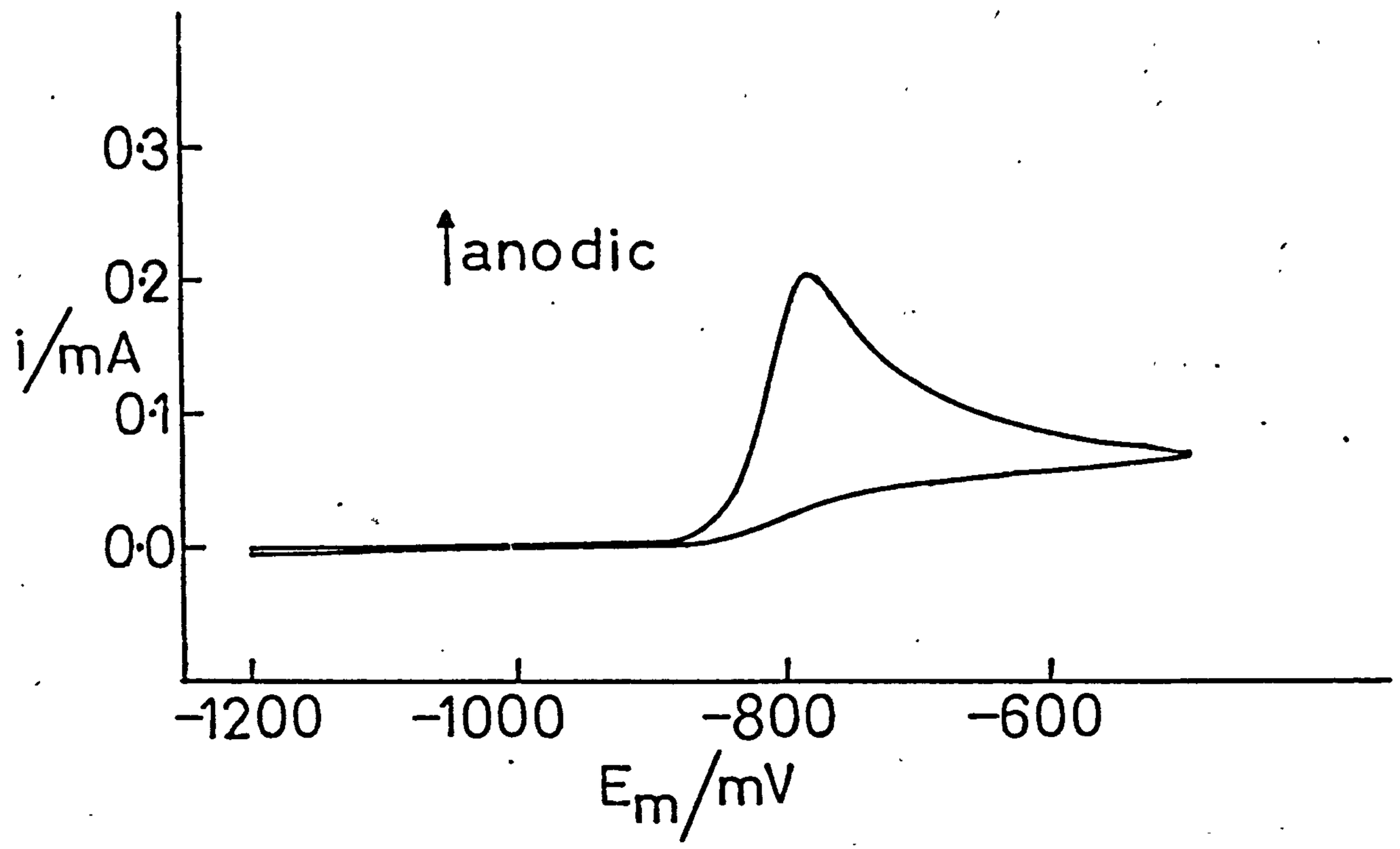

Fig. 6.39. Potential sweep on Amalgam C in 1M H_2SO_4 saturated with organic additive. (S)

(b) $v = 1\ V\ s^{-1}$

Y axis, 0.5 mA/division

X axis, 100 mV/division

Cathodic end -1200 mV E_m

(c) $v = 3.2\ V\ s^{-1}$

Y axis, 0.5 mA/division

X axis, 100 mV/division

Cathodic end -1200 mV E_m

(d) $v = 10\ V\ s^{-1}$

Y axis, 0.5 mA/division

X axis, 100 mV/division

Cathodic end -1200 mV E_m

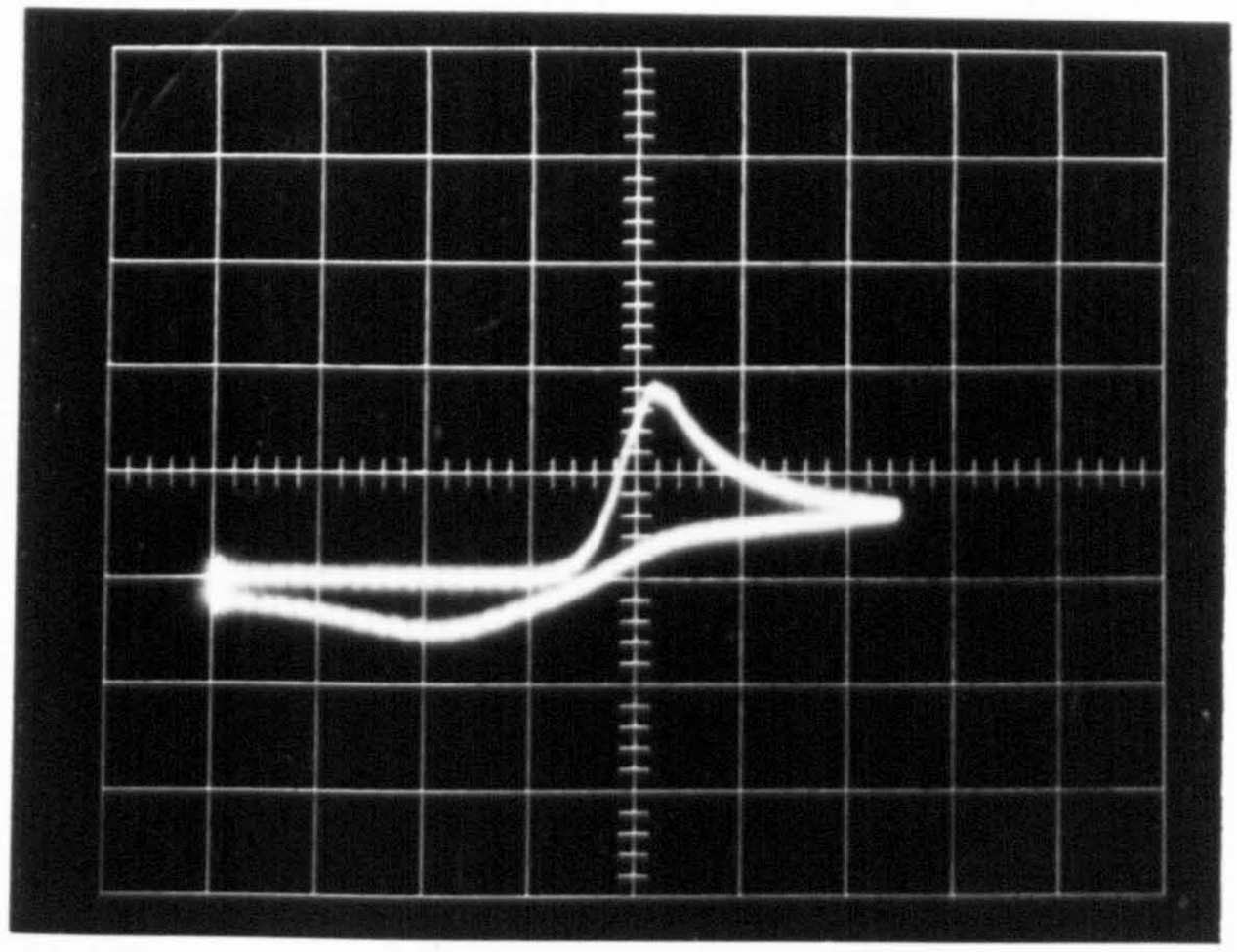

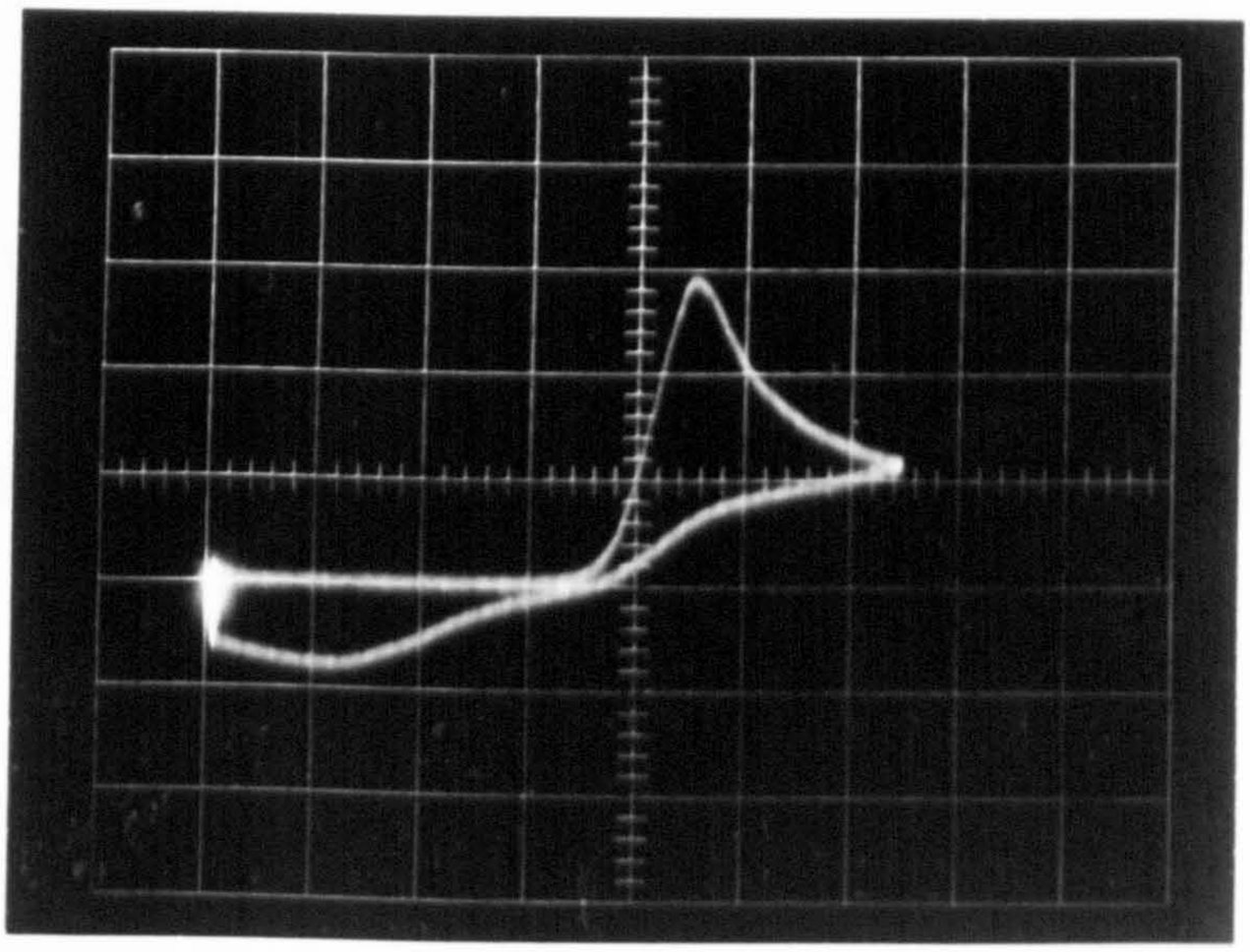

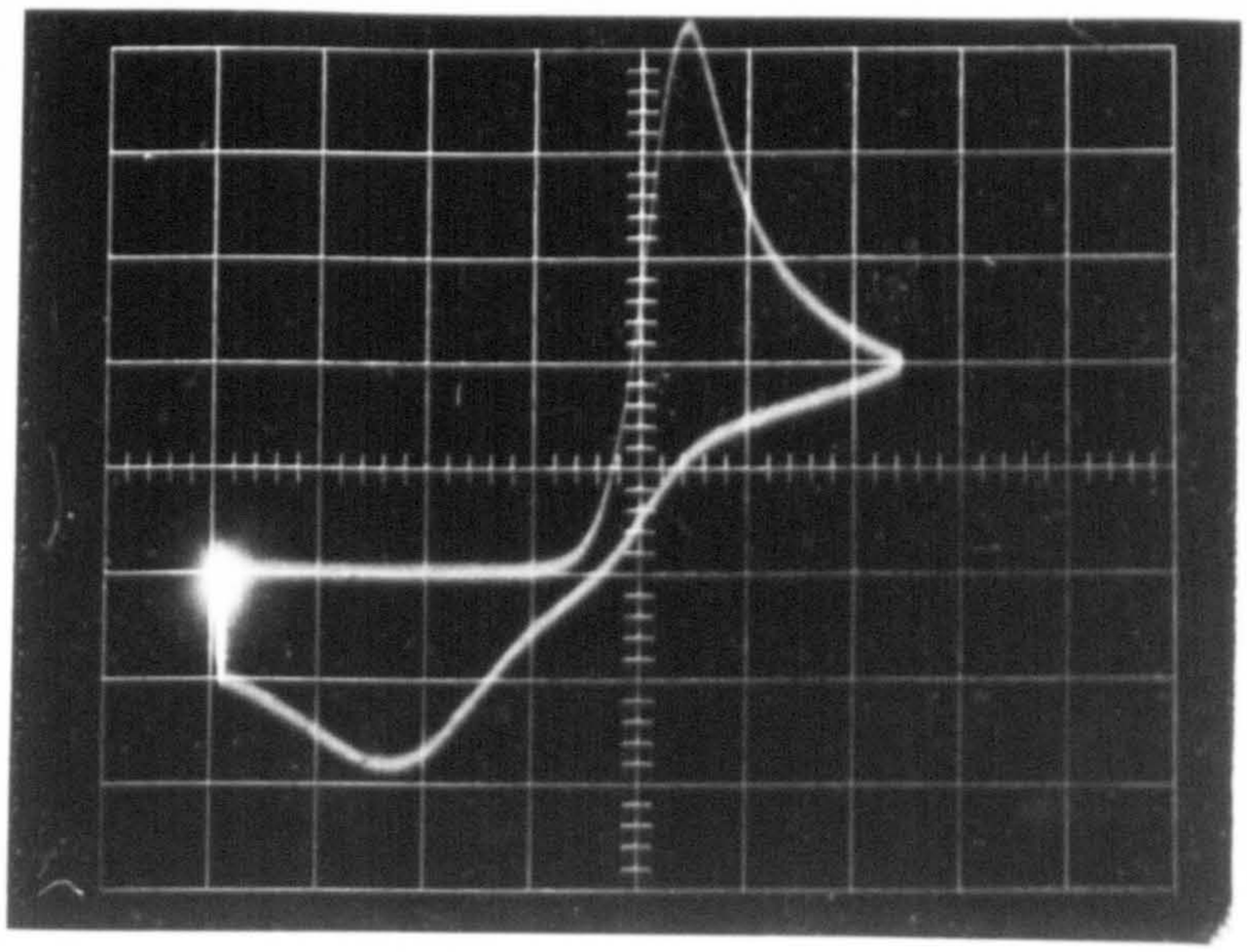

FIG. 6.40 LOG i vs E FOR AMALGAM C
$v = 0{\cdot}03\ V s^{-1}$

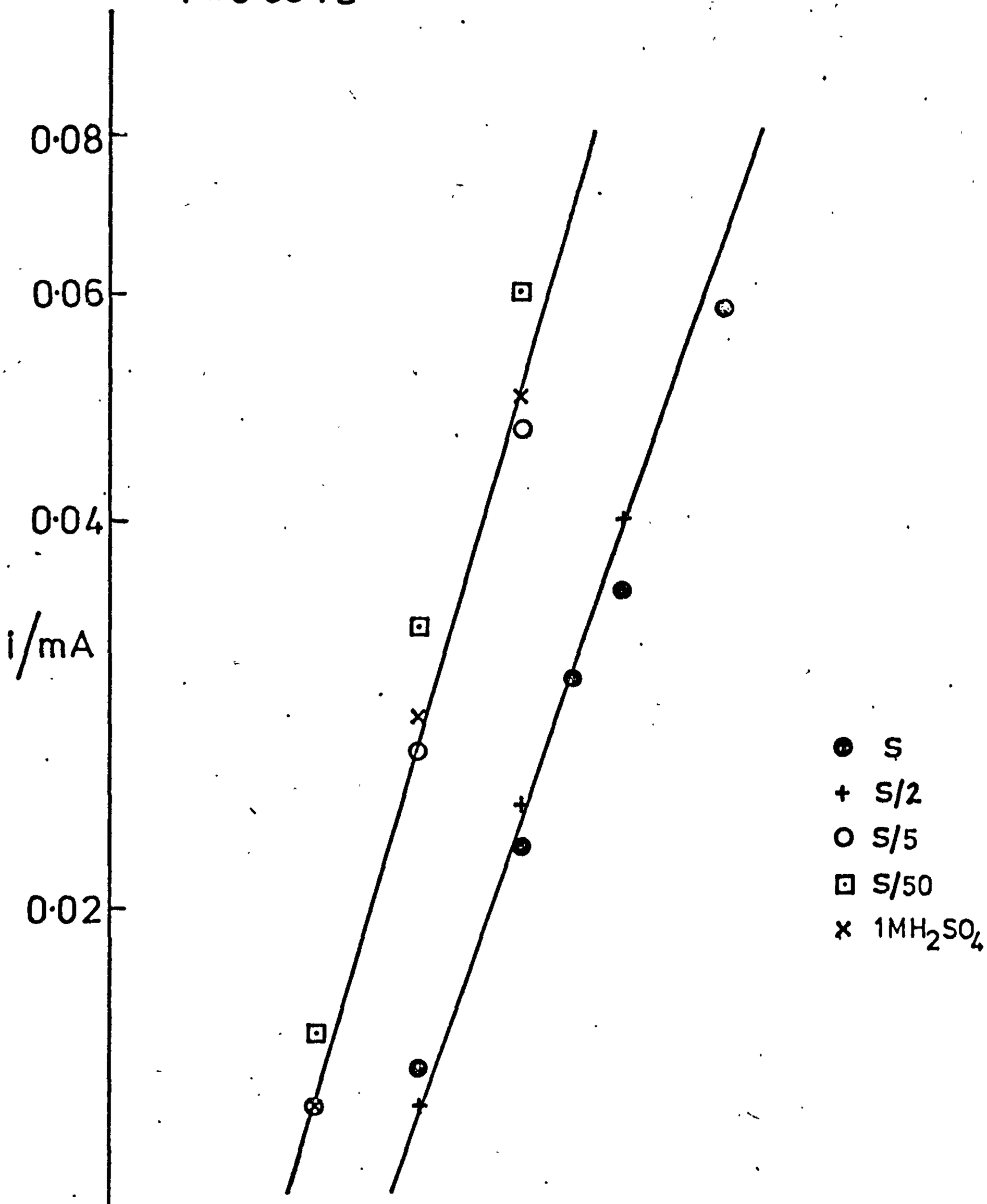

the action of the organic concentration on the current-voltage characteristic at the foot of the wave. Below $^{S}/_{5}$ the Tafel slope is independent of concentration and has a value near to 30 mV and the reversible dissolution reaction is only present. This is substantiated in Figures 6.41, a,b,c, where, the sweep curves are reproduced. The peaks are separated by 30 mV, independent of ν. At concentrations above $^{S}/_{5}$ the Tafel slope is still approximately 30 mV, however the curve is shifted to higher potentials and clearly represents an irreversible reaction. The complete sweep curves in Figure 6.41 agree with this conclusion. At lower sweep rates Figure 6.41,d, and Figure 6.41, e, the product is a soluble species. The anodic and cathodic peaks are separated by $\sim$60 mV which depends on ν. At very high sweep rate Figure 6.41f, a new phenomenon is seen, the soluble species reduction peak disappears and a new peak appears. This is very similar to the reduction peak of solid $PbSO_4$ which has been observed with the more concentrated amalgams and with solid Pb.

Discussion

Figure 6.42 is a simple diagram of the situation which is believed to exist, based on these measurements, at a Pb(Hg) surface in the presence of sulphuric acid saturated with organic additive. A layer of the bulky organic molecules is adsorbed onto the surface and is fully formed when the concentration of organic reaches a certain critical value. This corresponds to full coverage which maybe a monolayer. Transport through the layer of Pb^{2+} containing species is restricted so that it is slower than diffusion away into the solution. It will be assumed that $SO_4^{=}$ can move freely through the layer in the opposite direction. $SO_4^{=}$ is in equilibrium with H_2SO_4 so its concentration cannot be depleted.

Fig. 6.41 Potential sweeps on Amalgam C

(a) $v = 1\ V\ s^{-1}$, S/50
Y axis, 0.5 mA/division
X axis, 100 mV/division
Cathodic end -1200 mV E_m

(b) $v = 3.2\ V\ s^{-1}$, S/50
Y axis, 0.5 mA/division
X axis, 100 mV/division
Cathodic end -1200 mV E_m

(c) $v = 10\ V\ s^{-1}$, S/50
Y axis, 1 mA/division
X axis, 100 mV/division
Cathodic end -1200 mV E_m

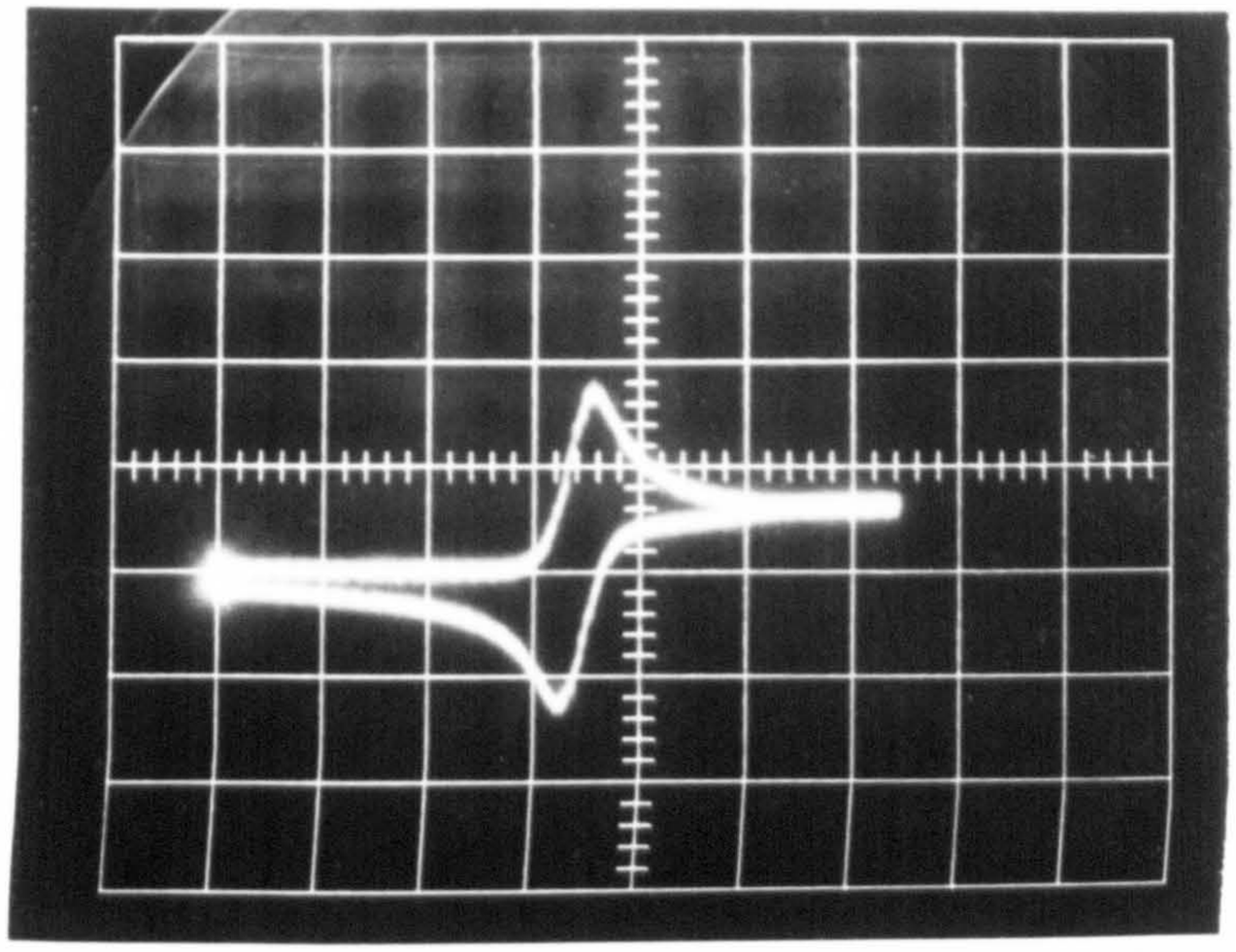

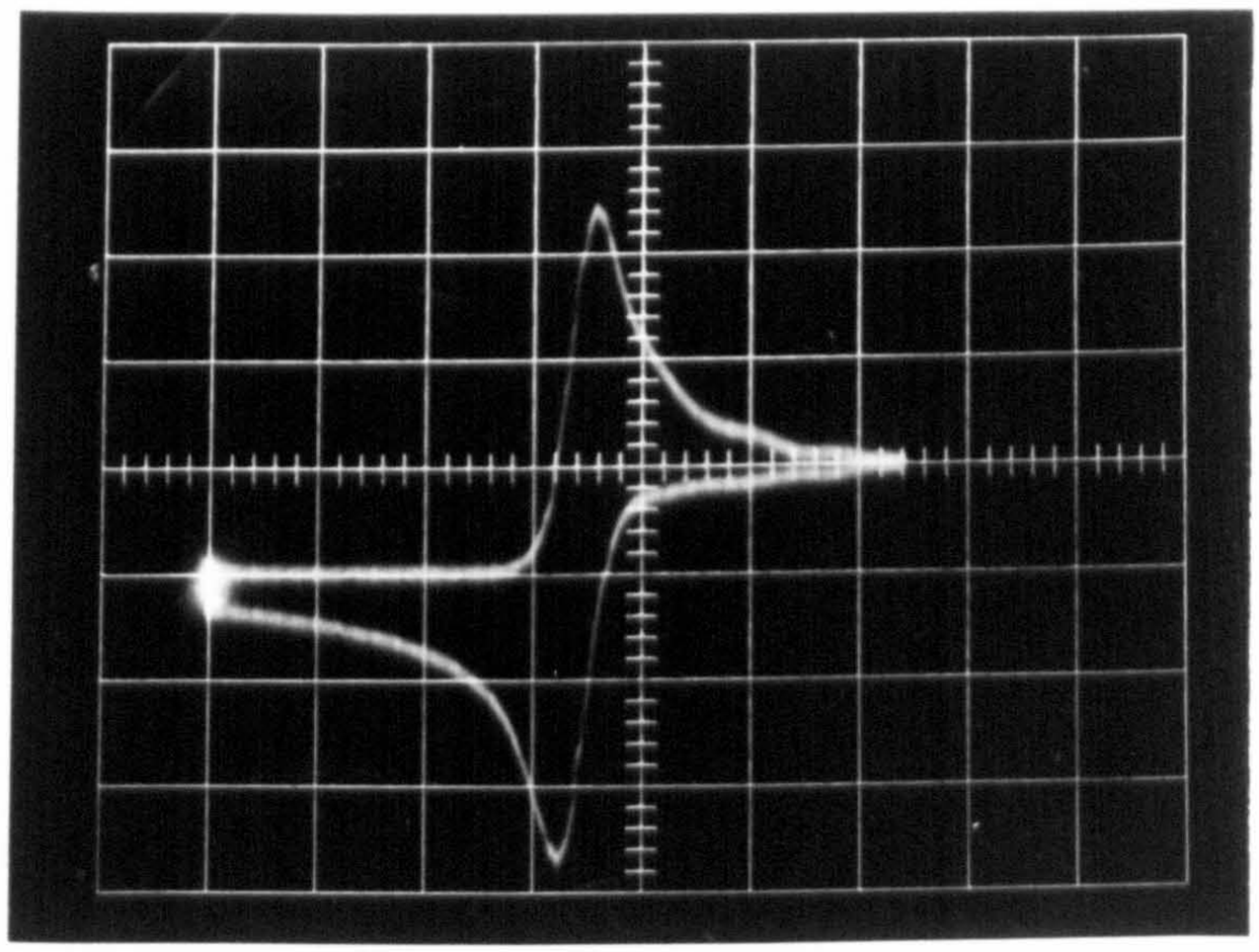

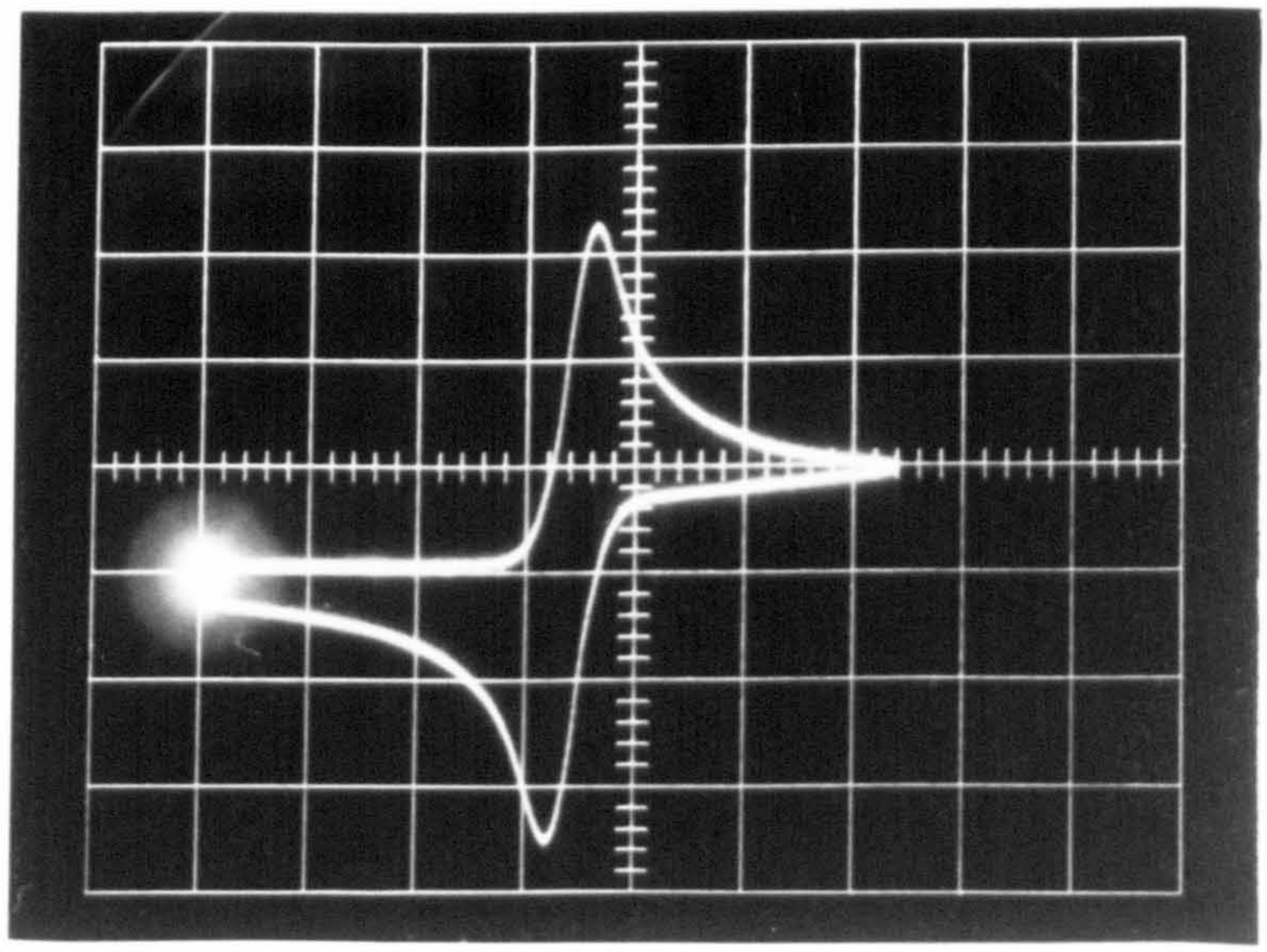

Fig. 6.41 Potential sweeps on Amalgam C

(d) $v = 1\ V\ s^{-1}$, S/5

Y axis, 0.5 mA/division

X axis, 100 mV/division

Cathodic end -1200 mV E_m

(e) $v = 3.2\ V\ s^{-1}$, S/5

Y axis, 0.5 mA/division

X axis, 100 mV/division

Cathodic end -1200 mV E_m

(f) $v = 10\ V\ s^{-1}$, S/5

Y axis, 1 mA/division

X axis, 100 mV/division

Cathodic end -1200 mV E_m

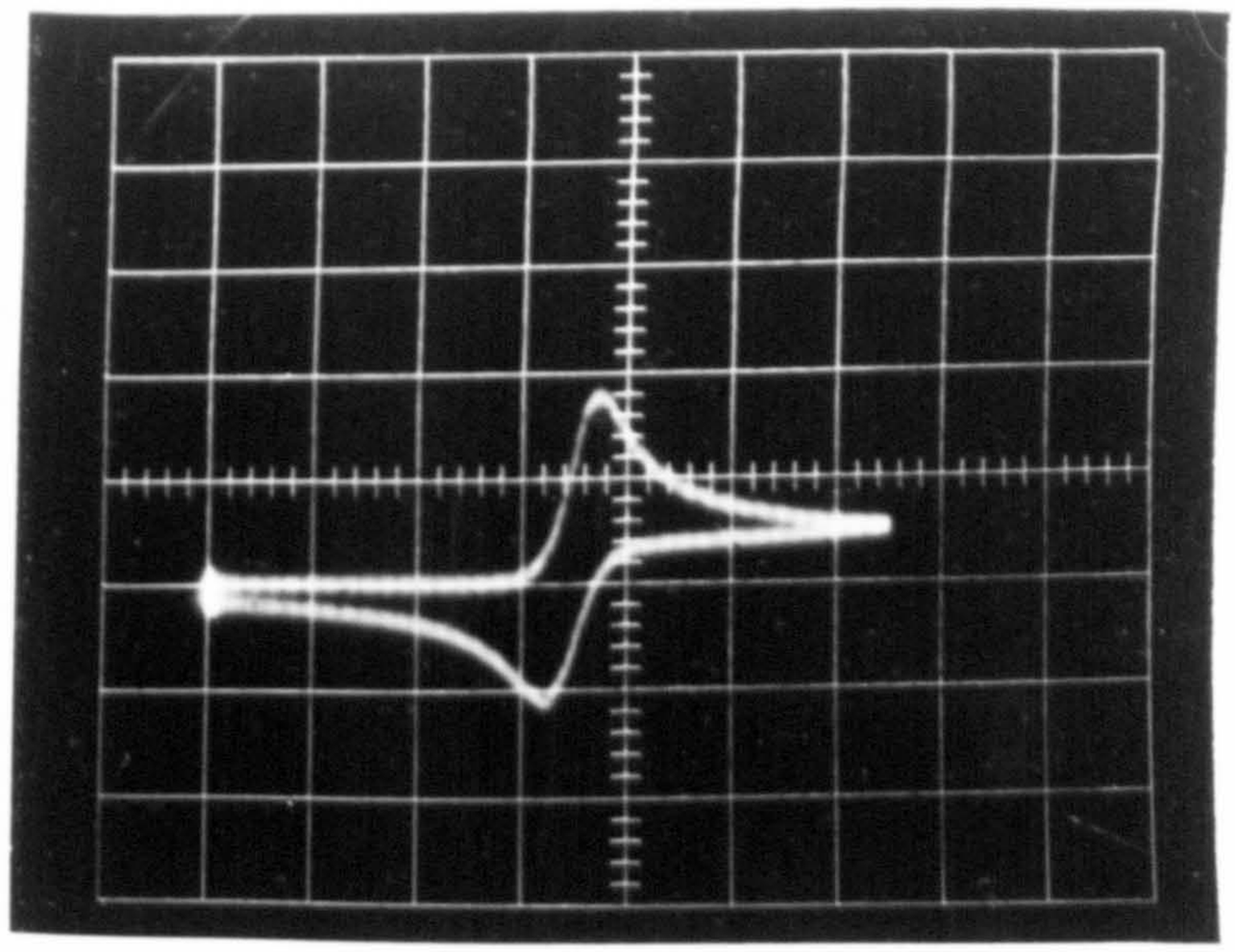

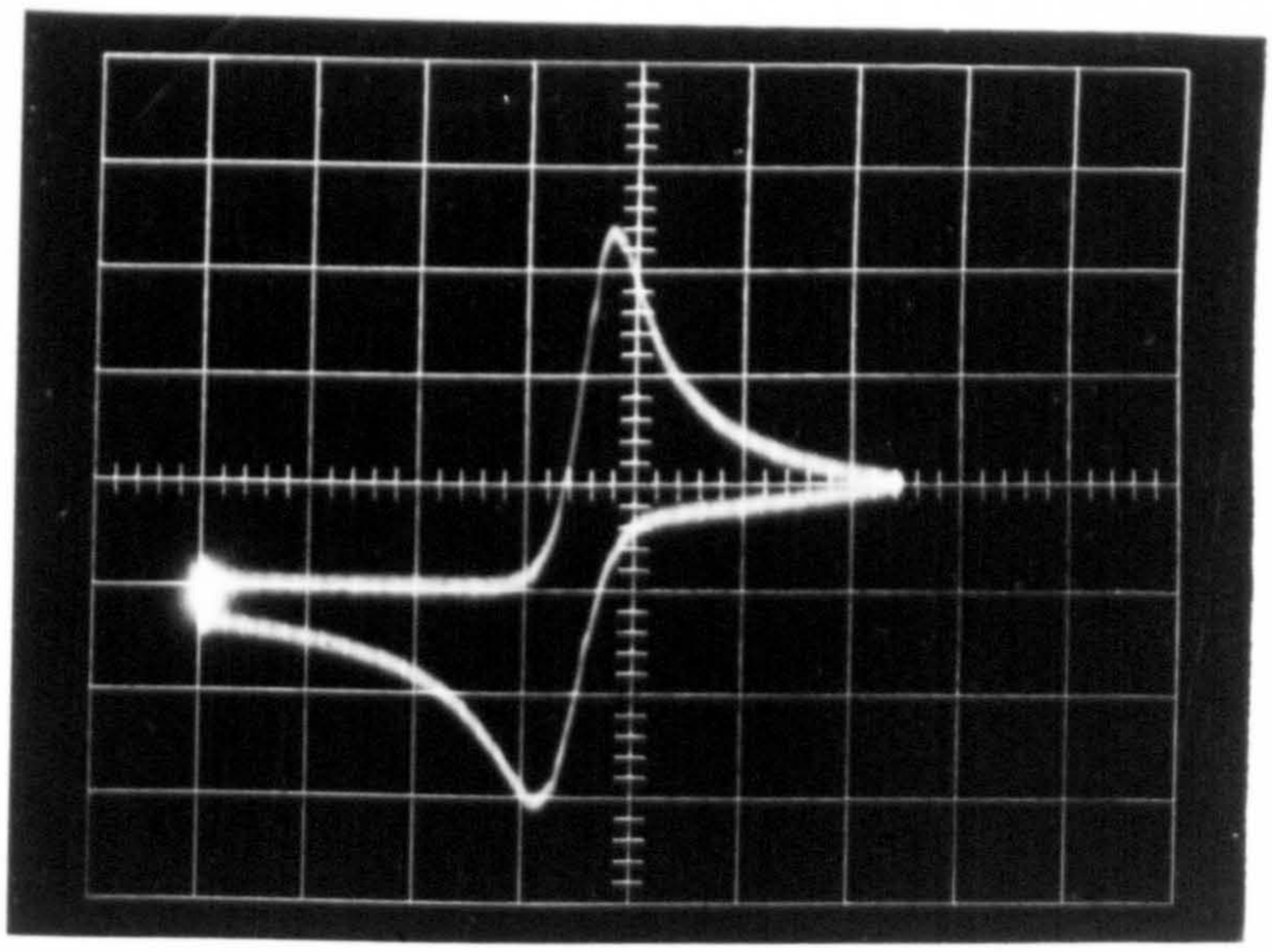

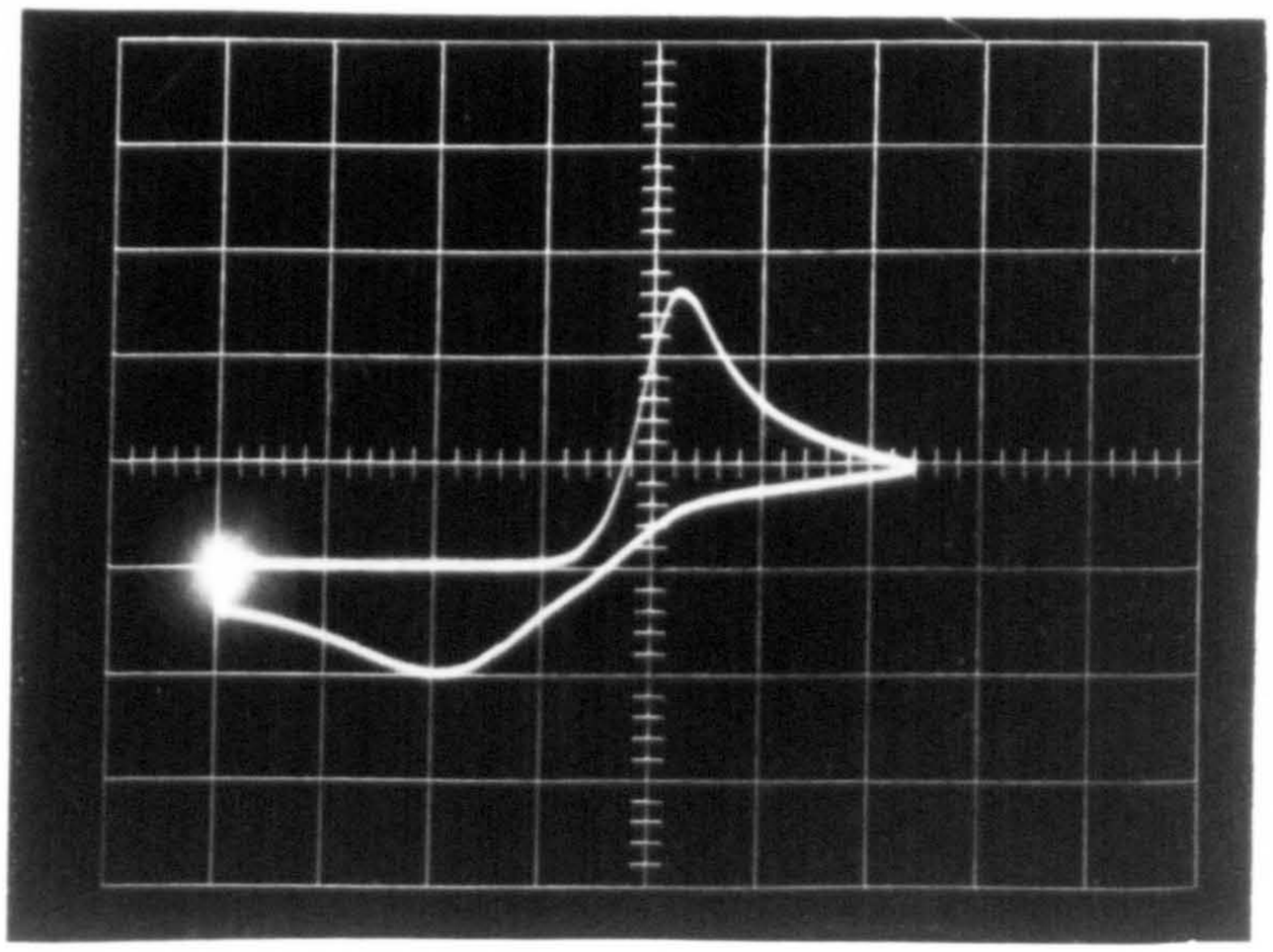

FIG. 6.42 A POSSIBLE SITUATION WHICH EXISTS AT A Pb(Hg) SURFACE IN THE PRESENCE OF ORGANIC ADDITIVE.

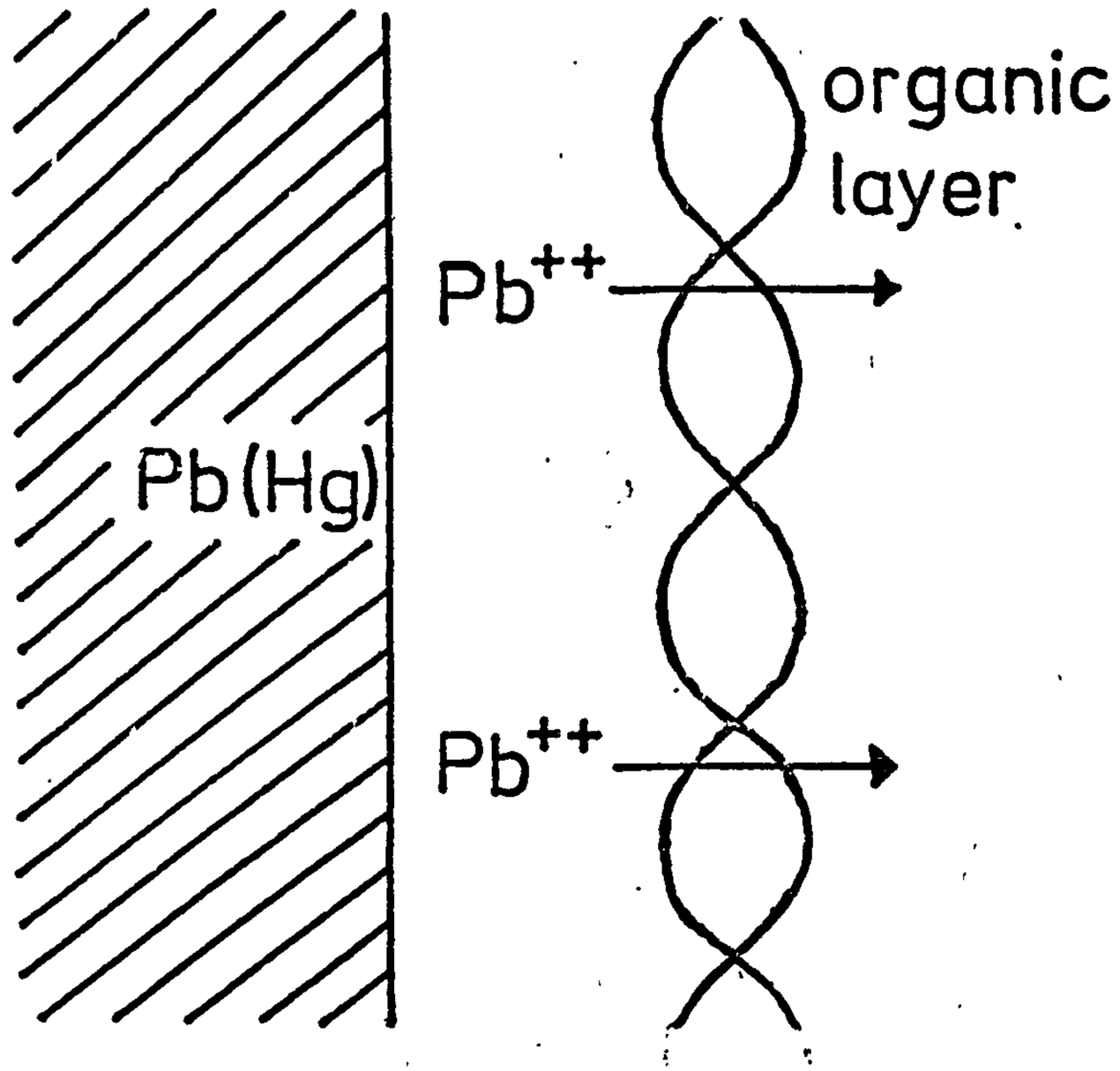

The Tafel slope will be calculated as

$$i = k[Pb^{2+}]_s$$

from the Nernst Equation

$$E - E^\circ = \frac{RT}{nF} \ln \frac{[Pb^{2+}]_s}{[Pb]_s}$$

If $[Pb]_s$ and the ionic activity coefficient of Pb^{2+} is constant then

$$i = k' \exp \frac{(E-E^\circ)nF}{RT}$$

i.e. will be approximately 30 mV. Because of the slow rate of transport through the layer the concentration of Pb^{2+} can exceed the solubility product and precipitate as $PbSO_4$. This is supported by the faster sweep experiments Figures 6.39b,c,d, Figure 6.41f. Here actual reduction peaks appear due to the reduction of a solid $PbSO_4$ phase which is formed between the organic layer and the Pb(Hg). The slower sweep experiments Figure 6.39a, Figure 6.41e, show no reduction peak. The rate of Pb^{2+} production does not exceed transport through the layer so there is no build up of Pb^{2+} in the layer and the concentration does not exceed that of the solubility product.

Solid lead

Figures 6.43a,b are potential sweeps at the base of the wave on solid lead with and without the additive. Similar behaviour is observed to the amalgams in the presence of organic, in which the soluble species is not reduced. Figure 6.44 shows a stationary current-voltage relationship taken from short time potentiostatic pulses at the rotating disc (in order to dissolve a minimum of the Pb). The effect of the organic is to displace the curve to more anodic potentials although it has a similar Tafel slope.

FIG. 6.43 POTENTIAL SWEEPS ON SOLID LEAD
$v = 0{\cdot}1\ V.s^{-1}$

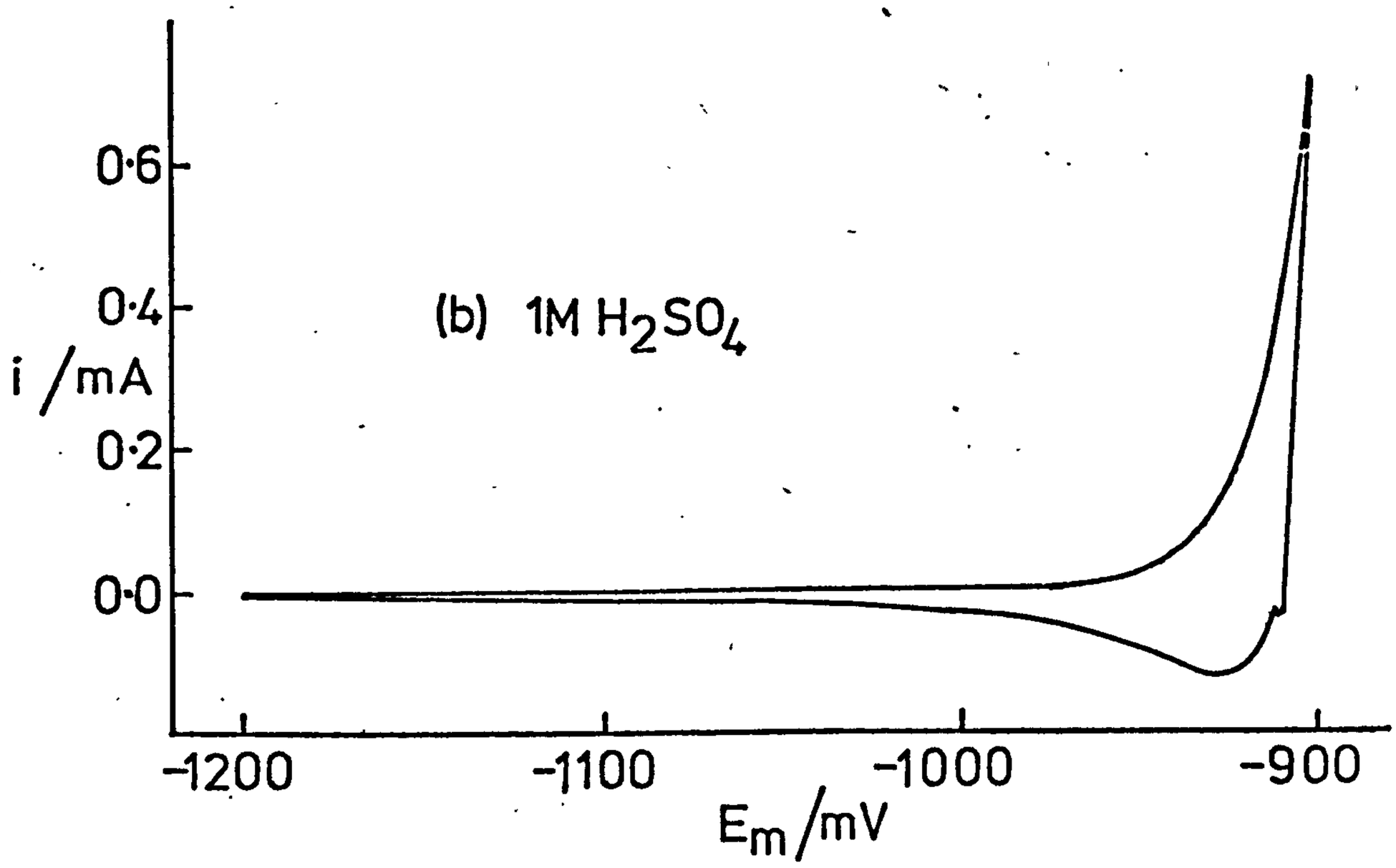

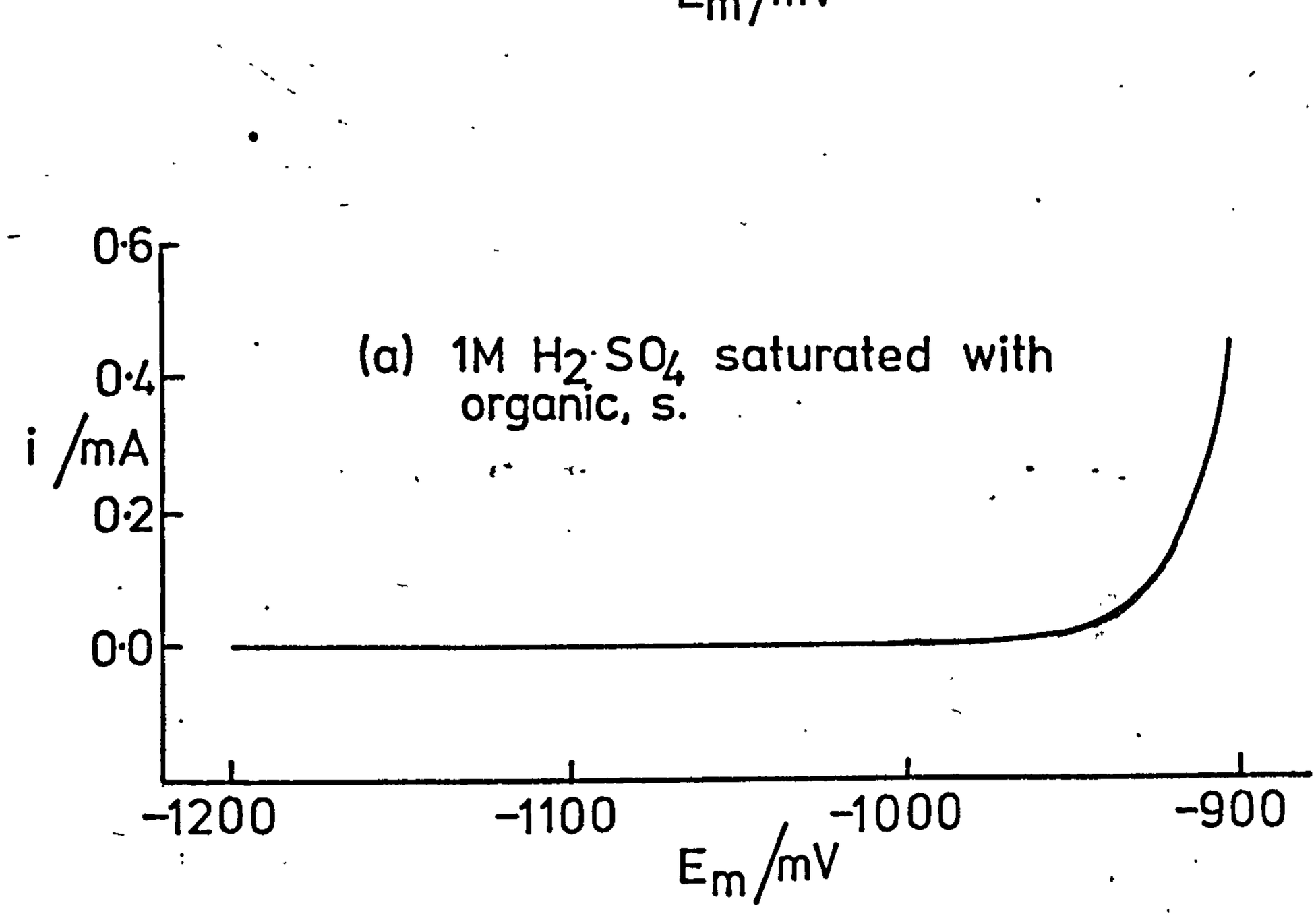

FIG. 6.44 LOGi vs E FROM SHORT TIME POTENTIOSTATIC PULSES ON A ROTATING LEAD ELECTRODE

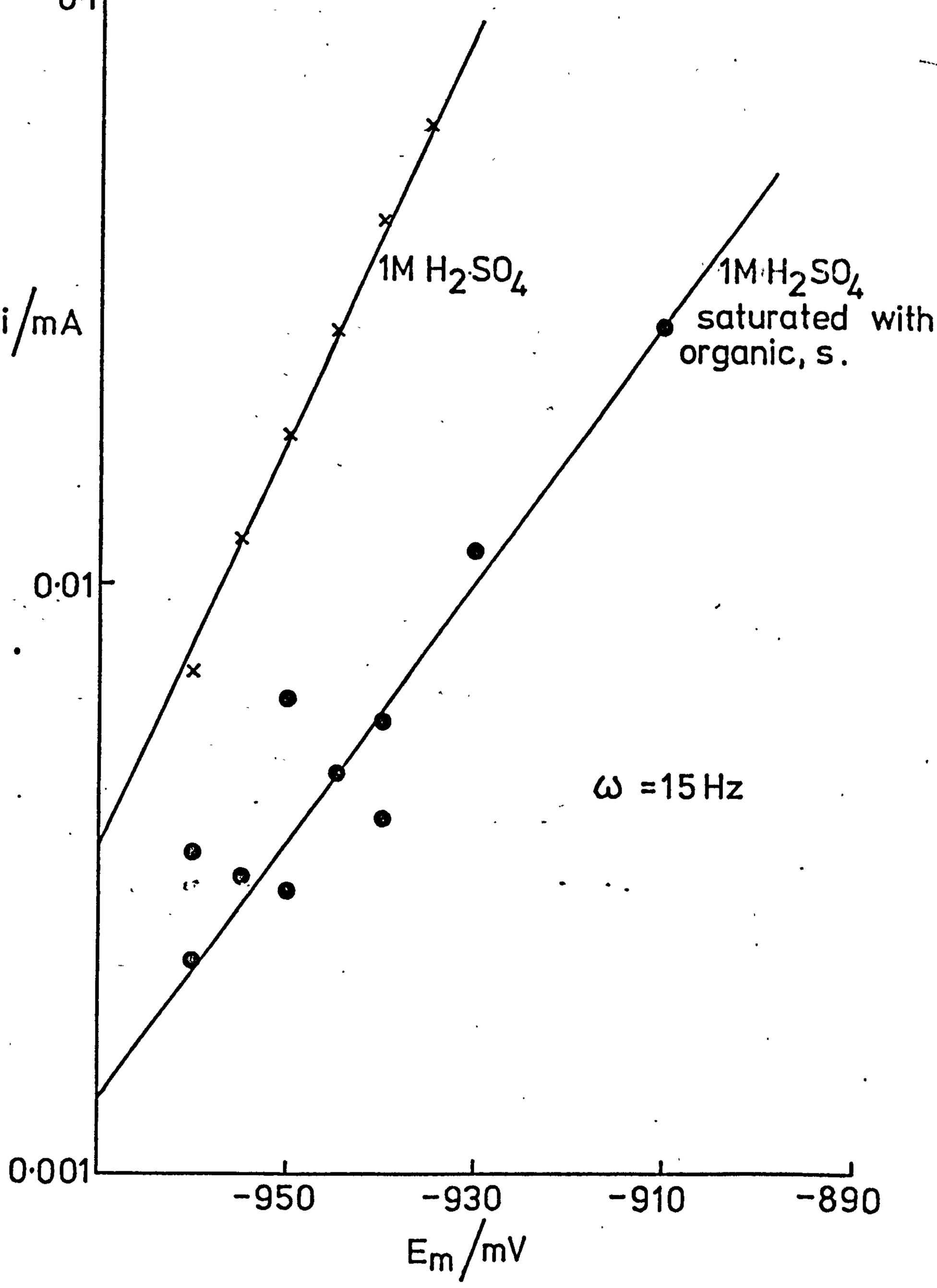

Unfortunately the experimental accuracy is not very high as only a limited range of low currents is available due to the onset of the solid state formation of $PbSO_4$.

The solid state reaction, typified by rising transients, which is not seen on amalgams until much more positive potentials is more important here since Pb is more readily available. The solid reaction is however suppressed in the presence of organic and appears approximately 15 mV later than solutions without the organic. At these low potentials a model similar to Figure 6.42 also seems to be operating on solid Pb. However at higher potentials Pb is readily available and the solid state reaction predominates.

6.6. The Pb/H_2SO_4 Battery

A s.l.i. battery can deliver 170A per cell for $\sim$3 min. If the surface area of the -ve plates measured by B.E.T. is 200 m^2/cell then under these conditions 0.1 mA cm^{-2} is flowing. It is not possible to make a direct comparison of the behaviour of a single negative plate with a flat electrode as the i - E characteristic and the response to a potentiostatic pulse of the plate is unknown. It seems likely that at such low currents the battery is operating mainly through a dissolution and precipitation mechanism for the formation of $PbSO_4$. In addition Figure 6.22 suggests that the solid state mechanism is undesirable as it eventually passivates the electrode. In order to be nearer to the actual conditions in a battery, measurements were made in 4.7M H_2SO_4 (the concentration of a fully charged battery acid) over a varying temperature range.

Effect of temperature

Figure 6.45 shows the dissolution currents, taken from potentiostatic pulses (at low η) vs E at -18°C, 0°C and 23°C for 4.7M H_2SO_4. Since large residual currents were observed due to hydrogen evolution and impurities, a correction derived by extrapolation was necessary. The Tafel slopes were as follows; 23°C, 29 mV/decade; 0°C, 29 mV/decade; -18°C, 27 mV/decade; theoretical slopes for a 2e reversible reaction at these temperatures are 30.4, 28.0, 26.2, mV/decade respectively. The dissolution current is observed to decrease with decreasing temperature for a fixed potential.

Figure 6.46, shows the dependence of the rate of solid reaction on potential. These results were taken from potentiostatic pulse measurements (at high η). Here the solid reaction is shifted to anodic potentials with decreasing temperature.

Effect of organic additives

Figure 6.47, shows the dependence of the dissolution reaction on potential in acid saturated with organic additive. The results are taken from potentiostatic measurements. The Tafel slopes are considerably altered from those without the additive; 23°C, 43 mV/decade; 0°C, 52 mV/decade; -18°C, 38 mV/decade. The dependence of the solid reaction is shown in Figure 6.46.

Both dissolution as a soluble species and solid reaction are suppressed by the presence of the organic. A similar mechanism to the one already described, probably operates.

FIG. 6.45 TAFEL PLOT i vs E TEMP. DEPEND.
4·7M H_2SO_4 ω=15 Hz.

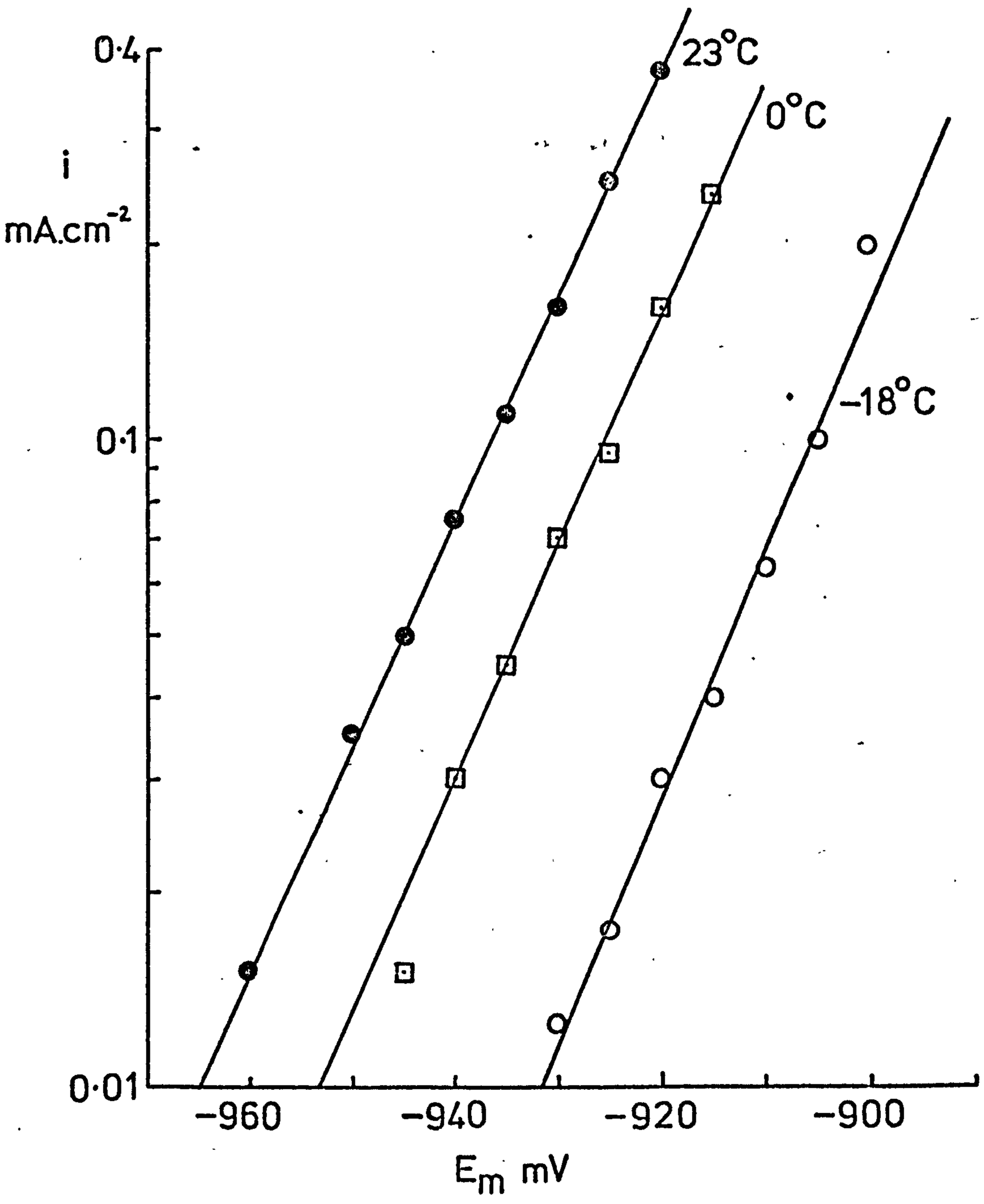

FIG. 6.46 i/t vs E FOR SOLID Pb

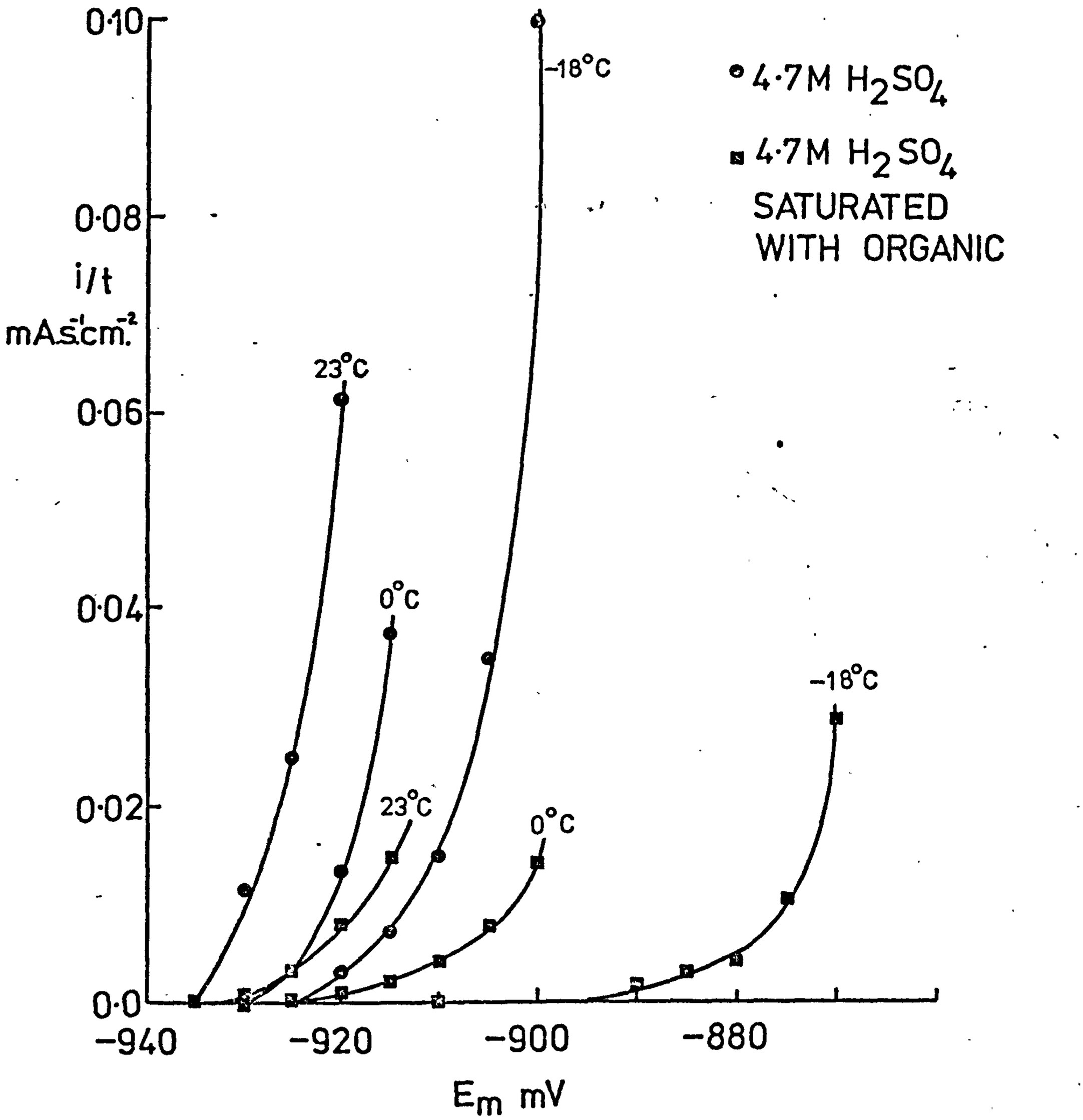

FIG. 6.47 TAFEL PLOT 4·7M H_2SO_4 SAT. WITH ORGANIC

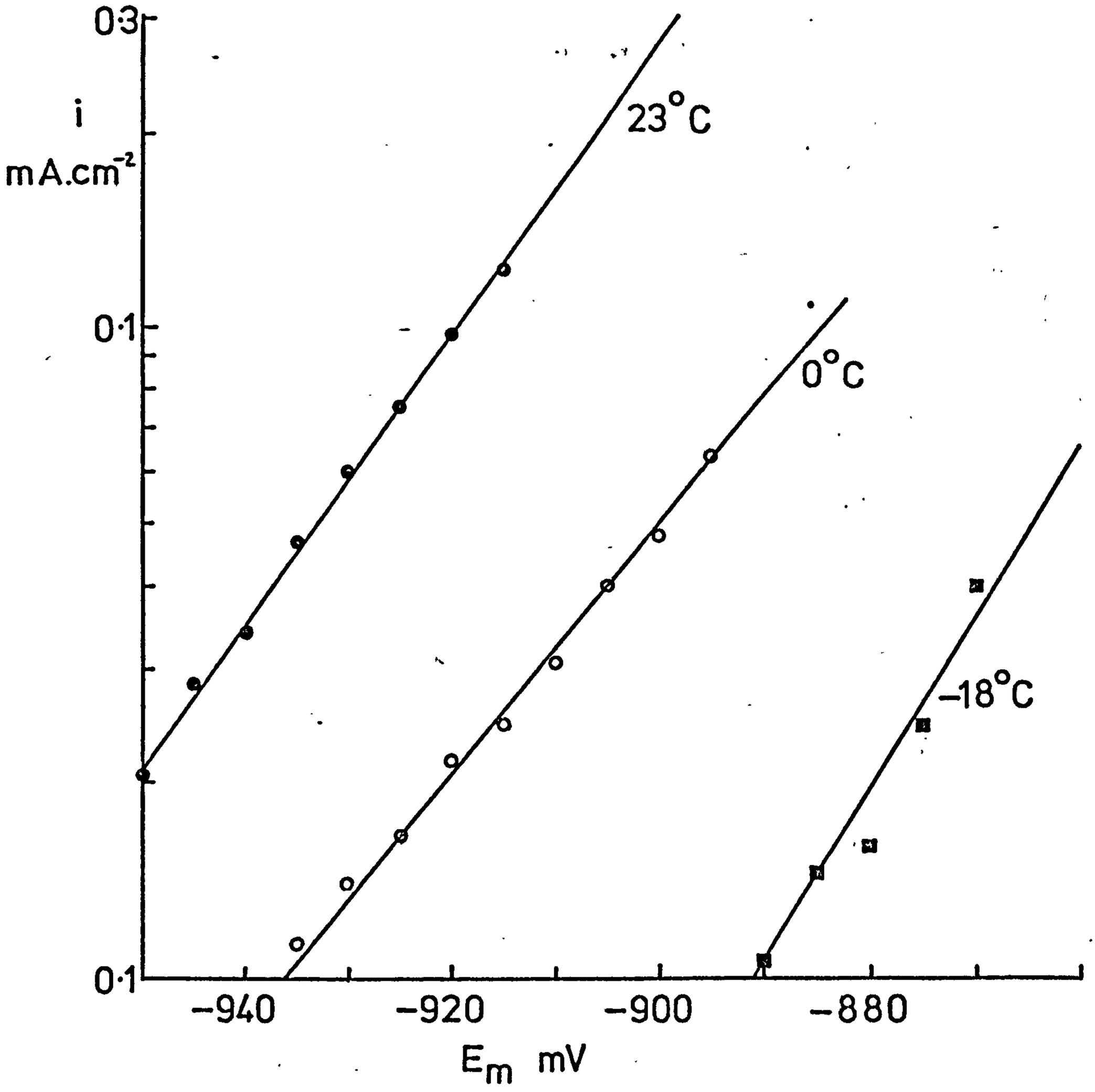

Cycling of a stationary electrode

Repetitive pulses between -926 mV E_m and -1200 mV E_m for mechanically and electropolished electrodes showed a steepening of the rising transient (i.e. i/t increasing) for successive pulses until after about 3 cycles, when the transients had the same shape and the anodic charge Q_a was approximately equal to the cathodic charge Q_c.

The effect of $BaSO_4$

If barium sulphate is rubbed into the surface of a lead electrode the solid reaction is enhanced, occurring at potentials anodic to -960 mV E_m and dissolution becomes negligible.

The effect of $BaSO_4$, C, and organic additive

Potential pulses were carried out on a lead rotating disc electrode (ω = 15 r.p.s.) in 1M H_2SO_4, saturated with Van Dyke Brown, and some with $BaSO_4$ and carbon rubbed into its surface. The results are summarised in Figure 6.48. The organic additive alone inhibits the current by approximately a factor of 100 suppressing both currents due to the solid state process and dissolution. However if the surface is impregnated with carbon and $BaSO_4$ the currents are increased. This is probably due to disruption of the organic layer.

Structure of the deposit

Stereoscan micrographs of the lead sulphate formed on lead with and without the organic additive are different Figures 6.49, 6.50. Micrographs of lead sulphate formed on lead in 1M H_2SO_4 show that the

FIG. 6.48 TAFEL PLOTS FROM PULSES

25°C ω =15Hz.

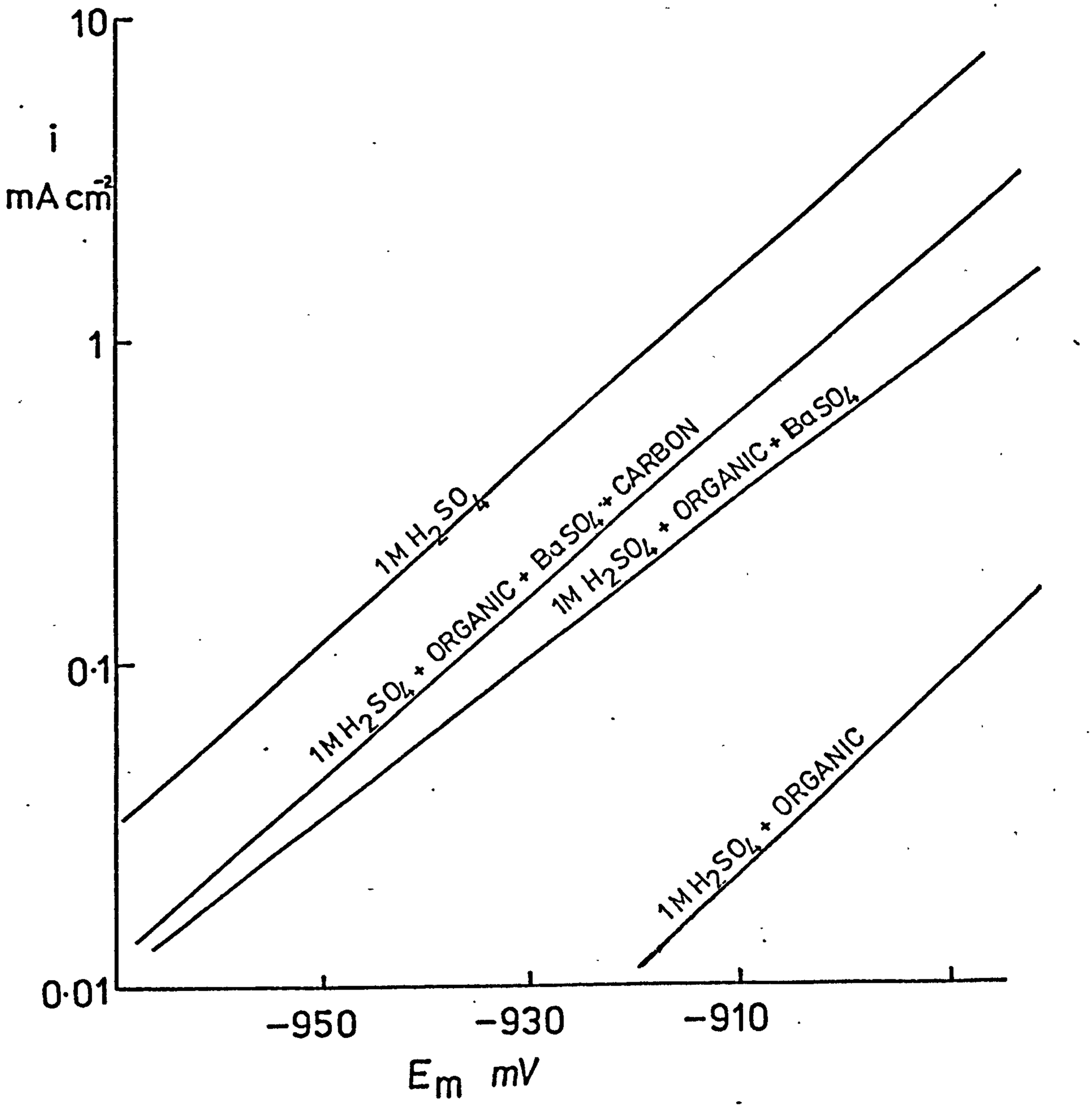

Fig. 6.49 $PbSO_4$ formed at -907 mV E_m (E_h = -245 mV) for 2 minutes in 1M H_2SO_4 saturated with organic (X810)

Fig. 6.50 $PbSO_4$ formed at -907 mV E_m for 2 minutes in 1M H_2SO_4 (X795)

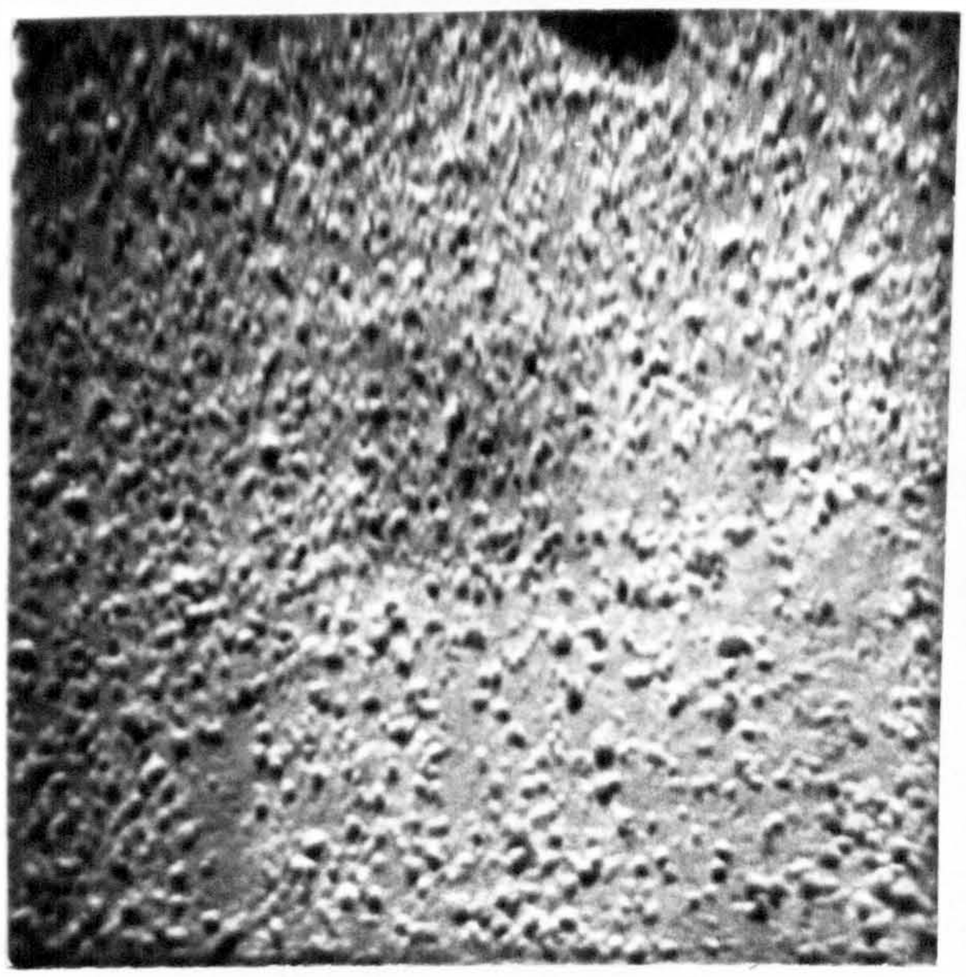

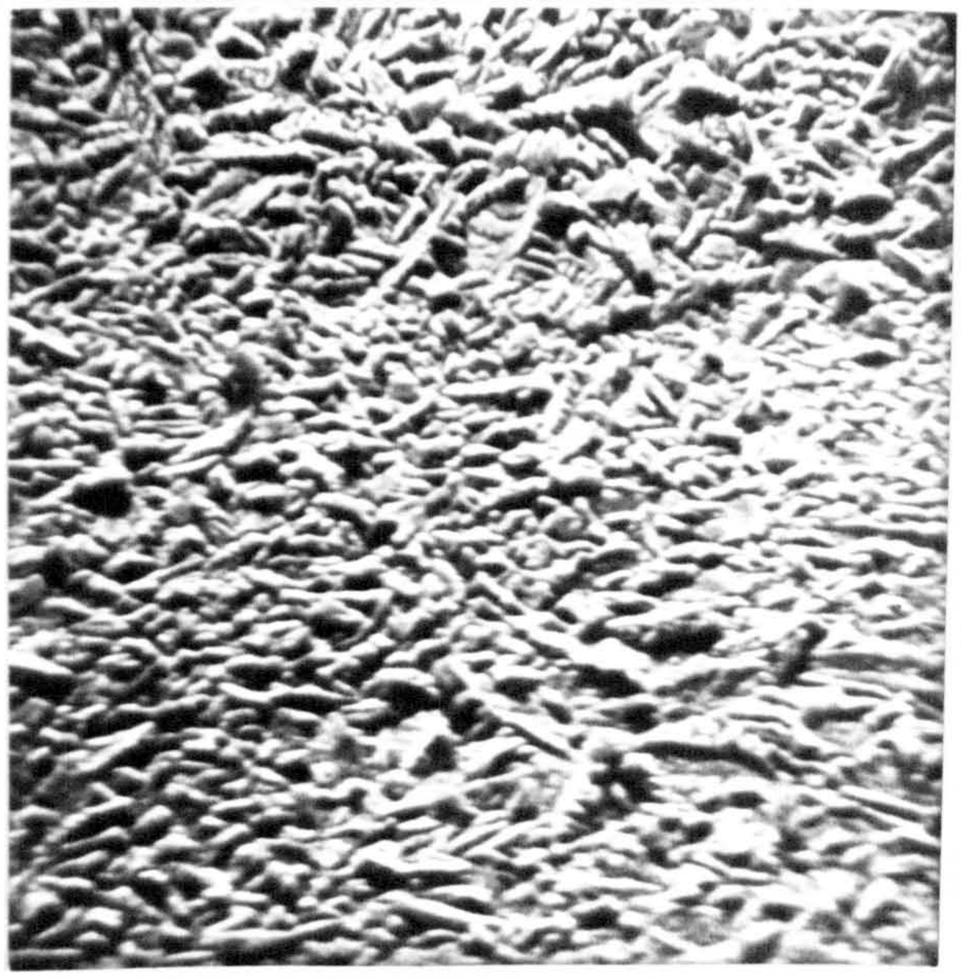

number of nuclei increase with time Figures 6.51,a,b,c. The crystals of lead sulphate formed depends on the formation potential.

6.7. Conclusions and Suggestions for further work

The anodic dissolution of Pb in H_2SO_4 has been investigated. The Pb dissolves as Pb^{2+} and $PbSO_4$ ions at low anodic potentials. At higher potentials solid $PbSO_4$ is formed by a solid state reaction.

Comparison of solid Pb and Pb(Hg)

The measurements of Figure (6.15d) and Figure (6.30) show that the solid state formation of $PbSO_4$ is much delayed in potential on Pb(Hg). $PbSO_4$ forms on solid Pb at -940 mV E_m and on Pb(Hg) at -910 mV E_m. The $Pb/PbSO_4$ E^o is -970 mV E_m. The charge recovered is approximately 100% on amalgams (Figure 6.26) whereas the same on solid lead is somewhat less (Figures 6.3, 6.4, 6.5). This is shown in Figure 6.1 even after prolonged reduction conditions, some lead sulphate remains. The solid Pb catalyses the formation of $PbSO_4$. The nature of the sites at which this happens is unknown.

$PbSO_4$ can also be formed in parallel by a solution-precipitation mechanism.

As already mentioned the critical potential for nucleation and growth on solid lead is -940 mV E_m. Cathodic to -940 mV E_m the current is steady for hours. The dissolution current flowing at this potential is approximately 0.2 mA cm^{-2} when the rotation speed is 15 Hz. Since 0.1 mA cm^{-2} is flowing (Section 6.6) under normal starting conditions on the negative plate is would seem reasonable that this current can be supplied by the dissolution process alone. If the surface is covered with

Fig. 6.51(a) $PbSO_4$ formed at -930 mV E_m in 1M H_2SO_4 after 20 seconds (X405)

Fig. 6.51(b) $PbSO_4$ formed at -930 mV E_m in 1M H_2SO_4 after 60 seconds (X405)

Fig. 6.51(c) $PbSO_4$ formed at -930 mV E_m in 1M H_2SO_4 after 116 seconds (X405)

lead sulphate formed by the solid state process the maximum current that can be supplied is approximately the same magnitude (Figures 6.22a,b,c); at very long times, when a thick layer is formed, the maximum current that can be supplied will presumably be lower. It has been shown[15] that during the discharge the negative plate operates at -0.3V (N.H.E.) (Figure 6.52). This corresponds to a potential of $\sim$ -960 mV E_m when 1M H_2SO_4 is used, i.e. the negative plate of the battery operates in the dissolution region.

Application of results to a porous battery electrode

It is only possible at this stage to make a qualitative conclusion. At the negative plate the overall reaction is

$$Pb + SO_4^{2-} \rightleftharpoons PbSO_4 + 2e$$

The requirement for a successful rechargeable battery is that one component, in this case Pb, should be electron conducting.

The advantages of using a porous electrode are primarily,

(i) Larger active surface area.

(ii) The pores provide areas in the electrode where the concentration of Pb^{2+} can exceed the solubility product, and lead sulphate precipitates as a porous layer which is presumably easily reduced(Stereoscan micrographs (Figures 6.1a,b) show $PbSO_4$ formed by the solid state process is not easily reduced).

Figure 6.53 shows how the process in a pore may operate. Lead dissolves from the walls of the pore. Inside the pore the concentration of $PbSO_4$

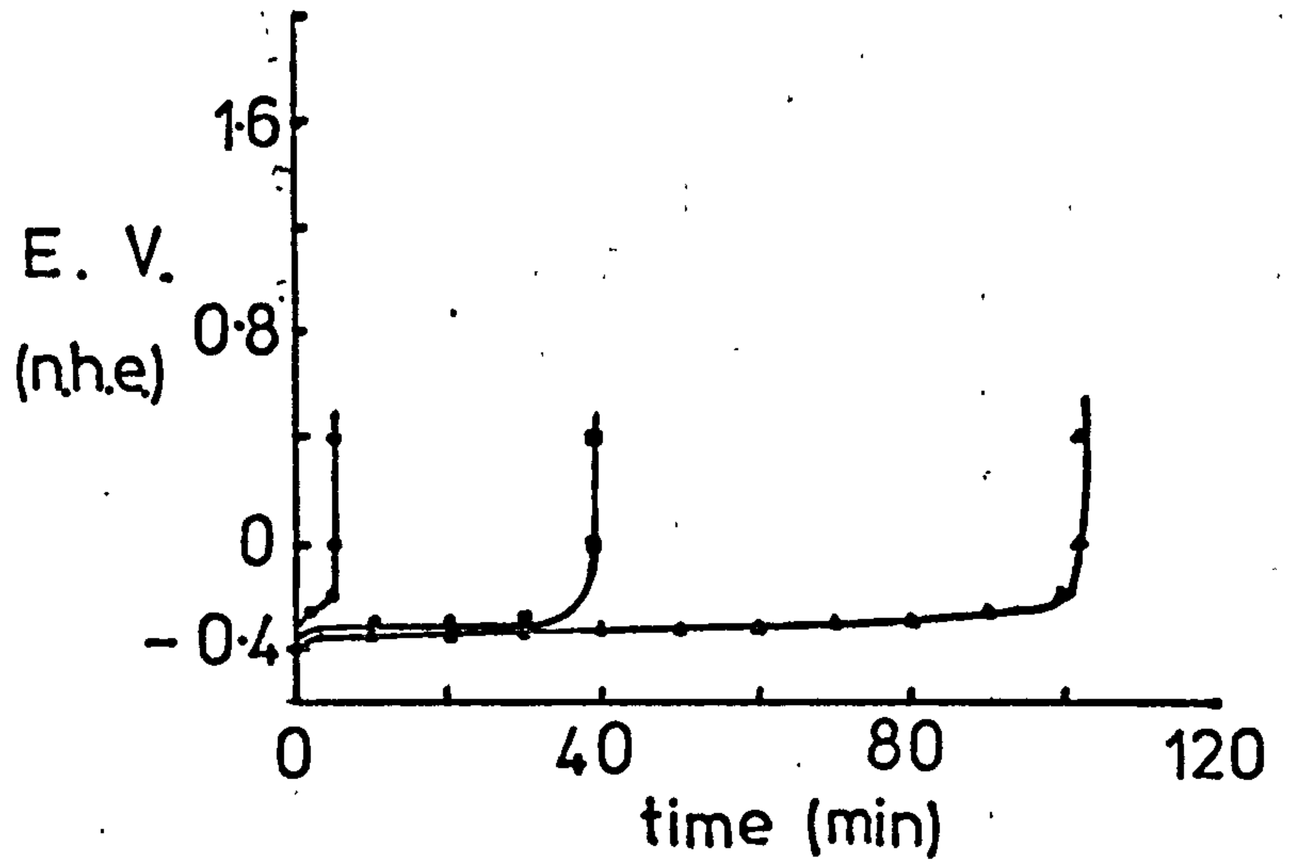

FIG. 6.52 Discharge characteristics of a –ve battery plate at 16°C. ▲, 21 mA cm^{-2}; ●, 41 mA cm^{-2}; ●, 165 mA cm^{-2}. (geometric surface area).

FIG. 6.53 PROCESS THAT MAY OPERATE IN A PORE.

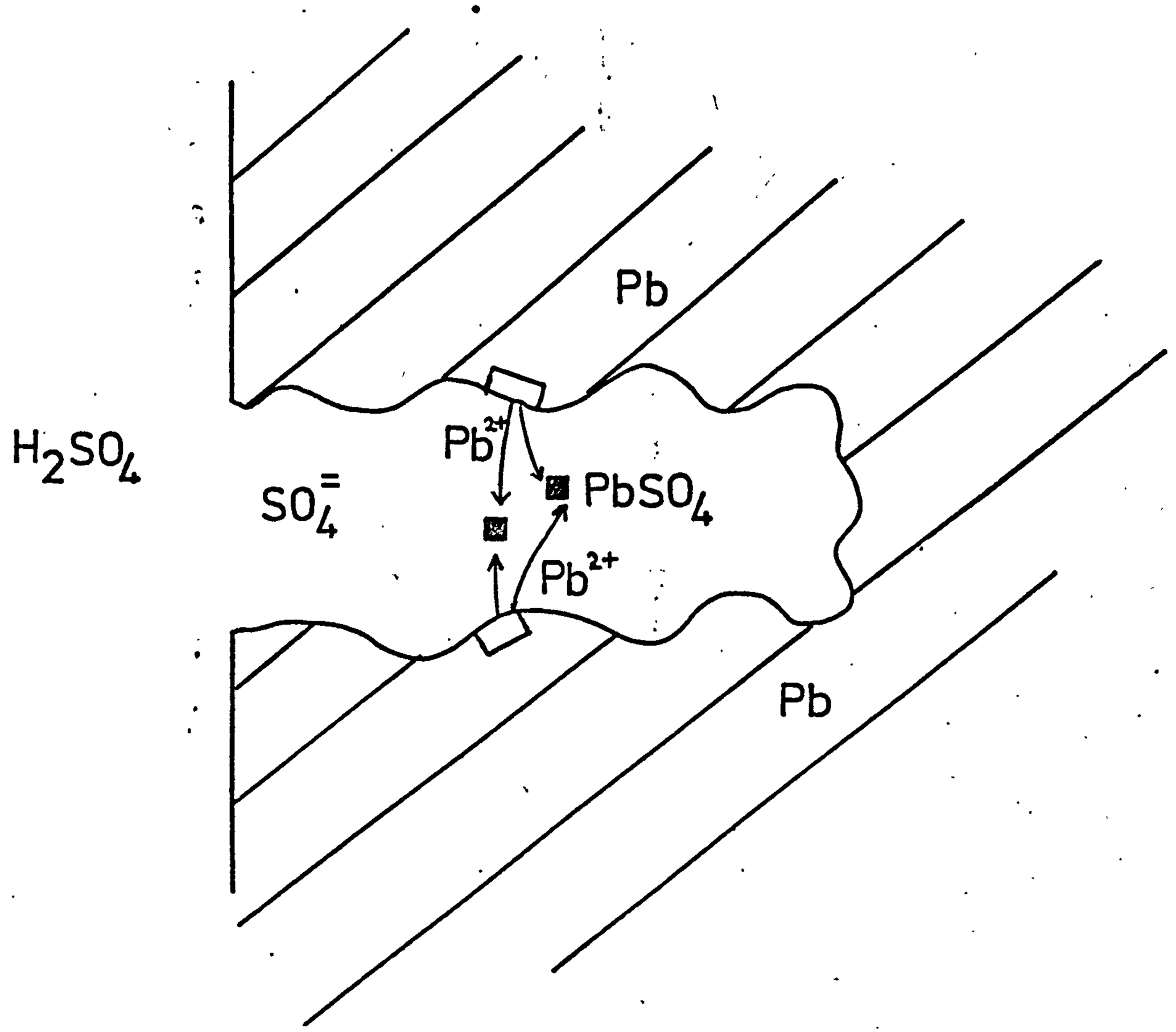

can exceed the solubility product and it precipitates forming a porous, easily reduced, layer.

A possible description of the action of organic additive is as follows:

1. The organic adsorbs strongly on the Pb surface and inhibits the solid state reaction to form $PbSO_4$. (Figures 6.49,6.50).

2. It ensures that precipitated $PbSO_4$, formed from a solution soluble species Pb^{2+} or $PbSO_4$ is well dispersed.

3. It cuts down the hydrogen evolution reaction, hence prevents loss of charge on open circuit.

4. As the temperature is lowered the current due to dissolution is lowered, however the organic ensures that the solid state reaction is suppressed. A more effective expander will suppress the solid state reaction without affecting the free dissolution.

$BaSO_4$ seems to encourage the solid state reaction and is probably undesirable. However it has not been possible as yet, to define its exact role.

The effect of these additives on solid lead is an interesting problem and provides a starting point for future work. The response of actual battery plates to potential pulses and sweeps could tie together the work in this project with the actual situation that exists in a battery.

REFERENCES

1. CHRISTIE, J.H. — J. Electroanal. Chem., 13, 79 (1967)

2. SCHWARZ, W.M. and SHAIN, J. — J. Phys. Chem., 69, 30 (1965)

3. CRAIG, D.N. and VINAL, G.W. — J. Research N.B.S., 22, 55 (1939)

4. VAN'T RIET, B. and KOLTHOFF, I.M. — J. Phys. Chem., 64, 1045 (1960)

5. LIESER, K.H., BEYER, G. and LAKATOS, E. — Z. Anorg. Chem., 339, 208 (1965)

6. Stability Constants, Special Publication No. 17, The Chemical Society, London, (1964)

7. Stability Constants, Supplement No. 1 to ref. 6, (1971)

8. ROBINSON, R.A. and STOKES, R.H. — 'Electrolyte Solutions', Butterworths, London (1968)

9. HARRISON,J.A. and THIRSK, H.R. — Electroanal. Chem. Vol.5 (ed. Bard, A.J.), Dekker, New York, (1971)

10. HARRISON, J.A. — J. Electroanal. Chem., 36, 71 (1972)

11. ARMSTRONG, R.D., FLEISCHMANN, M.F. and THIRSK, H.R. — J. Electroanal. Chem., 11, 208 (1966)

12. ARMSTRONG, R.D. and HARRISON, J.A. — J. Electroanal. Chem. 36, 79 (1972)

13.a. 'Computers in Chemistry and Instrumentation', Vol. 2, Mark, H.B. Jr., and Macdonald, H.C. Jr., (Eds.), Dekker, New York, 1972

13.b. FELDBERG, S.W. in Bard, A.J. (Ed) Electroanalytical Chemistry, Vol. 3, Dekker, New York, (1969)

14. GLADYSHEV, V.P. Soviet Electrochemistry, 7, No. 10, 1374 (1971)

15. BAIKIE, P.E., GILLIBRAND, M.I. and PETERS, K. Electrochim. Acta 17, 839 (1972)

LIST OF SYMBOLS

a	area, jump distance (equations 2.9, 2.10), cylindrical pore radius (Chapter 3), ion size parameter (Chapter 5)
a'	distance from an equilibrium site in the metal to an equilibrium site in the oxide film (equation 2.12)
a_i	activity of species i
A	area, constant (Chapter 5)
b	Tafel slope
B	constant
B'	constant
C	capacity
C^*	supersaturated solution, Bulk concentration outside a pore (Chapter 3)
$C_{x=0}$	concentration at the opening of a pore (Chapter 3)
C_o^s, C_R^s	surface concentrations of species O and R
C_o^b, C_R^b	bulk concentrations of species O and R
D	diffusion coefficient. Also with appropriate subscripts identifying species
D', D_E	effective diffusion coefficient
e	electronic charge, electron
E	potential of working electrode
E^o	standard potential
E_o	potential at open end of pore
E^*	critical potential for S.S. film formation

E_e	potential at which i = 0
E_f	flade potential
E_h	standard hydrogen scale
E_ℓ	potential at the bottom of a pore
E_m	$Hg/Hg_2SO_4/H_2SO_4$ potential scale
E_p	peak potential, passivation potential (Chapter 2)
E_{pp}	potential of complete passivity
f	F/RT
F	Faraday
h	height of Pb(Hg) drop
ΔH_s	enthalpy of sublimation
i	current in amps
i_f	forward current
i_b	backward current
i_d, i_D	diffusion limited current
i_R, i_D	current at ring, current at disc
$i_{x=0}$	current at opening of pore (Chapter 3)
i_o	exchange current density
i_p	peak current, passivation current (Chapter 2)
i(u)	current due to growth of a single area
I	total current, current density due to the interfacial reaction; that is the current after correction for diffusion effects
j	$\sqrt{-1}$
J	flux
k	Boltzmann constant

k_o, k'	constants
k_f	a forward rate constant
k_b	a backward rate constant
k_a	forward rate on the surface
k_1	rate of horizontal growth of a pyramid
k_1, k_{-1}	potential independent characteristic forward and backward rate constants
k_1, k_2	chemical rate constants
K	chemical equilibrium constant
K'	a constant
K_∞	specific conductivity
ℓ	pore length
L	film thickness
M	molecular weight
M^a	anode material
M^c	cathode material
M_1^*	concentration of species M_1 at $x = 0$
n	number of electrons transferred, a constant (Chapter 5)
n'	effective number of electrons involved
n_D	number of electrons in reaction at disc electrode
n_R	number of electrons in reaction at ring electrode
N	collection efficiency, number of mobile ions per unit volume (Chapter 2)
N'	concentration of atoms on the metal surface

Q_a anodic charge

Q_c cathodic charge

r radius of capillary (Chapter 5)

r_1 radius of disc electrode

r_2 radius from the centre of the disc electrode to the outer edge of the isolating ring

r_3 radius from the centre of the disc to the outer edge of the metal ring electrode

R gas constant, ohmic resistance of the electrolyte solution (Chapter 3)

R_{ct} charge transfer resistance

S a 1M H_2SO_4 solution saturated with organic additive

$S_{/x}$ a 1 M H_2SO_4 solution saturated with organic additive and diluted x times with 1M H_2SO_4

t time

t_i transport number of species i

T absolute temperature

v potential sweep rate

V volume, potential sweep rate, potential

V_2 rate of vertical growth

x distance from electrode surface, distance through the oxide (equations 2.9, 2.10), direction along pore axis

z charge on a particle (sometimes with a subscript)

Z impedance

Z_o impedance of a semi-infinite pore

Z' ratio of interfacial concentration and current (Chapter 3)

α transfer coefficient, temperature coefficient

γ activity coefficient

δ Nernst diffusion layer thickness

ξ $\frac{\alpha naF}{RT}$

η $(E - E_e)$

θ coverage, temperature

κ specific conductance

μ chemical activation energy

ν kinematic viscosity

ρ density, $(R/R_{ct})^{\frac{1}{2}}$

σ conductivity

ω frequency

$\omega, \omega_D, \omega_R$ rotation speed of rotating disc

grad $\tilde{\mu}$ the electrochemical potential gradient

grad ϕ total electric field

ACKNOWLEDGMENTS

I am greatly indebted to Dr. J.A. Harrison for his continued advice and guidance throughout the course of this work.

I would like to thank Dr. S.C. Barnes of Joseph Lucas (Batteries) Ltd. for his useful discussion and support with apparatus.

My thanks are due to Mr. E.H. Boult for assistance with the Stereoscan microscopy and to the Science Research Council for the provision of financial support.